ANNÉE 2017

UNIVERSITÉ DE RENNES 1

UNIVERSITE BRETAGNE LOIRE

THÈSE / UNIVERSITÉ DE RENNES 1
sous le sceau de l'Université Bretagne Loire

pour le grade de

DOCTEUR DE L'UNIVERSITÉ DE RENNES 1

Mention : Biologie

Ecole doctorale (BS)
Ecole Doctorale Biologie Santé

Julien Babic

Préparée à l'unité de recherche (IGDR UMR 6290)
Institut de Génétique et de Développement de Rennes
(UFR Sciences de la vie et de l'environnement)

New microfluidic systems for controlling the cell microenvironment during live-cell imaging

Thèse soutenue à l'IGDR
le 14/12/2017

devant le jury composé de :

Damien COUDREUSE
CR1 - IGDR / *Thesis director*

Jérémy CRAMER
CEO Cherry Biotech / *Thesis co-director*

Gilles CHARVIN
CR1 – IGBMC / *Examinator*

Isabelle SAGOT
DR2 – IGBC / *Examinator*

Reynald GILLET
PU – IGDR / *Reporter*

Régis GIET
DR2 - IGDR / *Reporter*

Acknowledgments

When I started my PhD, I was told that it would not be easy and many obstacles would be on my way. These three years did not pass without problems, and eventually the Murphy's Law also acted against my will. Thus, I am grateful to many people for helping me through the great challenge that is a PhD.

Above all, I would like to thank my supervisor Damien Coudreuse. First, thank you for accepting me in your research laboratory. As an engineer, the research environment was new to me, and I would like to thank you for everything that you have taught me and for the interesting discussions we have had during these three years. I really appreciated that you were opened and enthusiastic with the projects I was in charge of. I also would like to thank you for pushing me the way you did: you gave me the energy to work hard, sometimes during the night, sometimes when experiments were not working as expected, and without this energy I would never have accomplished my projects.

I would like to thank the co-director of my thesis, Jeremy Cramer, for accepting me in this thesis and welcoming me inside the Cherry team. I learnt a lot from being part of this team with the Cherry spirit. I really thank you for that and for your support and advices.

Also, I am grateful to Jenny Wu for her helpful advices and discussions. Thanks to all the members and past members of my team, and by my team I include the GDM team: Celine, Javier, Laurent, Maria, Nelson, Sarah, Vasantha (Synthecell team) and Anthony, Balveer, Blanca, Chris, Diane, Diego, Lilian, Miguel, Nena (GDM team). Thanks for the your help and support, for all interesting conversations about my project, thanks for listening for my (sometimes) bad jokes. About that, I would like to thank Mike Roscope and Mike Rofluidics for being there with me against Murphy. I also would like to thank my second team from Cherry Biotech (especially Thomas, Nadia, Damien, Erwan and Mathilde).

Also, I would like to thank all the people with whom I interacted in the institute, especially the Jaulin's team, the Gestion, Geraldine and Benedicte.

Thanks to all the members of my thesis jury, for accepting to be part of this committee, and for reading and correcting this (hopefully not too long or too boring) thesis manuscript.

Almost finally, I would like to thank my family, for each time trying to understand what I do and encouraging me throughout my PhD. Also, sorry that we could not have seen each other much lately, this is part of a PhD project I guess.

Almost almost finally, I also thank all my friends (that did or are still doing a PhD, or never did any but understand how time consuming it can be). Thanks for your presence and for all the fun time that we had, especially on Friday evenings…

Finally, I would like to thank Audrey for all the support you gave me, especially in difficult times, thanks for your enthusiastic sentence "So it worked?" when I was coming back late from the lab. Most of all, thanks for your encouragements and your patience, I could not have done it without you around.

Table of contents

Table of Figures

Introduction

General introduction

Life science is the study of living organisms, and is composed of a myriad of fields. Cell biology is one of these, and consists of the study of cells, their structures and their functions in order to understand nature in all its forms. Biologists try to explain cell biology principles through the observation of cells and their behaviors using microscopy. Microscope developments have evolved in parallel with our knowledge: time-lapse microscopy and live-cell imaging have made possible the observation of cells over a long period of time, and have improved our understanding of biological processes. Tools compatible with microscopy have been developed to control the cell microenvironment for a wide range of assays while being monitored under the microscope. However, using conventional methods, the control of such microenvironment parameters is not precise and dynamic. Advanced researches consist in visualizing fast cells responses for understanding their behavior and functions, and controlling dynamically the cell microenvironment is critical and challenging. As of today, there is no simple existing system that can dynamically, simultaneously and precisely control the cell microenvironment under microscopy observation. For that, recent approaches have emerged and microfluidics is one of the strategies to ensure such a control of the cell microenvironment.

Using microfluidics relies on the fabrication of miniaturized devices, adapted for the circulation of any fluids. At their scale, the physics are well understood, and fluid flows can be highly controlled and predicted. Additionally, these systems allow for the observation of single cells or populations of cells using microscopy. Thus, microfluidics is the best candidate to realize the control of the microenvironment while performing high-resolution microscopy. Myriad microfluidic systems have been developed for biological purposes, but there are still challenges that need to be addressed for live-cell imaging experiments.

The aim of my research is to build a versatile microfluidic system, which can provide simple solutions for a number of applications in the life sciences: an accurate, dynamic and simultaneous control of the cell microenvironment while performing live-cell imaging.

- It must be fabricated with biocompatible materials, which allow cell proliferation and are compatible with the drugs and biomolecules used in the laboratory.
- It must be adapted to high-resolution microscopy and live-cell imaging.
- It must be compatible with adherent and non-adherent models.
- It must allow for an accurate, dynamic and simultaneous control of the temperature, medium and drug concentration.
- It must be user-friendly and reusable.

In the first chapter of the introduction, I present some biological concepts and features relevant to my work. In the second chapter, I describe microfluidics basic concepts, and microfluidics fabrication methods and materials. The third chapter explains how, using microfluidics, it is possible to control the different parameters during live-cell imaging. Finally I conclude and present the objectives of my thesis project.

Chapter 1. Biological sciences: a necessity of understanding

1 Studying cell biology for understanding life

Biology is the study of all kind of systems from animals to plants to improve our knowledge of life and nature. Biologists have tried to understand nature in all its form and diversity, with a broad range of topics such as cell biology, biochemistry, genetics, developmental biology, immunology, evolution[1]. Cell Biologists aim to better understand the functions of organs, tissues, cells, organelles and DNA among other things, to explain the phenomena and processes that are yet not understood.

One fundamental process that is at the center of cell biology itself is the cell cycle, which is a series of biochemical and structural events regulating cell growth and division, and which plays a role in cell proliferation, stem cell renewal, or diseases. The cell cycle is composed of several phases, the deregulation of which is known to impact cell proliferation and is responsible for several diseases such as leukemia[2], Alzheimer[3], hepatitis[4] or cancer[5]. Biological discoveries could lead to prevention or treatment of these diseases.

2 The cell cycle: the process of proliferation

2.1 Definition of a cell

A cell is by definition the smallest structural, functional and biological unit of all organisms. Hypothetically, all existing cells derive from one ancestral cell that lived between 3 and 4 billion years ago[6,7]. Nowadays, various existing cells and organisms are present in the nature. Prokaryotic organisms are unicellular organisms that can be classified in two domains: Archaea and Bacteria. Prokaryotes are the most ancient form of life on Earth, and they have the particularity of having no nucleus. In this thesis I will focus on eukaryotic organisms[8]. Eukaryotes can be unicellular or multicellular, and eukaryotic cells are characterized by a nucleus where the DNA is encapsulated, and by membrane-bound organelles, separated from the cytoplasm, which perform specific functions critical for cell survival[9] (Figure 1).

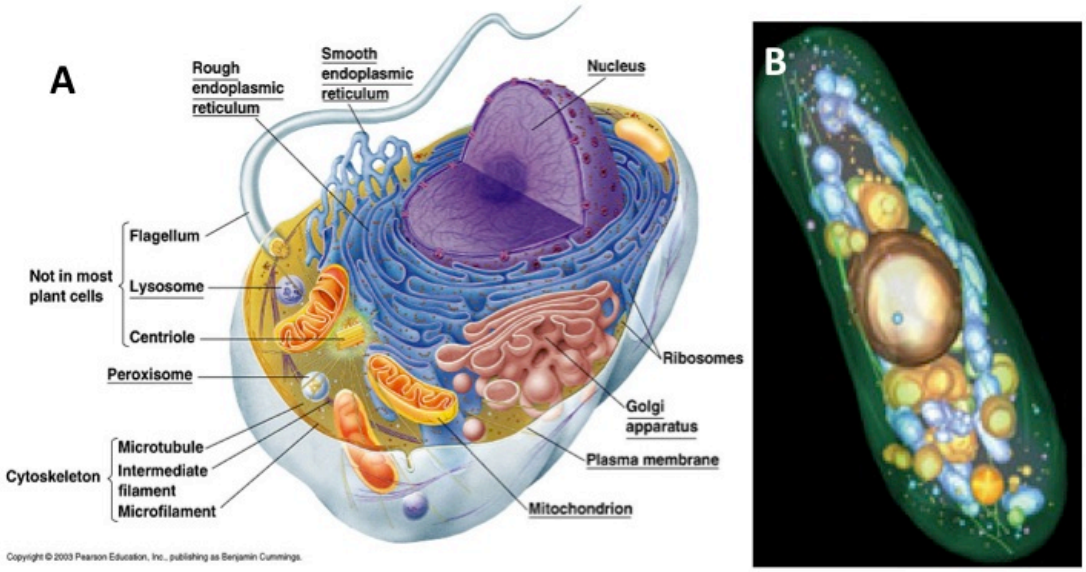

Figure 1: Definition of a cell. A - Detailed schematic of a eukaryotic cell containing a nucleus and organelles. B – Reconstruction of a whole yeast cell by electron tomography made by Johanna Höög/EMBL. The plasma membrane, microtubules and vacuoles are green, the nucleus is positioned at the center in gold, vacuoles and dark vesicles are gold, mitochondria and large dark vesicles are blue.

2.2 Definition of the cell cycle

The cell cycle can be described as a series of events that occur in a cell allowing it to divide into two daughter cells (Figure 2). It is constituted of two main steps: the duplication of the DNA (interphase) and the distribution of the genetic material into the daughter cells (mitosis).

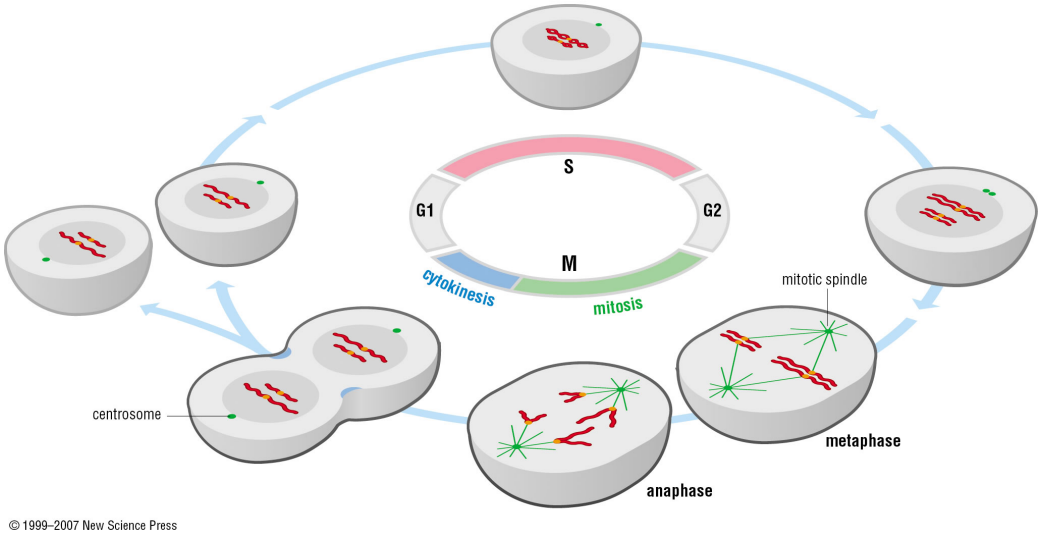

Figure 2: The four phases of the cell cycle. Picture taken from The Cell Cycle: Principles of Control by David O Morgan. The G1 phase starts the cell cycle process. Replication of the chromosomes and duplication of the cell components occur in S phase. After the G2 gap, M phase allows one cell to divide into two daughter cells, and can be separated into a mitosis phase (separation of the DNA content in the daughter cell) and a cytokinesis phase (physical separation of the mother cell into two cells).

2.2.1 The interphase

The interphase is composed of three stages: the S phase, G1 phase and G2 phase, and two major transitions: the G1/S and G2/M transitions.

- During the G1 phase or G1 gap, the cell grows.
- The S phase is the Synthesis phase: the cell replicates its DNA[10].
- The G2 phase or G2 gap: the cell continues its growth and production of organelles, and starts reorganizing its contents prior to mitosis.

2.2.2 Mitosis

Following the G2 gap is M phase, the stage of the cell cycle at which DNA is equally separated into two nuclei[11]. M phase comprises several steps. Higher eukaryotes such as *drosophila*, *C. elegans* or mammalian cells contain a nuclear envelope, which encapsulates the genome. During the prophase, which is the first stage of mitosis, their nuclear envelope disappears[12]. In all eukaryotes, the mitotic spindle forms, composed of an array of microtubules[13]. The centrosome (known as the spindle pole body in yeasts) is the main microtubule-organizing center. During metaphase, the sister chromatids are attached to the mitotic spindle, and are localized at the center of the nucleus, as shown in Figure 2. Anaphase is the phase at which the sister chromatids are separated, and the two copies of the chromosomes are distributed in the two daughter cells, respectively: the mitotic spindle forms a bipolar assembly[14] (Figure 2). This occurs as the cohesins, which hold the two sister chromatids together, are degraded[15]. Forces emanating from the mitotic spindle microtubules pull the separated sisters towards their respective centrosomes[16]. During the last phase of mitosis, known as telophase, the chromatids and other nuclear components are distributed in the two daughter cells. Under normal conditions, this distribution tends to be equal. The phenomenon that divides the cell in two is called cytokinesis (cytoplasmic division)[17].

Mitosis is a major focus in research, especially because problems in the chromosome segregation can lead to abnormalities and aneuploidy, source of diseases such as cancer.

2.2.3 The mechanisms involved in the cell cycle

The fidelity of the cell cycle through generations is the result of regulatory mechanisms that are well conserved throughout eukaryotes[18], and which occur in a precise order with specific timings[19]. This fine regulation of the cell cycle is allowed by cyclin-dependent kinases (CDK), enzymes that interact with various regulatory partners called cyclins[19]. The interaction of CDK with cyclins regulates the activity of CDK, which oscillates throughout the cell cycle[20], and is essential for cell cycle progression[21]. Specific mechanisms, known as checkpoints, ensure that one cell cycle event does not start prior to the completion of the previous one[22] . These checkpoints are controlling the activity of the CDK, as they can arrest the cell in its cycle temporarily if the conditions for continuing the cell cycle are unfavorable[23]. Checkpoints are thus surveillance mechanisms upon challenges to cells, and can make cells re-enter the cell cycle only until the problem is solved. We can cite the checkpoint at the G1/S transition, known as Start point for yeasts, or restriction point in mammalian cells[24,25], the mitotic entry checkpoint[26,27]. In short, both CDK and checkpoints form the cell cycle control network (complex regulatory network) that coordinates and regulates in time the cell cycle events[28].

The cell cycle machinery is universal[19]. Therefore biologists have the possibility to study various model organisms, whose functions and mechanisms are highly conserved.

3 The use of model organisms and their advantages for studying cell cycle processes

3.1 Model organisms and their advantages

Studying human cells is not ideal for biological research and investigation of the cell cycle. Their number of genes is estimated to be more than 19000[29], many of which are involved in more than one process and possess multiple functions. As a consequence, the complexity of human cells makes it challenging to find evidence on the functions of genes. Hence, for practical reasons, biologists use simpler living tools called "model organisms". These are non-human organisms chosen because of their simplicity and their particular experimental advantages. First, they are easy to manipulate and to grow in laboratories, from simpler ones like the yeasts *Schizossaccharomyces pombe*, *Saccharomyces cerevisiae*, the bacteria *Escherichia coli* to slightly more complex ones such as the fruit fly *Drosophila melanogaster*[30], the nematode *Caenorhabditis elegans*[31] or mammalian cells. Most model organisms have their genome fully sequenced, and their genetic manipulation methods are well established compared to that of human cells. The genomes of all species are different, but have similarities, and a large number of mechanisms, principles and genes are conserved between two different model organisms, and also between model organisms and human cells. As an example, in the fission yeast *Schizossaccharomyces pombe*, 50 genes have similarities with genes related to human diseases[32], and half of these genes are related with cancer. The cell cycle machinery is universal, and each model follows the same cell cycle steps. As Nobel laureate, Jacques Monod famously said: "What is true for *E.Coli* is true for the elephant". Thus, studying biological processes using one model organism can provide knowledge about another organism. For instance, discoveries made on model organism have led to significant insights about cell cycle regulation[33], apoptosis[34], signaling pathway such as the TGFβ pathway[35], circadian rhythms[36], or developmental processes, involving for instance HOX genes[37,38].

Although they follow the same cell cycle steps, the timings of each phase can differ from one model to the next, an important factor for choosing the model best adapted for the process of interest. Moreover, the short generation time of some model organisms can be an advantage for their study in laboratories, especially when performing evolutionary biology.

3.2 *S. pombe*: A reliable model organism for cell cycle studies

3.2.1 What is *S. pombe*?

Schizosaccharomyces pombe is a fission yeast used as a model for genetics and cell biology. *S. pombe* is a rod-shaped yeast, and the standard strains used in the laboratory have a length of 7 microns at birth, of 14 microns at division, and a diameter of 4 microns. During the cell cycle, its growth is made only through the cell tips. During cytokinesis, a septum forms at the center of the cell along the short axis for its division into two daughter cells. Moreover, this type of yeast divides symmetrically: the two daughter cells have the same size after division (Figure 3). One main advantage of using *S. pombe* cells is their short generation

time: for standard yeast strains used in the laboratory, a cell cycle can last between 2 and 4 hours, depending on the nutritional and physical conditions. These cells are considered as "non-adherent cells": In the laboratories with standard culture conditions, they do not attach to their substrate, growing in suspension in the medium[39].

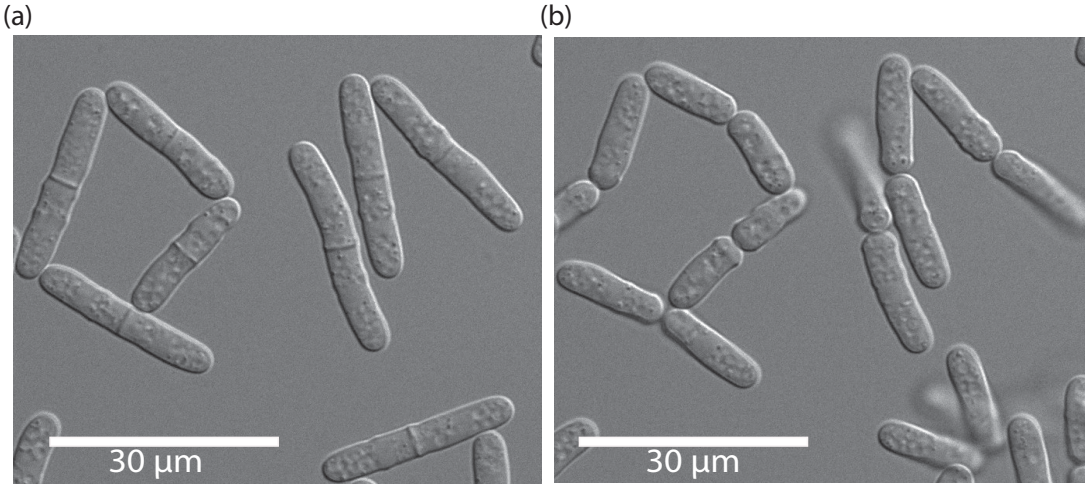

Figure 3: Pictures of *S. pombe* cells in transmission (DIC). Mutant cells sensitive to an ATP analogue inhibitor 3-MBPP1 were blocked in the cell cycle for synchronization. Pictures were taken after the release in normal medium. (a) All cells contain a septum, indicating their synchronization in the cell cycle. (b) Same cells after dividing, showing that the daughter cells have the same size. The division is symmetrical.

3.2.2 How is *S. pombe* useful for biological studies?

As a unicellular eukaryote, its studies represent a tremendous contribution for understanding cell mechanisms and processes. The genome of *Schizosaccharomyces pombe* was sequenced by the Sanger institute in 2002. It contains nearly 5000 genes along three chromosomes of a total size of 13,8 Mb[32]. Strains for various applications have generated a considerable collection of data and tools[40,41]. The ease of its genetic manipulation makes *S. pombe* an excellent model for studying fundamental processes. It is relatively easy to insert and delete genes in the genome and also to create mutants sensitive to specific drugs or temperatures[42-44]. Furthermore, *S. pombe* cells can proliferate in a haploid state, containing only one copy of the genome, enabling easier screening of mutations and avoiding the complication of having a second copy of the genes.

3.2.3 *S. pombe* cell cycle

As previously described, cyclin-dependant kinases (CDK) regulate the cell cycle. Their binding with cyclin subunits regulates distinct cellular events in the cell cycle. As opposed to human cells, the cell cycle in *S. pombe* yeasts is controlled by only one CDK, called Cdc2. The cyclins subunits that bind to Cdc2 are called Cdc13, Cig1, Cig2 and Puc[45] (Figure 4 - A).

3.2.4 Using a synthetic cell cycle

Originally, scientists thought that cell cycle control was driven qualitatively by different cyclin-CDK complexes at different stages of the cell cycle. However, this qualitative model of cell cycle regulation and cell proliferation was controversial, and a quantitative model was proposed in the yeast *S. pombe*, as the deletion of the Cig1, Cig2 and Puc1 cyclins did not appear to be lethal in the cell cycle, and Cdc13 was

discovered to be the only essential cyclin in fission yeast[46]. Other studies in mice have demonstrated that the deletions of CDK[47], or even one CDK alone was able to drive the whole cell cycle in mammalian cells[48]. This questioned the absolute necessity of having multiple complex cyclin-CDK driving the cell cycle[49], therefore quantitative models have been proposed and suggest that oscillations of the activity between thresholds drive cell cycle progression. These quantitative approaches led to the engineering of synthetic systems that allowed biologists to decrease the complexity of the cell cycle[50], which could be an obstacle for understanding the core engine and basic principles of cell proliferation. In yeasts, Coudreuse *et al.* developed a minimal cell cycle, in which Cdc13 and Cdc2 are fused[51] (Figure 4 - B), and the G1/S cyclins have been deleted. The idea is that the oscillation of a single Cdc13/Cdc2 complex is sufficient to drive cell cycle events and progression.

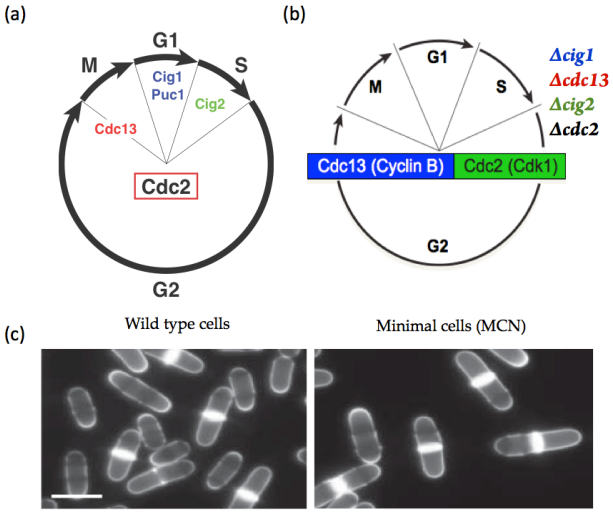

Figure 4: *S. pombe* cell cycles (a) Schematics of *S. pombe* cell cycle. The binding of the unique CDK (Cdc2) with four cyclins (Cdc13, Cig1, Puc1 and Cig2) is driving the different cell cycle phase of *S. pombe*. (b) Schematic of a synthetic *S. pombe* cell cycle. Cig1, Cdc13, Cig2 and Cdc2 have been deleted, and the fusion between cdc13 and cdc2 is driving cell cycle progression. (c) Picture of cells with blancophore of wild type cells on the left and of cells following a synthetic cell cycle. Generation time and length at division are similar.

3.3 Mammalian cell studies

As opposed to *S. pombe*, mammalian cells are larger in size but still require the use of a microscope for detailed analyses. Furthermore, most mammalian cells are adherent, they grow and proliferate on a biocompatible substrate material such as glass or polystyrene (Figure 5). Their cell cycle lasts between 12 and 28 hours, depending on the cell line and the nutritional conditions. Their standard growing temperature is 37˚C with constant renewal of carbon dioxide, required for maintaining a constant pH[52].

Mammalian cells used in a laboratory setting originate from specific tissues (liver, skin, etc.) and have been isolated and cultivated in artificial media in laboratories. As more complex cells than yeasts, mammalian cells are used for studying and understanding specific mechanisms and processes.

For biological studies, it is possible to use primary cells, taken directly from a subject. Their have a limited lifespan and their senescence prevents long-term cultures. Other cells lines are immortal and can be cultured for a long period of time. These particular cells have either been genetically modified, either they accumulated mutations (for instance *HeLa* cells), resulting in immortalization.

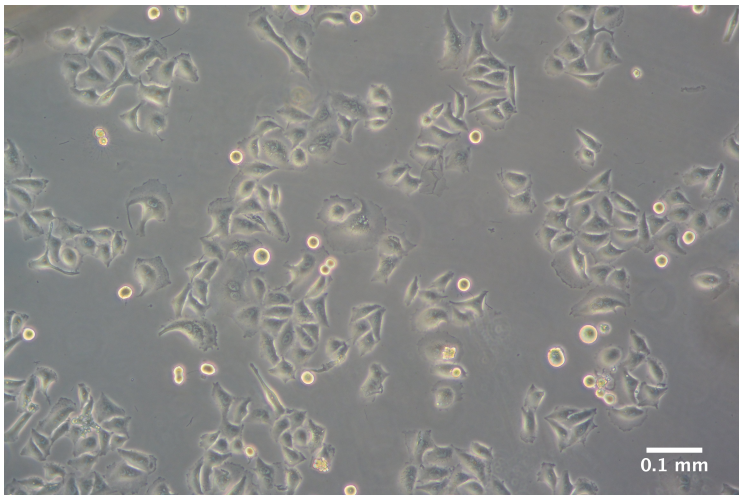

Figure 5: **Picture of *HeLa* cells in transmission. Cells are mostly adhering on the glass coverslip substrate. The round ones have partially detached and are in mitosis.**

Cell biology and life sciences in general are investigating the concepts of life by using simple model organisms. These models are following similar cell cycles and a number of principles and functions are well conserved throughout these organisms. Due to their small size, researchers need to use microscopy for understanding their functions, observing precisely their behavior and performing detailed analyses.

4 Microscopy imaging

4.1 From a standard microscopy image to live-cell imaging

4.1.1 Light microscopy imaging

The fine observation of cells with the naked eyes is almost impossible. For most applications, high-resolution microscopes have been developed for imaging small living cells and their components, and their resolution is adequate for studying cellular and subcellular structures.
Light microscopy used for cell biology can be classified into two classes: transmitted light microscopy and fluorescence light microscopy (Figure 6).

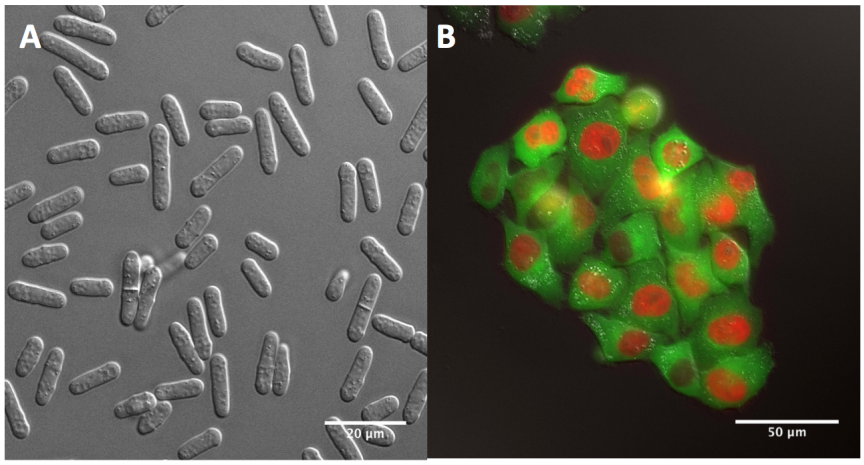

Figure 6: Microscopy: transmitted light versus reflective light. A – Picture of *S. pombe* cells using differential interference contrast (DIC), giving the appearance of reliefs. Scale bar is 20 µm. B – Picture using fluorescence microscopy of *HeLa* cells {H2B::mCherry ; tubulin::GFP}.

4.1.1.1 Transmitted light microscopy

The microscopes using transmitted light dispose of a light source, which emits a light that passes through the sample to 1) the objective lens, which magnifies the image of the sample and 2) an ocular to allow the user to see the image. Before reaching the sample, the light passes through a condenser, an optical tool that focuses the light to the substrate, for obtaining better illumination. This visualization using transmitted light, called bright-field microscopy, is not optimal: the attenuation of light by the sample creates a contrast, but as cells can be translucent, the visualization of detailed components or molecules is unsuitable. For enhancing cell observation further, optical strategies with different outputs were developed with the objective of improving cell contrast. These microscope techniques are the following: dark-field, phase contrast, polarization and differential interference.

Dark-field microscopy consists of illuminating the sample obliquely for creating a strong contrast between cells and their substrate. The objective lens does not receive direct light. The setup is simple, but the need of strong illumination can damage delicate samples.

Phase contrast microscopy exploits the fact that the light changes its phase while passing through the sample. The phase shift induces a change in the amplitude of the light wave, creating a contrast of intensity. Fine details, which are impossible to see using bright-field microscopy, can be observed using phase contrast. However, phase artifacts could lead to a distortion effect around the sample perimeter.

Polarization microscopes use the electromagnetic aspect of the light. The light is composed of electromagnetic oscillations that are perpendicular to the light path. By adding a polarized filter in the light path (polarizer), the oscillations occur only in one direction: the light is polarized. An analyzer, placed after the sample and perpendicularly to the polarizer, does not let the polarized light from the polarizer pass. It can however detect the light that went through the substrate due to the birefringence: when the light passes through the sample, its changes in magnetic orientations allow it to pass through the analyzer. The contrasts will thus depend on the orientation of the magnetic oscillations after the analyzer. The polarized microscopes are used when the polarized light interacts strongly with the sample. Thus, this technique is not appropriate for live-cell imaging, and is only used in mineralogy.

Differential interference contrast microscopy creates a 3D-like image with shades of grey, used especially for unstained and transparent samples. Two polarized light paths are used to illuminate the sample

and their interference creates the final image (Figure 6). This technique gets rid of the artifact effects of the phase contrast technique.

4.1.1.2 Fluorescence light microscopy

Microscopy using fluorescent light is called reflective microscopy. In the life sciences, tagged molecules called fluorophores emit fluorescent light after being excited, which can be seen due to their high intensity. This phenomenon can be explained briefly (Figure 7): The incident light coming from the objective excites the sample molecules, or fluorophores, which absorb a photon. They consequently reach an electronic state of higher energy. The excitation does not last long and the molecules must return to their fundamental energy level. The decrease of energy associated with the des-excitation is accompanied by the emission of a photon of another wavelength, which can be observed at the microscope.

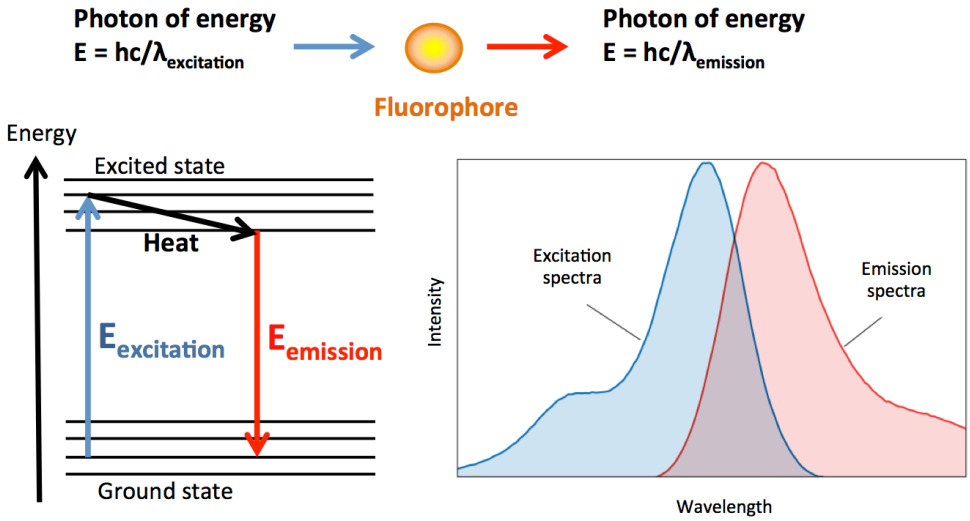

Figure 7: Schematics of the principle of fluorescence microscopy. The light coming towards the sample, associated with a photon of energy $E_{excitation}$, excites the fluorophore (excited state). While returning to its ground state, it first generate heat, then a photon of lower energy $E_{emission}$ is produced (higher wavelength) and seen by the observer.

Many fluorophores exist with different wavelengths of excitation, which define large spectra (Figure 8). Thus it is possible to track the localization and dynamics or different proteins, organelles or components at the same time using multiple fluorophores, and perform multicolor imaging.

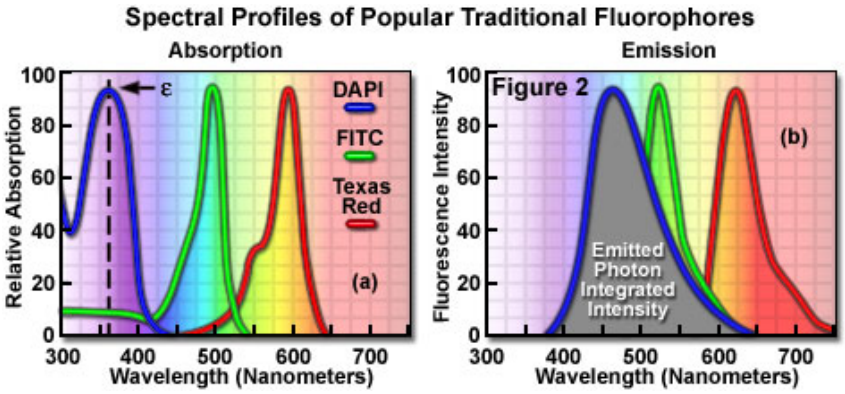

Figure 8: Spectra of different fluorophores (Carl Zeiss website). By superposing the images of each fluorophore it is possible to have a multicolor image. a – Excitation spectra. b – Emission spectra.

One advantage of reflective microscopy is the possibility of genetically modifying biological species so that the protein of interest is attached to a fluorescent molecule. Combining this genetic engineering with microscopy, the localization of the protein can be traced by the fluorescent signal, and it is possible to observe cell dynamic responses to perturbations of their microenvironment, especially during live-cell imaging.
The drawback of this type of microscopy is that the fluorescent staining is not permanent. Bleaching occurs as the sample is viewed and the intensity of the fluorescence decreases over time. Moreover, an over-exposure can degrade cells proteins or contents.

All these microscopy techniques improve the contrasts of cells to background. They all have advantages and limitations, and have to be chosen appropriately depending on the sample size, cell type, length of the experiment, of precision of details required. Any of these techniques requires the sample to be deposited on a high-grade glass coverslip, which is the standard material for microscopy, due to its high advantageous optical properties.

4.1.2 Live-cell imaging

For better understanding of biological processes, capturing motions and behaviors of live cells has become indispensable in the life sciences. In the past, photo-microscopy was used to decipher cell behavior over time[53]. Nowadays, microscopes are equipped with a camera for realizing video sequences, which can be programmed and automatized: time-lapse imaging[54]. These sequences are recorded and viewed at high speed to give an accelerated view of cell dynamics and processes. Live-cell imaging and time-lapse microscopy are thus powerful tools for understanding complex cellular processes, studying dynamic cellular responses to perturbation of the cell micro-environment and modulation of cell pathways, understanding the behaviors of individual cells or populations of cells.

4.2 The limitations of live-cell imaging using microscopy

For performing live-cell imaging, maintaining cells in their optimal growing conditions is essential. While observing cells using a microscope, trying to mimic their microenvironment for allowing their proliferation and circumventing possible cellular stress responses constitutes a great challenge. To this end, pH, medium composition and sample temperature should be controlled simultaneously and accurately to avoid interfering with the biological process of interest. Using conventional bench-top techniques, the manipulation of cells and the control of their microenvironment while doing microscopic observation remain

extremely difficult. Under static conditions without any medium renewal, the composition of medium changes, and wastes accumulate. Cultures in observation may have their temperature and pH modified over time, and evaporation can occur. Moreover, changing media manually can cause undesirable contaminations, hydrodynamic stresses, or changes in temperature and pH. Taken together, these issues are not solved by macroscopic perfusion systems. Besides, the flow control in such systems is not precise and reproducible.

Live-cell imaging constitutes a great tool for visualizing cells in their microenvironment, combining microscopy with biological samples. Regardless the microscopy techniques used, cells need to be in healthy conditions to proliferate. Static cell culture systems and macro-perfusion systems are insufficient for controlling the microenvironment and not best for performing robust experiments during live-cell imaging.

5 Conclusion

In the life sciences, live-cell imaging is an essential approach for studying cell behaviors and dynamics. For that, model organisms have been used especially for their simplicity. Their thin size requires the use of microscopes, and appropriate optical strategies allow for fine visualization of details or tagged regulatory molecules. The need of controlling the cell microenvironment while doing live-cell imaging is essential and difficult using macroscopic methods. Besides, it is challenging to control this microenvironment in a precise, dynamic and simultaneous way. One of the best candidates to achieve such multiplexed live-cell imaging assays is microfluidics. This science and technology has been developed during the past decades, and has already proven to be a good candidate for controlling all parameters influencing the cell and its microenvironment.

Chapter 2. Towards another approach for studying biology: microfluidics

1 Microfluidic basics and advantages

1.1 Definition of microfluidic

The term "Microfluidic" was first used at the beginning of the 21st century. As a pioneer in microfluidics, Georges Whitesides defines microfluidics as a science and a technology for the study of small volumes in channels of a micro-scale dimension[55]. Pr. Patrick Tabelling proposes a more engineer point of view, describing microfluidics as a field that studies the manipulation of flows of simple or complex fluids in microsystems fabricated with new technologies[56].

To summarize, microfluidics is both a science and a technology that consists in the production and use of miniaturized devices designed for fluid manipulation. Interestingly, biological research laboratories require the manipulation of cells and drugs, which are carried out in solutions, and microfluidic can be used as an adequate tool for controlling these fluids.

1.2 The evolution of microfluidics

Since their emergence, microfluidic systems have been compared to microelectronic devices: the circulation of fluids in microfluidic channels can be assimilated to the electron flow in micro-electronic cards. This analogy can be explained because microelectronic logics served as a base for microfluidic development. Microelectronics started with the replacement of lamps with mechanical transistors in the 1950's. Since, great efforts have been made in reducing the size of transistors, and miniaturization led to the emergence of electronic transistor-based devices called MEMS. The MEMS, or microelectromechanical systems, are usually between one and 300 microns in size. Interestingly, microfluidic systems were born when silicium-based MEMS technology was expanding, and the fabrication processes to generate MEMS, especially photolithography, were used and derived for producing microfluidic chips[56]. It was in the 1990's, when new techniques of molding of polymer materials had been developed, that microfluidics saw a faster expansion. In the 2000's, the reduction of fabrication times and costs led to a larger spread of microfluidics in laboratories, which could start creating their own custom-made miniaturized systems. In addition, standard protocols and methods for fabricating microfluidic chips started to be developed. Nowadays, microfluidics is commonly used in several domains: biology, chemistry, micro-electronic, energetic, pharmaceutical, and even clinical domains[57]. As a consequence, the microfluidics market is expanding particularly by the development of microfluidic-based companies and start-ups.

1.3 Microfluidics miniaturization and its consequences

As previously introduced, microfluidic devices are adapted and designed for fluidic manipulation. They are constituted with channels of a micro-scaled dimension in which fluids can circulate. This miniaturization changes drastically the physic laws applied in those systems in contrast to macroscopic

systems. This can be explained because at this scale, the dominant forces differ from the dominant ones applied in macroenvironments such as standard cell cultures or macroperfusion system.

1.3.1 The laminar flow

In most microfluidic chips, the flow inside the channels is characterized by a low Reynolds number[55]. This number is a dimensionless number that describes the ratio of inertial forces to viscous forces applied in a fluid. It is proportional to the fluid velocity, and inversely proportional to its dynamic viscosity, by the following equation:

$$R_e = \frac{\rho V L}{\mu}$$

where ρ is the density of the fluid (kg/m^3), V the velocity (m/s), L the channel diameter (m) and μ the dynamic viscosity (kg/m·s).
Three flow regimes exist and are defined accordingly to the Reynolds number: The laminar flow ($Re < 2000$), the semi-turbulent flow ($2000 < Re < 4000$) and the turbulent flow ($Re > 4000$). One considerable aspect of the turbulent domain is that flows undergo irregular and chaotic fluctuations in pressure and velocity (Figure 9 - a). At the macro-scale dimension, flows are mostly turbulent, as the Reynolds number is high. For instance, macroscopic perfusion systems have a Reynolds number relatively high, thus the flows involved are random, uncontrollable and non-reproducible. On the other hand, in most microfluidic systems, the small dimensions of the channels induce a laminar regime. This regime is particular because the fluid molecules move in straight lines without mixing (Figure 9 - a)[58]. As a consequence, the flow is highly predictable and easy and precise control of fluid dynamics can be achieved[59]. Takayama *et al*. demonstrated the possibility of targeting cell subcellular microdomains using laminar flow[60]. Keenan et al. described strategies involving laminar flow for building biomolecule gradients inside microfluidic chips[61]. Additionally, precise and controllable flows led to the development of microfluidic systems dedicated to hydrodynamic flow focusing[62], which result in cell alignments in continuous flow, analysis and sorting using flow cytometry[63].

On the other hand, the mixing of different fluids does not occur by convection, as they are flowing in paralleled lines. The molecular and chemical transport and mixing is mainly occurring by diffusion[59]. This diffusive property can be used as an advantageous strategy for nutritional delivery (see Chapter 3). In order to improve the mixing dynamics for biological purposes, specific setups are required, which actively or passively enhance mixing. The active mixing consists in using external energy to perturb the flow. Passive mixing results in slower but efficient mixing (by adjusting micro-channels geometries)[64,65]. For example, Williams et al. mixed reagents in laminar regime by using a herringbone mixer[65], which is a microfluidic chip containing serpentine channels designed to modify the flow trajectory and to increase the mixing while keeping a laminar flow (Figure 9 - b).

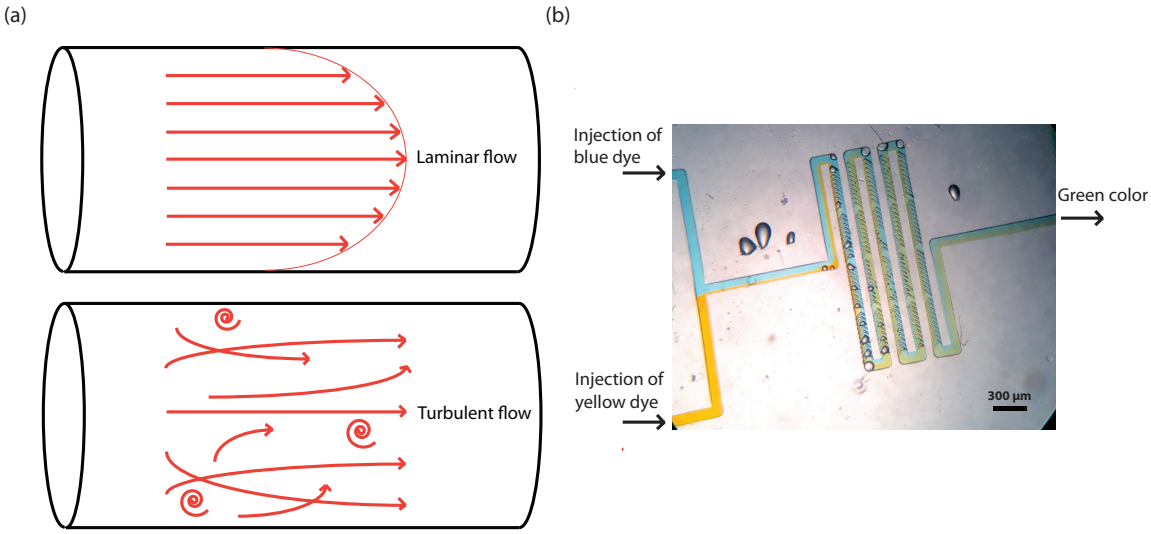

Figure 9: Laminar flow in microfluidics. (a) Schematic of laminar flows versus turbulent flows. (b) Pictures of a micromixer fabricated in our laboratory. Blue and yellow dyes are injected at the two inlets of the chip. (a) At the intersection of both channels, the dyes do not mixed, due to the laminar flows. The micromixer is composed of several structures that enhance passive mixing of the dyes. The observation of the green color at the outlet of the device indicates that both dyes have been mixed.

1.3.2 Capillary forces are dominating

At the micro-scale dimension, capillary forces can be preponderant over gravity. They refer to the movements of fluids through narrow spaces without the assistance of any other forces. The capillary forces are a combination of adhesion and cohesion.

- Adhesion

The adhesion describes the molecular forces of attraction between molecules or between the surfaces of bodies in contact. They can be mechanical (adhesive materials can fill the pores or voids of substrates and interlock their surfaces), chemical (ionic, covalent or hydrogen bonds), dispersive (Van der Waals forces), electrostatic, or diffusive (see "Chapter 2" section 2.2.3).

- Cohesion

A liquid is constituted with molecules linked together by cohesive forces. The neighboring molecules in the bulk of the fluid share these forces. However, the molecules at the surface are exposed to a lower amount of molecules. Therefore the cohesive forces are stronger between these molecules, creating a layer at the surface with high tension[66] (See Figure 12 - A). The surface tension of a fluid is thus defined by its resistance to external forces due to the cohesive forces, generally given in $mJ.m^{-2}$.
The surface tension of fluids (or surface energy) is always minimized. Thus, their surface areas are minimal. For instance, a drop of water has its surface energy minimized while having a spherical geometry.

In microfluidic devices, the adhesion forces of the substrate walls are often stronger than the cohesive forces that link the fluid molecules together. As a consequence, substrates will favor the adhesion of the fluid onto their surface. Interestingly, this property is used in microfluidic chips for loading cells inside the chambers without any air residue, which could be troublesome for cell proliferation, or for liquid medium perfusion in microfluidic chips with complex structures. The capillary forces drive fluids in

microchannels without the need of external forces such as gravity (Figure 10). Moreover, miniaturization improves the capillary effect, as the surface to volume ratio is largely increased.

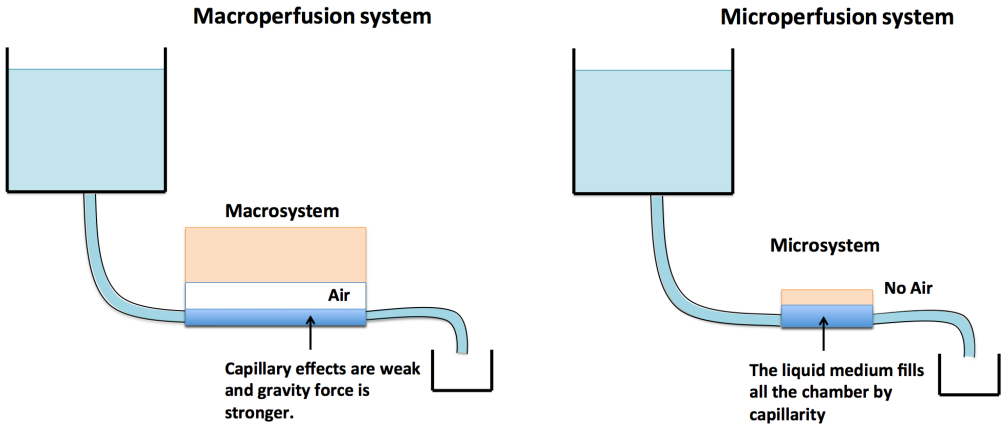

Figure 10: Schematics representing perfusion systems. On the left, a macroperfusion system is simplified, in which a channel in a macrosystem is perfused. The gravity exercising in the channel prevents the fluid to fill the entire channel. On the right, the scale of the system is smaller, and the fluid fills the channel by capillarity, avoiding any air residues.

Taking advantage of the capillary forces, various microfluidic systems have been created for scientific applications and also for common usage. One famous example is the portable glucometer allowing the blood transport by capillarity from a finger strip to an electro-chemical analyzer for measuring blood glucose[67] (See Figure 11). The volume of blood sample needed by different models is low and varies from 0,3 to 1 µL. One other application is the pregnancy test using urine propagation in test sticks.

Figure 11: Picture of the blood from the fingertip conducted a glucometer. The glucometer device is a qualified as a microfluidic device: Blood is transported to the device by capillarity through a plastic test strip. The glucose concentration in the blood is indicated on the device screen.

The affinity of the fluid with its substrate can be characterized by the wettability.

- Wettability

When the surface energy is higher than that of water, the result is a hydrophilic surface. The substrate surface will be qualified as “wet”. On the other hand, a surface with low energy is hydrophobic: the cohesive

forces are dominating over the adhesive ones and the surface between the liquid and the substrate is minimized. The wettability of a substrate can be determined by measuring the contact angle (Figure 12– B).

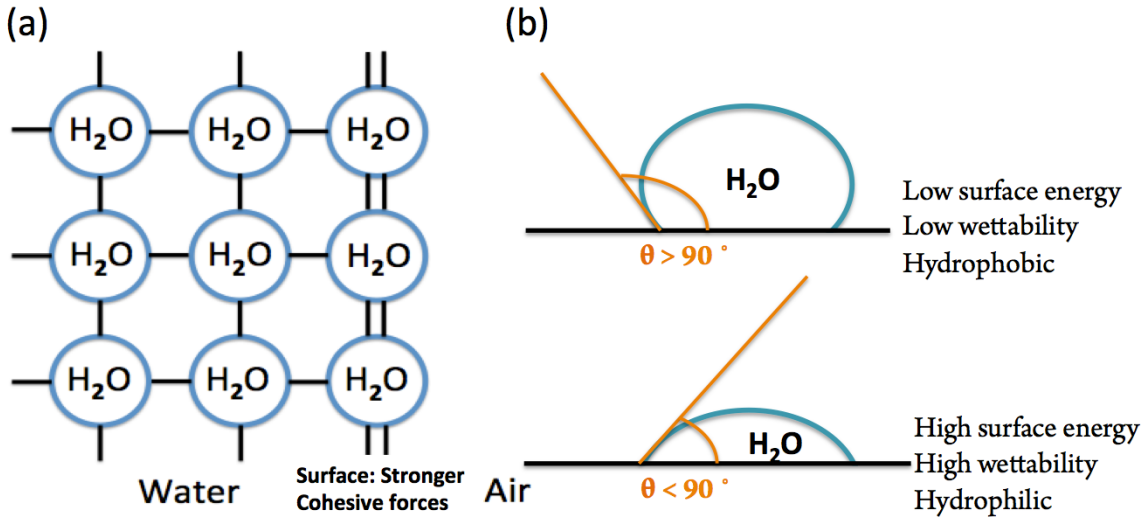

Figure 12: (a) Schematics of the cohesive forces in a fluid, stronger between molecules at the surface of the fluid. (b) Schematic of the contact angle depending on the wettability of the substrate. The top substrate is hydrophobic and the contact angle is high. The bottom one is hydrophilic, resulting in a low contact angle.

1.3.3 Miniaturization advantages in biology

One particular advantage of miniaturization is the reduction of the volumes of fluids injected. Biologists exploit this advantage in their experiments, as the consumption of samples, reagents and production of waste are reduced, resulting in a decrease of the global costs of their assays[68], the preservation of precious samples or samples of limited availability from primary patients[69,70].

Furthermore, as previously described, the physic laws of the micro-scaled dimension allow a predominant laminar flow in most microfluidic devices, making it highly predictable and controllable. Such control of the flow, especially the medium flow, constitutes a great advantage in cell biology. It enables the study of a population of cells or the study of single cell behaviors, as the flow can be addressed locally to control the microenvironment at the scale of a cell. This localized and precise environmental conditions are unreachable when conventional macroscopic tools are used. One common advantage of the laminar flow is the possibility of making chemical gradients. As opposed to gradients created using conventional methods (using for instance a macroscopic gradient generator), the microsystems enable precise, stable and reproducible gradients at a subcellular resolution, which are controlled spatially and temporally. These microscale gradients have been successful for investigating chemotaxis[71,72] or cell migration[73], cell morphology, cell growth and differentiation[74] among other studies.

Thus, microfluidic systems are advantageous for controlling with precision the medium flow while performing live-cell imaging experiments. Moreover, multi-parameters can be controlled precisely within a unique microfluidic chip, such as the temperature, pH level of the medium, oxygen concentration. At the small scale of the channels, the temperature and mass transfer diffusions are fast, hence allowing rapid environmental changes. Even if macroperfusion systems are capable of controlling the microenvironmental parameters, their accuracy, precision and dynamics are not reliable, robust and reproducible, as the flow in such systems is turbulent, hence difficult to control. In microfluidic chips, the flow is laminar, and the control of multi-parameters can be accurate, precise, dynamic and simultaneous.

Additionally, miniaturization allows to perform simultaneous independent operations within the same chip during live-cell imaging[75]. For instance, the monitoring of cells can be done while controlling flows, temperatures, or pH, measuring electrical signals, using electromagnetic fields, applying or measuring forces on cells[76], among other operations. Scientists take advantage of this miniaturization, conducting multiplexed and parallel high throughput assay: indeed, microfluidic channels allow performing multiple independent experiments at the same time, and has made possible the visualization of different cell types simultaneously[77], or the same cells under different conditions.

To conclude, microfluidics relies on miniaturization, and the forces that are dominating at this scale allow for a highly precise spatio-temporal control of the flow. This control is advantageous for achieving robust experiments under high-resolution microscopy.

2 Microfluidics: materials and fabrication

Since microfluidics emerged, myriad microfluidic devices have been conceived, and the expansion of microfluidics in all scientific domains makes the systems highly specific to an application. Microfluidics chips differ by their designs, structures and materials. The choice of material includes many criteria such as its optical and mechanical properties, its biocompatibility, or even its availability. This diversity of materials allows different microfabrication processes, functionalities and applications.

2.1 The photolithography

A general method for fabricating microfluidics chip is photolithography. In microfluidics, the photolithography process consists in fabricating a substrate mold, which contains the negative structures of the future microchannels[78]. On this mold will be cast a moldable polymer, which will harden and contain the microchannels.

The substrates molds are commonly photosensitive resin polymers, or photoresists, deposited on a substrate, generally a silicon wafer. The most commonly used resin is called SU8. Depending on the channel thickness desired, different formulations of the resin can be used. These resins are sensitive to UV-light: the resins called “positive” become soluble to a photoresist developer after their exposition to UV-light, whereas the “negative” resins become insoluble to the developer after being exposed, and only the unexposed parts are dissolved in the developer. Engineers took advantage of photoresists for creating microstructures. The strategy is to use a mask, either transparent and containing black patterns, or channels, either with a dark background containing transparent patterns, depending on the photoresist type. The mask is designed by CAD software, which allows the design of virtual patterns later reproduced onto the photoresist. Depending on the resolution of the channels, the mask can be realized from the design with different technics: laser printed overhead (250 microns resolution), high-resolution print on polymer (30 microns resolution) or chrome mask (chromium deposited on quartz with 600 nm resolution)[79]. The mask is applied against the resin under direct exposition to UV light and the channel structures appear after the treatment with the developer (Figure 13). The thickness of the channels depends on specific parameters: the photoresist type, the light exposition wavelength, the exposure time and intensity and the resin curing time and temperature after the light exposition step[80].

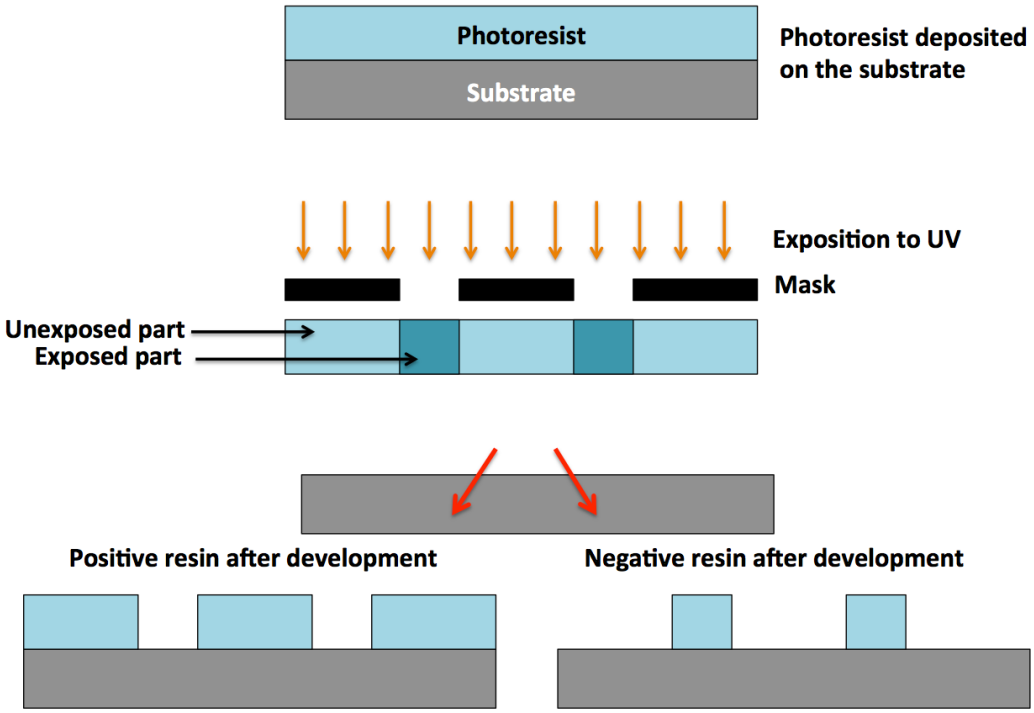

Figure 13: Schematics of the photolithography process. First, the photoresist (generally SU-8) is deposited on the substrate. Then a mask is applied against the photoresist and the photoresist is exposed to UV. Depending on the photoresist type, the exposed parts, or unexposed parts will be dissolved in the developer and removed. Straight channels can be realized by irradiating the photoresist perpendicularly.

After the mold is generated, a moldable polymer is poured onto the resin and contains the negative structures of the mold after curing: the microchannels (Figure 14).

The classical polymer that has been used for decades is the PDMS (polydimethylsiloxane). When poured onto the resin, this material hardens when heated at 70˚C for generally 2 hours. Then, PDMS is peeled-off from the resin. In order to facilitate PDMS detachment from the resin, and avoid undesired cracks (on the polymer or on the resin), the use of ultra-thin silane coating (generally a few nanometers) has proven to be efficient. Using needles or disposable biopsy punches, holes can be drilled through the PDMS material to allow fluidic circulation in and out of the chip. Finally, the PDMS can bond to a glass coverslip, which is the standard material for microscopy, after having its surface modified with a plasma treatment.

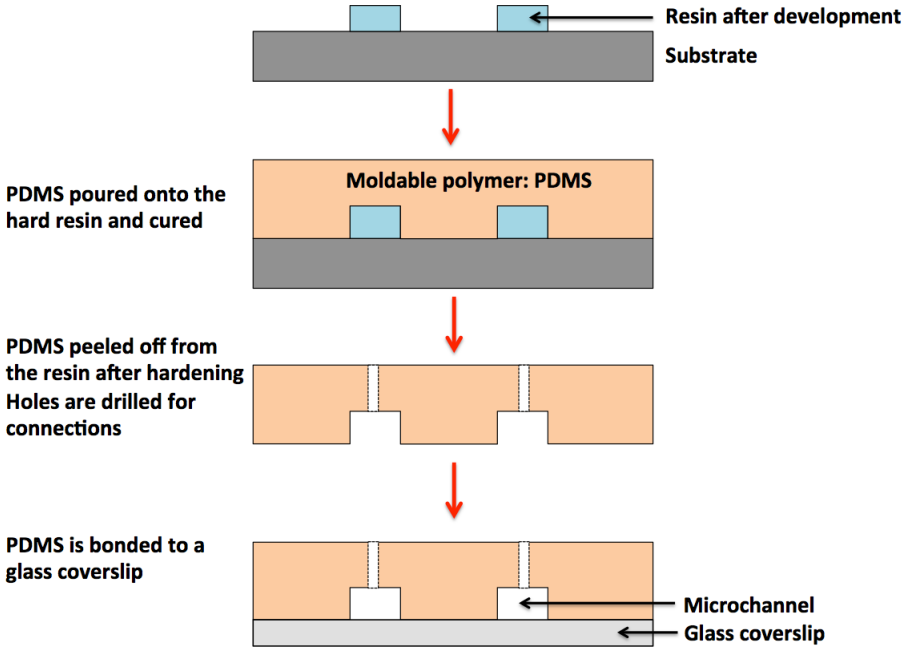

Figure 14: Schematics of the PDMS chip fabrication. The PDMS is poured onto the resin and cured. After hardening, the PDMS is removed from the resin and the substrate, containing microchannels. Holes are made in the PDMS for allowing further inputs and outputs of the microfluidic chip. Finally, the PDMS bonds to a glass coverslip after a plasma treatment.

To conclude, the photolithography process started the microfluidic revolution, associated with its standard material: PDMS. Myriad protocols have been developed depending on the microfluidic chip of interest. Nowadays, full kits are provided for realizing custom-made microfluidic chips. These kits allow the production of any PDMS chip, however, despite their simple protocols, the process of photolithography remains not trivial and time-consuming.

2.2 The standard microfluidic material: PDMS

2.2.1 Brief description of PDMS

For decades, the PDMS has been the standard and most widely used material for fabricating microfluidic devices. This material is a polymeric organo-silicon whose formula is $CH_3[Si(CH_3)_2O]_nSi(CH_3)_3$ (Figure 15), composed of inorganic siloxane groups SI-O linked to methyl groups CH_3.

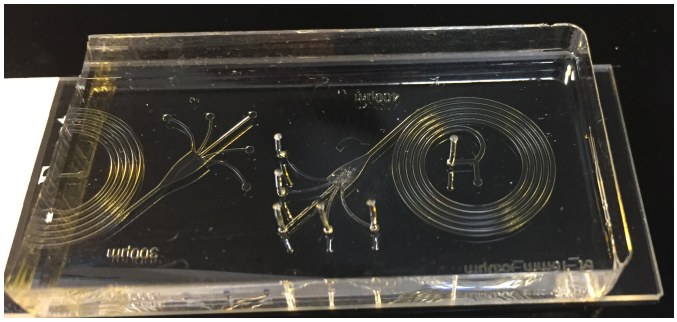

Figure 15: The PDMS material. Picture of a PDMS block produced in the laboratory containing channels. The PDMS is stuck to a glass coverslip after a plasma treatment.

PDMS is an elastomer whose glass transition temperature is below ambient, making it soft and flexible. Different formulations of this elastomer are commercially available and the most commonly used in laboratories is Sylgard 184 (Dow Corning, United States). The PDMS is the result of a mixture between two reagents: a cross-linker and a curing agent. The mechanical properties of the PDMS will be dependent on the ratio of the two agents: for instance, an increase of the cross-linker will increase the rigidity of the elastomer after curing[81]. Besides, as a heat-activated elastomer, PDMS mechanical properties depend on its curing time and temperature[82].

The PDMS has the attracting ability to replicate structures after casting on a substrate mold with high precision (Figure 14). Indeed, it possesses the advantageous property of releasing from the substrate molds after being cured. This property of PDMS has enlarged the number of potential applications of microfluidic considering the range of the channel size achievable, making PDMS the standard microfluidic material.

2.2.2 PDMS advantages and drawbacks

In fact, PDMS has been proven to be biocompatible[83] and has offered a tremendous potential for biological applications. It is a transparent material whose auto-fluorescence is low from the ultraviolet to the infrared wavelengths, thus suitable for any microscopic observation using transmission light or for biological strains with fluorescent markers.

Moreover, its ability to form micro and nanochannels using soft-lithography makes it a material of choice, as this scale is usually of the same order of magnitude as a cell size, allowing the observation of single cells in PDMS structures[84,85], or populations of cells. The PDMS offers the advantage of being highly deformable, and engineers took profit of this properties for building pneumatic valves within microsystems[86]. However, as a deformable polymer, PDMS is unsuited for applications involving high pressures, resulting in alterations of channel geometries and uncontrollable flows[87].

PDMS is permeable to gas and permits oxygen and carbon dioxide to diffuse through its matrix, which renewal is crucial for cell-based experiments[88]. On the other hand, its permeability to gas can lead to evaporation, affecting several types of cells and any experiments involving precise medium composition[89].

The PDMS can covalently bond to oxidized surfaces, and is then suitable for bonding treated glass coverslips, standard support for microscopy in biology[90], or to PDMS itself[91]. Therefore the need of additional layers for bonding PDMS to glass or other substrates can be avoided.

Moreover, its extreme hydrophobicity is an important issue when the filling of the micro-channels is not complete and air is trapped in the system[92].

The PDMS material is prone to release uncrosslinked oligomers, which were shown to have impacts on the proliferation of living cells[93 94].

2.2.3 The main drawback of PDMS: the absorption

2.2.3.1 Introduction

Despite all its advantages, PDMS has a critical drawback, which is absorption, that makes it incompatible with many standard biological assays[57]. As a hydrophobic rubber elastomer, PDMS possesses the particularity of absorbing small molecules, which are often hydrophobic or composed of hydrophobic regions[95]. The absorption is a major inconvenient in microfluidic devices because at this scale the ratio of potentially absorbing surface to volume is increased, thus the absorption effect significantly increases and results in uncontrolled concentrations, preventing any experiments involving low or precise drug concentrations[96].
Even though this absorption feature can be used for chemical applications[97], it is generally a problem for biological experiments[96,98].

The absorption is a well-known and described phenomenon, and despite this non-desired property, scientists have kept using this material for its advantages. Recently, the control of highly precise drug concentrations is required for myriad applications, and this absorption issue has become a major challenge to overcome.

2.2.3.2 Reducing the absorption of PDMS: still an actual challenge

Circumventing the absorption of PDMS has recently become a major focus, and two main options have been considered: 1) chemical or physical modifications of its surface and 2) its replacement by other candidate materials which do not absorb.

One approach is to oxidize its surface using UV light, oxygen plasma or corona discharges[99,100]. This treatment is used to modify the chemical properties of the surface of the elastomer to make it hydrophilic[101]. As most biomolecules are hydrophobic, they would potentially stop penetrating inside the bulk of PDMS. Another approach is the coating of PDMS surface. Wang *et al*. proved that the addition of silica and glass on its surface has a significant effect on reducing the absorption of PDMS[101]. Roman *et al.* chemically modified PDMS surfaces using Sol/Gel treatment in tetraethyl orthosilicate (TEOS)[102]. This method consists in incorporating silica nanoparticules into the PDMS matrix, and considerably reduced the diffusion of small molecules inside the PDMS, while keeping its advantageous properties such as biocompatibility, oxygen permeability and transparency[103]. Other coatings have been proven to reduce PDMS hydrophobicity by using APTES and TEOS[104], sulfuric acid[93] or parylene[105].

To some extend, these modifications of the PDMS surfaces have shown improved hydrophobicity, however none of these coatings have totally prevented the absorption of the material, especially because the PDMS tends to recover his hydrophobicity within a few hours[99,106]. This effect is due to the PDMS uncross-linked chains in the bulk, which diffuse to the surfaces and change its hydrophobicity[107]. Jokinen et al. also proved that this hydrophobic recovery was similar in other materials such as PMMA, PC and SU-8[108].

One must bear in mind that miniaturized devices significantly increase the absorption effect. In our laboratory, we have tested the NOA material, which has been already characterized as a non-absorptive material. Our work on this material has demonstrated a slight absorption when microchannels are made in this material[109] (See Results, Chapter 1). The impossibility of completely circumventing PDMS absorption has thus led to considering new materials for constituting microfluidic chips.

2.3 The emergence of thermoplastic materials in microfluidics

2.3.1 From PDMS to thermoplastic materials

In a microfluidic device, considering the high surface to volume ratio, the surface properties of the materials have a major impact on cells and their microenvironment, and choosing the appropriate material for biological applications is critical and challenging. The PDMS drawbacks drove scientists to seek for other types of materials. Thermoplastics have been proven to be compatible with microfluidics as we can pattern them (see below) thus fabricate microchannels. They were an easy competitive alternative to elastomers like PDMS[110] due to their low costs.

The typical thermoplastics used in microfluidics are polystyrene[111,112], polycarbonate[113], polyethylene[114], PVC[115], cyclin olefin co-polymer[116-118] and PMMA[119-121]. The high-grade optical properties of these materials make them suitable for microscopy applications[113]. They are usually purchased as rigid materials after a thermo-molding treatment[122]. These polymers differ from elastomers with their hardness at ambient temperature and their higher Young modulus. This hardness comes from their glass transition temperature that is higher than ambient temperature.

These materials are compatible with biological experiment and their low absorption allows them to be used with low and precise concentrations of drugs. However, fabricating a microfluidic chip using thermoplastics is not trivial, as it is challenging to 1) create channels, or microchannels, on their surface and 2) bond these materials to other hard materials for sealing the microfluidic chip, especially to glass coverslips for biological purposes using microscopy.

2.3.2 Generating a micro-channel in a thermoplastic material

The fabrication of thin channels in plastic materials has been a first challenge. As opposed to PDMS, thermoplastics are usually not compatible with photolithography techniques but require the same initial approach. The high glass transition temperature has been exploited for fabricating micro-channels in these materials: after elevating the temperature near their glass transition temperature, they become softer and the possibility of making channels or patterns within the plastic materials has been demonstrated[123]. To this end, researchers have developed molding protocols using hydraulic presses, which constitute the typical strategy for fabricating plastic-based microfluidic chips by hot embossing[124]. The technique consists of transferring the structures of a mold, generally a PDMS mold, to the thermoplastic by pressing the two materials against each other using specific pressure and temperature parameters[125,126] (Figure 16). This process has been largely exploited for creating channels inside thermoplastics but is also a cause of channels deformation[127].

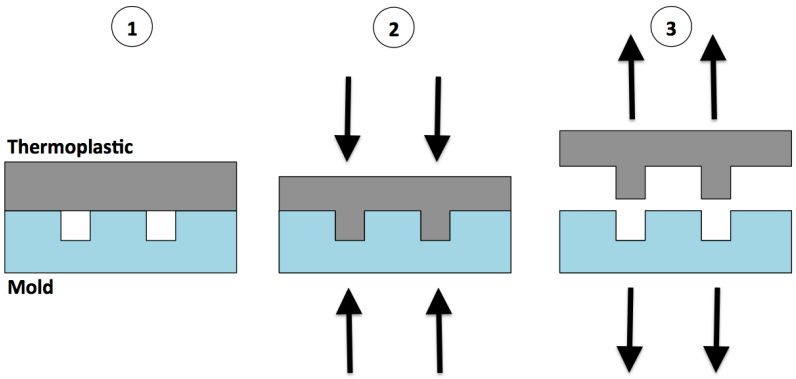

Figure 16: Schematic of a hot embossing process. 1) The mold and thermoplastic are placed against each other. 2) They are heated and pressed against each other. The pressurization allows the replication of the channels in the plastic material. 3) Both materials are cooled down and separated. The replication depends on three main parameters: pressure, temperature and time.

Another technique for fabricating polymer-based chips is injection molding[128]. During this process, the plastic is heated to its liquid state and injected on the surface of a mold with inverted patterns[129]. The microchannels are created once the polymer hardens and is peeled-off from the mold. For instance, Alexander *et al.* used liquid-based PMMA poured in a silicon master mold containing micro-channels then cured it using UV treatment[130]. Yao *et al.* used hydrogel as a master mold[131].

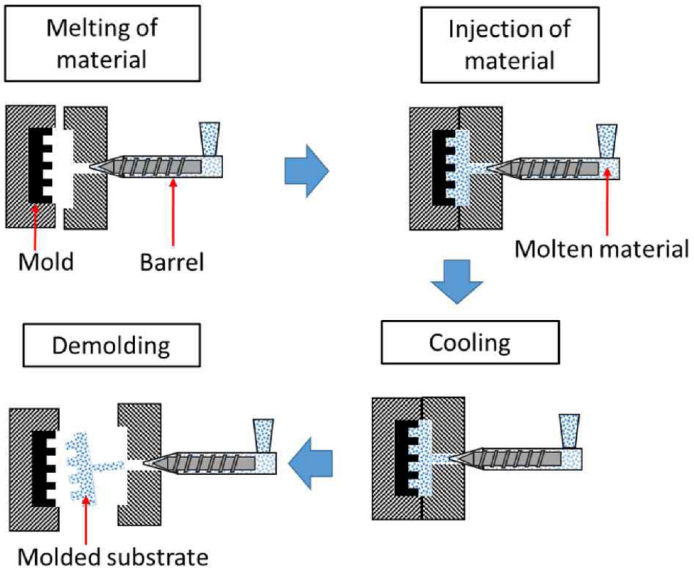

Figure 17: Schematics of the injecting molding process: 1) The material constituting the microfluidic manifold is melted. 2) The liquid plastic is injected on the surface of a mold containing the inverted structures. 3) The liquid plastic hardens after cooling or being exposed to UV. 4) The thermoplastic containing the channels is peeled-off from the mold substrate.

Moreover, recent techniques have been used for directly fabricating channels inside hard polymer materials using milling machines. The use of this machining process has made prototyping easy and fast, as it is controlled by computers[132]. This so-called "micromilling" consists in engraving microchannels and cutting the substrate materials using milling cutters of the appropriate size.

Finally, the laser ablation technique has been exploited for producing channels in thermoplastics, and was first utilized by Costela *et al.* in 1995[133]. In fact, the energy of a condensed CO_2 laser is needed for

cutting plastic materials[134-136]. The laser allows highly precise and robust cutting of micro-structures [137], as well as precise engraving of micro-channels. The prototyping of microfluidic chips can then be automated and is highly reproducible. The drawback of this method is the formation of bulges at the borders of the cut structures[138]. These bulges are located in a heat affected zone (HAZ)[139] accompanied with micro-fissures which can be seen after the laser ablation, leading to a lower solvent resistance. This inconvenient can be circumvented by pre-heating the cut material to re-polymerize the cut surfaces[140], or post-heating (Figure 18).

Figure 18: Pictures of PMMA blocks cut using a CO_2 laser-cutter (Speedy 100, Trotec, Austria). The PMMA on the left side was untreated and the PMMA on the right side was heated at 90˚C for two hours after being cut. Both PMMA blocks were placed in acetone for two hours. The pre-heated PMMA block showed improved chemical resistance. The few visible marks on the pre-heated PMMA are due to the honeycomb of the laser-cutting machine.

Techniques for making channels in thermoplastics are well known and used in laboratories and the equipment for realizing them (hot presses, laser cutting machines, CNC machines) is available.

2.3.3 Plastic materials: easy and fast production, but challenging bonding

In general, microfluidic chips require closed channels and opened inputs and outputs for allowing fluid circulation. For this reason, the materials constituting the microfluidic chip need to be sealed together[141] or to other materials. The low surface energy of plastic materials makes it challenging to bond these materials with each other, and also to other materials, especially glass coverslips commonly used for biological applications using microscopy. Bonding methods for microfluidic devices are categorized in two classes: direct bonding and indirect bonding.

2.3.3.1 Direct bonding of plastic materials

Most plastic materials have their glass transition temperature comprised between 100 and 350 ˚C, and the typical bonding strategy used is thermo-bonding. This technique consists of bonding two surfaces using a proper combination of pressure and temperature[142]. Plastic surfaces can soften and depolymerize with heat, and by applying pressure on two substrates against each other, molecules of both surfaces penetrate inside the bulk of the other (adhesion by diffusion). When the temperature decreases, both materials re-polymerize and the two parts are sealed together. Higher pressures and temperatures lead to stronger bonding, however they increase the probability of deformation of the channel structures[143] (Figure 19).

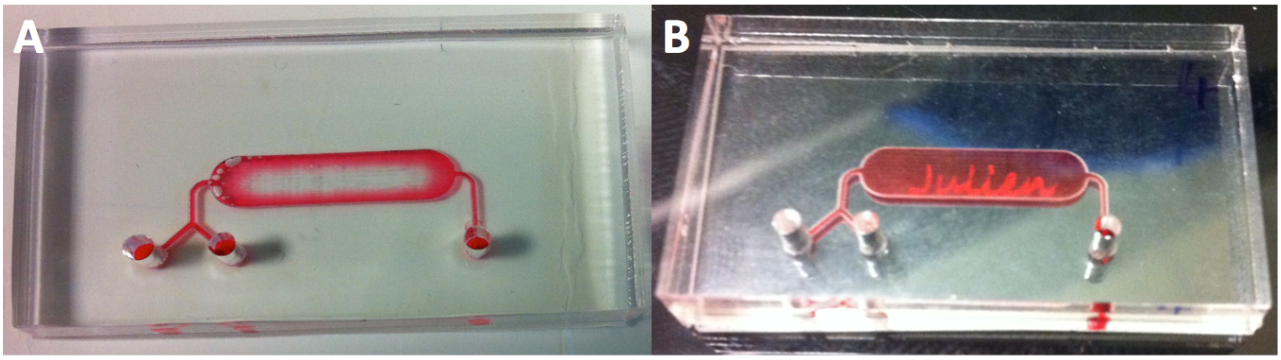

Figure 19: Pictures of full PMMA microfluidic chips. Both chips contain a 2 mm-thick layer and a 6 mm-thick layer, bonded together using a thermo-press. The 6 mm thick PMMA contains holes for allowing fluidic circulation, and the 2 mm thick PMMA was engraved (channel). A red dye was injected in the engraved channel. A – The thermo-bonding was made at 131 °C using a pressure of 1500 kg. Pressure and temperature were too high: both layers are bonded together but the channel is deformed. B – Thermo-bonding made at 126 °C with a pressure of 800 kg. No deformation was noticed. A laser-cut engraving was made after the bonding on the other side of the 2mm-thick PMMA.

Chemical bonding is the second approach. Modifying or adding a supplementary thin layer onto the surface of the hard material has been used for enhancing the bonding properties of the material. In fact, it increases the surface energy, enhancing stronger intermolecular bonds. This allows better interdiffusion of chains, as well as mechanical interlocking. For instance, the use of APTES for functionalizing PMMA surface has been demonstrated by Vlachopoulou *et al.* to facilitate its bonding to PDMS[144]. Keller *et al.* recently enhanced COC bonding by using a mix of cyclohexane and acetone[145], Tang et al. used a silane treatment of APTES combined with GPTMS for bonding PDMS to PMMA and PDMS to PC[146].

These bonding methods are often not reproducible and sometimes inefficient, as the bonded materials can be removed easily.

2.3.3.2 Indirect bonding of plastic materials

Finally, one common strategy for bonding two hard substrates is the use of indirect methods by intercalating a layer of glue, adhesive or laminated film. This choice is of high interest for fabrication simplicity, but can be detrimental if the excess of glue clogs the channel, or in the other case if dead volumes are created when the substrates wall or not flush with the adhesive layer[143]. The dead volumes would lead to air trapping inside the chip, which could prevent cell culturing and proliferation.

The use of an intercalating layer can be adequate in order to make channels with various thicknesses, from 20 to more than 200 microns thick. Pressure sensitive adhesives (PSA) have been reported for their easy and fast prototyping of microfluidic devices. One standard PSA substrate is the double-sided adhesive, which can be cut precisely and rapidly using a laser-cutting machine[147]. Double-sided adhesives are generally constituted with a substrate in a hard material, which grants rigid properties and is thin, allowing the whole layer to be flexible and to be manipulated easily. This material is surrounded by thin adhesive layers. For instance, Khashayar *et al.* used double-sided tapes in polyester surrounded by acrylate adhesive for producing their electrochemical biosensors[148]. Serra *et al.* demonstrated the possibility of using PCR sealing tapes made in polyolefin and silicone adhesive for bonding a wide range of thermoplastics used for microfluidic applications[149].

Other adhesive sheets called “transfer tapes” can also be used in microfluidics[150], with the particularity of not having a hard substrate layer. These adhesives are constituted with glue between two liners. After removing the first liner, the adhesive is stuck to the substrate. The second liner is then removed while the glue stays on the substrate. These particular adhesives are suitable for performing rapid prototyping of thin channels (usually around 50 microns thick). However, the glue that constitutes most of these adhesive sheets is usually made in acrylic, which can potentially absorb small biomolecules, and the bonding surface is not always homogeneous.

Alternatively, harder materials have been used for bonding two hard materials and showed a limited absorption. First, the use of UV-curing adhesive has been in rapid expansion in research laboratories: the liquid glue hardens due to the polymerization of polymer chains occurring with UV exposure, thus creating a solid bond between materials[151]. Satyanarayana *et al.* developed the proof of concept of a stamping method for producing their microfluidic chip using UV glue[152,153]. UV curing adhesive such as NOA (Norland Optical Adhesives) have been frequently used for sealing microdevices[152], Bartolo *et al.* developed full NOA chips[154]. Another example of UV-sensitive epoxy is the Ostemer, which is a mixture of a curing agent and an accelerator, which hardens using UV-light[155]. Moreover, epoxy-based adhesives have been used for sealing microdevices[156]. The use of wax as a bonding layer has also been proven to be compatible with experiments using biological samples[157]. In our team, we have sealed COC with glass coverslips using wax. For that, the wax needs to be heated at 80 ˚C using low pressure for covering the surfaces of both materials in contact by capillarity[109] (See Results, Chapter 1).

Thus, indirect bonding consists in adding a supplementary layer in the microfluidic chip. The use of adhesive sheets allows good reproducibility from one chip to another, and fast prototyping can be achieved. However, as they are constituted with glues, small molecule absorption can occur is fluids are in direct contact. The use of epoxy, UV glues, or wax prevents the absorption, however the increased surface to volume ratios may slightly have an effect on the absorption. Using plastic material, simple chip fabrication is hard to achieve, and a reproducible thickness of the bonding layer is challenging.

2.4 Conclusion

This chapter shows that a myriad of materials and fabrication processes can be used for fabricating microfluidics chips. Simple protocols have been developed for fabricating all kind of microfluidic devices. However, the fabrication of such devices is time-consuming, and often requires expensive specific equipment. In the biological field, the standard material PDMS recently tends to be avoided, especially because of its absorption drawback. Thermoplastics overcome this absorption, and have led to fast and cheap prototyping of microfluidic chips. However, despite all the fabrication and bonding techniques that were developed, there are still challenges remaining for fabricating low-cost, easy-to-use and robust microfluidic chips that allow live-cell imaging and a precise and dynamic control of the environmental parameters.

Chapter 3. Microfluidics and live-cell imaging

1 Microfluidics: a new trend in biology

At first, microfluidics was a field focusing on chemistry and physics at the microscale dimension. The fundamental aspects of these dimensions had to be understood clearly prior to the integration of these technologies for complex biological experiments[158]. Moreover, microfluidics early development was essentially conducted in clean rooms with high-end photolithography equipment. Only a few laboratories could have access to such clean rooms. The complexity of the microfluidic fabrication methods and availability of the specific equipment was preventing the usage of microfluidics in laboratories. During the past two decades, the development of simpler processes and approaches, such a soft-lithography, or the use of cheap plastic materials has made microfluidics expand in laboratories. Clean rooms were not fundamental anymore for prototyping simple microfluidic chips, and makerspaces, or grey rooms, were used for allowing low-cost device developments[159]. These makerspaces allowed the introduction of photolithography equipment, laser-cutting machines, 3D printers[160], xurography equipment[161] and hot presses.

Nowadays, microfluidic potential has been known and used in laboratories. Microsystems have allowed cell culture experiments, single cell analysis or studies of entire populations of cells. They have been designed and optimized for the study of various model organisms, such as bacteria and yeast, full *C.elegans* worms, *drosophila* or mice embryos[162].

Moreover, microfluidics has brought live-cell imaging to a whole new level. The advantages of microfluidics allow the control of all the microenvironment parameters in a much precise, accurate and dynamic way[163]. These parameters include the temperature, renewal of medium, injection of drugs with precise concentrations, or pH, O_2 and CO_2 level.

2 Controlling the microenvironment while doing live-cell imaging

2.1 The temperature control

One essential parameter to control for performing live-cell imaging is temperature. It is an omnipresent physical parameter influencing chemical and biochemical reactions[164]. Its variations across space and time can lead to dramatic effects on cell physiology and behavior[165]. The need of understanding cell mechanisms and processes involving precise temperatures or temperature switches has led to new approaches for controlling the temperature with precision while doing high-resolution microscopy.

Simple solutions or accessories have allowed temperature control at the microscope. One of the simplest and most frequent tools is the incubation chamber, consisting of a Plexiglas box surrounding the microscope and allowing the control of the environment inside the box (Temperature, pH, CO2 and humidity). However, the temperature is not homogeneous inside the box. Additionally, the box windows, allowing the passage of microfluidic connections or the hands of the user for manipulating the sample, increase this temperature gradient and may lead to inaccurate temperatures. Finally, those windows are small, hence the accessibility to the microfluidic chip inside the chamber is limited, and its manipulation is difficult. Other systems have been implemented for live-cell imaging, such as objective heaters, or heated

microscope plates[166-168]. Nevertheless, these accessories may not be fully accurate and are incompatible with fast temperature dynamics.

Other solutions have also been conceived directly within microfluidic chips, allowing rapid temperature switches. For instance, advanced techniques consist of integrating micro-heaters directly inside a microfluidic chamber[169]. In fact, the Joule effect of heating resistors can be used for controlling temperature inside microfluidic systems[170,171], notably the indium-tin-oxide resistors[172,173]. These systems allow precise temperature control and fast switching dynamics, but as they are composed of electrodes, they are difficult to fabricate and manipulate, and as they are deposited on glass coverslips they are fragile and not always reusable.

Alternatively, fluids have been used to control the temperature inside microfluidic chips. Mao *et al.* built a PDMS-based microfluidic system which uses pre-heated fluids on both sides of a PDMS microchannel for achieving a temperature gradient thought the PDMS walls[174]. Das *et al.* used the same principle for analyzing mammalian cells behaviors and migration by varying temperature gradients[175](Figure 20). One disadvantage of this chip is the temperature gradient inside the cell channel. Besides, as the heat is transferred from the thermalized channels to the cell channel, heat losses occur in the PDMS that separates the two chambers, and a reproducible width is essential for avoiding temperature variations from one chip to the next. Moreover, the PDMS absorbs, and washing the cell chamber after usage may be difficult and could prevent any reuse of the chip.

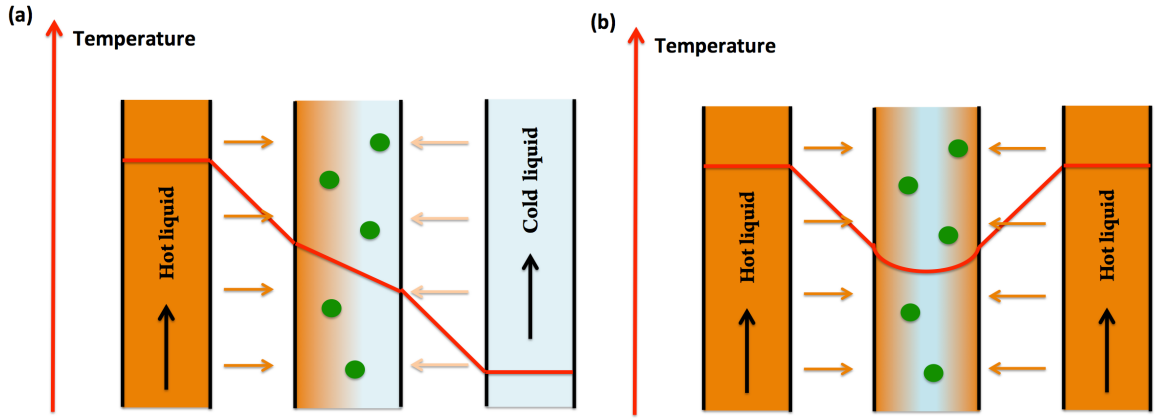

Figure 20: Schematics of the principle of heat transfer using pre-heated fluids circulating in side channels. High and low temperatures are represented in dark orange and clear orange, respectively. (a) Having two heated channels on both sides at different temperature allows for thermal gradients inside the cell channel. (b) Drawback of the system. Having a uniform temperature inside the cell channel is challenging, as a temperature gradient can still be seen within the cell channel.

Finally, the use of Peltier elements as heating or cooling systems has been in rapid expansion in biological laboratories during the past decades. For instance, Yang *et al*. have developed Peltier elements for achieving thermal cyclings[176], allowing ultrafast PCR reactions[177].

Peltier elements have also been implemented for generating temperature gradients in microfluidic chips[178,179]. To this end, VelveCasillas *et al*. developed a microfluidic system in which a pre-heated fluid is injected in one channel, and heats the medium underneath a glass coverslip substrate by thermal conduction (Figure 21). Two Peltier elements are connected to the microchip and using valves, it is possible to switch temperature within ten seconds[180].

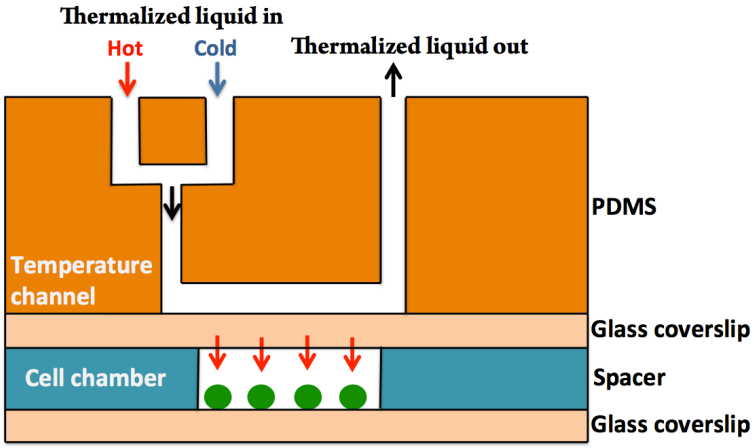

Figure 21: Schematic of the temperature controlled microfluidic chip using Peltier elements for controlling the temperature inside the cell channel.

The thermalized liquids are pre-heated and a calibration has to be performed for compensating the heat loss by the objective, tubings and materials constituting the microfluidic chip[109] (See Results, Chapter 1). The heat loss from the objective is made through the oil drop, which allows the contact between the objective and the sample. Consequently, if a microfluidic channel is larger than the oil area, there will be a temperature gradient inside the chip (Figure 22).

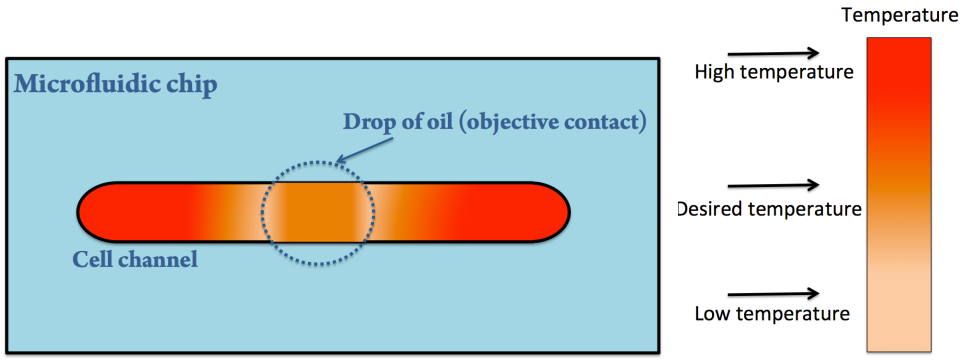

Figure 22: Schematic of a temperature gradient in a microfluidic chip using the temperature control with Peltier elements. In this example, the desired temperature in the cell channel is higher than the temperature of the microscope objective. The gradient is mainly due to the objective heat loss. The temperature is accurate in the area of the drop of oil. However, the other parts of the cell channel are not at the desired temperature and keeping focusing on the same area during live-cell imaging is essential.

All these temperature systems have their advantages and drawbacks, and allow the control of the temperature while doing live-cell imaging. During my thesis, I mostly used Peltier elements as a temperature control, represented on Figure 21, as it allows a simple, robust and fast temperature control, and I could adapt it to various microfluidic chips.

2.2 The flow control

2.2.1 Microfluidic systems for controlling the cell microenvironment

The perfusion allows constant delivery of fresh medium to cells, as well as the removal of biological wastes. Additionally, it allows the possibility of changing medium composition, as well as injecting drugs with precision[181]. As previously said, performing static cell culture without renewal of medium can lead to the alteration of medium composition and thus alter cell physiology and proliferation. Thus, static cell cultures are inadequate for long-term studies under microscope.

Macrofluidic perfusion system exists, but present several drawbacks compared to microperfusion systems. First, they require large volumes of medium to maintain cells healthy over time. The setups of such systems require space and may not be adequate for microscopy usage. Moreover, their lack of precision and reproducibility makes them unsuitable for biological assays involving precise and dynamic control of the microenvironment.

Microfluidics advantages allow such control of the cell microenvironment and have led to the development of microfluidic perfusion systems dedicated to live-cell imaging[182,183]. Robust perfusion systems are challenging to fabricate and operate, as they include specific requirements depending on the biological assay. Typically, decisions have to be taken regarding the perfusion control (see next paragraph), the choice of materials, microfluidic networks, fabrication processes, macro-scale components and connections. Most importantly, materials constituting the perfusion chambers have to be biocompatible and chemically compatible.

To conclude, microfluidic perfusion systems are more challenging to fabricate and operate compared to conventional static systems, but allow a more precise control over the cell microenvironment.

2.2.2 Flow control in microfluidic perfusion systems

Microfluidic systems are ideal for achieving precise and dynamic flow control within cell culture chambers. To this end, biologists have the possibility to use different systems of control, depending on their biological application, their microfluidic chip (and respective fluidic resistance, tubings, etc.) and the precision, accuracy and stability they require.

The first and simplest way to inject a flow inside a microfluidic chip is the use of gravity and hydrostatic pressure. Fundamentally, the hydrostatic pressure applied while varying the altitude of a reservoir is sufficient to move fluids from the outlet of the reservoir to the microfluidic[184] (Figure 23). The flow rate in such microsystems is not precise and not controllable: it is dependent on the height between the reservoir medium and the exit of the perfusion tubing (See Figure 23), and also on the fluidic resistance both tubings and microfluidic chip. As a consequence, during an experiment using gravity to control the medium flow, the flow rate fluctuates as the medium is consumed. To counter this effect and achieve a constant flow, this only complicated solution would be to place the reservoir on a plate, which could change its altitude with a variable velocity, calculated in function of the flow rate.

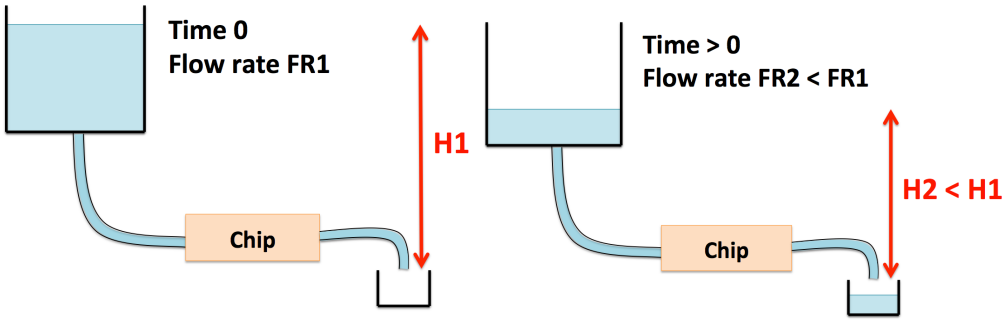

Figure 23: Schematics of a microfluidic perfusion system using gravity and hydrostatic pressure. At time 0 the height of the medium reservoir is at its highest position and the flow rate is maximal. When the experiment starts, the gravity is exercising and the height of medium in the reservoir decreases, as a consequence the flow rate decreases.

Another simple method is the use of capillary forces: hydrophilic channels in the chip generate a spontaneous filling of the microchannels with water or media. Moreover, media switch can be realized by using a porous material, which could absorb the medium by capillarity. The drawback of these methods is the lack of control of the dynamics and precision media switches and flow rates.

Regulation of perfusion flows using powerful external flow control systems have been implemented in laboratories[168,185] for circulating fresh medium to cells previously injected in the microfluidic channels. This renewal of medium can be either continuous or sequential[186], and allows a precise and dynamic control of the flow by controlling either the flow rate or the pressure in the system.

- Controlling the pressure

The concept of controlling the pressure in a microfluidic perfusion system is simple: Using reservoirs of fluids that are pressurized with an air pressure controller, fluids are circulating inside the microfluidic chip. Controlling the pressure allows fast switching dynamics. However, it induces variations from chip to chip, as the flow rate is proportional to the fluidic resistance (in microchannels or in tubings), which may vary from one chip to the next. This control of the microenvironment using pressure is thus insufficient for having a reproducible and precise flow rate, and thus for realizing robust experiments using biological samples.

- Controlling the flow rate

On the other hand, syringe pumps control the flow rate independently of the fluidic resistance of the microfluidic channels. They were first used for medical applications and then were adapted in microfluidic setups[168,187]. These systems have less versatility in term of reservoir volumes. The main drawbacks of these systems are the fluctuation while having low flow rates and the stability while changing flow rates.

To circumvent the issues that both methods present, the pressure controller can be coupled with flow sensors, and a feedback loops allows the regulation of the flow rate by adjusting the pressures in the system (Figure 24). Thus, for having a constant flow rate, the pressure controller will induce small adjustments of the pressure over time. Combined with valves, this setup allows fast medium switches, precise and accurate perfusion flow reproducible from chip to chip.

Additionally, systems such as peristaltic pumps, electro-osmosis pumps can be used for flow control, but their usage is rare in biological laboratories.

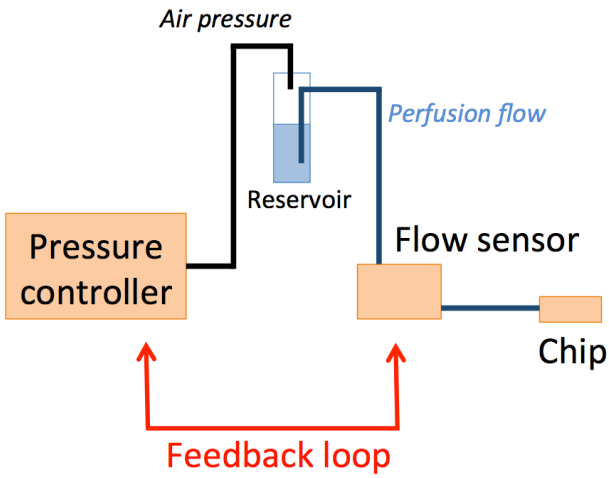

Figure 24: Flow control setup using feedback loops between a pressure controller and a flow sensor. The feedback loop regulates the pressure for maintaining a constant flow rate.

Multiple systems are available for controlling cell microenvironment. Depending on the application and the level of control required, simple systems using gravity exists, or more engineered systems using feedback loops between flow rate and pressure can be used, allowing precise, dynamic and accurate control of the perfusion in microfluidic devices during live-cell imaging.

2.3 Perfusion and cells

As opposed to static cell cultures, perfusion cultures are more challenging to implement: the microfluidic chips and setups need to be optimized, and several steps are required for allowing constant nutrient delivery in optimal conditions. The first challenges of perfusion systems that I will describe below are 1) the accumulation of bubbles in the microfluidic channel and 2) the hydrodynamic shear stress on cells.

2.3.1 Bubbles in microfluidics: still a challenging phenomenon to control

Bubbles inside a microfluidic devices can be a major issue for cell culture experiments[158]. When already inside the chip, they create flow fluctuations[188], optical perturbations, channel clogging[189]. In addition, one major problem is that growth of the bubbles may lead to cell death or cell flushing of the chip (Figure 25). Bubble formation and expansion is not fully understood. They can nucleate in small cavities, or appear when temperature varies. Lochovsky *et al.* postulated that the dissolution of gases, effective when the liquid perfused changes from room temperature to 37 ˚C, may be a cause for bubble formation[190]. Even a tiny bubble already inside a channel has the ability to increase in size and circulate inside the microfluidic network.

To solve this problem, bubble traps have been introduced for avoiding bubbles to reach the studied cells. They can be either dynamical, as Schonburg *et al.* showed by collecting air bubbles in a tube by centrifugal forces[191], either diffusive. The bubble traps, using diffusion as a way to filter bubbles out of the microfluidic chip, are connected upstream the microchip, and integrate a gas-permeable membrane. Van Lintel *et al*. used a PTFE membrane and managed to get rid of the air bubbles[192]. Sung and Shuler used a

microfluidic chip constituted with a double chamber separated with a PDMS membrane for capturing bubbles[193]. To efficiently remove the bubbles trapped in specific chambers, the need of vacuum through the membrane is sometimes needed[194].

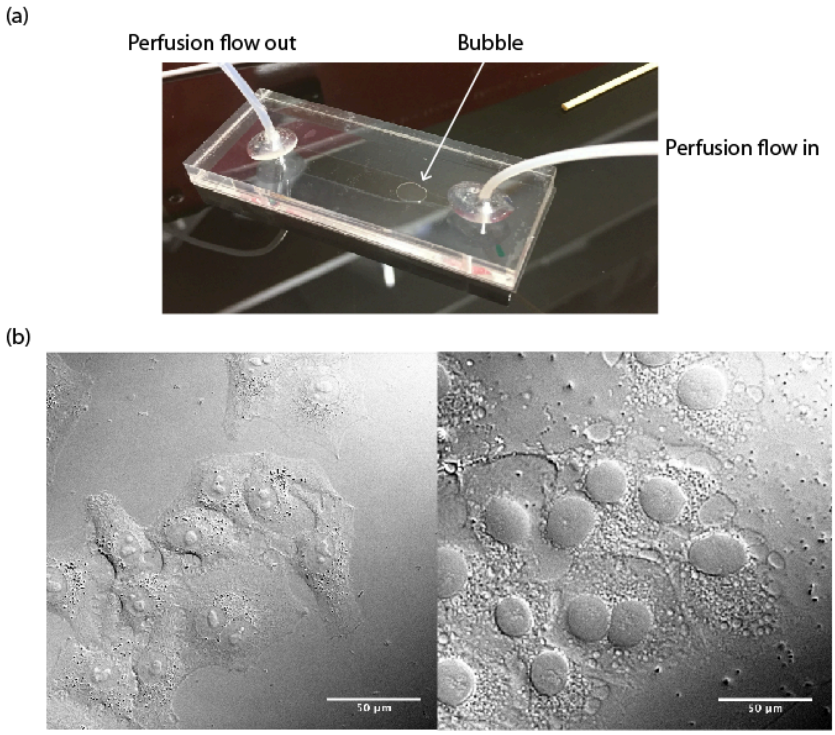

Figure 25: Bubbles in microfluidic chip (a) Picture of a microfluidic containing a bubble that has grown in size after several hours of perfusion. (b) Pictures of mammalian cells inside a microfluidic chip during live-cell imaging. On the left, picture before the passage of a bubble. On the right, cells after the bubble passage. Scale bar is 50 µm.

These trapping systems do not completely prevent bubbles inside microfluidic channels. I have used commercial bubble traps using vacuum through a membrane material, which was efficient to remove big bubbles, but tiny ones would eventually accumulates during long-term experiments. For evacuating these bubbles we implemented a vacuuming system within the microfluidic channel, which removes the bubbles intermittently and can be automated (See Results, Chapter 4).

2.3.2 Shear stress in perfusion systems

In perfusion systems, cells are constantly under medium flow and are subjected to hydrodynamic shear stress. This stress may cause detrimental effects on the perfused cells.

Shear stress in microfluidic chips can be estimated by the formula: $t = \frac{6\mu Q}{wh^2}$, where μ is the dynamic fluidic viscosity, Q is the flow rate, w and h are the width and height of the channel respectively. As a consequence, the mechanical shear stress is linearly proportional to the flow rate.

Shear stress while constant perfusion can modulate cell behavior[195] and morphology[57], as well as genetic expression, cell-cell and cell-matrix interactions and extracellular matrix protein secretion[196]. Typically, the transduction of the mechanical forces is an important factor for studying endothelial cells in

their microenvironment[197], as the mechanical shear stress mimics blood vessels pressure and flow[198]. Importantly, the mechanical forces resulting on cells can also be converted into biochemical signals that impact cell functions and processes[199,200].

Thus, depending on model organism studied, the processes involved or the applications, mechanical shear stresses are often undesired. A simple solution is to use low flow velocity to renew the microenvironment while ensuring cell viability[201] (See Results, Chapter 2). Given the microfluidic channel dimensions, the velocity of the perfusion flow may still flush cells out, for both adherent and non-adherent cells. To this end, regarding the cell type, different strategies can be used for performing live-cell imaging combined with perfusion.

2.4 Cell injection and observation in perfusion systems

2.4.1 The sterilization of the microfluidic device

Before any cell injection, the microfluidic device has to be sterilized for avoiding any contamination. The most effective method consists of autoclaving the microfluidic chip. This solution is simple for PDMS-based microsystems[202], however it is incompatible with a broad range of microfluidic components, particularly with plastics materials, which can deform when autoclaved. Other alternatives for sterilization are ethanol wash[203], UV exposition[204] or dense carbon dioxide gas[205].

After the sterilization process, perfusion assays are composed of two main steps: the injection of cells prior to the experiment followed by the perfusion experiment itself.

2.4.2 Adherent cells in perfusion systems

Adherent cells firmly attach to their substrate[206]. They need to be injected inside microfluidic chips while they are in suspension (Figure 26). They do not bond to substrates similarly, depending on several parameters, such as the substrate material and its hydrophobicity, the surface tension, the cell type and morphology. For that reason, they may need cell attachment proteins such as fibronectin[206,207], poly-L-lysin, laminin, collagen[206,208] or gelatin.

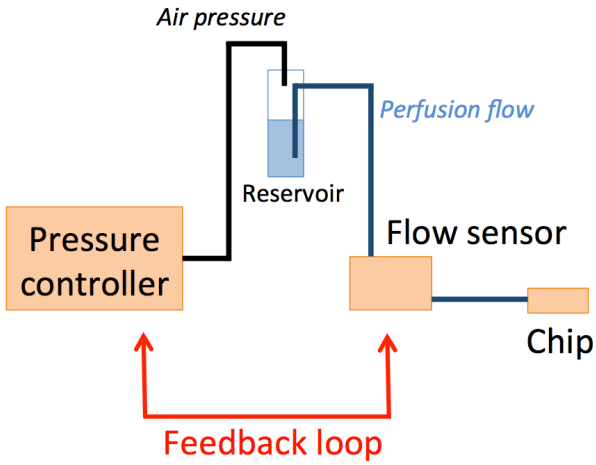

Figure 26: Pictures of *HeLa* cells inside a microfluidic chip (magnification x20). The substrate is a glass coverslip. A – Picture taken 30 minutes after the injection of the cells. The cells are not attached to the glass coverslip. B – Picture taken 24h after the injection of cells. All cells have adhered to the glass substrate.

their microenvironment[197], as the mechanical shear stress mimics blood vessels pressure and flow[198]. Importantly, the mechanical forces resulting on cells can also be converted into biochemical signals that impact cell functions and processes[199,200].

Thus, depending on model organism studied, the processes involved or the applications, mechanical shear stresses are often undesired. A simple solution is to use low flow velocity to renew the microenvironment while ensuring cell viability[201] (See Results, Chapter 2). Given the microfluidic channel dimensions, the velocity of the perfusion flow may still flush cells out, for both adherent and non-adherent cells. To this end, regarding the cell type, different strategies can be used for performing live-cell imaging combined with perfusion.

2.4 Cell injection and observation in perfusion systems

2.4.1 The sterilization of the microfluidic device

Before any cell injection, the microfluidic device has to be sterilized for avoiding any contamination. The most effective method consists of autoclaving the microfluidic chip. This solution is simple for PDMS-based microsystems[202], however it is incompatible with a broad range of microfluidic components, particularly with plastics materials, which can deform when autoclaved. Other alternatives for sterilization are ethanol wash[203], UV exposition[204] or dense carbon dioxide gas[205].

After the sterilization process, perfusion assays are composed of two main steps: the injection of cells prior to the experiment followed by the perfusion experiment itself.

2.4.2 Adherent cells in perfusion systems

Adherent cells firmly attach to their substrate[206]. They need to be injected inside microfluidic chips while they are in suspension (Figure 26). They do not bond to substrates similarly, depending on several parameters, such as the substrate material and its hydrophobicity, the surface tension, the cell type and morphology. For that reason, they may need cell attachment proteins such as fibronectin[206,207], poly-L-lysin, laminin, collagen[206,208] or gelatin.

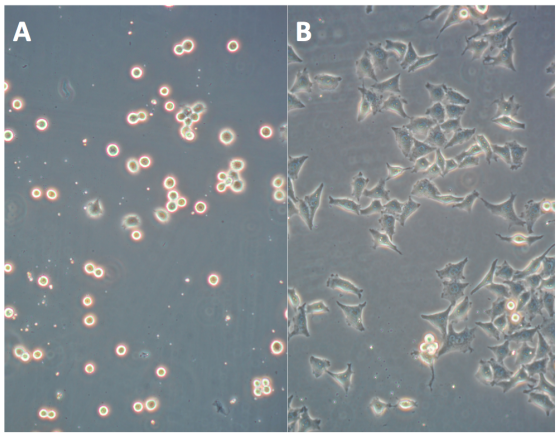

Figure 26: Pictures of *HeLa* cells inside a microfluidic chip (magnification x20). The substrate is a glass coverslip. A – Picture taken 30 minutes after the injection of the cells. The cells are not attached to the glass coverslip. B – Picture taken 24h after the injection of cells. All cells have adhered to the glass substrate.

2.4.3 Non-adherent cells in perfusion systems

For non-adherent cells, their study under perfusion flow is more complicated, as they can be flushed out easily. Using live-cell imaging, it is essential to track cells at the microscope and follow their behavior over time. Nowadays, two strategies have been used for observing non-adherent cells at the microscope while having a constant flow of medium: the coating of the substrate to immobilize cells, or the engineering of the channel designs to trap cells.

2.4.3.1 Coating the substrate to immobilize cells

The simplest solution is to chemically immobilize cells by using specific coatings onto the substrate, especially on glass coverslips for microscopy, generally by poly-l-lysin[209] or lectin (See Results, Chapter 2).

2.4.3.2 Trapping systems in the flow

Alternatively, technical trapping strategies have been engineered for allowing cell observation under perfusion flow. The first strategy consists in subjecting cells to direct perfusion flow but preventing their movements by specific channel designs[210-212] (Figure 27). For example, Bell *et al.* developed a system dedicated to hydrodynamic yeast trapping using small wells fabricated in the walls of the micro-channels, favoring cell immobilization and observation[210]. Other perfusion systems have integrated cell trapping sites in PDMS structures[213-216], and can take advantage of the perfusion to flush undesired cells[217].

Additionally, cells can be immobilized in polymer scaffolds. In fact, the scaffold is used as a mechanical support and the cell is encapsulated in its matrix. These polymers are called hydrogels: they are composed with more than 99% of water and the polymer chains are hydrophilic. Using hydrogels, the cell receives nutrients on their whole surface, compared to cells attached to the substrate[218]. These gels are commonly calcium alginate[219], agarose[220], chitosan[221], PEG [222], collagen[223] and cellulose[224].

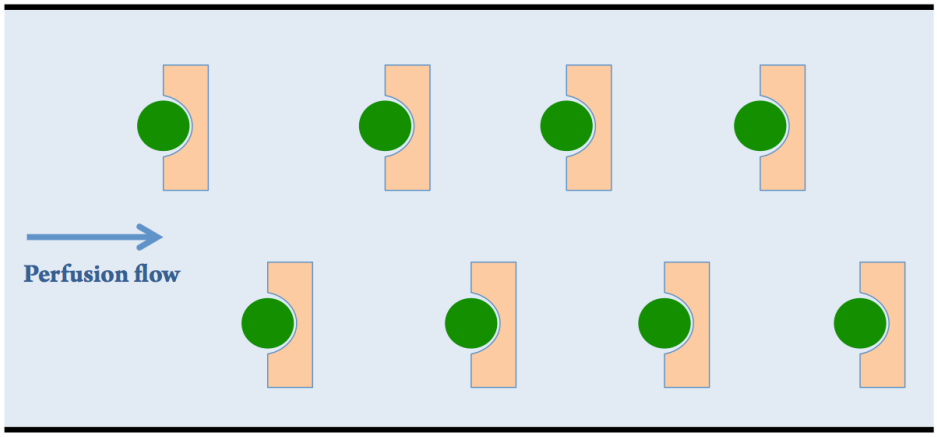

Figure 27: Scheme of a microfluidic device constituted with several trapping arrays. In green, cells are trapped in these arrays.

Cells in such systems using traps are directly in the flow and are subjected to hydrodynamic shear stress. For this reason the velocity of the flow has to be reduced for minimizing this stress.

2.4.3.3 Trapping systems in side chambers

Other strategies have been conceived for trapping cells and lowering shear stress. They consist in using side chambers for trapping non-adherent cells. These chambers are along the perfusion channel on the sides, and the nutrients and drugs are brought by diffusion. Indeed, it lowers the shear stress on cells, but as a consequence, the timings of medium switches are slower. Furthermore, loading cells in such device is challenging because air may be trapped in the chambers. Wang *et al.* used vacuum through PDMS chambers to get the air out of the chamber due to PDMS gas permeability, while injecting their cells[225,226] (Figure 28-A). When PDMS is avoided in the microfluidic chip, for its negative absorption effects, the loading of cells is challenging. In the PDMS-free microfluidic system we fabricated (See Results, Chapter 1), we used side chambers in between two perfusion channels, and cells are injecting inside the chambers by adjusting the fluidic resistances while blocking one input and one output[109] (Figure 28– B).

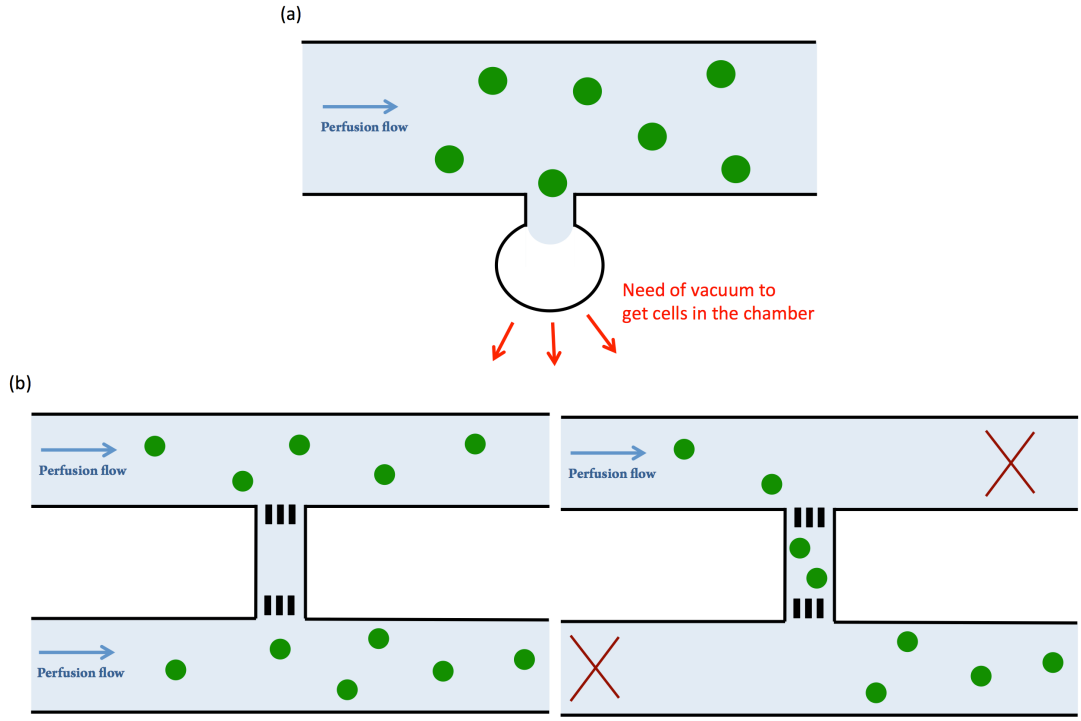

Figure 28: Examples of cell trapping using side chambers. A – Schematic of a microfluidic system constituted with a side chamber. No cells were trapped in the chamber after injection. Air trapped need to be removed by using vacuum to allow cell to enter the chamber. B – Schematics of a side chamber between two perfusion channels. Cells are injected in the chamber while varying the fluidic resistance.

2.4.3.4 Conclusion

As a matter of facts, perfusion systems while observing cell behavior during live-cell imaging is no longer a challenge, as already several options are available. Hence, strategic choices need to be taken, regarding the biological questions addressed. Having cells directly in the perfusion flow is compatible with dynamic medium switches, as cells directly receive fresh medium. These systems subject cells to hydrodynamic shear stress, which can have an affect on their proliferation and morphology. Nevertheless, high shear stresses could be used for mimicking in vivo environments. Perfusion flow can be compared to

blood flow, and can be advantageous for investigating endothelial cell functions and adhesion[227]. On the other hand, strategies to avoid hydrodynamic shear stress involve nutrient supplies by diffusion and require complex designs, fabrication methods and challenging cell loadings. Fluid convection in such systems is reduced. As a consequence, medium change dynamics are slower.

Alternatively, porous membranes in microfluidic systems have been implemented for avoiding shear stress on cells while having high perfusion flow rates.

2.5 Membranes integration: an alternative strategy for avoiding shear stress

Another alternative for reducing shear stress while having a constant renewal of medium is the introduction of a porous membrane in the microfluidic chip. This membrane is sandwiched between the cell chamber and the perfusion channel, prevents convection in the cell chamber and allows nutrient diffusion (Figure 29) (See Results, Chapter 3).

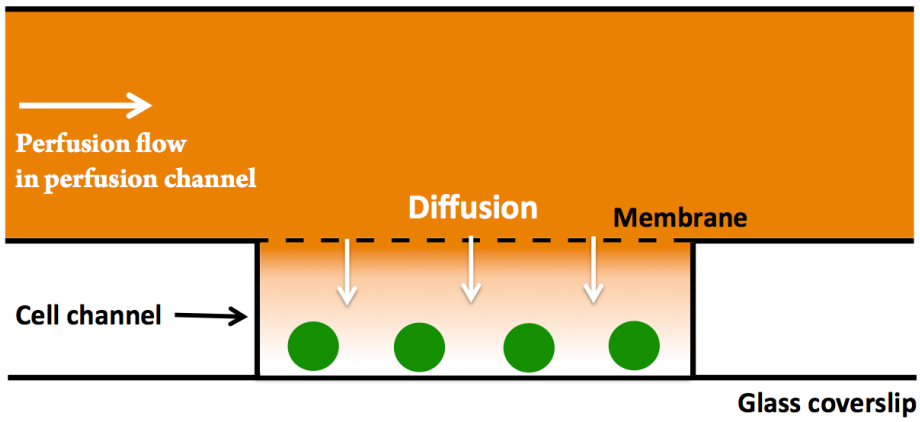

Figure 29: Schematic of a membrane integrated between two microfluidic channels. The medium is renewal continuously and cells are fed by diffusion. The orange gradient represents the concentration gradient. There is no convection inside the cell chambers and shear stress is limited.

2.5.1 What is a membrane?

A membrane is by definition a semi-permeable barrier, allowing molecules through, and blocking others. For this reason, membranes in microfluidics have been widely used to control flow transport[228,229]. The permeation of particles inside membranes is influenced by concentration, thermal, pressure or electrical gradients. These forces are dependent on the potential difference at both sides of the membranes and the thickness of the membrane, by the relation $F = \Delta X/I$, where ΔX is the potential difference and I the thickness of the membrane.

It exists two types of membranes. On the one hand, dense membranes are material dependent, composed of dense structure where no pore can be detected. They are permeable to single molecules[230]. On the other hand, porous membranes are constituted with pores, through which the transport occurs. This transport is dependent of the morphology of the membrane and the nature of the material. The morphology is defined by 1) the porosity, or fraction of the volume of voids over the total volume of the membrane, 2) the pore size, and 3) the tortuosity, or ratio between the average length of the path through the pores and the membrane

thickness[229]. Porous membranes are characterized by their permeability P (capacity of the membrane) and the molecular weight cut-off (MWCO), defined as the lowest molecular weight at which greater than 90% of the solute is retained by the membrane, which reflects the pore size of the membrane.

Depending on the application, a strategic choice of membrane has to be taken. First, considerations on the membrane material and type are essential for insuring the compatibility with the targeted experiment. For instance, membranes can be dense or porous, soft or hard. Their width is to be considered for diffusion timings, as well as their pore sizes and density. Secondly, the fabrication methods and assembly of the membrane is also an important parameter to be considered. InFigure 30, Jong *et al.* recommend choosing the membrane material and type prior to the fabrication and assembly methods[229].

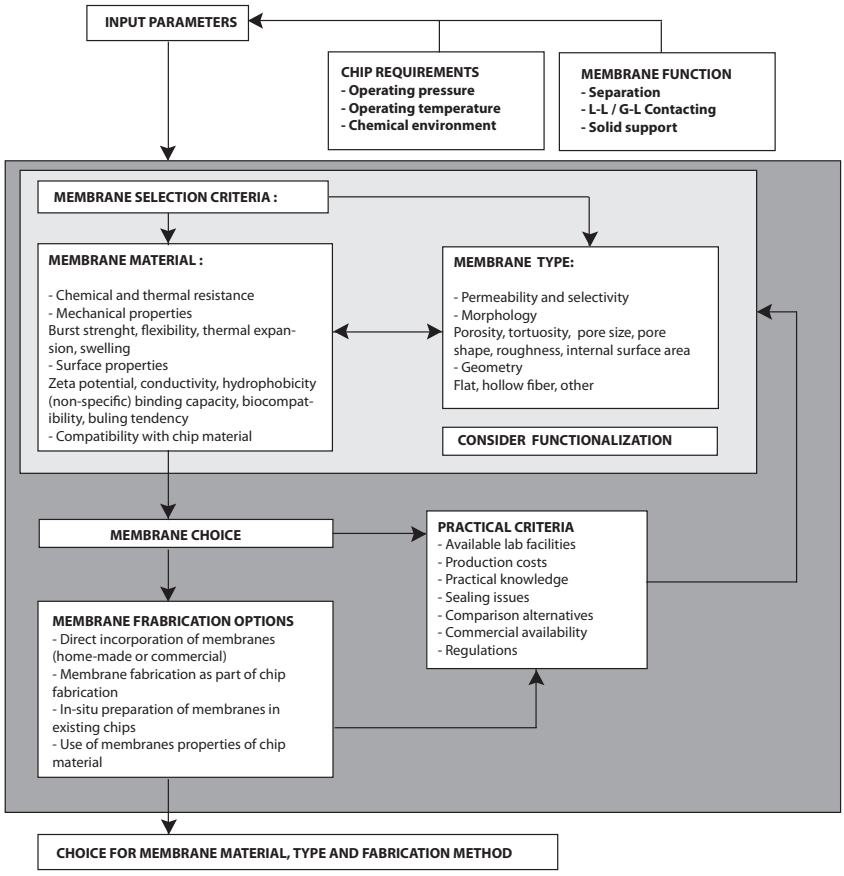

Figure 30: Schematic reproduced from [229] and cited with permission presenting the membrane selection criteria. Several parameters are involved in the membrane choice: the material, type of membrane, fabrication methods and practical criteria.

2.5.2 Engineering the sealing of a membrane

One common challenge in microfluidics is the implementation of a membrane in a chip. As they are often constituted with pores, membranes are not trivial to integrate because of sealing instability: due to capillary forces, any fluid can easily penetrate between the membrane and the substrate. Thus different approaches have been considered for ensuring proper sealing and avoiding any leakage[231].

2.5.2.1 Fabricating the membrane in a laboratory

One approach is to fabricate and bond directly the membrane to a substrate during the chip fabrication process. This requires semiconductor technologies and hence is not suitable for simple fabrication processes. The advantage of using such technique is a good control of the membrane thickness, pore size and distribution, as well as the direct bonding of the membrane on the substrate material. For instance, Heyderman *et al*. fabricated their membrane by etching a deposited substrate[232], Steigert *et al.* used electro-deposition to fabricate their membrane[116]. However, simpler photolithography techniques have also been utilized for fabricating membranes in PDMS[233], SU8[234,235] or NOA[235]. However, these methods are time-consuming and require the use of photolithography equipment. Besides, their thickness may not be reproducible from one chip to the next.

2.5.2.2 Using commercial membranes

A simpler option consists of using commercial flat membranes. In this case, the incorporation of the membrane can be done by clamping or gluing. Standard microfluidic systems have used PDMS as a scaffold because of the ability of PDMS to bond to itself, clamping the membrane between two PDMS blocks[231,236,237]. For instance, Kimura *et al.* used a 10-microns thick polyester semi-permeable membrane sandwiched between two PDMS blocks for perfusion culture and monitoring of intestinal tissue models[238]. Charvin *et al*. used a 30-microns thick cellulose membrane for trapping budding yeast cells, and the diffusion time was calculated to be approximately 40 seconds[167]. PDMS-free systems can be constituted with adhesive layers for bonding the membrane to hard substrates[239], even though gluing the membrane may not be trivial as the glue could eventually fill the pores and block the fluid flow[240] (See Results, Chapter 3).

2.6 Conclusion:

The ideal perfusion system must be compatible with live-cell imaging, easy to fabricate and user-friendly. It must allow fast media switching, avoid any shear stress on cells, and its temperature must be controlled precisely and dynamically. Building such a system is challenging, and considerations have to be made on the microfluidic chip used, the cell type of interest, the perfusion system and the temperature control.

Choosing a system in which cells are directly in the flow allows fast media switches but hydrodynamic shear stress on cells. Microfluidic chips constituted with traps or sides chambers reduce the shear stress, however the timings of medium switch are slower, as they are diffusion-dependent. Moreover, such systems are difficult to produce, especially when made with thermoplastic materials. Building microchips using membranes is the second strategy, even if the membrane is complicated to integrate, they prevent shear stress, but the diffusion timings are mostly membrane-dependent.

General conclusion

Perfusion systems for live-cell imaging have already been engineered and protocols have been established for fabricating microsystems, sterilization, injecting various model organisms, trapping and observing them with microscopes. Most perfusion systems utilize PDMS as the main chip material, which presents the non-desired absorption property. Changing this material to thermoplastics makes challenging the sealing of the microfluidic chips, cell injections, cell trapping, membrane integration. On one hand, simple perfusion systems compatible with microscopy already exist and are commercially available, composed of simple channels in which cells are subjected to shear stress during perfusion. As consumables, they cannot be reused and may not be adequate for integrating temperature control, de-bubbling, or valves for fast medium switches. Other simple systems may use gravity for driving flows. Similarly, simple temperature control can be achieved using for instance a thermalization chamber at the microscope. These systems are not adequate for performing experiments involving dynamic and precise control of the medium flow and temperature. However, high precision, accuracy and fast dynamics are required for performing robust experiments. Such a fine control of the microenvironmental parameters adds complexity in the microsystems and setups used. The simultaneous control of these parameters using a microfluidic chip that is simple to fabricate and to use constitutes a great challenge.

Thesis objectives

The objective of my thesis was to build an ideal system dedicated to live-cell imaging. The ideal system must be compatible with the state-of-the-art applications using high-resolution microscopy. As a versatile system, it must be compatible with adherent cells and non-adherent cells. For allowing cells to proliferate, temperature and medium flow must be controlled precisely and accurately, and fast changes in temperature or media must be possible to investigate cell functions and behaviors. Moreover, fine control of drug concentrations must be possible. Therefore the absorptive PDMS material must be avoided. Additionally, shear stress on cell must be negligible.

As mentioned above, building such a system is challenging. Making it simple to fabricate, user-friendly and reusable is even more challenging. Considering these last specifications, we realized that the unique ideal system would be impossible to realize. We therefore opted for a different strategy: building three different systems, which respective advantages and drawbacks would cover the entire needs and possible applications in cell biology. In all three systems, the materials need to be compatible with microscopy, and the temperature and perfusion flow need to be controlled precisely, dynamically and simultaneously.

We first aimed at a system compatible with precise concentration of drugs or small biomolecules, no matter how complex (to fabricate or to use) it is. Thus, it must be fully made of materials that do not absorb small biomolecules. Also, it will allow the study of various cell types (adherent and non-adherent cells) and shear stress will be limited. Therefore, the need of side chambers, where nutrients are brought by diffusion, is essential. The greatest challenge in such a system is the fabrication and assembly of the microfluidic chip (Results, Chapter 1).

We aimed at building a less powerful system, that is simpler to fabricate and to use, and reusable, with the inconvenient of having shear stress on cells, as they will be in the medium flow. This system will therefore be compatible with fast media switches and allow the monitoring of cell responses in real time, and will represent a considerable tool for biologists (Results, Chapter 2).

The third system will also be easy to fabricate and user-friendly. This system will be fabricated so that the shear stress on cells is completely avoided. For that, a membrane will be integrated to separate the cell channel from the perfusion one, and allow medium and drug exchange by diffusion. The materials in this system need to be compatible with precise concentrations of drug (Results, Chapter 3).

References

1. Lynch, M. *et al.* Evolutionary cell biology: two origins, one objective. *Proc. Natl. Acad. Sci. U.S.A.* **111,** 16990–16994 (2014).
2. Schnerch, D. *et al.* Cell cycle control in acute myeloid leukemia. *Am J Cancer Res* **2,** 508–528 (2012).
3. Webber, K. M. *et al.* The cell cycle in Alzheimer disease: a unique target for neuropharmacology. *Mech. Ageing Dev.* **126,** 1019–1025 (2005).
4. Yeh, C. T., Wong, S. W., Fung, Y. K. & Ou, J. H. Cell cycle regulation of nuclear localization of hepatitis B virus core protein. *Proc. Natl. Acad. Sci. U.S.A.* **90,** 6459–6463 (1993).
5. Williams, G. H. & Stoeber, K. The cell cycle and cancer. *The Journal of Pathology* **226,** 352–364 (2011).
6. Wolpert, L. The evolution of 'the cell theory'. *Curr. Biol.* **6,** 225–228 (1996).
7. Glansdorff, N., Xu, Y. & Labedan, B. The last universal common ancestor: emergence, constitution and genetic legacy of an elusive forerunner. *Biol. Direct* **3,** 29 (2008).
8. Vellai, T. & Vida, G. The origin of eukaryotes: the difference between prokaryotic and eukaryotic cells. *Proc. Biol. Sci.* **266,** 1571–1577 (1999).
9. Archibald, J. M. Endosymbiosis and Eukaryotic Cell Evolution. *Curr. Biol.* **25,** R911–21 (2015).
10. Takeda, D. Y. & Dutta, A. DNA replication and progression through S phase. *Oncogene* **24,** 2827–2843 (2005).
11. McIntosh, J. R. Mitosis. *Cold Spring Harb Perspect Biol* **8,** a023218 (2016).
12. Yam, C., He, Y., Zhang, D., Chiam, K.-H. & Oliferenko, S. Divergent strategies for controlling the nuclear membrane satisfy geometric constraints during nuclear division. *Curr. Biol.* **21,** 1314–1319 (2011).
13. Walczak, C. E. & Heald, R. in *A Survey of Cell Biology* **265,** 111–158 (Elsevier, 2008).
14. Blackwell, R. *et al.* Physical determinants of bipolar mitotic spindle assembly and stability in fission yeast. *Sci Adv* **3,** e1601603 (2017).
15. Brooker, A. S. & Berkowitz, K. M. The roles of cohesins in mitosis, meiosis, and human health and disease. *Methods Mol. Biol.* **1170,** 229–266 (2014).
16. Rogers, G. C. *et al.* Two mitotic kinesins cooperate to drive sister chromatid separation during anaphase. *Nature* **427,** 364–370 (2003).
17. Guertin, D. A., Trautmann, S. & McCollum, D. Cytokinesis in Eukaryotes. *Microbiology and Molecular Biology Reviews* **66,** 155–178 (2002).
18. Nurse, P. Regulation of the eukaryotic cell cycle. *Eur. J. Cancer* **33,** 1002–1004 (1997).
19. Morgan, D. O. CYCLIN-DEPENDENT KINASES: Engines, Clocks, and Microprocessors. *Annual Review of Cell and Developmental Biology* **13,** 261–291 (1997).
20. Morgan, D. O. Principles of CDK regulation. *Nature* **374,** 131–134 (1995).
21. Pardee, A. B., Dubrow, R., Hamlin, J. L. & Kletzien, R. F. Animal cell cycle. *Annu. Rev. Biochem.* **47,** 715–750 (1978).
22. Hartwell, L. H. & Weinert, T. A. Checkpoints: controls that ensure the order of cell cycle events. *Science* **246,** 629–634 (1989).
23. Elledge, S. J. Cell cycle checkpoints: preventing an identity crisis. *Science* **274,** 1664–1672 (1996).
24. Johnson, A. & Skotheim, J. M. Start and the restriction point. *Current Opinion in Cell Biology* **25,** 717–723 (2013).
25. Bertoli, C., Skotheim, J. M. & de Bruin, R. A. M. Control of cell cycle transcription during G1 and S phases. *Nat. Rev. Mol. Cell Biol.* **14,** 518–528 (2013).
26. Chin, C. F. & Yeong, F. M. Safeguarding entry into mitosis: the antephase checkpoint. *Molecular and Cellular Biology* **30,** 22–32 (2010).
27. Russell, P. Checkpoints on the road to mitosis. *Trends Biochem. Sci.* **23,** 399–402 (1998).
28. Fisher, D., Krasinska, L., Coudreuse, D. & Novák, B. Phosphorylation network dynamics in the control of cell cycle transitions. *J. Cell. Sci.* **125,** 4703–4711 (2012).
29. Ezkurdia, I. *et al.* Multiple evidence strands suggest that there may be as few as 19 000 human

protein-coding genes. *Human Molecular Genetics* **23,** 5866–5878 (2014).
30. Jennings, B. H. Drosophila – a versatile model in biology & medicine. *Materials Today* **14,** 190–195 (2011).
31. Koelle, M. in *Genetic Models in Cardiorespiratory Biology* **20013058,** 21–33 (CRC Press, 2013).
32. Wood, V. *et al.* The genome sequence of Schizosaccharomyces pombe. *Nature* **415,** 871–880 (2002).
33. Tang, Z. in *Cell Cycle Oscillators* (eds. Coutts, A. S. & Weston, L.) **1342,** 21–57 (Springer New York, 2016).
34. Peden, E., Killian, D. J. & Xue, D. Cell death specification in C. elegans. *Cell Cycle* **7,** 2479–2484 (2008).
35. Hu, X. & Zuckerman, K. S. Transforming Growth Factor: Signal Transduction Pathways, Cell Cycle Mediation, and Effects on Hematopoiesis. *Journal of Hematotherapy & Stem Cell Research* **10,** 67–74 (2001).
36. Matsu-Ura, T. *et al.* Intercellular Coupling of the Cell Cycle and Circadian Clock in Adult Stem Cell Culture. *Mol. Cell* **64,** 900–912 (2016).
37. Patterson, L. T. & Potter, S. S. Hox genes and kidney patterning. *Current Opinion in Nephrology and Hypertension* **12,** 19–23 (2003).
38. Lappin, T. R. J., Grier, D. G., Thompson, A. & Halliday, H. L. HOX genes: seductive science, mysterious mechanisms. *Ulster Med J* **75,** 23–31 (2006).
39. Petersen, J. & Russell, P. Growth and the Environment of Schizosaccharomyces pombe. *Cold Spring Harb Protoc* **2016,** pdb.top079764 (2016).
40. Wood, V. *et al.* PomBase: a comprehensive online resource for fission yeast. *Nucleic Acids Res.* **40,** D695–9 (2012).
41. Murray, J. M., Watson, A. T. & Carr, A. M. Molecular Genetic Tools and Techniques in Fission Yeast. *Cold Spring Harb Protoc* **2016,** pdb.top087601 (2016).
42. Ding, D. Q. *et al.* Large-scale screening of intracellular protein localization in living fission yeast cells by the use of a GFP-fusion genomic DNA library. *Genes Cells* **5,** 169–190 (2000).
43. Kim, D.-U. *et al.* Analysis of a genome-wide set of gene deletions in the fission yeast Schizosaccharomyces pombe. *Nat. Biotechnol.* **28,** 617–623 (2010).
44. Bonatti, S., Simili, M. & Abbondandolo, A. Isolation of temperature-sensitive mutants of Schizosaccharomyces pombe. *J. Bacteriol.* **109,** 484–491 (1972).
45. Forsburg, S. L. & Nurse, P. Identification of a Gl-type cyclin puc1 + in the fission yeast Schizosaccharomyces pombe. *Nature* **351,** 245–248 (1991).
46. Fisher, D. L. & Nurse, P. A single fission yeast mitotic cyclin B p34cdc2 kinase promotes both S-phase and mitosis in the absence of G1 cyclins. *EMBO J.* **15,** 850–860 (1996).
47. Kozar, K. *et al.* Mouse development and cell proliferation in the absence of D-cyclins. *Cell* **118,** 477–491 (2004).
48. Santamaría, D. *et al.* Cdk1 is sufficient to drive the mammalian cell cycle. *Nature* **448,** 811–815 (2007).
49. Sherr, C. J. Living with or without cyclins and cyclin-dependent kinases. *Genes Dev.* **18,** 2699–2711 (2004).
50. Coudreuse, D. Insights from synthetic yeasts. *Yeast* **33,** 483–492 (2016).
51. Coudreuse, D. & Nurse, P. Driving the cell cycle with a minimal CDK control network. *Nature* **468,** 1074–1079 (2010).
52. Masters, J. R. & Stacey, G. N. Changing medium and passaging cell lines. *Nat Protoc* **2,** 2276–2284 (2007).
53. Wheals, A. E. Size control models of Saccharomyces cerevisiae cell proliferation. *Molecular and Cellular Biology* **2,** 361–368 (1982).
54. Albrecht, D. R. *et al.* Microfluidics-integrated time-lapse imaging for analysis of cellular dynamics. *Integr Biol (Camb)* **2,** 278–287 (2010).
55. Whitesides, G. M. The origins and the future of microfluidics. *Nature* **442,** 368–373 (2006).
56. Jacobs, K. Introduction to Microfluidics. By Patrick Tabeling. *Angewandte Chemie International Edition* **45,** 7875–7875 (2006).
57. Halldorsson, S., Lucumi, E., Gómez-Sjöberg, R. & Fleming, R. M. T. Advantages and challenges of microfluidic cell culture in polydimethylsiloxane devices. *Biosens Bioelectron* **63,** 218–231 (2015).

58. Stroock, A. D. & Whitesides, G. M. Controlling Flows in Microchannels with Patterned Surface Charge and Topography. *Accounts of Chemical Research* **36,** 597–604 (2003).
59. Bayraktar, T. & Pidugu, S. B. Characterization of liquid flows in microfluidic systems. *International Journal of Heat and Mass Transfer* **49,** 815–824 (2006).
60. Takayama, S. *et al.* Laminar flows: Subcellular positioning of small molecules. *Nature* **411,** 1016–1016 (2001).
61. Keenan, T. M. & Folch, A. Biomolecular gradients in cell culture systems. *Lab Chip* **8,** 34–57 (2008).
62. Mark, D., Haeberle, S., Roth, G., Stetten, von, F. & Zengerle, R. Microfluidic lab-on-a-chip platforms: requirements, characteristics and applications. *Chem Soc Rev* **39,** 1153–1182 (2010).
63. Huh, D., Gu, W., Kamotani, Y., Grotberg, J. B. & Takayama, S. Microfluidics for flow cytometric analysis of cells and particles. *Physiol Meas* **26,** R73–98 (2005).
64. Lee, C.-Y., Chang, C.-L., Wang, Y.-N. & Fu, L.-M. Microfluidic mixing: a review. *Int J Mol Sci* **12,** 3263–3287 (2011).
65. Williams, M. S., Longmuir, K. J. & Yager, P. A practical guide to the staggered herringbone mixer. *Lab Chip* **8,** 1121–1129 (2008).
66. Thull, R. Physicochemical principles of tissue material interactions. *Biomolecular Engineering* **19,** 43–50 (2002).
67. Whitesides, G. M. Cool, or simple and cheap? Why not both? *Lab Chip* **13,** 11–13 (2013).
68. Velve-Casquillas, G., Le Berre, M., Piel, M. & Tran, P. T. Microfluidic tools for cell biological research. *Nano Today* **5,** 28–47 (2010).
69. Barkefors, I. *et al.* Endothelial cell migration in stable gradients of vascular endothelial growth factor A and fibroblast growth factor 2: effects on chemotaxis and chemokinesis. *J. Biol. Chem.* **283,** 13905–13912 (2008).
70. Wang, S.-J., Saadi, W., Lin, F., Minh-Canh Nguyen, C. & Li Jeon, N. Differential effects of EGF gradient profiles on MDA-MB-231 breast cancer cell chemotaxis. *Exp. Cell Res.* **300,** 180–189 (2004).
71. Li Jeon, N. *et al.* Neutrophil chemotaxis in linear and complex gradients of interleukin-8 formed in a microfabricated device. *Nat. Biotechnol.* **20,** 826–830 (2002).
72. Mao, H., Cremer, P. S. & Manson, M. D. A sensitive, versatile microfluidic assay for bacterial chemotaxis. *Proc. Natl. Acad. Sci. U.S.A.* **100,** 5449–5454 (2003).
73. Irimia, D. *et al.* Microfluidic system for measuring neutrophil migratory responses to fast switches of chemical gradients. *Lab Chip* **6,** 191–198 (2006).
74. Chung, B. G. *et al.* Human neural stem cell growth and differentiation in a gradient-generating microfluidic device. *Lab Chip* **5,** 401–406 (2005).
75. Vyawahare, S., Griffiths, A. D. & Merten, C. A. Miniaturization and Parallelization of Biological and?Chemical Assays in Microfluidic Devices. *Chemistry & Biology* **17,** 1052–1065 (2010).
76. Guck, J. *et al.* Optical deformability as an inherent cell marker for testing malignant transformation and metastatic competence. *Biophys. J.* **88,** 3689–3698 (2005).
77. Shin, Y. *et al.* Microfluidic assay for simultaneous culture of multiple cell types on surfaces or within hydrogels. *Nat Protoc* **7,** 1247–1259 (2012).
78. Whitesides, G. M., Ostuni, E., Takayama, S., Jiang, X. & Ingber, D. E. Soft Lithography in Biology and Biochemistry. *Annu Rev Biomed Eng* **3,** 335–373 (2001).
79. Qin, D., Xia, Y. & Whitesides, G. M. Soft lithography for micro- and nanoscale patterning. *Nat Protoc* **5,** 491–502 (2010).
80. Zhang, J., Tan, K. L., Hong, G. D., Yang, L. J. & Gong, H. Q. Polymerization optimization of SU-8 photoresist and its applications in microfluidic systems and MEMS. *Journal of Micromechanics and Microengineering* **11,** 20–26 (2000).
81. Lamberti, A., Marasso, S. L. & Cocuzza, M. PDMS membranes with tunable gas permeability for microfluidic applications. *RSC Adv.* **4,** 61415–61419 (2014).
82. Johnston, I. D., McCluskey, D. K., Tan, C. K. L. & Tracey, M. C. Mechanical characterization of bulk Sylgard 184 for microfluidics and microengineering. *Journal of Micromechanics and Microengineering* **24,** 035017 (2014).
83. Lee, J. N., Jiang, X., Ryan, D. & Whitesides, G. M. Compatibility of mammalian cells on surfaces of poly(dimethylsiloxane). *Langmuir* **20,** 11684–11691 (2004).

84. Crane, M. M., Clark, I. B. N., Bakker, E., Smith, S. & Swain, P. S. A microfluidic system for studying ageing and dynamic single-cell responses in budding yeast. *PLoS ONE* **9,** e100042 (2014).
85. Eyer, K., Kuhn, P., Stratz, S. & Dittrich, P. S. A microfluidic chip for the versatile chemical analysis of single cells. *J Vis Exp* e50618 (2013). doi:10.3791/50618
86. Unger, M. A., Chou, H. P., Thorsen, T., Scherer, A. & Quake, S. R. Monolithic microfabricated valves and pumps by multilayer soft lithography. *Science* **288,** 113–116 (2000).
87. Sollier, E., Murray, C., Maoddi, P. & Di Carlo, D. Rapid prototyping polymers for microfluidic devices and high pressure injections. *Lab Chip* **11,** 3752–3765 (2011).
88. Mukhopadhyay, R. When PDMS isn't the best. *Anal. Chem.* **79,** 3248–3253 (2007).
89. Heo, Y. S. *et al.* Characterization and Resolution of Evaporation-Mediated Osmolality Shifts That Constrain Microfluidic Cell Culture in Poly(dimethylsiloxane) Devices. *Anal. Chem.* **79,** 1126–1134 (2007).
90. Bhattacharya, S., Datta, A., Berg, J. M. & Gangopadhyay, S. Studies on surface wettability of poly(dimethyl) siloxane (PDMS) and glass under oxygen-plasma treatment and correlation with bond strength. *Journal of Microelectromechanical Systems* **14,** 590–597 (2005).
91. Eddings, M. A., Johnson, M. A. & Gale, B. K. Determining the optimal PDMS–PDMS bonding technique for microfluidic devices. *Journal of Micromechanics and Microengineering* **18,** 067001 (2008).
92. Hu, S. *et al.* Tailoring the Surface Properties of Poly(dimethylsiloxane) Microfluidic Devices. *Langmuir* **20,** 5569–5574 (2004).
93. Gitlin, L., Schulze, P., Ohla, S., Bongard, H.-J. & Belder, D. Surface modification of PDMS microfluidic devices by controlled sulfuric acid treatment and the application in chip electrophoresis. *Electrophoresis* **36,** 449–456 (2015).
94. Regehr, K. J. *et al.* Biological implications of polydimethylsiloxane-based microfluidic cell culture. *Lab Chip* **9,** 2132–2139 (2009).
95. van Meer, B. J. *et al.* Small molecule absorption by PDMS in the context of drug response bioassays. *Biochemical and Biophysical Research Communications* **482,** 323–328 (2017).
96. Toepke, M. W. & Beebe, D. J. PDMS absorption of small molecules and consequences in microfluidic applications. *Lab Chip* **6,** 1484–1486 (2006).
97. Choi, S.-J. *et al.* A polydimethylsiloxane (PDMS) sponge for the selective absorption of oil from water. *ACS Appl Mater Interfaces* **3,** 4552–4556 (2011).
98. Futrega, K. *et al.* Polydimethylsiloxane (PDMS) modulates CD38 expression, absorbs retinoic acid and may perturb retinoid signalling. *Lab Chip* **16,** 1473–1483 (2016).
99. Makamba, H., Kim, J. H., Lim, K., Park, N. & Hahn, J. H. Surface modification of poly(dimethylsiloxane) microchannels. *Electrophoresis* **24,** 3607–3619 (2003).
100. Zhou, J., Ellis, A. V. & Voelcker, N. H. Recent developments in PDMS surface modification for microfluidic devices. *Electrophoresis* **31,** 2–16 (2010).
101. Wang, J. D., Douville, N. J., Takayama, S. & ElSayed, M. Quantitative analysis of molecular absorption into PDMS microfluidic channels. *Ann Biomed Eng* **40,** 1862–1873 (2012).
102. Roman, G. T., Hlaus, T., Bass, K. J., Seelhammer, T. G. & Culbertson, C. T. Sol−Gel Modified Poly(dimethylsiloxane) Microfluidic Devices with High Electroosmotic Mobilities and Hydrophilic Channel Wall Characteristics. *Anal. Chem.* **77,** 1414–1422 (2005).
103. Gómez-Sjöberg, R., Leyrat, A. A., Houseman, B. T., Shokat, K. & Quake, S. R. Biocompatibility and reduced drug absorption of sol-gel-treated poly(dimethyl siloxane) for microfluidic cell culture applications. *Anal. Chem.* **82,** 8954–8960 (2010).
104. Beal, J. H. L., Bubendorfer, A., Kemmitt, T., Hoek, I. & Mike Arnold, W. A rapid, inexpensive surface treatment for enhanced functionality of polydimethylsiloxane microfluidic channels. *Biomicrofluidics* **6,** 36503 (2012).
105. Sasaki, H., Onoe, H., Osaki, T., Kawano, R. & Takeuchi, S. Parylene-coating in PDMS microfluidic channels prevents the absorption of fluorescent dyes. *Sensors and Actuators B: Chemical* **150,** 478–482 (2010).
106. Bodas, D. & Khan-Malek, C. Hydrophilization and hydrophobic recovery of PDMS by oxygen plasma and chemical treatment—An SEM investigation. *Sensors and Actuators B: Chemical* **123,** 368–373 (2007).
107. Eddington, D. T., Puccinelli, J. P. & Beebe, D. J. Thermal aging and reduced hydrophobic recovery

of polydimethylsiloxane. *Sensors and Actuators B: Chemical* **114,** 170–172 (2006).
108. Jokinen, V., Suvanto, P. & Franssila, S. Oxygen and nitrogen plasma hydrophilization and hydrophobic recovery of polymers. *Biomicrofluidics* **6,** 016501 (2012).
109. Chen, T. *et al.* A drug-compatible and temperature-controlled microfluidic device for live-cell imaging. *Open Biol* **6,** 160156 (2016).
110. Ren, K., Zhou, J. & Wu, H. Materials for Microfluidic Chip Fabrication. *Accounts of Chemical Research* **46,** 2396–2406 (2013).
111. Cao, Y., Bontrager-Singer, J. & Zhu, L. A 3D microfluidic device fabrication method using thermopress bonding with multiple layers of polystyrene film. *Journal of Micromechanics and Microengineering* **25,** 065005 (2015).
112. Li, H., Fan, Y., Kodzius, R. & Foulds, I. G. Fabrication of polystyrene microfluidic devices using a pulsed CO2 laser system. *Microsystem Technologies* **18,** 373–379 (2011).
113. Ogo czyk, D., W grzyn, J., Jankowski, P., D browski, B. & Garstecki, P. Bonding of microfluidic devices fabricated in polycarbonate. *Lab Chip* **10,** 1324–1327 (2010).
114. Chou, J. *et al.* Hot embossed polyethylene through-hole chips for bead-based microfluidicdevices. *Biosens Bioelectron* **42,** 653–660 (2013).
115. Zhang, X. *et al.* A low cost and quasi-commercial polymer film chip for high-throughput inertial cell isolation. *RSC Adv.* **6,** 9734–9742 (2016).
116. Steigert, J. *et al.* Rapid prototyping of microfluidic chips in COC. *Journal of Micromechanics and Microengineering* **17,** 333–341 (2007).
117. Jena, R. K., Yue, C. Y. & Lam, Y. C. Micro fabrication of cyclic olefin copolymer (COC) based microfluidic devices. *Microsystem Technologies* **18,** 159–166 (2011).
118. Lee, J.-H., Peterson, E. T. K., Dagani, G. & Papautsky, I. Rapid prototyping of plastic microfluidic devices in cyclic olefin copolymer (COC). in (eds. Papautsky, I. & Chartier, I.) **5718,** 82 (SPIE, 2005).
119. Hong, T.-F. *et al.* Rapid prototyping of PMMA microfluidic chips utilizing a CO2 laser. *Microfluidics and Nanofluidics* **9,** 1125–1133 (2010).
120. Qi, H., Wang, X., Chen, T., Ma, X. & Zuo, T. Fabrication and characterization of a polymethyl methacrylate continuous-flow PCR microfluidic chip using CO2 laser ablation. *Microsystem Technologies* **15,** 1027–1030 (2009).
121. Chen, Y., Zhang, L. & Chen, G. Fabrication, modification, and application of poly(methyl methacrylate) microfluidic chips. *Electrophoresis* **29,** 1801–1814 (2008).
122. Becker, H. & Gärtner, C. Polymer microfabrication technologies for microfluidic systems. *Analytical and Bioanalytical Chemistry* **390,** 89–111 (2007).
123. Becker, H. & Locascio, L. E. Polymer microfluidic devices. *Talanta* **56,** 267–287 (2002).
124. Gerlach, A. *et al.* Microfabrication of single-use plastic microfluidic devices for high-throughput screening and DNA analysis. *Microsystem Technologies* **7,** 265–268 (2002).
125. Pemg, B.-Y., Wu, C.-W., Shen, Y.-K. & Lin, Y. Microfluidic chip fabrication using hot embossing and thermal bonding of COP. *Polymers for Advanced Technologies* **21,** 457–466 (2009).
126. Leech, P. W. Hot embossing of cyclic olefin copolymers. *Journal of Micromechanics and Microengineering* **19,** 055008 (2009).
127. Wu, C.-L., Li, C.-C., Lu, C.-F. & Yang, S.-Y. Development of two step carbon dioxide assisted thermal fusion PMMA bonding process. *Microsystem Technologies* **18,** 409–414 (2012).
128. Rötting, O., Röpke, W., Becker, H. & Gärtner, C. Polymer microfabrication technologies. *Microsystem Technologies* **8,** 32–36 (2002).
129. Hansen, T. S., Selmeczi, D. & Larsen, N. B. Fast prototyping of injection molded polymer microfluidic chips. *Journal of Micromechanics and Microengineering* **20,** 015020 (2009).
130. Alexander Muck, Jr *et al.* Fabrication of Poly(methyl methacrylate) Microfluidic Chips by Atmospheric Molding. **76,** 2290–2297 (2004).
131. Yao, X., Chen, Z. & Chen, G. Fabrication of PMMA microfluidic chips using disposable agar hydrogel templates. *Electrophoresis* **30,** 4225–4229 (2009).
132. Guckenberger, D. J., de Groot, T. E., Wan, A. M. D., Beebe, D. J. & Young, E. W. K. Micromilling: a method for ultra-rapid prototyping of plastic microfluidic devices. *Lab Chip* **15,** 2364–2378 (2015).
133. Costela, A. *et al.* Laser ablation of polymeric materials at 157 nm. *Journal of Applied Physics* **77,**

2343–2350 (1995).
134. Chung, C. K. & Tu, K. Z. Application of metal film protection to microfluidic chip fabrication using CO2 laser ablation. *Microsystem Technologies* **20,** 1987–1992 (2013).
135. Herbst, L., Klaft, I., Wenzel, T. & Rebhan, U. High-repetition-rate excimer laser for micromachining. in (eds. Davis, S. J. & Heaven, M. C.) **4971,** 87 (SPIE, 2003).
136. Waddell, E. A. Laser ablation as a fabrication technique for microfluidic devices. *Methods Mol. Biol.* **321,** 27–38 (2006).
137. Jensen, M. F., Noerholm, M., Christensen, L. H. & Geschke, O. Microstructure fabrication with a CO2 laser system: characterization and fabrication of cavities produced by raster scanning of the laser beam. *Lab Chip* **3,** 302–307 (2003).
138. Chung, C. K. & Lin, S. L. On the fabrication of minimizing bulges and reducing the feature dimensions of microchannels using novel CO 2laser micromachining. *Journal of Micromechanics and Microengineering* **21,** 065023 (2011).
139. Cheng, J.-Y., Wei, C.-W., Hsu, K.-H. & Young, T.-H. Direct-write laser micromachining and universal surface modification of PMMA for device development. *Sensors and Actuators B: Chemical* **99,** 186–196 (2004).
140. Huang, Y., Liu, S., Yang, W. & Yu, C. Surface roughness analysis and improvement of PMMA-based microfluidic chip chambers by CO2 laser cutting. *Applied Surface Science* **256,** 1675–1678 (2010).
141. Temiz, Y., Lovchik, R. D., Kaigala, G. V. & Delamarche, E. Lab-on-a-chip devices: How to close and plug the lab? *Microelectronic Engineering* **132,** 156–175 (2015).
142. Roy, S., Yue, C. Y., Wang, Z. Y. & Anand, L. Thermal bonding of microfluidic devices: Factors that affect interfacial strength of similar and dissimilar cyclic olefin copolymers. *Sensors and Actuators B: Chemical* **161,** 1067–1073 (2012).
143. Park, T., Song, I.-H., Park, D. S., You, B. H. & Murphy, M. C. Thermoplastic fusion bonding using a pressure-assisted boiling point control system. *Lab Chip* **12,** 2799–2802 (2012).
144. Vlachopoulou, M.-E. *et al.* A low temperature surface modification assisted method for bonding plastic substrates. *Journal of Micromechanics and Microengineering* **19,** 015007 (2008).
145. Keller, N. *et al.* Tacky cyclic olefin copolymer: a biocompatible bonding technique for the fabrication of microfluidic channels in COC. *Lab Chip* **16,** 1561–1564 (2016).
146. Tang, L. & Lee, N. Y. A facile route for irreversible bonding of plastic-PDMS hybrid microdevices at room temperature. *Lab Chip* **10,** 1274–1280 (2010).
147. Patko, D. *et al.* Microfluidic channels laser-cut in thin double-sided tapes: Cost-effective biocompatible fluidics in minutes from design to final integration with optical biochips. *Sensors and Actuators B: Chemical* **196,** 352–356 (2014).
148. Khashayar, P. *et al.* Rapid prototyping of microfluidic chips using laser-cut double-sided tape for electrochemical biosensors. *Journal of the Brazilian Society of Mechanical Sciences and Engineering* **39,** 1469–1477 (2016).
149. Serra, M. *et al.* A simple and low-cost chip bonding solution for high pressure, high temperature and biological applications. *Lab Chip* **17,** 629–634 (2017).
150. Nath, P. *et al.* Rapid prototyping of robust and versatile microfluidic components using adhesive transfer tapes. *Lab Chip* **10,** 2286–2291 (2010).
151. Arayanarakool, R., Le Gac, S. & van den Berg, A. Low-temperature, simple and fast integration technique of microfluidic chips by using a UV-curable adhesive. *Lab Chip* **10,** 2115–2121 (2010).
152. Satyanarayana, S., Karnik, R. N. & Majumdar, A. Stamp-and-stick room-temperature bonding technique for microdevices. *Journal of Microelectromechanical Systems* **14,** 392–399 (2005).
153. Mokkapati, V. R. S. S., Bethge, O., Hainberger, R. & Brueckl, H. Microfluidic chips fabrication from UV curable adhesives for heterogeneous integration. in 1965–1969 (IEEE, 2012). doi:10.1109/ECTC.2012.6249109
154. Bartolo, D., Degr, G., Nghe, P. & Studer, V. Microfluidic stickers. *Lab Chip* **8,** 274–279 (2008).
155. Martin, A., Teychené, S., Camy, S. & Aubin, J. Fast and inexpensive method for the fabrication of transparent pressure-resistant microfluidic chips. *Microfluidics and Nanofluidics* **20,** 355 (2016).
156. Riegger, L., Strohmeier, O., Faltin, B., Zengerle, R. & Koltay, P. Adhesive bonding of microfluidic chips: influence of process parameters. *Journal of Micromechanics and Microengineering* **20,** 087003 (2010).

157. Gong, X. *et al.* Wax-bonding 3D microfluidic chips. *Lab Chip* **10,** 2622–2627 (2010).
158. Young, E. W. K. & Beebe, D. J. Fundamentals of microfluidic cell culture in controlled microenvironments. *Chem Soc Rev* **39,** 1036–1048 (2010).
159. Walsh, D. I., III, Kong, D. S., Murthy, S. K. & Carr, P. A. Enabling Microfluidics: from Clean Rooms to Makerspaces. *Trends in Biotechnology* **35,** 383–392 (2017).
160. Waheed, S. *et al.* 3D printed microfluidic devices: enablers and barriers. *Lab Chip* **16,** 1993–2013 (2016).
161. Bartholomeusz, D. A., Boutte, R. W. & Andrade, J. D. Xurography: rapid prototyping of microstructures using a cutting plotter. *Journal of Microelectromechanical Systems* **14,** 1364–1374 (2005).
162. Swain, J. E., Lai, D., Takayama, S. & Smith, G. D. Thinking big by thinking small: application of microfluidic technology to improve ART. *Lab Chip* **13,** 1213–1224 (2013).
163. Paguirigan, A. L. & Beebe, D. J. Microfluidics meet cell biology: bridging the gap by validation and application of microscale techniques for cell biological assays. *Bioessays* **30,** 811–821 (2008).
164. Schulte, P. M. The effects of temperature on aerobic metabolism: towards a mechanistic understanding of the responses of ectotherms to a changing environment. *J. Exp. Biol.* **218,** 1856–1866 (2015).
165. Sengupta, P. & Garrity, P. Sensing temperature. *Curr. Biol.* **23,** R304–7 (2013).
166. Tazawa, H., Sato, K., Tsutiya, A., Tokeshi, M. & Ohtani-Kaneko, R. A microfluidic cell culture system for monitoring of sequential changes in endothelial cells after heat stress. *Thromb. Res.* **136,** 328–334 (2015).
167. Charvin, G., Cross, F. R. & Siggia, E. D. A microfluidic device for temporally controlled gene expression and long-term fluorescent imaging in unperturbed dividing yeast cells. *PLoS ONE* **3,** e1468 (2008).
168. Angione, S. L., Oulhen, N., Brayboy, L. M., Tripathi, A. & Wessel, G. M. Simple perfusion apparatus for manipulation, tracking, and study of oocytes and embryos. *Fertil. Steril.* **103,** 281–90.e5 (2015).
169. Fang, C., Ji, F., Shu, Z. & Gao, D. Determination of the temperature-dependent cell membrane permeabilities using microfluidics with integrated flow and temperature control. *Lab Chip* **17,** 951–960 (2017).
170. de Mello, A. J., Habgood, M., Lancaster, N. L., Welton, T. & Wootton, R. C. R. Precise temperature control in microfluidic devices using Joule heating of ionic liquids. *Lab Chip* **4,** 417–419 (2004).
171. Vigolo, D., Rusconi, R., Piazza, R. & Stone, H. A. A portable device for temperature control along microchannels. *Lab Chip* **10,** 795–798 (2010).
172. Lin, L., Wang, S.-S., Wu, M.-H. & Oh-Yang, C.-C. Development of an integrated microfluidic perfusion cell culture system for real-time microscopic observation of biological cells. *Sensors (Basel)* **11,** 8395–8411 (2011).
173. Tazawa, H., Sunaoshi, S., Tokeshi, M., Kitamori, T. & Ohtani-Kaneko, R. An Easy-to-Use Polystyrene Microchip-based Cell Culture System. *Anal Sci* **32,** 349–353 (2016).
174. Mao, H., Yang, T. & Cremer, P. S. A microfluidic device with a linear temperature gradient for parallel and combinatorial measurements. *J. Am. Chem. Soc.* **124,** 4432–4435 (2002).
175. Das, S. K., Chung, S., Zervantonakis, I., Atnafu, J. & Kamm, R. D. A microfluidic platform for studying the effects of small temperature gradients in an incubator environment. *Biomicrofluidics* **2,** 034106 (2008).
176. Yang, J. *et al.* High sensitivity PCR assay in plastic micro reactors. *Lab Chip* **2,** 179–187 (2002).
177. Maltezos, G. *et al.* Exploring the limits of ultrafast polymerase chain reaction using liquid for thermal heat exchange: A proof of principle. *Appl Phys Lett* **97,** 264101 (2010).
178. Velve-Casquillas, G., Costa, J., Carlier-Grynkorn, F., Mayeux, A. & Tran, P. T. A fast microfluidic temperature control device for studying microtubule dynamics in fission yeast. *Methods Cell Biol.* **97,** 185–201 (2010).
179. Velve-Casquillas, G. *et al.* Fast microfluidic temperature control for high resolution live cell imaging. *Lab Chip* **11,** 484–489 (2011).
180. Houssin, T. *et al.* Ultrafast, sensitive and large-volume on-chip real-time PCR for the molecular diagnosis of bacterial and viral infections. *Lab Chip* **16,** 1401–1411 (2016).

181. Eribol, P., Uguz, A. K. & Ulgen, K. O. Screening applications in drug discovery based on microfluidic technology. *Biomicrofluidics* **10,** 011502 (2016).
182. Kim, L., Toh, Y.-C., Voldman, J. & Yu, H. A practical guide to microfluidic perfusion culture of adherent mammalian cells. *Lab Chip* **7,** 681–694 (2007).
183. Du, G., Fang, Q. & Toonder, den, J. M. J. Microfluidics for cell-based high throughput screening platforms - A review. *Anal. Chim. Acta* **903,** 36–50 (2016).
184. Lee, K. *et al.* Gravity-oriented microfluidic device for uniform and massive cell spheroid formation. *Biomicrofluidics* **6,** 14114–141147 (2012).
185. Hung, P. J., Lee, P. J., Sabounchi, P., Lin, R. & Lee, L. P. Continuous perfusion microfluidic cell culture array for high-throughput cell-based assays. *Biotechnol. Bioeng.* **89,** 1–8 (2005).
186. Tourovskaia, A., Figueroa-Masot, X. & Folch, A. Differentiation-on-a-chip: a microfluidic platform for long-term cell culture studies. *Lab Chip* **5,** 14–19 (2005).
187. Xu, X. *et al.* Probing the cytoadherence of malaria infected red blood cells under flow. *PLoS ONE* **8,** e64763 (2013).
188. VANSTEIJN, V., KREUTZER, M. & KLEIJN, C. Velocity fluctuations of segmented flow in microchannels. *Chemical Engineering Journal* **135,** S159–S165 (2008).
189. Jensen, M. J., Goranovi, G. & Bruus, H. The clogging pressure of bubbles in hydrophilic microchannel contractions. *Journal of Micromechanics and Microengineering* **14,** 876–883 (2004).
190. Lochovsky, C., Yasotharan, S. & G nther, A. Bubbles no more: in-plane trapping and removal of bubbles in microfluidic devices. *Lab Chip* **12,** 595–601 (2012).
191. Schönburg, M. *et al.* Significant reduction of air microbubbles with the dynamic bubble trap during cardiopulmonary bypass. *Perfusion* **16,** 19–25 (2001).
192. van Lintel, H., Mernier, G. & Renaud, P. High-Throughput Micro-Debubblers for Bubble Removal with Sub-Microliter Dead Volume. *Micromachines* **3,** 218–224 (2012).
193. Sung, J. H. & Shuler, M. L. Prevention of air bubble formation in a microfluidic perfusion cell culture system using a microscale bubble trap. *Biomed Microdevices* **11,** 731–738 (2009).
194. Skelley, A. M. & Voldman, J. An active bubble trap and debubbler for microfluidic systems. *Lab Chip* **8,** 1733 (2008).
195. Steward, R., Tambe, D., Hardin, C. C., Krishnan, R. & Fredberg, J. J. Fluid shear, intercellular stress, and endothelial cell alignment. *Am. J. Physiol., Cell Physiol.* **308,** C657–64 (2015).
196. Shemesh, J. *et al.* Flow-induced stress on adherent cells in microfluidic devices. *Lab Chip* **15,** 4114–4127 (2015).
197. Helmke, B. P., Goldman, R. D. & Davies, P. F. Rapid displacement of vimentin intermediate filaments in living endothelial cells exposed to flow. *Circulation Research* **86,** 745–752 (2000).
198. Yeh, C.-H., Tsai, S.-H., Wu, L.-W. & Lin, Y.-C. Using a co-culture microsystem for cell migration under fluid shear stress. *Lab Chip* **11,** 2583–2590 (2011).
199. Li, Y.-S. J., Haga, J. H. & Chien, S. Molecular basis of the effects of shear stress on vascular endothelial cells. *Journal of Biomechanics* **38,** 1949–1971 (2005).
200. Tsao, C.-W., Cheng, Y.-C. & Cheng, J.-H. Fluid Flow Shear Stress Stimulation on a Multiplex Microfluidic Device for Rat Bone Marrow Stromal Cell Differentiation Enhancement. *Micromachines* **6,** 1996–2009 (2015).
201. Tkachenko, E., Gutierrez, E., Ginsberg, M. H. & Groisman, A. An easy to assemble microfluidic perfusion device with a magnetic clamp. *Lab Chip* **9,** 1085–1095 (2009).
202. Leclerc, E., Sakai, Y. & Fujii, T. Microfluidic PDMS (polydimethylsiloxane) bioreactor for large-scale culture of hepatocytes. *Biotechnol. Prog.* **20,** 750–755 (2004).
203. Pawell, R. S., Inglis, D. W., Barber, T. J. & Taylor, R. A. Manufacturing and wetting low-cost microfluidic cell separation devices. *Biomicrofluidics* **7,** 56501 (2013).
204. Gao, Y. *et al.* A versatile valve-enabled microfluidic cell co-culture platform and demonstration of its applications to neurobiology and cancer biology. *Biomed Microdevices* **13,** 539–548 (2011).
205. Karajanagi, S. S. *et al.* Application of a dense gas technique for sterilizing soft biomaterials. *Biotechnol. Bioeng.* **108,** 1716–1725 (2011).
206. Khalili, A. A. & Ahmad, M. R. A Review of Cell Adhesion Studies for Biomedical and Biological Applications. *Int J Mol Sci* **16,** 18149–18184 (2015).
207. Gu, W., Zhu, X., Futai, N., Cho, B. S. & Takayama, S. Computerized microfluidic cell culture using elastomeric channels and Braille displays. *Proc. Natl. Acad. Sci. U.S.A.* **101,** 15861–15866

(2004).
208. Heino, J. The collagen family members as cell adhesion proteins. *Bioessays* **29,** 1001–1010 (2007).
209. Colville, K., Tompkins, N., Rutenberg, A. D. & Jericho, M. H. Effects of poly(L-lysine) substrates on attached Escherichia coli bacteria. *Langmuir* **26,** 2639–2644 (2010).
210. Bell, L. *et al.* A microfluidic device for the hydrodynamic immobilisation of living fission yeast cells for super-resolution imaging. *Sensors and Actuators B: Chemical* **192,** 36–41 (2014).
211. Jin, S. H. *et al.* Monitoring of chromosome dynamics of single yeast cells in a microfluidic platform with aperture cell traps. *Lab Chip* **16,** 1358–1365 (2016).
212. Nobs, J.-B. & Maerkl, S. J. Long-term single cell analysis of S. pombe on a microfluidic microchemostat array. *PLoS ONE* **9,** e93466 (2014).
213. Lee, P. J., Helman, N. C., Lim, W. A. & Hung, P. J. A microfluidic system for dynamic yeast cell imaging. *BioTechniques* **44,** 91–95 (2008).
214. Lee, P., Helman, N., Lim, W. & Hung, P. A microfluidic system for dynamic yeast cell imaging. *BioTechniques* **44,** 91–95 (2008).
215. Di Carlo, D., Aghdam, N. & Lee, L. P. Single-cell enzyme concentrations, kinetics, and inhibition analysis using high-density hydrodynamic cell isolation arrays. *Anal. Chem.* **78,** 4925–4930 (2006).
216. Tan, W.-H. & Takeuchi, S. A trap-and-release integrated microfluidic system for dynamic microarray applications. *Proc. Natl. Acad. Sci. U.S.A.* **104,** 1146–1151 (2007).
217. Nilsson, J., Evander, M., Hammarström, B. & Laurell, T. Review of cell and particle trapping in microfluidic systems. *Anal. Chim. Acta* **649,** 141–157 (2009).
218. Huang, G. Y. *et al.* Microfluidic hydrogels for tissue engineering. *Biofabrication* **3,** 012001 (2011).
219. Braschler, T., Johann, R., Heule, M., Metref, L. & Renaud, P. Gentle cell trapping and release on a microfluidic chip by in situ alginate hydrogel formation. *Lab Chip* **5,** 553 (2005).
220. Gong, Y., Su, K., Lau, T. T., Zhou, R. & Wang, D.-A. Microcavitary Hydrogel-Mediating Phase Transfer Cell Culture for Cartilage Tissue Engineering. *Tissue Engineering Part A* **16,** 3611–3622 (2010).
221. Zamora-Mora, V., Velasco, D., Hernández, R., Mijangos, C. & Kumacheva, E. Chitosan/agarose hydrogels: Cooperative properties and microfluidic preparation. *Carbohydrate Polymers* **111,** 348–355 (2014).
222. Chiu, Y.-C., Larson, J. C., Isom, A., Jr. & Brey, E. M. Generation of Porous Poly(Ethylene Glycol) Hydrogels by Salt Leaching. *Tissue Engineering Part C: Methods* **16,** 905–912 (2010).
223. Lu, H., Ko, Y.-G., Kawazoe, N. & Chen, G. Cartilage tissue engineering using funnel-like collagen sponges prepared with embossing ice particulate templates. *Biomaterials* **31,** 5825–5835 (2010).
224. Yue, Z. *et al.* Preparation of three-dimensional interconnected macroporous cellulosic hydrogels for soft tissue engineering. *Biomaterials* **31,** 8141–8152 (2010).
225. Wang, L. *et al.* Self-loading and cell culture in one layer microfluidic devices. *Biomed Microdevices* **11,** 679–684 (2009).
226. Kolnik, M., Tsimring, L. S. & Hasty, J. Vacuum-assisted cell loading enables shear-free mammalian microfluidic culture. *Lab Chip* **12,** 4732–4737 (2012).
227. Khan, O. F. & Sefton, M. V. Endothelial cell behaviour within a microfluidic mimic of the flow channels of a modular tissue engineered construct. *Biomed Microdevices* **13,** 69–87 (2011).
228. Inamdar, N. K., Griffith, L. G. & Borenstein, J. T. Transport and shear in a microfluidic membrane bilayer device for cell culture. *Biomicrofluidics* **5,** 022213 (2011).
229. de Jong, J., Lammertink, R. G. H. & Wessling, M. Membranes and microfluidics: a review. *Lab Chip* **6,** 1125–1139 (2006).
230. Bazzarelli, F., Giorno, L. & Piacentini, E. in *Encyclopedia of Membranes* **45,** 530–532 (Springer Berlin Heidelberg, 2016).
231. Chueh, B.-H. *et al.* Leakage-free bonding of porous membranes into layered microfluidic array systems. *Anal. Chem.* **79,** 3504–3508 (2007).
232. Heyderman, L. J. *et al.* High volume fabrication of customised nanopore membrane chips. *Microelectronic Engineering* **67-68,** 208–213 (2003).
233. Firpo, G., Angeli, E., Repetto, L. & Valbusa, U. Permeability thickness dependence of polydimethylsiloxane (PDMS) membranes. *Journal of Membrane Science* **481,** 1–8 (2015).
234. Ravetto, A., Hoefer, I. E., Toonder, den, J. M. J. & Bouten, C. V. C. A membrane-based microfluidic device for mechano-chemical cell manipulation. *Biomed Microdevices* **18,** 31 (2016).

235. Zheng, Y., Dai, W., Ryan, D. & Wu, H. Fabrication of freestanding, microperforated membranes and their applications in microfluidics. *Biomicrofluidics* **4,** 36504 (2010).
236. Epshteyn, A. A. *et al.* Membrane-integrated microfluidic device for high-resolution live cell imaging. *Biomicrofluidics* **5,** 46501–465016 (2011).
237. Chiang, H.-J., Yeh, S.-L., Peng, C.-C., Liao, W.-H. & Tung, Y.-C. Polydimethylsiloxane-polycarbonate Microfluidic Devices for Cell Migration Studies Under Perpendicular Chemical and Oxygen Gradients. *J Vis Exp* e55292–e55292 (2017). doi:10.3791/55292
238. Kimura, H., Yamamoto, T., Sakai, H., Sakai, Y. & Fujii, T. An integrated microfluidic system for long-term perfusion culture and on-line monitoring of intestinal tissue models. *Lab Chip* **8,** 741 (2008).
239. Vereshchagina, E., Mc Glade, D., Glynn, M. & Ducr e, J. A hybrid microfluidic platform for cell-based assays via diffusive and convective trans-membrane perfusion. *Biomicrofluidics* **7,** 034101 (2013).
240. Wang, C., Gao, X., Mawatari, K. & Kitamori, T. Clogging-Free Irreversible Bonding of Polycarbonate Membranes to Glass Microfluidic Devices. *Journal of The Electrochemical Society* **164,** B3087–B3090 (2017).

Results

Chapter 1: the wax chip

This chapter presents a novel PDMS-free microfluidic system dedicated to live-cell imaging. As the PDMS (polydimethylsiloxane), which is the most widely used material for microfluidic applications, has proven to be detrimental for cell proliferation, thermoplastic materials have emerged as replacements in microfluidics for performing experiments with live-cells. However, the fabrication of devices made of plastic, and especially the bonding of these rigid materials to glass coverslips, which are necessary for performing high-resolution microscopy, remains challenging. We have tested the compatibility of several materials with drugs commonly used in the laboratory, and we have chosen COC (cyclin olefin copolymer), which absorption of small molecules is negligible, allowing the possibility of injecting media with highly precise drug concentrations. In this chapter, we present a novel method for bonding this plastic COC to microscopy-grade glass coverslip using wax. The COC contains microchannels where cells are inserted, and is versatile, allowing complex channel designs and structures. We achieved a high degree of control of the microenvironment. Using the fission yeast *S. pombe*, we demonstrated the possibility of performing fast media switches. We also implemented a temperature control channel, which allows a precise and accurate temperature inside the system, and provides the possibility of performing fast media switches while observing cells at the microscope.

A drug-compatible and temperature-controlled microfluidic device for live-cell imaging
Tong Chen, Blanca Gomez-Escoda, Javier Munoz-Garcia, Julien Babic, Laurent Griscom, Pei-Yun Jenny Wu, Damien Coudreuse
Published in Open Biology 10 August 2016.DOI: 10.1098/rsob.160156

OPEN BIOLOGY

rsob.royalsocietypublishing.org

Research

Cite this article: Chen T, Gomez-Escoda B, Munoz-Garcia J, Babic J, Griscom L, Wu P-YJ, Coudreuse D. 2016 A drug-compatible and temperature-controlled microfluidic device for live-cell imaging. *Open Biol.* **6**: 160156. http://dx.doi.org/10.1098/rsob.160156

Received: 26 May 2016
Accepted: 11 July 2016

Subject Area:
biotechnology/cellular biology

Keywords:
live-cell imaging, cell biology, microfluidics, control of cellular environment, microscopy

Authors for correspondence:
Pei-Yun Jenny Wu
e-mail: pei-yun.wu@univ-rennes1.fr
Damien Coudreuse
e-mail: damien.coudreuse@univ-rennes1.fr

†These authors contributed equally to this study.

Electronic supplementary material is available at http://dx.doi.org/10.1098/rsob.160156.

THE ROYAL SOCIETY PUBLISHING

A drug-compatible and temperature-controlled microfluidic device for live-cell imaging

Tong Chen[1,†], Blanca Gomez-Escoda[2,†], Javier Munoz-Garcia[1,†], Julien Babic[1], Laurent Griscom[1], Pei-Yun Jenny Wu[2] and Damien Coudreuse[1]

[1]SyntheCell team, and [2]Genome Duplication and Maintenance team, Institute of Genetics and Development, CNRS UMR 6290, 2 avenue du Pr. Léon Bernard, 35043 Rennes, France

DC, 0000-0003-2534-1621

Monitoring cellular responses to changes in growth conditions and perturbation of targeted pathways is integral to the investigation of biological processes. However, manipulating cells and their environment during live-cell-imaging experiments still represents a major challenge. While the coupling of microfluidics with microscopy has emerged as a powerful solution to this problem, this approach remains severely underexploited. Indeed, most microdevices rely on the polymer polydimethylsiloxane (PDMS), which strongly absorbs a variety of molecules commonly used in cell biology. This effect of the microsystems on the cellular environment hampers our capacity to accurately modulate the composition of the medium and the concentration of specific compounds within the microchips, with implications for the reliability of these experiments. To overcome this critical issue, we developed new PDMS-free microdevices dedicated to live-cell imaging that show no interference with small molecules. They also integrate a module for maintaining precise sample temperature both above and below ambient as well as for rapid temperature shifts. Importantly, changes in medium composition and temperature can be efficiently achieved within the chips while recording cell behaviour by microscopy. Compatible with different model systems, our platforms provide a versatile solution for the dynamic regulation of the cellular environment during live-cell imaging.

1. Background

The study of cellular behaviours and interactions has been a central focus of biologists for almost 200 years, since the initial definition of the cell as the structural and functional unit of life by Schleiden and Schwann. Recent advances in microscopy have resulted in unprecedented insights into cell physiology and have led to ever more demanding experiments for the quantitative dissection of cellular events *in vivo*. In particular, direct monitoring of cells in real time in specific and changing environments has become a valuable strategy for understanding biological processes. In this context, novel approaches using microfluidic technologies coupled with high-resolution live-cell imaging provide the possibility to study cells at both single and multicellular levels while controlling cell growth and environmental stimuli [1–5]. For instance, the combination of microfluidic systems with chemical genetics is a powerful method to selectively perturb cellular function while observing the associated physiological responses. As microchip architecture is entirely customizable, these tools can be tailored to the needs of specific cell types, co-cultures and assays [6]. This versatile technology therefore offers the potential to manipulate cells and measure their behaviour in previously unachievable ways, and represents a key turning point in our investigation of cellular mechanisms.

However, despite its vast potential in biological research, microfluidics remains underexploited in cell biological studies, due in part to the restrictions intrinsic to currently available microsystems. In the field of microfluidics for the life sciences, the design and fabrication of microchips has largely relied on the use of a transparent polymer, polydimethylsiloxane (PDMS). PDMS rapidly became the most prevalent substrate in commercially available and laboratory produced microdevices, as it possesses a number of properties that make it a material of choice: it is easy to manipulate, even outside of high-end microfabrication facilities and clean rooms, and it can be reliably bonded via plasma treatment to glass coverslips, the ideal interface for high-resolution microscopy. In addition, the possibility to deform PDMS using pressure allows the integration of valves within microsystems [7]. Nevertheless, the use of PDMS can be problematic for in-chip cell culture and manipulation [4,8–10]. Leaching of uncrosslinked oligomers, deformation of channels and cell chambers, as well as gas permeability, which can lead to evaporation and changes in medium composition and osmolarity, are some of the well-documented disadvantages of PDMS that have implications for cell physiology. Even more prohibitive is the interference of PDMS with a number of compounds: its porous and hydrophobic nature contributes to a strong absorption of small molecules and adsorption of proteins [11,12]. As previously suggested, the features that allow such molecules to cross the cell membrane—their low molecular weight and hydrophobicity—are the same as those that favour absorption by PDMS [13]. The characteristics of PDMS-based devices therefore not only preclude the accurate use of a variety of compounds in microchips, but also call into question the control of growth conditions and cellular microenvironment. Indeed, the absorption, retention and subsequent slow release of molecules make it difficult to ensure quantitative and reliable results, counterbalancing the advantages offered by microfluidic technologies. To address this often overlooked though crucial issue, a number of studies have described post-fabrication processing and treatments of PDMS devices. All of these improve the compatibility of PDMS with chemical compounds [13–16], but as we show in this study, such methods are insufficient to resolve this critical problem.

Owing to the major disadvantages associated with PDMS, the search for alternative materials for microfabrication has gained interest and urgency [8,17,18]. One group of materials with clear potential is thermoplastics, which are impermeable and show limited interaction with the chemical compounds classically used in biological studies. Thermoplastics such as polystyrene (PS) have been widely employed in conventional cell culture and are found in a range of experimental products, from tubes to Petri dishes. Importantly, they are easy to prototype with simple and affordable techniques such as hot embossing, which involves the stamping of a micropattern into a heat-softened plastic polymer [8]. In fact, a number of thermoplastics have previously been integrated in cell culture microchips, including poly(methyl methacrylate) (PMMA) [19], polycarbonate (PC) [20], cyclic olefin copolymer (COC) [21] and PS [8,22]. To date, these materials have not replaced PDMS in imaging-driven experiments, despite their purity and favourable optical properties: unlike PDMS, they cannot be easily bonded to microscopy-grade glass coverslips.

In this study, we develop a method for the simple and cost-effective fabrication of microdevices dedicated to live-cell imaging that allow for dynamic temperature control and are compatible with the use of small molecules. First, we establish a sensitive cell-based assay to demonstrate that the treatment of PDMS with previously described methods is insufficient to counteract its absorption of small hydrophobic molecules. We then identify the thermoplastic COC and paraffin wax as biocompatible materials that do not interfere with these compounds, and we construct a cell microsystem consisting of a COC chip bonded to a glass coverslip using wax as a sealant. Its fabrication does not require a complex facility, and it can be adapted to different designs of microfluidic channels, including multi-level structures. This microdevice shows no absorption of chemical compounds in our biological assays, is able to sustain cell growth and proliferation for long periods for both yeast and human cells, and is fully compatible with fluorescence microscopy. It also integrates an additional microfluidic layer that allows for dynamic control of sample temperature both above and below ambient. We further demonstrate the possibility to perform in-chip media switches as cells remain under microscopic observation. Our method therefore provides a versatile microfluidic platform for live-cell imaging and lays the foundation for new ways to investigate biological processes through modulating the cellular environment while recording real-time responses in cellular behaviour.

2. Material and methods

2.1. Fission yeast strains and methods

Standard media and methods were used [23,24]. Strains used in this study were PN1 (*972 h*$^-$), DC240 (*leu1Δ:Pcdc13::cdc13-L-cdc2as::cdc13-3′UTR::ura4*$^+$ *cdc2Δ::kanMX6 cdc13Δ::natMX6 cig1Δ::ura4*$^+$ *cig2Δ::ura4*$^+$ *puc1Δ::ura4*$^+$ *ura4−D18 h*$^+$) [25], DC450 (*leu1Δ:Pcdc13::cdc13-L-cdc2as::cdc13-3′UTR::ura4*$^+$ *cdc2Δ::kanMX6 cdc13Δ::natMX6 cig1Δ::hphMX6 cig2Δ::kanMX6 puc1Δ::leu2*$^+$ *ura4-D18 h*$^+$), MBY7519 (*Pact1::LAmGFP::leu1*$^+$ *ade6-210 ura4-D18 leu1-32 h*$^+$) [26], PN292 (*cdc25-22 h*$^+$), PN2483 (*nda3-km311 h*$^-$) and JW1001 (*ura4::eGFP::pcn1*$^+$ *h*$^-$). The *cdc2* and *cdc13* deletions as well as the Cdc13-L-Cdc2 and the Cdc13-L-Cdc2as fusion proteins were previously described [25]. Deletions of the cyclin-encoding genes *cig1*, *cig2* and *puc1* in DC450 completely remove their coding sequences. The *cdc25-22* and *nda3-km311* mutations as well as the eGFP::Pcn1/PCNA fusion were previously described [27–29]. All experiments were carried out in minimal medium plus supplements (EMM6S) at 32°C except where otherwise noted. The 3-MBPP1 and 1-NmPP1 inhibitors (A602960 and A603003, Toronto Research Chemicals Inc.) were dissolved in DMSO at stock concentrations of 10 mM and added to liquid cultures at the indicated concentrations. For cell size measurements, live cells were stained with Blankophor (MP Biochemicals) except for figure 5*a*, where DIC images were used. Cell size was determined from microscopy images using Fiji (National Institutes of Health) and the Pointpicker plug-in.

2.2. Mammalian cell culture

For figure 5*c*, HeLa Kyoto cell lines stably expressing an H2B::mCherry fusion protein (from plasmid 21045, Addgene) were used (Gregory Eot-Houllier 2014, unpublished data).

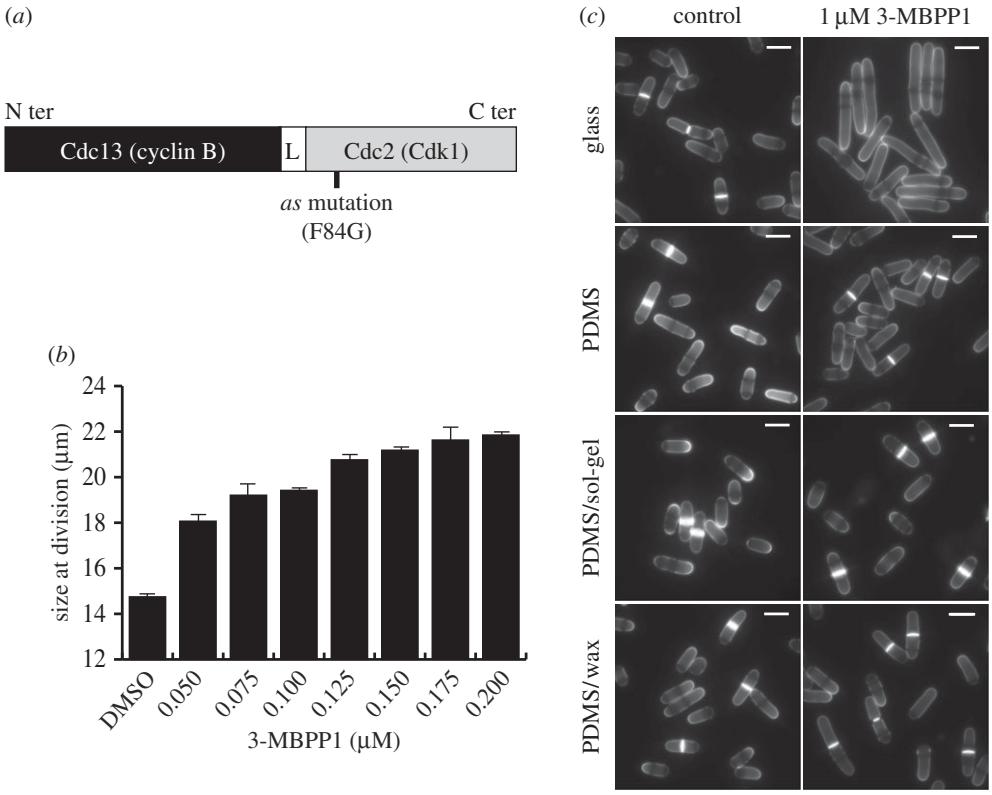

Figure 1. Standard treatments of PDMS are insufficient for preventing the absorption of small hydrophobic molecules. (*a*) Schematic representation of the Cdc13-L-Cdc2 fusion protein driving the fission yeast cell cycle in the strains used in this study (L = linker). The presence of the F84G mutation in the Cdc2 moiety of the protein renders the system sensitive to inhibition by characterized ATP analogues. *as*: analogue sensitive. (*b*) Cell size at division reflects the concentration of inhibitor to which cells are exposed. Batch cultures of cells operating with the inhibitor-sensitive cell cycle control module (Cdc13-L-Cdc2as fusion protein) were incubated with the indicated concentrations of 3-MBPP1 for 2 h 40 min at 32°C, and cell size at division was measured. Bars represent standard errors of three independent experiments ($n > 50$ for each independent experiment). (*c*) Drop assays were performed with inhibitor-sensitive cells on the indicated materials in the presence of 1 µM 3-MBPP1 for 2 h 40 min at 32°C. On glass, this resulted in G2 arrest with elongated, non-dividing cells. By contrast, cells grown on PDMS continued to divide, highlighting the strong absorption of such molecules by this polymer. Importantly, treatments of PDMS previously shown to limit absorption using fluorescent dye tests were revealed by this assay to be insufficient to prevent absorption, as cells kept dividing in the presence of the inhibitor. Blankophor staining. Scale bars, 10 µm.

Cells were grown in DMEM GlutaMAX (Gibco) with 10% FCS and 0.5 µg ml^{-1} puromycin. To assess the biocompatibility of the materials in our microdevices with these cells, single-channel (two ports, 300 µm wide, 40 µm high) COC/wax chips were first rinsed with growth medium, and cells were loaded at one port and allowed to fill the channels by applying a vacuum on the opposite port of the chips. The entire devices were then incubated in humid chambers at 37°C in a CO_2 incubator, with 300 µl drops of medium deposited at each of the ports every 12 h to prevent evaporation and drying of the samples. As a control, cells were inoculated at a similar starting density in glass bottom dishes (Mat Tek Corporation) and grown at 37°C.

2.3. Microscopy

All microscopy experiments were performed on an inverted Zeiss Axio Observer (Carl Zeiss Inc.) equipped with a Lumencor Spectra X illumination system (figures 1–5*b* and 7; electronic supplementary material, figures S1 and S3) or a laser bench (Visitron GmbH) and spinning disc confocal head (figure 5*c*; electronic supplementary material, figure S4). Images were acquired with a Hamamatsu Orca Flash 4.0V2 sCMOS camera through VisiView (Visitron GmbH) and subsequently analysed using Fiji.

2.4. Microfabrication materials

PDMS was prepared from the Sylgard 184 silicone elastomer kit (Dow Corning, USA). Styrene-ethylene/butylene-styrene (SEBS) blocks are a product of Kraton Polymer. NOA81 UV glue is a product of Norland Products Inc. (USA). COC pellets and sheets (Topas 5013) were purchased from Topas Advanced Polymers Inc. (USA). Paraffin wax (#411663) was purchased from Sigma-Aldrich (USA). Dymax UV glue is a product of Dymax Corp. (USA). Superglue is a cyanoacrylate-based glue from Loctite (Henkel, Germany). PR5 is a cyanoacrylate-based glue from 3M (USA). The double-sided adhesive tape used for the temperature control layer is ARcare 90445 from Adhesive Research Inc. (USA). Extruded PMMA for the fabrication of the manifold was purchased from Weber-Metaux (France).

2.5. Polydimethylsiloxane treatments, styrene-ethylene/butylene-styrene preparation and NOA81 chip fabrication

For sol-gel treatment [13], PDMS blocks were immersed in pure TEOS (Sigma-Aldrich) for 30 min under constant shaking. The treated blocks were then rapidly rinsed with ethanol followed by deionized water. They were subsequently immersed in a 4% (v/v) solution of methylamine (Sigma-Aldrich) for a

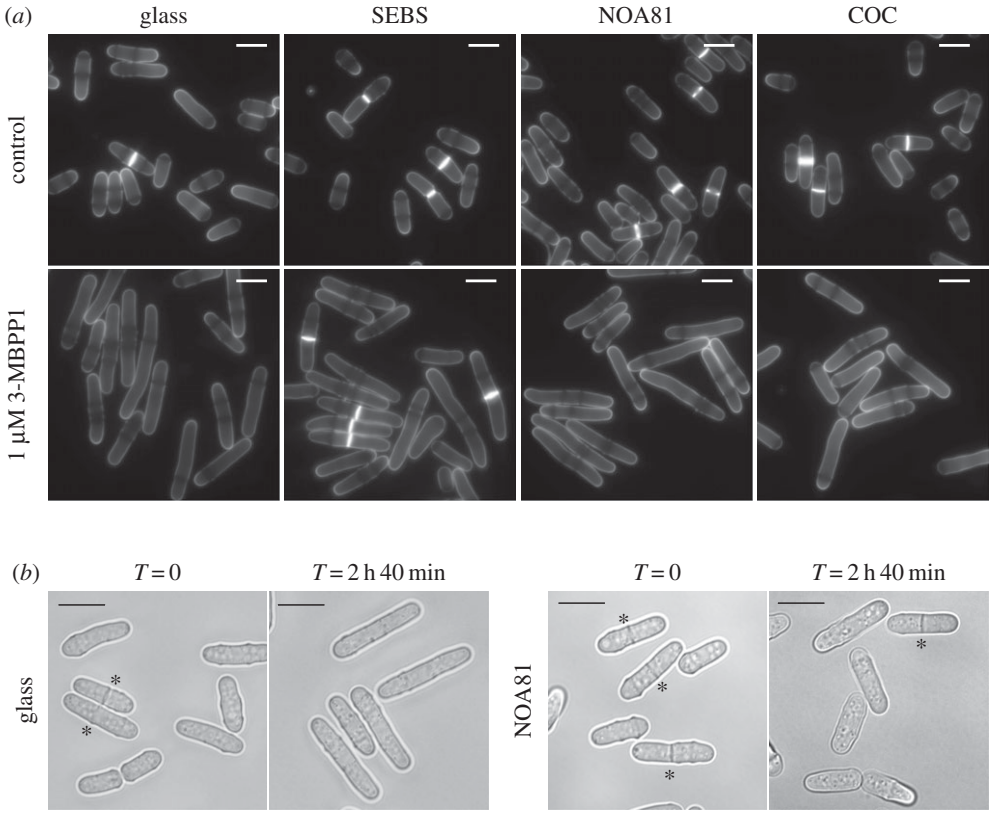

Figure 2. Identification of alternative materials for microfabrication. (*a*) Drop assays using inhibitor-sensitive cells on the indicated materials in the presence of 1 µM 3-MBPP1 for 2 h 40 min at 32°C. While cells on SEBS kept dividing, although at a longer size, cells on glass, NOA81 and COC showed a complete arrest of the cell cycle, suggesting no absorption of the molecule. Blankophor staining. Scale bars, 10 µm. (*b*) Inhibitor-sensitive cells were grown in microfluidic channels made of NOA81 in the presence of 1 µM 3-MBPP1 for 2 h 40 min at 32°C. In contrast with the experiment in (*a*), these cells kept dividing despite the presence of the compound, showing its significant absorption by NOA81 at a high surface area to volume ratio. Asterisks indicate septated (dividing) cells. DIC images. Scale bars, 10 µm.

minimum of 15 h, and then in water for 24 h to ensure biocompatibility [13]. For paraffin wax treatment, PDMS blocks were immersed for 5 min in pure paraffin wax melted in a glass container at 100°C, removed from the solution and allowed to cool down to room temperature [15]. For preparing SEBS layers, SEBS was dissolved in toluene (20–35%) and de-gassed under vacuum for 5–10 min. Dissolved SEBS was deposited on a glass slide and baked at 60°C for 5 h and then 95°C for 8 h [17]. Full NOA81 chips mounted on glass coverslips were fabricated as described [31].

2.6. Screening for materials compatible with small molecules

All the initial tests for small molecule absorption (figures 1, 2*a*, 3*a–c*; electronic supplementary material, figure S1) were performed using 'drop assays': exponentially growing cells were treated with the indicated concentrations of inhibitor and 10–20 µl drops of the cultures were immediately and directly deposited on the indicated materials. The set-ups were then incubated in humid chambers at the appropriate temperatures, and samples were taken for analyses of cell proliferation and size at division at the indicated times. For the LatA experiment in figure 3*d*, 1.5 µl of non-treated fission yeast cell cultures was deposited on the indicated substrates. LatA was then added to a final concentration of 50 µM (1.5 µl of 100 µM LatA) and coverslips were placed on the samples, allowing rapid live imaging of the effects of the drug.

2.7. Fabrication of polydimethylsiloxane moulds for cyclic olefin copolymer hot embossing and polydimethylsiloxane chips

PDMS moulds for hot embossing and PDMS chips were fabricated similarly by casting PDMS on SU-8 (2005 and 2050, MicroChem Corp., USA) master moulds as previously described [32]. Briefly, the master moulds were obtained by spin-coating thin layers of SU-8 (5–100 µm) on silicon wafers using a spincoater (Laurell Technologies, USA) according to manufacturer's instructions. Microstructures were then generated using high-resolution printed masks (JD phototools, UK) and 365 nm UV exposure (UV KUB 2, Kloe, France) followed by PGMEA (Sigma-Aldrich) development. The master moulds were then treated with trichloromethyl-silane (Acros Organics, Belgium) by vapour deposition (room temperature overnight under vacuum). PDMS moulds for hot embossing were produced by casting a 5 : 1 PDMS mixture on these SU-8 master moulds and curing at 75°C for 30 min followed by an additional baking step (200°C for 1 h). These moulds were used for direct hot embossing of COC at high temperatures (up to 200°C), accommodating pressures up to 1 tonne without significant deformation of the structures. PDMS chips were fabricated using a similar protocol, but with a 10 : 1 PDMS mixture and a single-step curing at 75°C for 1 h. For the mounting of closed PDMS devices, both chips and coverslips were plasma-treated for 1 min (Harrick Plasma), allowing direct and reliable bonding.

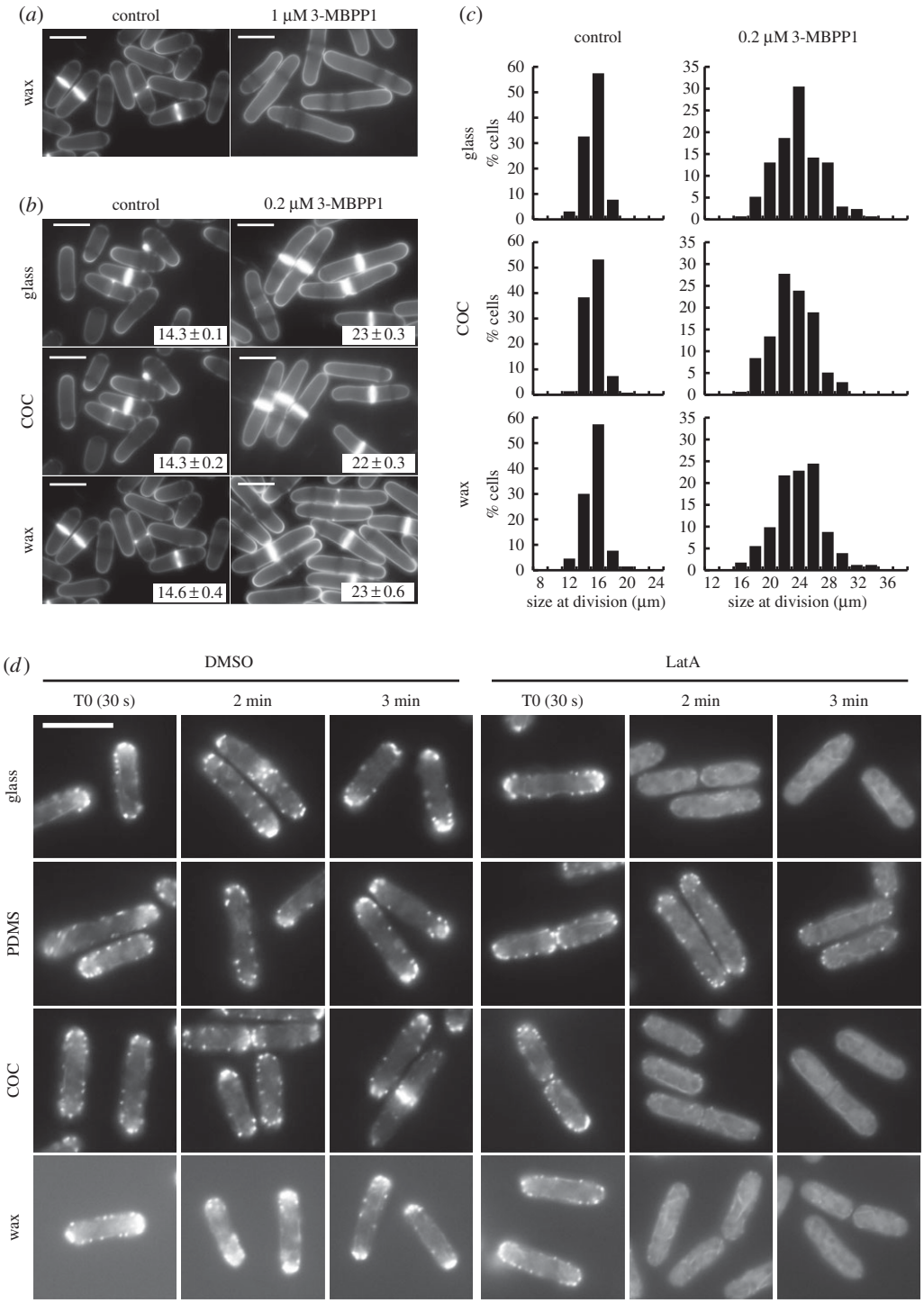

Figure 3. Paraffin wax as a sealant for bonding COC chips to glass coverslips. (*a*) Inhibitor-sensitive cells grown on a wax layer in the presence of 1 µM 3-MBPP1 behaved similarly to the glass control (drop assay, 2 h 40 min at 32°C, cf. figure 2*a*). Blankophor staining. Scale bars, 10 µm. (*b*) To confirm the lack of absorption, drop assays were performed on glass, COC and wax with 0.2 µM 3-MBPP1 for 2 h 40 min at 32°C, and cell size at division was determined. Images show cells stained with blankophor (scale bars, 10 µm) with the size at division in insets (average of three independent experiments; $n > 50$ for each experiment; standard errors are indicated). Drop assays were used in this study for material screening purposes. While they allow for rapid identification of promising materials, they show a higher variability than batch cultures or chip assays with regard to cell size at division. The difference observed between glass, COC and wax in this assay was not considered to be significant. This was further demonstrated by the results of figure 5*a*. (*c*) Size distribution in the populations of cells grown on glass, COC and wax in the presence of 0.2 µM 3-MBPP1 for 2 h 40 min at 32°C. Data are from the drop assays in figure 3*b* (includes all measurements from the three independent experiments in each assay). No differences were observed between the different materials. (*d*) Cells expressing the F-actin marker LAGFP [26,30] were treated with 50 µM LatA glass, PDMS, COC and wax and monitored by live-cell imaging (see Material and methods section for the specifics of the LatA assay). After 2 min, patches of F-actin were only visible in cells grown on PDMS. The stronger background fluorescence for the wax assay resulted from the poor optical properties of wax. Scale bar, 10 µm.

2.8. Fabrication of cyclic olefin copolymer chips

COC chips were fabricated using two different protocols. Initially, a thin sheet was generated from COC pellets (COC 5013) melted at 180°C under 16 MPa of pressure using a manual hydraulic press equipped with heated plates (Specac, UK). The obtained COC films of approximately 150–200 µm thickness were then placed on the PDMS moulds (see above)

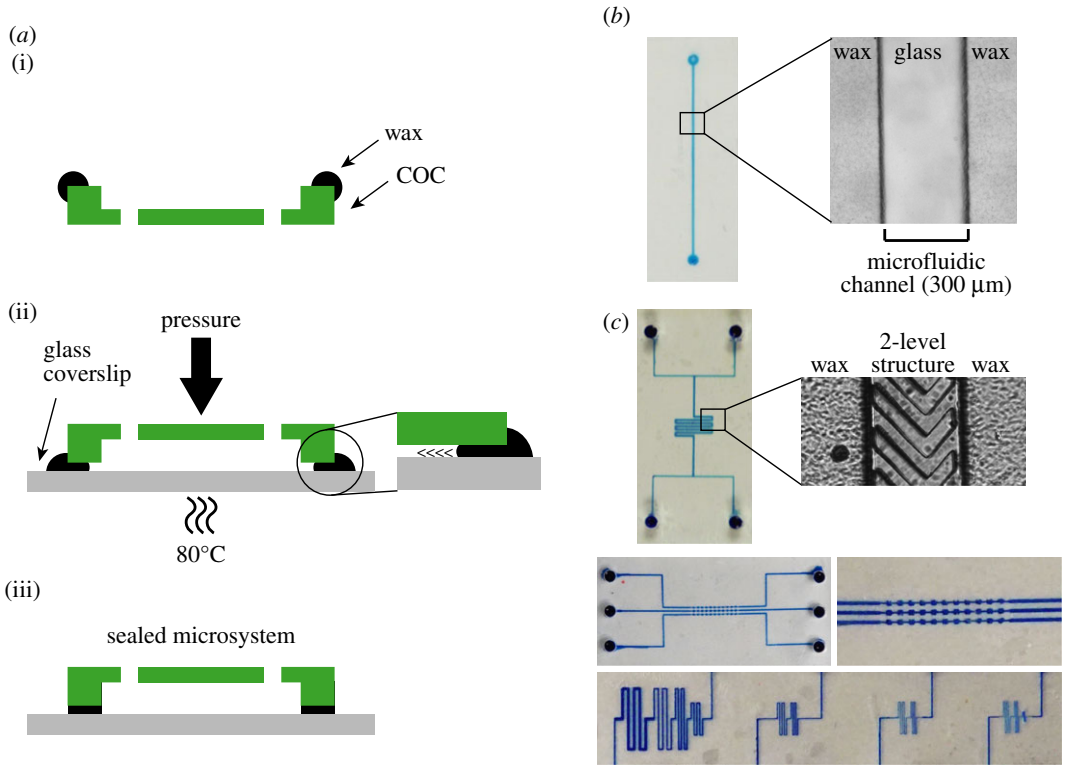

Figure 4. Fabrication of closed COC/wax microchips. (*a*) Schematic representation of the different steps of the wax-bonding protocol. (i) Pre-melted wax is deposited around the edge of the chip and allowed to rapidly harden at room temperature. (ii) The microsystem is then mounted on a glass coverslip and put under pressure on a hot plate at 80°C, allowing the wax to melt and spread between the COC chip and the glass coverslip. (iii) The microsystem is cooled to room temperature, generating a strongly sealed chip. (*b*) A single-channel (two ports, 300 µm wide and 40 µm high) microchip was mounted on a glass coverslip with the wax protocol. The flow of melted wax between the COC chip and the glass coverslip stopped when it encountered microchannels. Left: a bromophenol blue solution was injected for visualization. Right: microscopy image of the channel (transmitted light) showing the wax bonding. (*c*) The limits of the wax-bonding protocol were tested for channels of various sizes and structures as well as for multi-level devices (see the electronic supplementary material, figure S2, for detailed schematics of the test designs). In total, 40 µm in width and height were identified as the lower limits for the dimensions of channels required for the reliable bonding of the COC chips. Smaller structures could be achieved but with lower success rates.

and hot-embossed at 180°C under 250 kPa of pressure. This allowed faithful reproduction of all the microstructures tested. A single PDMS mould could be used to fabricate several COC chips. To generate more reproducible systems, we then switched to pre-made COC sheets of accurate thicknesses (150 and 250 µm, Topas Advanced Polymers Inc., USA) in which we directly hot-embossed the microchannels as described above.

2.9. Bonding of cyclic olefin copolymer chips to microscopy-grade coverslips

Classical methods such as thermo-bonding or solvent-bonding were first tested but remained unreliable for achieving proper adhesion to glass and for maintaining the integrity of small features in the COC chips. Paraffin wax was selected as a sealing material because it is biocompatible with no absorptive properties (see the Results section). To assemble the COC device on a glass coverslip, melted wax (melting temperature: 65°C) was deposited on the edge of the chip and allowed to harden. The microsystem was subsequently placed on a 0.17 mm microscopy-grade coverslip that had been pre-cleaned with isopropanol and dried for 20 min at 70°C. The set-up was then put on a hot plate at 80°C at the indicated pressures for 1–2 min, allowing spreading of the melted wax by capillary action and bonding of the whole chip upon return to room temperature. The thickness of the wax layer was determined using a profilometer (KLA-Tencor Alpha-step IQ surface profilometer). For the tests of bonding strength, water was injected in a closed chip at various pressures using a 0–2 bar pressure controller (Elvesys, France).

2.10. Structures of the microfluidic networks used in this study

For figures 5*b*,*c* and 6*b*, and electronic supplementary material, figure S3, we used a single-channel design (two ports, 300 µm wide, 40 µm high). For figures 2*b*, 5*a*, 6*c* and 7, and electronic supplementary material, figures S4 and S5, we used a design that was compatible with the maintenance of a flow of medium through the cell compartment of the chip without flushing out non-adherent fission yeast cells. This consisted of two parallel channels (500 µm wide, 40 µm high) to accommodate the flow of medium, connected to lateral cell chambers (165 × 300 µm, 12 µm high) through small channels (15 × 100 µm, 12 µm high). A flow of medium was applied for the experiments in figure 7*a*,*d*.

2.11. Rhodamine assay

For the Rhodamine assay in the electronic supplementary material, figure S3, 50 µM Rhodamine B (Sigma-Aldrich) was injected in the microchannels and incubated for 5 min. Rhodamine B was then thoroughly washed by flowing

(a)

	3-MBPP1		
	control	0.2 µM	1 µM
glass	13.8 ± 0.1	23.2 ± 0.2	arrested
PDMS chip	14.2 ± 0.0	15.6 ± 0.2	15.7 ± 0.4
COC chip	14.3 ± 0.2	23 ± 0.5	arrested

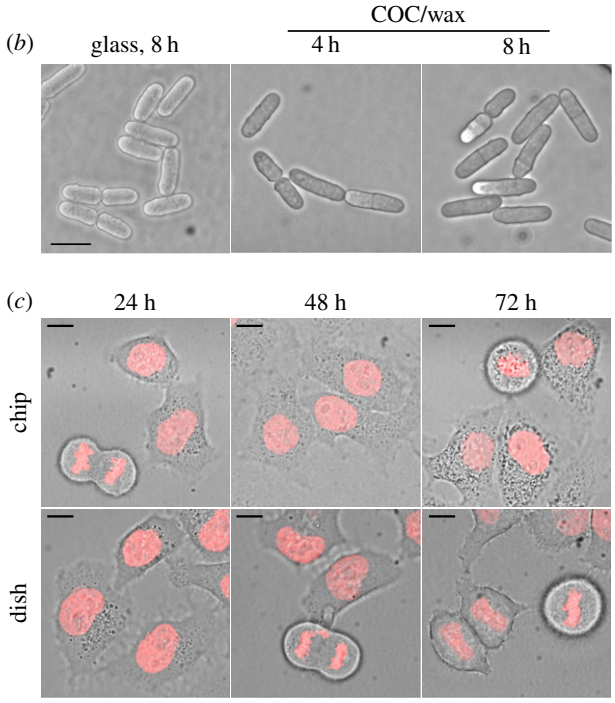

Figure 5. COC/wax microsystems are compatible with small molecules and can be used with different model systems. (*a*) Size at division (in micrometres) of inhibitor-sensitive cells grown at 32°C for 2 h 40 min in the presence of different concentrations of 3-MBPP1 in full PDMS or COC/wax microchips or between two glass coverslips. Average of three independent experiments with standard errors ($n > 50$ for each experiment). Identical results were obtained for glass and the COC/wax device, while PDMS showed strong absorption of the inhibitor. (*b*) Inhibitor-sensitive cells were grown in a closed COC/wax microchip at 32°C for 8 h. No defects in cell growth and morphology could be observed. DIC images. Scale bar, 10 µm. (*c*) HeLa cells expressing an H2B::mCherry fusion protein were grown in a COC/wax chip or in standard culture dishes for 72 h at 37°C. No differences between the two experimental set-ups were observed after 48 h, while a slight increase in the number of apoptotic cells was detected at 72 h in the chip, probably due to the very small volume of non-renewed growth medium in a gas-impermeable chamber. This could affect the pH, nutritional composition and/or partial pressure of oxygen and carbon dioxide in the medium. This assay demonstrated the possibility of performing live imaging of mammalian cells in our system for at least 48–72 h, and probably more if applying a constant flow of fresh medium through the chip to circumvent the problems mentioned above. Pictures are overlays of DIC images with maximum projections of Z stacks acquired to visualize H2B::mCherry. Scale bar, 10 µm.

10 ml of water through the microsystems. Fluorescence intensity was measured by microscopy.

2.12. Assembly and control of the thermalization system on cyclic olefin copolymer/wax chips

The temperature control system used in our devices consists of a large chamber (7 × 16 mm) through which a flow of water pre-thermalized by Peltier elements is constantly maintained [33]; this chamber is positioned above the cell compartment (figure 6*a*). It was produced by cutting 81 µm thick double-sided tape (ARcare 90445) using a 60 W CO_2 laser cutter (Speedy 100, Trotec, Austria). The pre-cut tape was then intercalated between the COC chip and a PMMA manifold (engineered from extruded PMMA plates of 6 mm thickness using the same laser cutter), paying particular attention to the alignment of all the ports required for the fluidic connections (figure 6*b*). The adhesion provided by the tape withstands a wide range of temperatures (10–70°C). Control of the flow rate and regulation of the temperature of the injected water was achieved using the CherryTemp system (Cherry Biotech, France). To bond the entire PMMA/temperature control/COC device to a glass coverslip, the same wax sealing protocol was used as for COC chips alone.

2.13. Calibration of the temperature control system

Calibration of the temperature control system required the measurement of the temperature of the sample directly within the microsystem. To this end, the complete COC microfluidic chips with the built-in temperature device were mounted on modified coverslips using the wax-bonding protocol. These consisted of standard microscopy-grade glass coverslips onto which a circuit of four electrodes linked to a resistance temperature detector (RTD) was fabricated by electrodeposition of successive metallic layers: (i) 5 nm titanium for adhesion; (ii) 70 nm platinum as a conductive element; (iii) 300 nm silicon nitride as an insulator; (iv) 2 µm Ag to reinforce the areas onto which the measurement device (model 34972A from Agilent Technologies) was connected [34].

We first calibrated the temperature detectors themselves, correlating the resistance of the RTD with its temperature, a relationship that is specific to each measurement system. To this end, the cell compartment of the chip was filled with water and a constant current was applied through two of the electrodes after precisely heating the entire microsystem to 24, 29 and 35°C (as determined by a thermistor) in incubation chambers. The voltage between the two other electrodes, which takes into account the RTD, was then measured. As the current was constant and the resistance varies linearly with the temperature, the changes in voltage directly reflected the changes in temperature.

This pre-calibrated set-up was then mounted on an inverted microscope, in contact with the oil on the immersion lens. This allowed us to determine the relationship between the temperature of the injected thermalization fluid (water, temperature measured by a PT100 sensor), the temperature of the microscope lens (measured by a second PT100 sensor) and the temperature within the microchambers (determined by the resistance of the electrodes). This was performed at 1°C intervals from 18°C to 40°C. We then established the linear equation linking the difference in temperature between the injected water and the lens with that between the sample and the lens. For a given objective temperature, this provides the exact temperature at which to set the Peltier elements in order to reach a specific target temperature in the cell compartment of any chip of the same design. Importantly, a minimum amount of oil was required to provide sufficient contact between the lens and the coverslip, and to ensure proper regulation of the temperature. Furthermore, we did not observe changes in the temperature

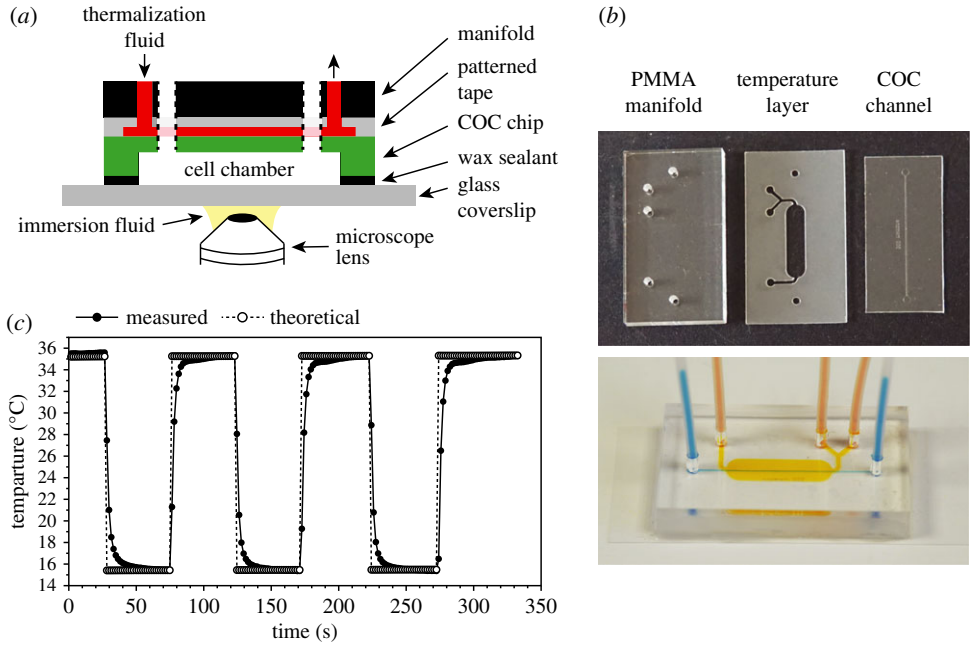

Figure 6. Integration of a microfluidic-based temperature control system. (*a*) Schematic representation of the full microsystem. Dashed lines represent the connections between the cell chamber and the manifold; the temperature channel is designed so that there is no fluid exchange between the cell (white) and thermalization (red) chambers. (*b*) Top panel: picture of the different elements constituting the device. Bottom panel: picture of a device mounted on a coverslip using the wax protocol. For ease of visualization, bromophenol blue and orange G dyes were injected in the cell compartment and thermalization channel, respectively. (*c*) Dynamics of temperature switches using the built-in temperature system. A COC/wax system was mounted on a glass coverslip containing temperature measurement electrodes (see Material and methods) and installed on the microscope stage, in contact with the oil of the immersion lens. The temperature within the microchannels was determined during a series of temperature shifts. The experimental data were compared with the calculated sample temperature (theoretical values) based on the measured lens and thermalization fluid temperatures at each time point and the calibration equation of the chip (similar to that provided as an example in electronic supplementary material, figure S5*a*).

when switching from a 63× to a 100× immersion lens (electronic supplementary material, figure S5*b*). Note that each type of thermalization fluid requires a specific calibration.

2.14. Temperature shift assays

For the temperature shift assays, cells were injected in the chips and the set-up was mounted on an inverted microscope. All subsequent changes in temperature (figure 7) were performed using the built-in temperature device while monitoring cell division in real time. For the control experiments with *cdc25-22* cells, batch cultures were grown at 25°C in glass flasks and shifted to 36.5°C by transfer to a pre-warmed water bath for 4 h. Release was achieved by rapidly cooling the cultures down to 25°C through shaking of the flasks in an ice/water mix prior to incubation in a 25°C water bath. For the *nda3-km311* mutant, cells grown at 32°C were shifted to the restrictive temperature of 18°C by transfer to a cooled water bath for 6 h. Release was achieved through rapid shift to a 32°C pre-warmed water bath.

3. Results

3.1. A sensitive biological readout for testing the compatibility of microfluidic systems with small molecules

A significant advantage of using microfluidics in experimental cell biology is the ability to finely and dynamically modulate the culture microenvironment, including the concentrations of specific compounds and biomolecules to which cells are exposed. In particular, the coupling of these technologies with chemical genetic strategies is poised to become a mainstream approach for the targeted regulation of cellular functions. One such method involves the specific inhibition of kinases through modifications in their catalytic pockets to accept bulky, non-reactive analogues [35–37]. These molecules bind only to the modified proteins, making possible the highly selective, dose-dependent and reversible alteration of enzyme activities. In the fission yeast *Schizosaccharomyces pombe*, we have previously engineered a system that allows for the control of cell proliferation using this technique [25]. In these cells, the Cdc2/Cdk1 protein, a conserved member of the cyclin-dependent protein kinase (CDK) family that drives both DNA replication and mitosis in fission yeast [29,38], is fused to the B-type cyclin Cdc13. This single protein module (referred to as Cdc13-L-Cdc2; L = linker) is sufficient to autonomously drive cell cycle progression. Importantly, incorporation of a mutation in the ATP binding pocket of the Cdc2 moiety of the fusion protein (Cdc2as, as: analogue sensitive) enables precise modulation of CDK activity levels through addition of non-hydrolysable ATP analogues (e.g. 1-NmPP1, 3-MBPP1) in the culture medium (figure 1*a*) [25]. Treatment with high concentrations of inhibitor results in a complete G2 block, where cells are elongated and show no nuclear or cell division [25] (also see figure 1*c*). At lower amounts, even modest alterations in inhibitor levels can be detected: small incremental increases in the applied doses of 3-MBPP1 result in cells that divide at increasingly longer sizes due to the induced mitotic delays (figure 1*b*).

In probing the possibility of using this system in the context of conventional PDMS-based chips, we evaluated

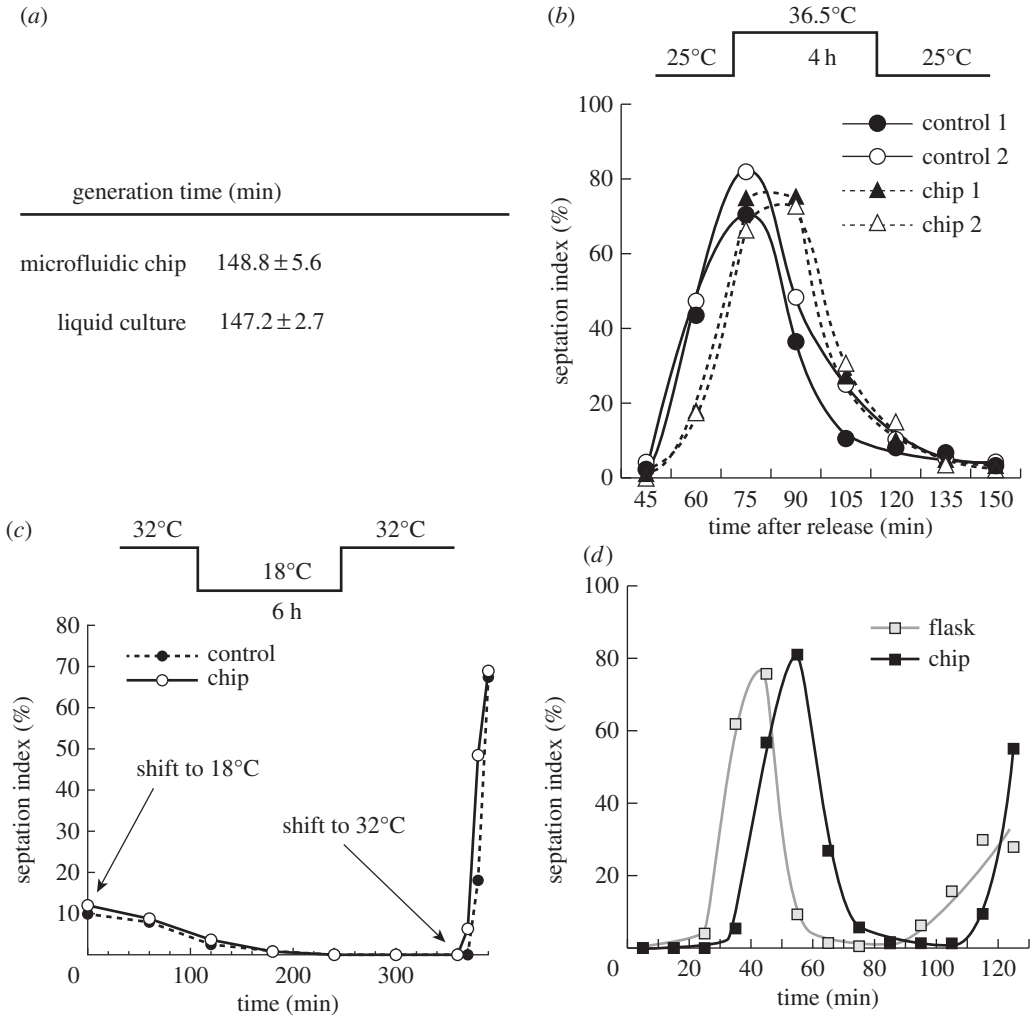

Figure 7. In-chip temperature and media switches. (*a*) Generation time of cells grown at 32°C in COC/wax chips with the built-in temperature control. Images were acquired every 5 min over several hours and division times were determined for 33 independent cells. Average generation time with standard deviation is shown. For the control liquid cultures, average of three experiments with standard error is shown. (*b,c*) Efficacy of the built-in thermalization system for shifting temperatures. (*b*) *cdc25-22* temperature-sensitive cells were blocked for 4 h at 36.5°C and released by shift down to 25°C using the temperature device. DIC images were acquired every 15 min, and septation index was monitored ($n > 80$ for each time point). No dividing cells were observed prior to and until 45 min after release (data not shown). (*c*) For below-ambient shifts, *nda3-km311* cold-sensitive cells were shifted from 32°C to 18°C for 6 h and released to 32°C. DIC images were acquired every hour during the 18°C block and every 10 min after release, and septation index was monitored ($n > 100$ for each time point). In (*b*) and (*c*), control cells grown in flasks were subjected to the same shifts (see Material and methods). Panel (*b*) shows two independent experiments for both chip and control. (*d*) Media switch during imaging. Analogue-sensitive cells initially grown at 32°C in batch cultures were injected in a microchip adapted to media switches (see Material and methods) and maintained at 32°C using the built-in temperature controller. Constant medium flow was applied at 40 µl min^{-1}. After 1 h, medium with 1 µM 3-MBPP1 was injected for 2 h 40 min, resulting in G2 arrest. Cells were then followed for 2 h after switching back to inhibitor-free medium ($T = 0$) and septation index was determined in DIC images ($n > 50$ for each point). While cells re-entered the cell cycle with a 5–10 min delay compared with the control due to medium exchange by diffusion rather than filtration, their synchrony was similar to that in the flasks.

the effect of the inhibitor on cells in contact with different substrates (referred to as a 'drop assay'; see the Material and methods section). While cells treated with 1 µM 3-MBPP1 and incubated on a glass coverslip showed complete arrest in G2 phase, as expected, the same concentration of inhibitor had no impact on cells on PDMS (figure 1*c*). Absorption was also observed with 1-NmPP1 (data not shown), which we previously used to efficiently inhibit the analogue-sensitive fusion protein [25]. This demonstrates that PDMS strongly interferes with these compounds, consistent with its documented absorption of a wide variety of molecules used in biological studies [8,11,12].

As treatments of PDMS have been previously proposed to address this issue [13,15,16], we assessed their efficacy using the drop assay. We focused on the two protocols that can be performed without high-end, complex and expensive equipment, and that were validated by standard fluorescent dye-based tests for molecule absorption [13,15]. Surprisingly, we found that coating PDMS with sol-gel, which produces a glass-like surface that increases its chemical resistance [13], did not result in any detectable improvement based on our biological readout (figure 1*c*). Similarly, adding a thin layer of paraffin wax onto PDMS, which has been suggested to provide a surface that limits small molecule absorption [15], had only minor effects (figure 1*c*). We also investigated a number of undocumented alternative treatments of PDMS, from silanization of the surface to coating with UV glues, none of which led to promising results based on either biocompatibility or interference with small molecules (data not shown). Taken together, our findings highlight the sensitivity of our cell-based approach compared with conventional analyses of molecule absorption and show that well-characterized PDMS treatments fail to provide a robust solution for this problem. We therefore took advantage of our biological assay to identify

alternative materials, focusing on those that may be suitable for using microfluidics in imaging-based, cell biological experiments.

3.2. Identification of alternative materials for microfabrication

To select new substrates for microfluidic devices compatible with live-cell microscopy, we exploited our chemical genetic system in fission yeast as a quantitative test for small molecule absorption. We chose three potential candidates based on their chemical nature, ease of manipulation, optical properties and previous reports of their integration in microdevices: (i) SEBS, a thermoplastic elastomer [17]; (ii) NOA81, a UV-glue that has been used in the microfabrication of complete NOA81/glass chips [31]; and (iii) COC, which is chemically resistant and commonly incorporated in a wide range of medical products [39]. Based on the same drop assay as above, our results demonstrated that SEBS provides a mild improvement compared with PDMS (compare figure 1*c* and figure 2*a*). By contrast, neither NOA81 nor COC exhibited small molecule interference: cells arrested in the cell cycle upon inhibitor treatment, identically to the glass control (figure 2*a*). However, while the drop assays are useful for screening purposes, they only evaluate the behaviour of cells deposited on flat substrates, at a low surface-area-to-volume ratio. This ratio is much higher in a microfluidic environment, increasing the impact of small molecule absorption by the microsystem. This prompted us to test the effect of the inhibitor within microchips in order to fully validate the selected materials. As protocols for the fabrication of complete NOA81/glass chips have previously been established [31], we assessed the absorption of 3-MBPP1 at high concentration (1 µM) in NOA81 channels. Interestingly, we found that cells continue to divide and do not arrest in the cell cycle in these conditions, thus excluding this UV-glue as a good candidate for PDMS-free microdevices (figure 2*b*). While COC remained a promising material for the fabrication of non-absorptive cell culture microsystems, similar 'in-chip' validation required the assembly of closed COC chips on glass. As mentioned previously, there are no methods for the reliable bonding of thermoplastic chips to glass, highlighting the need to develop a robust approach to mount such devices.

3.3. Construction of closed, microscopy-compatible cyclic olefin copolymer chips

Our results show that the thermoplastic COC does not interfere with small molecules in our assay, and its ability to be moulded to produce complex microfluidic networks makes it one of the best candidates for PDMS-free microchips. However, one of its limitations remains the lack of a simple method to seal it to glass coverslips, which is essential for its integration in microscopy set-ups. We therefore tested a number of glues and sealing materials, first assessing their biocompatibility using drop assays as above (electronic supplementary material, figure S1). Most of them induced cell death or changed cellular behaviour. Interestingly, paraffin wax, which has been used for the prototyping of basic microsystems [40–42], presented all the required characteristics for the fabrication of COC microdevices. First, it showed no absorption when using high concentrations of 3-MBPP1 inhibitor in drop assays (compare figure 3*a* and figure 2*a*). Moreover, at lower inhibitor concentrations, measurements of cell size at division further indicated that COC and wax are non-absorptive materials (figure 3*b*,*c*). We also tested the difference between glass, PDMS, COC and paraffin wax when using a fast-acting molecule with a dynamic readout that can be monitored more rapidly than that of our cell cycle assay. To this end, we treated cells with Latrunculin A (LatA), which triggers depolymerization of F actin (figure 3*d*) [26,30]. Both COC and wax behaved similarly to glass when cells were incubated with LatA. This is in contrast with cells on PDMS, where a clear delay in LatA action could be observed. Although the poor optical properties of wax render it less suitable for use as the primary material for microscopy-compatible systems, in particular in the context of multi-level devices, we hypothesized that it could serve as a sealant for mounting COC chips to glass.

To construct a closed COC microsystem on glass, we developed a method for using wax as a bonding compound. Paraffin wax melts at temperatures above 65°C, far below the transition temperature of the grade of COC ($T_g = 130$°C) used in our experiments. Owing to the speed with which melted wax hardens at room temperature, we found that stamping wax on the entire surface of the COC chip to seal it with a coverslip was unreliable, often leading to leaky or jammed channels. However, we reasoned that melted wax applied to the interface between the COC chip and the coverslip would spread by capillary action to bond the two surfaces. We also surmised that channels of a sufficient height and width would serve as barriers for the flow of wax, preventing it from filling the cell chambers. In our approach, small amounts of pre-melted wax were deposited on the edges of COC chips obtained by standard hot embossing (figure 4*a*; for the microfluidic networks used in this study, see Material and methods). After cooling and solidification of the wax, the systems were mounted on isopropanol-cleaned glass coverslips and placed on a hot plate at 80°C for 1–2 min under constant bonding pressure (see below). As anticipated, we observed melting and flowing of the wax between the two surfaces, with the wax front systematically stopping at the edge of the microfluidic channels (figure 4*b*). Upon return to room temperature, this adhesive layer provided strong bonding to produce a sealed microsystem (see below).

3.4. Physical and biological characterization of the cyclic olefin copolymer/wax chips

We next characterized the properties and potential limitations of the wax-mounted COC microsystems. First, we assessed the thickness of the intercalated wax layer as a function of the pressure applied during the assembly process (figure 4*a*). Pressures of approximately 4, 8 and 15 kPa were tested for these experiments. In all cases, the thickness of the bonding wax was in the range of a few micrometres, indicating that this technique can be applied to devices harbouring relatively fine structures (table 1). Lower bonding pressures (less than 4 kPa) increased the frequency of wax penetrating and clogging the channels, while higher bonding pressures (more than 15 kPa) led to small deformations of the COC microchannels; our results showed 4 kPa to be the most reliable. In addition, extending the time at 80°C was

Table 1. Physical characterization of the COC/wax chips. The thickness of the adhesive wax layer that resulted from using various pressures for mounting the chips (figure 4*a*) was measured using a profilometer. For each applied pressure, the indicated values are means and standard deviations of independent measurements for five chips.

mounting pressure (kPa)	wax thickness (μm)
4	11 ± 1.0
8	5 ± 0.5
15	4 ± 0.5

unnecessary and occasionally resulted in collapse of the microfluidic network. We then determined the bonding strength of the wax within the microsystems using a tensile load test. To this end, water was injected using a pressure controller in microsystems whose outputs were blocked. As a proxy for the maximum bonding strength, we evaluated the pressure required to detach the COC chip from the coverslip and generate leaks in the device (table 2). At temperatures commonly used in cell culture experiments (from 20°C to 40°C), our microchips withstood pressures up to 90 kPa, much greater than those used in standard microfluidic experiments: for instance, only 1.5 kPa was necessary to generate a high flow rate of 80 μl min^{-1} through the same test chips. Finally, we assessed the minimal size of microchannels required to delimit the spreading of melted wax during the mounting process. Using test COC chips with channels of different structures and dimensions (figure 4*c*; electronic supplementary material, figure S2), we found 40 μm to be the lower limit for both channel width and height to obtain reliable, non-obstructed microsystems. Smaller structures could also be efficiently mounted, although with a lower success rate. In addition, these assays demonstrated that our method can be used to fabricate complex microsystems, including multi-level and multi-channel chips (figure 4*c*; electronic supplementary material, figure S2). Apart from some limitations when very narrow or shallow microchannels are required, these data indicate that our platform is versatile and compatible with different applications and microfluidic circuits.

The successful assembly of complete COC/wax devices allowed us to ascertain their absorptive properties. As mentioned above, this is particularly important because interference with any small molecule is enhanced by the high surface-area-to-volume ratio in microfluidic systems. Analogue-sensitive cells (Cdc13-L-Cdc2as) were exposed to 0.2 and 1 μM of the 3-MBPP1 within a chip for 2 h 40 min (figure 5*a*). Cells in the COC/wax chips showed the same response to the inhibitor as those grown directly on a glass coverslip. This was in contrast to the results obtained with cells in PDMS chips, which remained largely unaffected by the addition of 3-MBPP1. This difference was also confirmed using the conventional Rhodamine-based absorption assay (electronic supplementary material, figure S3). These data demonstrate that our microfluidic systems permit the use of small molecules and offer a more precise control of the environment when growing and treating cells within microdevices.

Next, we investigated the ability of our microchips to sustain long-term cell growth. To this end, we assessed the proliferation of two different model systems: fission yeast and mammalian cells. Fission yeast cells that were maintained

Table 2. Bonding strength of the COC/wax chips. The bonding strength of the wax layer was determined by injecting medium at different pressures into microchips whose outputs were blocked. This was achieved using a high precision pressure control system (see Material and methods). '+' indicates no leaks. Pressures that are incompatible with our bonding method resulted in failure of the device ('leak'). To test the effect of temperature on the bonding strength, these experiments were performed at various temperatures using precision hot plates.

P (kPa)	20°C	33°C	37°C	40°C
10	+	+	+	+
15	+	+	+	+
20	+	+	+	+
25	+	+	+	+
30	+	+	+	+
35	+	+	+	+
40	+	+	+	+
45	+	+	+	+
50	+	+	+	+
55	+	+	+	+
60	+	+	+	+
65	+	+	+	+
70	+	+	+	+
75	+	+	+	+
80	+	+	+	+
85	+	+	+	+
90	+	+	+	+
95	+	+	+	leak
100	+	+	+	leak

in our microdevice at an optimal growing temperature of 32°C for 8 h (approx. three generations) showed no apparent phenotypes (figure 5*b*). Similarly, HeLa cells were observed to grow and proliferate in a wax-bonded COC chip at 37°C (figure 5*c*). Over a period of 48 h, we did not detect any differences between cells in the chip and the control culture. After 72 h, while cells in the microdevice continued to divide, there was a slight increase in the number of apoptotic cells (data not shown). While this may represent an intrinsic limitation of our device, the application of a constant flow to renew the medium in the chip may resolve this issue.

Finally, we validated our complete system for fluorescence microscopy applications. First, compared with glass, COC itself did not increase background fluorescence at the most commonly used excitation wavelengths (table 3; see glass, PDMS and COC). Second, we acquired images of cells harbouring fluorescently tagged proteins in chips and on glass coverslips. Using as a reference an eGFP-Pcn1/PCNA fusion protein, which forms discrete foci during S phase, we obtained similar results between glass, PDMS and COC/wax chips, with no detectable differences in signal to noise ratio (electronic supplementary material, figure S4).

Taken together, these experiments demonstrate the advantages of our COC/wax chips, which are compatible with small compounds, provide a reliable control of the cell culture conditions and are adapted for live-cell imaging studies using different biological models.

Table 3. Background fluorescence in microdevices. For these measurements, culture medium was injected between two coverslips (glass), between a coverslip and a thin layer of PDMS (PDMS) or COC (COC), and within full PDMS (PDMS full) and COC/wax chips integrating the temperature control (COC full). The indicated values are means and standard deviations (more than 2000 points along a diagonal line scan). All images were acquired with a spinning disc confocal microscope (300 ms exposure at 20% laser power).

	excitation wavelengths				
	405	445	488	515	561
glass	101.1 ± 1.9	100.3 ± 1.6	102.4 ± 2.3	100.7 ± 1.8	100.6 ± 1.8
PDMS	101 ± 1.9	100.3 ± 1.7	102.3 ± 2.2	100.7 ± 1.9	100.6 ± 1.7
COC	101 ± 1.9	100.3 ± 1.8	102.2 ± 2.1	100.7 ± 1.8	100.6 ± 1.8
PDMS full	103 ± 2.5	100.4 ± 1.9	102.4 ± 2.3	100.6 ± 1.8	100.7 ± 2
COC full	103 ± 2.4	100.3 ± 1.6	102.4 ± 2.4	100.7 ± 1.8	100.6 ± 1.8

3.5. Implementation of a thermalization layer

While our microsystem allows for the regulation of different aspects of the cell environment, it is also critical to control the temperature of the biological sample during microscopy experiments. Although there are a number of methods to achieve this, including incubation chambers and heated platforms, few are compatible with the rapid changes in temperature necessary for the use of temperature-sensitive mutations and with experiments that must be performed below-ambient temperature. We therefore extended our COC/wax device, adding a built-in, microfluidic-based temperature control unit. This system consists of a miniaturized thermalization chamber mounted above the cell culture channels (figure 6*a*) that accommodates a flow of water cooled or heated to a target temperature by Peltier elements [33]. This layer was produced by cutting channels in a sheet of double-sided medical adhesive (figure 6*b*; see Material and methods), and it was intercalated between the COC chip and a micromanifold made of PMMA (figure 6*a*,*b*). To favour heat exchange between the thermalization and sample compartments, we limited the thickness of the COC layer above the cell culture channels to 200 µm (see Material and methods). These additional elements did not increase the fluorescence background (table 3, COC full).

For accurate control of the sample temperature, it is crucial to account for the heat exchanges that occur between the device and its surroundings, in particular through contact between the coverslip and the microscope objective when using an immersion lens. We therefore calibrated our system by establishing the relationships between (i) the temperature of the water set by the Peltier elements, (ii) the temperature of the microscope lens in contact with the device through the immersion fluid and (iii) the temperature of the sample [33] (electronic supplementary material, figure S5*a*). A detailed description of the calibration protocol is presented in the Material and methods section. It integrates metal electrodes that are deposited on the microsystem's coverslip, allowing for direct measurements of the temperature in the cell chambers. For a given lens temperature, this calibration establishes the temperature that must be imposed by the Peltier elements in order to achieve the proper target temperature in the cell channels. We noted that switching the lens had no effect on the sample temperature (electronic supplementary material, figure S5*b*), suggesting that the use of different objectives does not require specific calibrations. Importantly, once this procedure has been performed for a microsystem, it remains valid for any chip of the same design. Next, we assessed the capacity of our microdevice to produce rapid and accurate temperature switches. Taking advantage of the same electrodes as those used for the calibration procedure, we measured the kinetics and reproducibility of the shifts. Sample temperature was within 0.5°C of the target temperature in 10–15 s when shifting down and in 15–25 s when shifting up (figure 6*c*). These results showed that our microchip allows for tight and dynamic control of the temperature of the sample at the microscope.

3.6. Temperature and medium control in a biological context

The data presented so far suggest that our microdevice could be a powerful platform for controlling the cellular environment during live-cell imaging experiments, and we validated its use in a biological context. First, we tested the ability of the system to maintain a constant temperature, taking advantage of the well-characterized generation time of fission yeast cells in minimal medium at 32°C. The division time of cells grown in the chips was determined by live-cell imaging and compared with standard batch cultures. To prevent any potential nutritional bias, a constant flow of fresh medium was applied throughout the experiment (10 µl min^{-1}; at this flow rate, we observed no influence of the injection of medium on the temperature of the sample; see electronic supplementary material, figure S5*c*). This required the use of a specific chamber design in which non-adherent cells are maintained outside of the direct path of the flow of medium (see Material and methods). Our results showed identical cell cycle times between the two approaches, validating the stability of our system for sustaining a given temperature (figure 7*a*).

To evaluate the performance of the temperature shift, we then conducted experiments using temperature-sensitive fission yeast mutants (figure 7*b*,*c*). The *cdc25-22* mutation [29] inactivates the Cdc25 phosphatase, required for entry into mitosis [43], at a restrictive temperature of 36.5°C. *cdc25-22* cells proliferate at the permissive temperature of 25°C, and shifting to 36.5°C results in G2 arrest and cell elongation. After 4 h at restrictive temperature, a shift back to the permissive temperature allows for the activation of the mitotic machinery and synchronous cell cycle re-entry [44]. In addition, to test the use of the system for temperatures

below ambient, we assayed a cold-sensitive mutation of *nda3*, which encodes for beta tubulin. The *nda3-km311* mutant proliferates normally at 32°C, while growth at 18°C results in a mitotic block [27]. After 6 h at the restrictive temperature, a shift back to 32°C results in synchronous progression through mitosis and the subsequent cell cycle phases. When these strains were subjected to the appropriate temperature shifts in the microfluidic chips using the integrated temperature control system, we found that the timing and synchrony of cell cycle progression were similar to standard experiments performed with batch cultures grown in glass flasks (figure 7*b*,*c*). These analyses demonstrate the ability of our device to generate rapid and accurate changes in temperature both above and below ambient. This not only enables the use of heat- and cold-sensitive mutations during live-cell imaging but also makes possible the assessment of temperature-sensitive processes in real time.

Finally, we demonstrated that our system allows for in-chip media switches, using treatment with 3-MBPP1 as an assay. Inhibitor block followed by release into normal medium in batch cultures is a well-characterized method for obtaining synchronous populations of cells [25]. Cells initially maintained at 32°C with a constant flow rate of fresh medium within the chip were arrested for 2 h 40 min by switching to medium containing 1 µM inhibitor. As expected, this resulted in complete cell cycle arrest, with cells elongating without undergoing mitosis. Switching back to inhibitor-free medium resulted in synchronous entry into the cell cycle (figure 7*d*). A small delay in this process was observed when using the chip, resulting from the time required for medium exchange by diffusion compared with filtration in the control cultures. This is inherent to microfluidic devices designed to avoid mechanical and shear stresses that can be induced if cells are maintained directly in the medium flow. However, the degree of synchrony was identical to that obtained when filtering batch cultures. Importantly, all the different shifts were performed while cells were under microscopic observation. Taken together, these results demonstrate that our microsystem allows for the dynamic control of both the temperature and medium composition during live-cell-imaging experiments. Coupling various media and temperature changes represents a powerful approach to study complex processes at the cell biological level.

4. Discussion

The introduction of microfluidic approaches in the life sciences has resulted in exciting possibilities for the investigation of cellular behaviour. By allowing for the control of cell growth and external stimuli at high temporal and spatial resolution, these methodologies pave the way for a new quantitative dimension in cell biology. One essential aspect of these technologies is the ability to reproducibly manipulate the cellular environment in customized microsystems. Paradoxically, the most widely used material for microfluidics, PDMS, has been shown to interfere with a variety of compounds. This is particularly true for small hydrophobic molecules, a class that includes a large number of cell biological reagents. For microscopy-based experiments, no effective solutions were available. In this context, finding alternatives to PDMS-based microsystems has become essential for exploiting the full potential of microfluidic devices. In this study, we have used one such small hydrophobic molecule, the ATP analogue 3-MBPP1, as a model compound to establish a sensitive and quantitative cell-based assay for absorption. This enabled us to assess the properties of potential microfabrication materials and identify appropriate substrates for PDMS-free microsystems compatible with high-resolution microscopy. We developed a new approach to produce microfluidic devices for live-cell imaging in which temperature and medium composition can be dynamically modulated. Our method is relatively cost-effective, and does not require high-end equipment and facilities. Importantly, it accommodates the design of custom networks of channels and can potentially be applied to bond any rigid microdevice to glass. This versatile tool therefore makes it possible to perform reproducible, highly controlled quantitative experiments in a broad range of contexts where cellular behaviour and responses to external stimuli must be monitored in real time.

Data accessibility. The datasets supporting this article have been uploaded as part of the electronic supplementary material.

Authors' contributions. T.C. identified the non-absorptive materials and performed proof-of-concept experiments for the wax-bonding protocol. B.G.-E. and J.M.-G. performed the majority of the biological experiments. J.B. adapted and calibrated the temperature control device. L.G. performed the photolithography for the chips used in this study and participated in the optimization of the fabrication protocol. P.-Y.J.W. and D.C. jointly supervised the study and wrote the manuscript. All authors gave final approval for publication.

Competing interests. P.-Y.J.W. and D.C. have established a CNRS collaboration contract with the company Cherry Biotech, from whom the equipment to control the flow and temperature of the thermalization fluid in our chips was purchased. Funded by the Région Bretagne, the subject of this contract is distinct from this study. B.G.-E. and J.B. are part of this collaboration.

Funding. T.C. was supported by a grant from the CNRS under the ATIP-AVENIR programme. B.G.-E. was supported by a grant from Worldwide Cancer Research (grant no. 11-0685) and a collaborative grant from the Région Bretagne. J.B. was supported by a grant from the Direction Générale des Armées (DGA). P.-Y.J.W. was supported by funding from the CNRS/INSERM under the ATIP-AVENIR programme. J.M.-G. and D.C. were supported by funding from the ERC under the European Union's Seventh Framework programme (FP7/2007-2013)/ERC Grant agreement no. 310849. The funding bodies had no role in the design and progress of this study.

Acknowledgements. We thank Olivier de Sagazan from the NanoRennes core facility for the fabrication of the metal electrodes and Gregory Eot-Houllier for sharing unpublished mammalian cell lines. We are grateful to Michael O'Brien from Adhesives Research Ireland for advice on the use of double-sided adhesives in our chips. We thank Jeremy Cramer from Cherry Biotech for his help with modifying the CherryTemp platform and adapting it to our experiments.

References

1. El-Ali J, Sorger PK, Jensen KF. 2006 Cells on chips. *Nature* **442**, 403–411. (doi:10.1038/nature05063)
2. Folch A, Toner M. 2000 Microengineering of cellular interactions. *Annu. Rev. Biomed. Eng.* **2**, 227–256. (doi:10.1146/annurev.bioeng.2.1.227)
3. Lee P, Gaige T, Hung P. 2011 Microfluidic systems for live cell imaging. *Methods Cell Biol.* **102**, 77–103. (doi:10.1016/B978-0-12-374912-3.00004-3)

4. Paguirigan AL, Beebe DJ. 2008 Microfluidics meet cell biology: bridging the gap by validation and application of microscale techniques for cell biological assays. *Bioessays* **30**, 811–821. (doi:10.1002/bies.20804)
5. Whitesides GM. 2006 The origins and the future of microfluidics. *Nature* **442**, 368–373. (doi:10.1038/nature05058)
6. Velve-Casquillas G, Le Berre M, Piel M, Tran PT. 2010 Microfluidic tools for cell biological research. *Nano Today* **5**, 28–47. (doi:10.1016/j.nantod.2009.12.001)
7. Unger MA, Chou HP, Thorsen T, Scherer A, Quake SR. 2000 Monolithic microfabricated valves and pumps by multilayer soft lithography. *Science* **288**, 113–116. (doi:10.1126/science.288.5463.113)
8. Berthier E, Young EWK, Beebe D. 2012 Engineers are from PDMS-land, biologists are from Polystyrenia. *Lab Chip* **12**, 1224–1237. (doi:10.1039/c2lc20982a)
9. Halldorsson S, Lucumi E, Gomez-Sjoberg R, Fleming RMT. 2015 Advantages and challenges of microfluidic cell culture in polydimethylsiloxane devices. *Biosens. Bioelectron.* **63**, 218–231. (doi:10.1016/j.bios.2014.07.029)
10. Regehr KJ, Domenech M, Koepsel JT, Carver KC, Ellison-Zelski SJ, Murphy WL, Schuler LA, Alarid ET, Beebe DJ. 2009 Biological implications of polydimethylsiloxane-based microfluidic cell culture. *Lab Chip* **9**, 2132–2139. (doi:10.1039/b903043c)
11. Toepke MW, Beebe DJ. 2006 PDMS absorption of small molecules and consequences in microfluidic applications. *Lab Chip* **6**, 1484–1486. (doi:10.1039/b612140c)
12. Wang JD, Douville NJ, Takayama S, ElSayed M. 2012 Quantitative analysis of molecular absorption into PDMS microfluidic channels. *Ann. Biomed. Eng.* **40**, 1862–1873. (doi:10.1007/s10439-012-0562-z)
13. Gomez-Sjoberg R, Leyrat AA, Houseman BT, Shokat K, Quake SR. 2010 Biocompatibility and reduced drug absorption of sol-gel-treated poly(dimethyl siloxane) for microfluidic cell culture applications. *Anal. Chem.* **82**, 8954–8960. (doi:10.1021/ac101870s)
14. Makamba H, Kim JH, Lim K, Park N, Hahn JH. 2003 Surface modification of poly(dimethylsiloxane) microchannels. *Electrophoresis* **24**, 3607–3619. (doi:10.1002/elps.200305627)
15. Ren K, Zhao Y, Su J, Ryan D, Wu H. 2010 Convenient method for modifying poly(dimethylsiloxane) to be airtight and resistive against absorption of small molecules. *Anal. Chem.* **82**, 5965–5971. (doi:10.1021/ac100830t)
16. Sasaki H, Onoe H, Osaki T, Kawano R, Takeuchi S. 2010 Parylene-coating in PDMS microfluidic channels prevents the absorption of fluorescent dyes. *Sensors Actuators B Chem.* **150**, 478–482. (doi:10.1016/j.snb.2010.07.021)
17. Borysiak MD, Bielawski KS, Sniadecki NJ, Jenkel CF, Vogt BD, Posner JD. 2013 Simple replica micromolding of biocompatible styrenic elastomers. *Lab Chip* **13**, 2773–2784. (doi:10.1039/c3lc50426c)
18. Liu K, Fan ZH. 2011 Thermoplastic microfluidic devices and their applications in protein and DNA analysis. *Analyst* **136**, 1288–1297. (doi:10.1039/c0an00969e)
19. Wang Y, Vaidya B, Farquar HD, Stryjewski W, Hammer RP, McCarley RL, Soper SA, Cheng Y-W, Barany F. 2003 Microarrays assembled in microfluidic chips fabricated from poly(methyl methacrylate) for the detection of low-abundant DNA mutations. *Anal. Chem.* **75**, 1130–1140. (doi:10.1021/ac020683w)
20. Wabuyele MB, Ford SM, Stryjewski W, Barrow J, Soper SA. 2001 Single molecule detection of double-stranded DNA in poly(methylmethacrylate) and polycarbonate microfluidic devices. *Electrophoresis* **22**, 3939–3948. (doi:10.1002/1522-2683(200110)22:18<3939::AID-ELPS3939>3.0.CO;2-9)
21. Ahn CH, Choi JW, Beaucage G, Nevin J, Lee JB, Puntambekar A, Lee RJY. 2004 Disposable smart lab on a chip for point-of-care clinical diagnostics. *Proc. IEEE* **92**, 154–173. (doi:10.1109/JPROC.2003.820548)
22. Young EWK, Berthier E, Guckenberger DJ, Sackmann E, Lamers C, Meyvantsson I, Huttenlocher A, Beebe DJ. 2011 Rapid prototyping of arrayed microfluidic systems in polystyrene for cell-based assays. *Anal. Chem.* **83**, 1408–1417. (doi:10.1021/ac102897h)
23. Hayles J, Nurse P. 1992 Genetics of the fission yeast *Schizosaccharomyces pombe*. *Annu. Rev. Genet.* **26**, 373–402. (doi:10.1146/annurev.ge.26.120192.002105)
24. Moreno S, Klar A, Nurse P. 1991 Molecular genetic analysis of fission yeast *Schizosaccharomyces pombe*. *Meth. Enzymol.* **194**, 795–823. (doi:10.1016/0076-6879(91)94059-L)
25. Coudreuse D, Nurse P. 2010 Driving the cell cycle with a minimal CDK control network. *Nature* **468**, 1074–1079. (doi:10.1038/nature09543)
26. Huang J *et al.* 2012 Nonmedially assembled F-actin cables incorporate into the actomyosin ring in fission yeast. *J. Cell Biol.* **199**, 831–847. (doi:10.1083/jcb.201209044)
27. Hiraoka Y, Toda T, Yanagida M. 1984 The NDA3 gene of fission yeast encodes beta-tubulin: a cold-sensitive nda3 mutation reversibly blocks spindle formation and chromosome movement in mitosis. *Cell* **39**, 349–358. (doi:10.1016/0092-8674(84)90013-8)
28. Meister P, Poidevin M, Francesconi S, Tratner I, Zarzov P, Baldacci G. 2003 Nuclear factories for signalling and repairing DNA double strand breaks in living fission yeast. *Nucleic Acids Res.* **31**, 5064–5073. (doi:10.1093/nar/gkg719)
29. Nurse P, Thuriaux P, Nasmyth K. 1976 Genetic control of the cell division cycle in the fission yeast *Schizosaccharomyces pombe*. *Mol. Gen. Genet.* **146**, 167–178. (doi:10.1007/BF00268085)
30. Riedl J *et al.* 2008 Lifeact: a versatile marker to visualize F-actin. *Nat. Methods* **5**, 605–607. (doi:10.1038/nmeth.1220)
31. Bartolo D, Degré G, Nghe P, Studer V. 2008 Microfluidic stickers. *Lab Chip* **8**, 274–279. (doi:10.1039/b712368j)
32. McDonald JC, Whitesides GM. 2002 Poly(dimethylsiloxane) as a material for fabricating microfluidic devices. *Acc. Chem. Res.* **35**, 491–499. (doi:10.1021/ar010110q)
33. Velve-Casquillas G *et al.* 2011 Fast microfluidic temperature control for high resolution live cell imaging. *Lab Chip* **11**, 484–489. (doi:10.1039/c0lc00222d)
34. Childs PRN, Greenwood JR, Long CA. 2000 Review of temperature measurement. *Rev. Sci. Instrum.* **71**, 2959–2978. (doi:10.1063/1.1305516)
35. Bishop AC *et al.* 2000 A chemical switch for inhibitor-sensitive alleles of any protein kinase. *Nature* **407**, 395–401. (doi:10.1038/35030148)
36. Gregan J, Zhang C, Rumpf C, Cipak L, Li Z, Uluocak P, Nasmyth K, Shokat KM. 2007 Construction of conditional analog-sensitive kinase alleles in the fission yeast *Schizosaccharomyces pombe*. *Nat. Protoc.* **2**, 2996–3000. (doi:10.1038/nprot.2007.447)
37. Lopez MS, Kliegman JI, Shokat KM. 2014 The logic and design of analog-sensitive kinases and their small molecule inhibitors. *Meth. Enzymol.* **548**, 189–213. (doi:10.1016/B978-0-12-397918-6.00008-2)
38. Nurse P, Bissett Y. 1981 Gene required in G1 for commitment to cell cycle and in G2 for control of mitosis in fission yeast. *Nature* **292**, 558–560. (doi:10.1038/292558a0)
39. Miserere S, Mottet G, Taniga V, Descroix S, Viovy J-L, Malaquin L. 2012 Fabrication of thermoplastics chips through lamination based techniques. *Lab Chip* **12**, 1849–1856. (doi:10.1039/c2lc21161k)
40. Carrilho E, Martinez AW, Whitesides GM. 2009 Understanding wax printing: a simple micropatterning process for paper-based microfluidics. *Anal. Chem.* **81**, 7091–7095. (doi:10.1021/ac901071p)
41. Díaz-González M, Baldi A. 2012 Fabrication of biofunctionalized microfluidic structures by low-temperature wax bonding. *Anal. Chem.* **84**, 7838–7844. (doi:10.1021/ac301512f)
42. Gong X, Yi X, Xiao K, Li S, Kodzius R, Qin J, Wen W. 2010 Wax-bonding 3D microfluidic chips. *Lab Chip* **10**, 2622–2627. (doi:10.1039/c004744a)
43. Russell P, Nurse P. 1986 cdc25+ functions as an inducer in the mitotic control of fission yeast. *Cell* **45**, 145–153. (doi:10.1016/0092-8674(86)90546-5)
44. Forsburg SL, Rhind N. 2006 Basic methods for fission yeast. *Yeast* **23**, 173–183. (doi:10.1002/yea.1347)

SUPPLEMENTARY MATERIAL

Supplementary Figure 1. Identification of a sealant for COC chips.

The biocompatibility of several glues and sealing components were tested for the fabrication of closed COC chips on glass coverslips. Most of them induced strong lethality of fission yeast cells (data not shown). Drop assays (wild-type cells, 6 h at 32 ºC) on representative compounds are shown here. Dymax and SuperGlue were not biocompatible. While the PR5 compound had no negative impact on cell proliferation, cells appeared to adhere to the glue. Paraffin wax, however, did not have detectable side effects (compare to Glass in Figure 2a). Blankophor staining. Scale bars = 10 µm. (PDF).

Supplementary Figure 2. Limits of the wax bonding protocol.

A-C. Schematics of the designs used in Figure 4c, with all the sizes, dimensions and heights of the channels indicated. In A, the middle and right panels detail the multi-level structures of the design shown in the left panel. (PDF).

Supplementary Figure 3. Rhodamine test for small molecule absorption.

50 µM Rhodamine B was injected in PDMS and COC/Wax microchips, incubated for 5 min and washed with 10 ml water. Images were acquired before and after washing the channels (left panel). Identical microscope acquisition settings were used for each set of images for comparison between PDMS and COC. Right panel: line scans of the intensity measured through the channels (vertical scans from images in the left panel). After washing, the COC/Wax chip exposed to Rhodamine showed similar signals that filled with water. In contrast, a significantly stronger signal remained in the PDMS chip. (PDF).

Supplementary Figure 4. Compatibility of the complete device with fluorescence microscopy.

A. Fission yeast cells expressing an eGFP-Pcn1/PCNA fusion protein were imaged between standard glass slides and coverslips, in PDMS chips or in complete COC/Wax devices integrating the temperature control system. No differences were observed between the different conditions. Maximum projections of z-stacks (0.2 µm steps). Scale bar = 10 µm. **B.** Quantification of the signal and background fluorescence from the images in A. No differences in signal to noise ratio were observed between the conditions. Average nuclear fluorescence intensity was measured using maximum projections of the acquired z-stacks. *n*=100 for each measurement. Cells with strong foci where excluded to avoid bias in the measurements. For the background values (Bkg), quantifications were performed using similar surface areas in different regions of the images that did not contain any cells. Box-and-whiskers plot using interquartile ranges; dots represent outliers. (PDF).

Supplementary Figure 5. Characterization of the temperature control system.

A. Example of a chip calibration. Graph showing the linear relationship linking the differences in temperature 1) between the thermalization fluid (water) injected in the system (T_i) and the microscope lens (T_{lens}) and 2) between the sample (T_{sample}) and the microscope lens (T_{lens}), as determined by our calibration protocol (see Materials and Methods). The associated equation is shown, providing the temperature at which to set the Peltier elements in order to reach a specific target in the cell chamber, after measuring the temperature of the microscope lens. **B.** Impact of changing microscope lens on the temperature control system. Complete COC/Wax chips were mounted on glass coverslips with integrated temperature measurement electrodes. Fixed temperatures were applied for the thermalization fluid and the temperatures within the microdevice were monitored using

the electrodes. No differences in temperature could be detected between the 63X and 100X oil immersion objectives. **C.** Impact of flowing fresh medium at room temperature through the cell compartment of the chip on the temperature of the samples. A COC/Wax chip integrating the temperature control device was mounted on a glass coverslip integrating temperature measurement electrodes and set up on a microscope stage in contact with the objective through immersion oil. A constant temperature of 45 ºC was set at the Peltier elements for the thermalization fluid. The temperature in the cell chamber was then monitored while applying different flow rates of medium. Although the highest flow rate of 60 µl/min altered the temperature of the sample, lower rates (15 and 30 µl/min) had no impact. For comparison, the total volume of a chamber of 1 cm diameter and 100 µm high is about 8 µl, which indicates that the rates allowed by the temperature system are compatible with rapid exchange of medium in the chips. (PDF).

Supplementary Figure 1

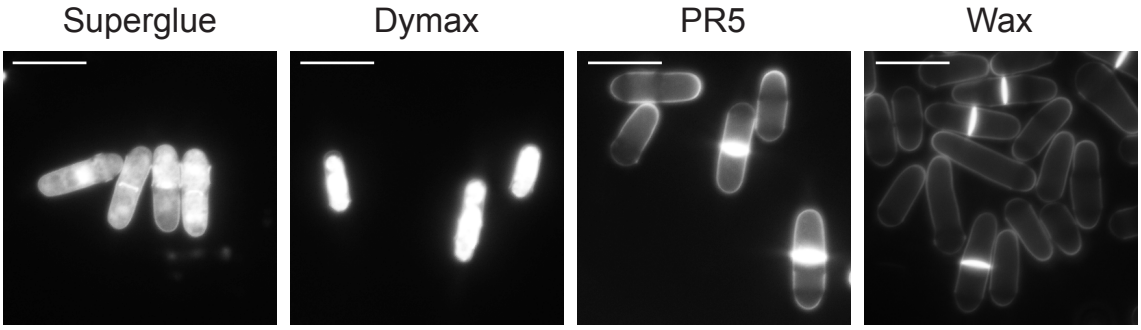

Supplementary Figure 2

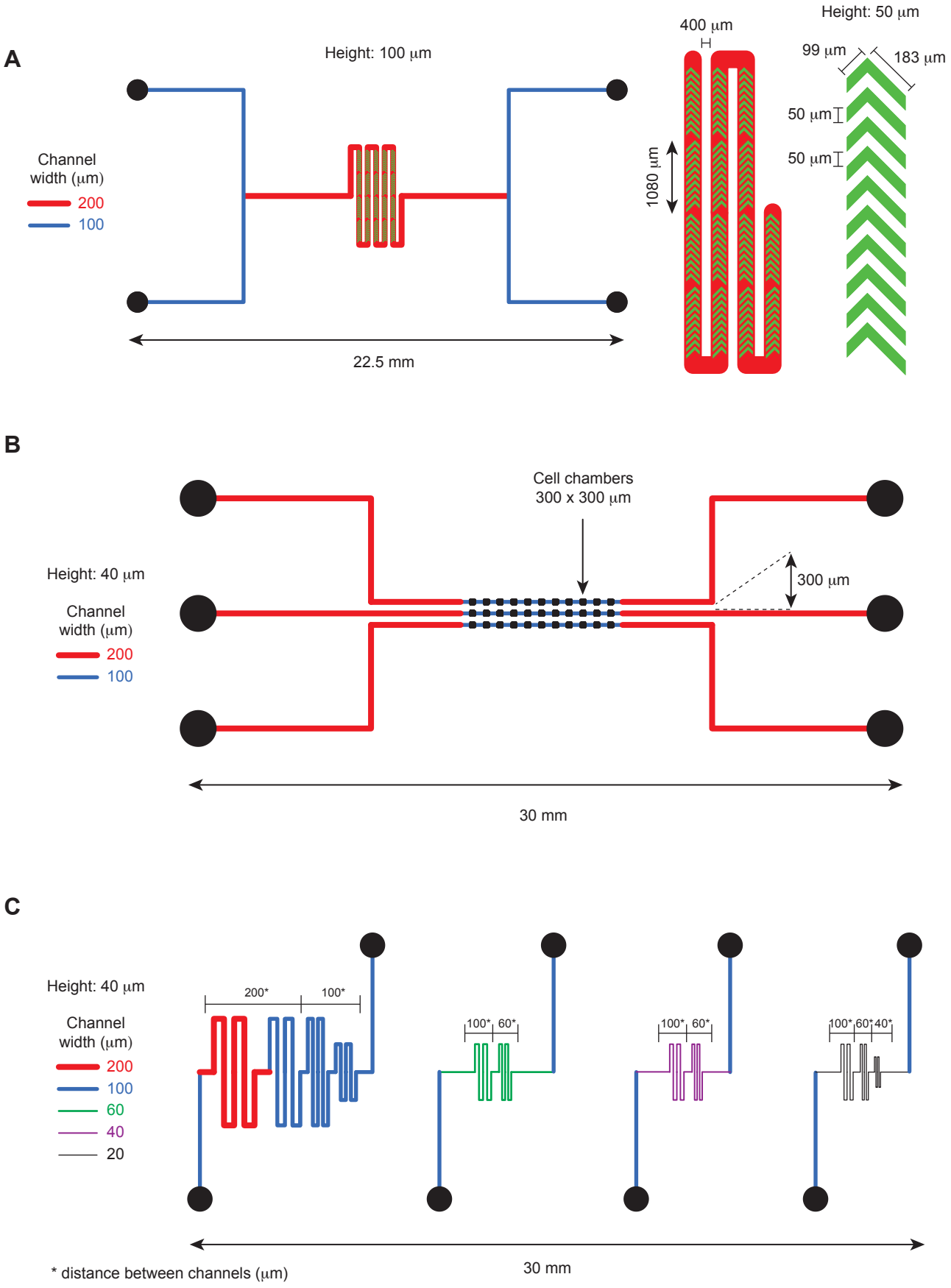

Supplementary Figure 3

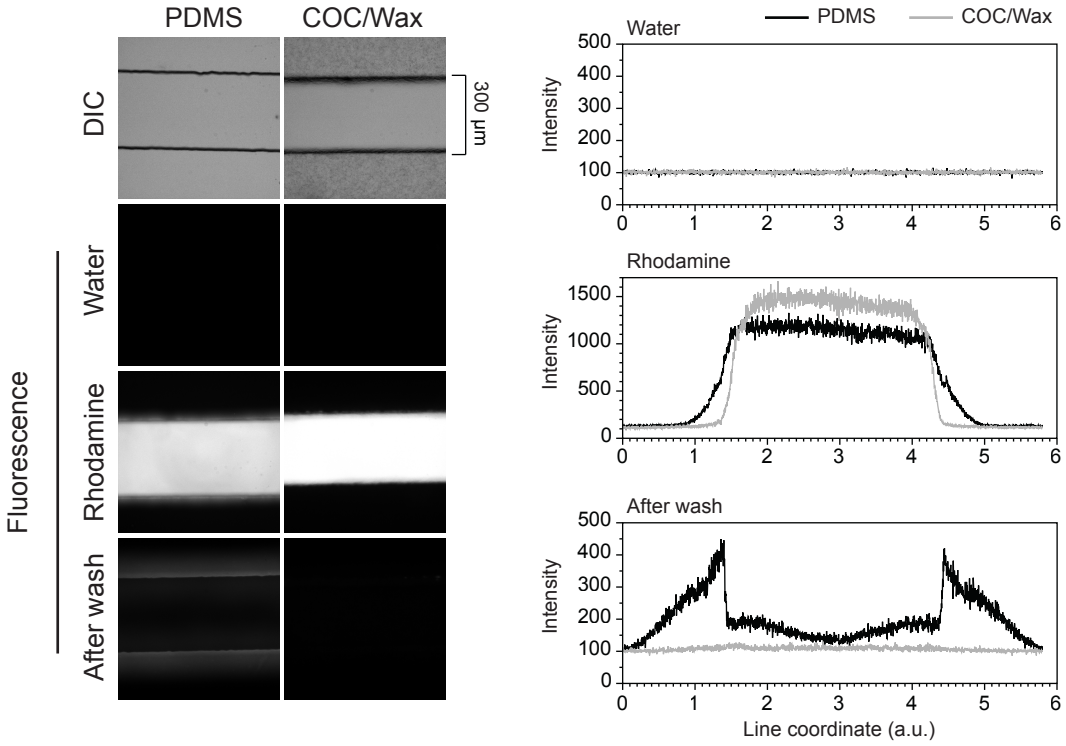

Supplementary Figure 4

A

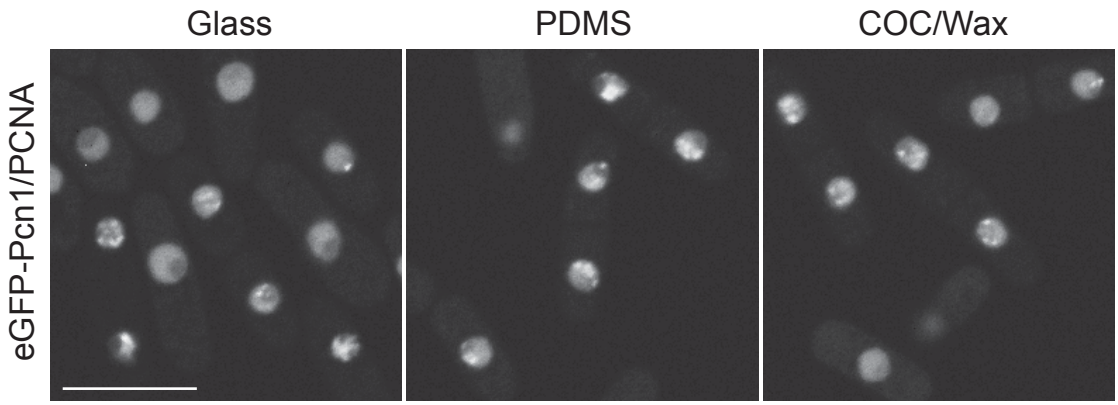

B

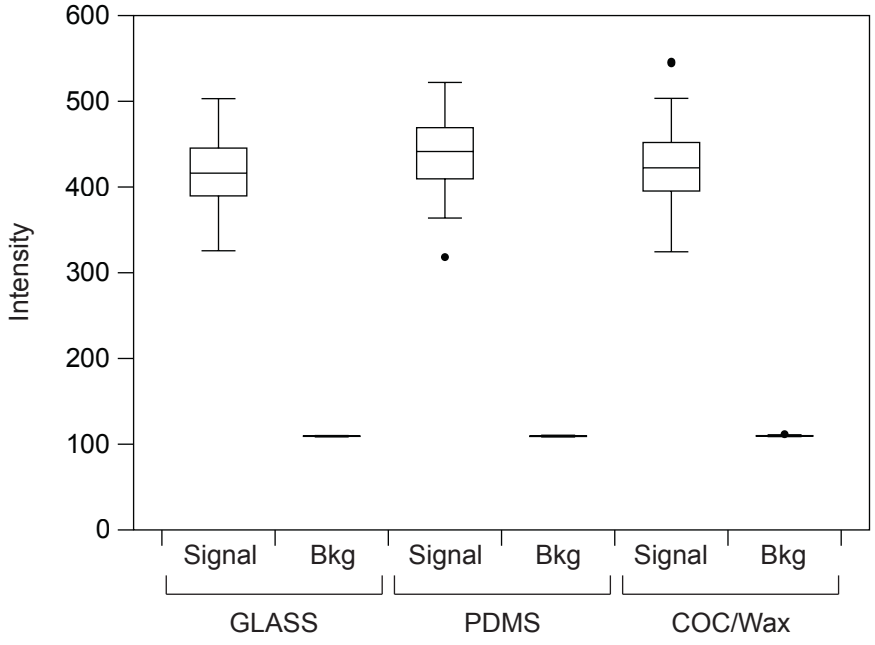

Supplementary Figure 5

A

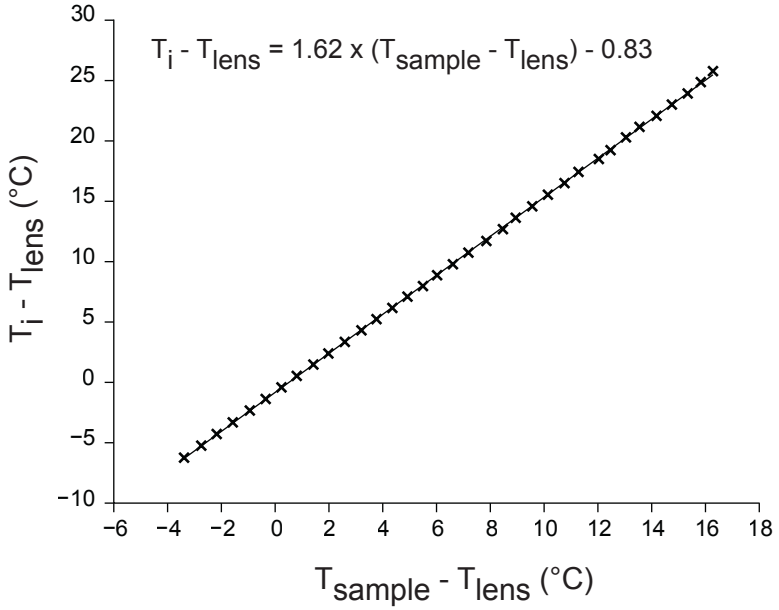

B

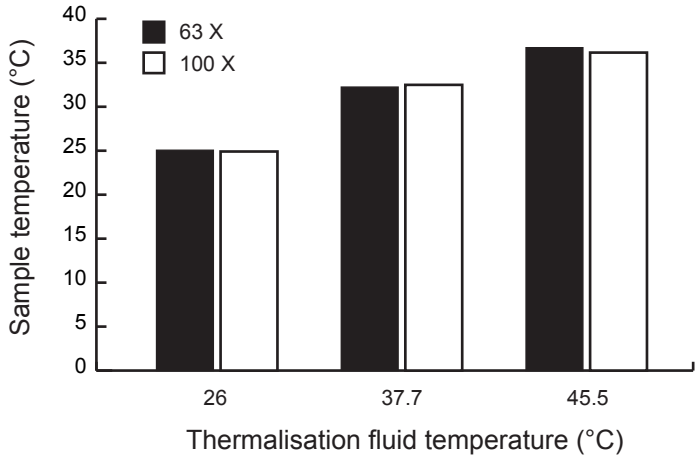

C

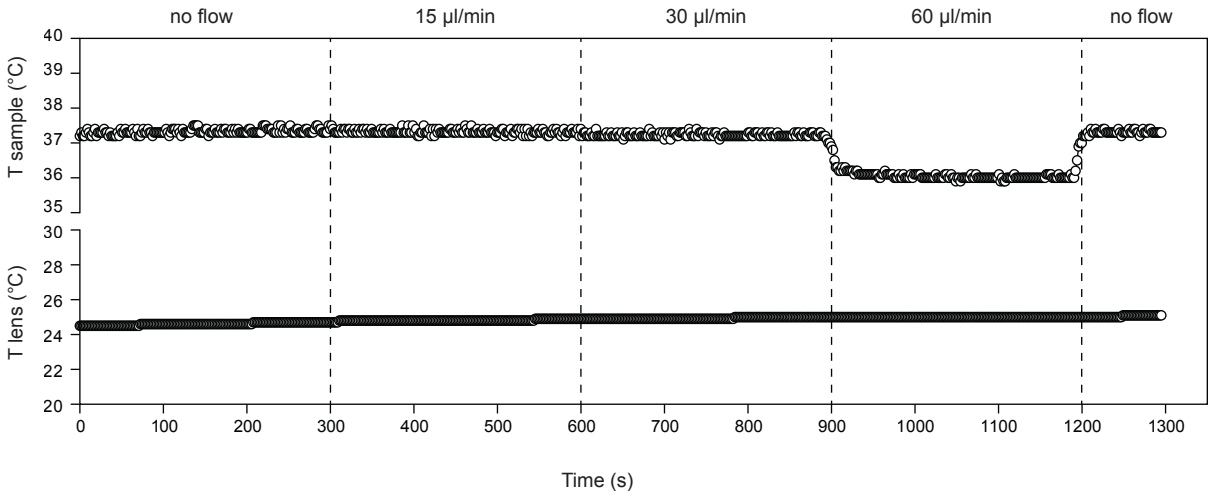

Chapter 2: The perfusion chip

Even though microfluidics have spread in biology laboratories, the complexity of microfluidic systems and the cost-effective equipments have prevented biologists to take full advantage of such technologies in laboratories. In this chapter, we focused on developing a versatile system dedicated to live-cell imaging, easy to use and to fabricate, which could be integrated as a standard system in biology laboratories. We focused on developing a microsystem in which simplicity was a crucial parameter to consider, while still possessing a number of advantages associated with microfluidics. The microchip we developed is composed of an elastomeric material constituting the main channel. The elastomer allows the sealing of the channel and the re-usability of the chip. The perfusion channel provides a constant delivery of fresh medium at the microscope. Consequently, cells are directly in the flow and are subjected to shear stress, which did not alter cell physiology while testing with the non-adherent fission yeasts *S. pombe* and adherent cells *HeLa*. However, the absorptive properties of the elastomer is preventing assays involving low or precise amount of drugs, even if the perfusion flow makes the absorption negligible when focusing on cells further from the channel border. We have used the same control systems as for the wax chip to generate robust perfusion and temperature control in this chip, therefore allowing fast media switches and temperature dynamics. All materials constituting this chip are cut using a CO_2 laser-cutting machine, however we have proven that this chip could be customizable and made without laser, thus accessible to any user. Moreover, the flows and temperature control could be achieved without external controllers, if the accuracy and time are less critical.

Manuscript submitted.

An easy-to-build and re-usable microfluidic system for live-cell imaging

Julien Babic[1], Laurent Griscom[1], Jeremy Cramer[2] and Damien Coudreuse[1,*]

[1]SyntheCell team, Institute of Genetics and Development of Rennes, France
[2]Cherry Biotech, Rennes, France

[*]Corresponding author: damien.coudreuse@univ-rennes1.fr

ABSTRACT

Real-time monitoring of the response of cells to dynamic changes in their environment during live-cell imaging experiments has become a critical approach in cell biology. However, such strategy has remained difficult to achieve with precision, and the simultaneous alteration of multiple parameters is still a challenge for most research laboratories. Recently, microfluidics have provided powerful solutions for such analyses, bringing an unprecedented level of control over the composition of the medium in which cells under microscopic observation are grown. Nevertheless, such technologies remain under-exploited, largely as a result of the complexity associated with microfabrication procedures when versatile systems are essential. In this study, we have developed simple though powerful microfluidic systems dedicated to live-cell imaging. These devices are affordable, easy-to-build without the need of sophisticated equipments, customizable and re-usable multiple times. Importantly, the possibility of dynamically controlling the cellular environment in microchips that can be fabricated and used by any laboratory will allow a broader spectrum of research teams to benefit from the advantages provided by microfluidics.

INTRODUCTION

Deciphering cell biological processes and understanding the dynamics that underlie fundamental functions in living cells has greatly benefited from the continual development of advanced methods in microscopy. It has become clear that investigating biological processes at a range of time scales, from immediate responses to various stimuli to long-term behaviors is an integral part of our understanding of cell biology. However, while complex time-lapse acquisitions have become a standard approach in the life sciences, the real-time monitoring of cellular responses to changes in their environment or to specific treatments has not progressed at the same pace. Indeed, most approaches still rely on basic perfusion systems that lack versatility and time resolution. Recently, microfluidic technologies coupled to high-resolution microscopy have brought a number of solutions to the limitations that are intrinsic to standard perfusion systems. These include the requirement for large volumes, the limited time resolution, their general incompatibility with non-adherent cells, as well as the difficulty of multiplexing assays in a single experiment and of simultaneously altering several parameters of the cellular environment(Young & Beebe, 2010). Relying on the manipulation of microvolumes and the well-established properties of the fluid flows within microchannels(Bayraktar & Pidugu, 2006), these miniaturized devices provide the capacity to control the cellular environment with unprecedented flexibility, accuracy and dynamics(Velve-Casquillas, Le Berre, Piel, & Tran, 2010; Young & Beebe, 2010). Furthermore, their emergence has been accompanied by the ongoing development of more advanced chip structures(Friend & Yeo, 2010), opening new doors of investigation for researchers (Whitesides, 2006). From ever more complex fluidic circuits to the use of microsystems for assessing the physical properties of living cells(Yuchao Chen et al., 2014), the advantages of microfluidics for the life sciences are undisputed, and the design of novel microdevices has become a dedicated area of research.

Nevertheless, the impact of microfluidics and their popularization in research laboratories that investigate biological processes have not yet been as significant as one may have predicted(Whitesides, 2006). One of the major obstacles to expanding the use of microdevices for biology is the complexity of their fabrication and usage(Whitesides, 2013). Indeed, the building of microfluidic chips adapted to live-cell imaging is a time consuming process that requires costly equipments, in particular for photolithography procedures(Qin, Xia, & Whitesides, 2010), dedicated spaces and often highly-controlled clean rooms, as well as specific and significant expertise. Furthermore, modulating the flow and composition of the growth medium in a chip while monitoring cells by microscopy is not simple. It relies on a clear understanding of various notions such as the impact of the fluidic resistances at different points in the network. In addition, flows in microchannels are laminar(Stroock & Whitesides, 2003) and their mixing therefore requires additional microstructures(Lee, Chang, Wang, & Fu, 2011; Williams, Longmuir, & Yager, 2008). All together, these different aspects of the use of microfluidic systems have hampered their integration in most research groups.

While a number of commercial systems have recently tried to circumvent these issues, offering high-end and expensive plug-and-play devices, they do not allow any customization of the fluidic networks, a property that is an integral part of what microfluidics can offer for research in the life sciences. Adopting microfluidic technologies within a research group therefore remains an endeavor that is time consuming and costly. Importantly, the race toward complexity and ever more powerful microfluidic devices has lost sight of the needs of the majority of research teams. The ideas of lab-on-chips(Haeberle & Zengerle, 2007) or even organ-on-chips(Bhatia & Ingber, 2014), although very promising in the long-run, do not reflect what is currently critical for a large number of investigations in cell biology. It is therefore crucial to establish methods and protocols for

the fabrication and use of simple customizable microsystems by non-experts{Yamada:2017}. This is an essential step for fully taking advantage of these revolutionary tools.

In this study, we have developed a novel microfluidic system dedicated to live-cell imaging that is easy-to-build, customizable and cost-effective while possessing a number of the advantages associated with microfluidics. This device consists of an elastomer that is commercially available in a range of precise thicknesses, in which different types of microfluidic networks can be easily engineered without the need for high-end equipment. We show that this transparent elastomer can be bonded to microscopy-grade glass coverslips and is not autofluorescent at the most common excitation wavelengths used when imaging living cells, two essential features for performing advanced microscopy assays. Interestingly, we find that the elastomer layer can be re-used several times, a significant advantage for its implementation in research laboratories. We next provide evidence that it can be coupled with precise controllers, allowing for rapid, accurate and simultaneous control of various parameters of the cellular environment such as the temperature of the sample and the composition of the growth medium. Importantly, we then detail proof-of-concept experiments that demonstrate the biocompatibility of these microdevices with different types of cells, namely the fission yeast *Schizosaccharomyces pombe* and mammalian cells (HeLa). Finally, we show that using a constant flow of medium, the absorption of small hydrophobic molecules, which is a common feature of a number of materials classically used for microfabrication, can be circumvented, and that this system is well-adapted for the real-time monitoring of cellular responses to dynamic perturbations of their environment. Taken together, our results describe an affordable, easy-to-build and re-usable microfluidic system that will be an asset for research teams in cell biology and contribute to the expansion of microfluidics in the life sciences.

MATERIALS AND METHODS

Fission yeast strains and methods

Standard media and methods were used(Hayles & Nurse, 1992; Moreno, Klar, & Nurse, 1991). The strain used in this study was DC450(Tong Chen et al., 2016) (*leu1Δ:Pcdc13::cdc13-L-cdc2as::cdc13-3'UTR::ura4*$^+$ *cdc2Δ::kanMX6 cdc13Δ::natMX6 cig1Δ::hphMX6 cig2Δ::kanMX6 puc1Δ::leu2*$^+$ *ura4-D18 h*$^+$). The inihibitor-sensitive Cdc13-L-Cdc2as fusion protein was previously described(Coudreuse & Nurse, 2010). All experiments were carried out in minimal medium plus supplements (EMM6S) at 32˚C. The 3-MBPP1 inhibitor (A603003, Toronto Research Chemical Inc.) was dissolved in DMSO at a stock concentration of 10 mM and added to the medium at the indicated concentrations. Size at division was determined from DIC images using Fiji. Generation time of cells grown in the chips was determined as the time between two successive septation events.

Mammalian cell lines and methods

All experiments were performed using HeLa Kyoto cell lines stably expressing an H2B::mCherry fusion protein (from plasmid 21045, Addgene; Gregory Eot-Houllier, unpublished data). Cells were grown in DMEM GlutaMax medium (Thermo Fisher Scientific) supplemented with 10% Fetal Calf Serum, 0.05 g/L streptomycin (Life Technologies), 50000 units/L penicillin (Life Technologies) and 25 mM HEPES (Sigma Aldrich). The CDK inhibitor RO-3306 (Calbiochem) was used at 6 μM final. All control experiments were performed in 12-well polystyrene dishes. For injection in the microdevices, cells were washed with PBS, treated with trypsin and resuspended in culture medium.

Microscopy

Images in figures 2C-E, 3B-D, 4A-B, 5A-B and 6A were performed using an inverted Zeiss Axio Observer (Carl Zeiss Inc.) equipped with a Lumencor Spectra X illumination system and a Hamamatsu Orca Flash 4.0V2 sCMOS camera. Figures 1F and 3C were obtained using a similar setup but equipped with a spinning disc confocal head and a laser bench (Visitron GmbH). For both systems, images were acquired using Visiview (Visitron GmbH). The images displayed in Figures 1C-E (bottom panel) and 4C were acquired using a Zeiss Axio Vert. A1 (Carl Zeiss Inc.) equipped with a Nikon 1 J3 camera and a PlasDIC system. All analyses were performed using Fiji (National Institutes of Health).

Microfabrication

Materials:

6 mm-thick extruded PMMA for the chip manifolds was purchased from Weber-Metaux. The double-sided adhesive tape (142 μm thick) used for the temperature control layer is ARcare 90880 (Adhesive Research Inc.). The 250 μm-thick elastomer used for fabricating all the perfusion channels is HT6240 40SH from Silex Silicones. Glass coverslips (170 μm thick) and plastic coverslips (Rinzel 72261-60, 280 μm thick) were purchased from Menzel-Gläser and Electron Microscopy Sciences, respectively. Bonding of the plastic coverslips to the PMMA manifolds (Figures 4C and 6B) was achieved using epoxy adhesive (Sader).

Chip dimensions:

The dimensions of the different layers constituting the chips used in this study are presented in Supplementary Fig. 2.

Fabrication of chips for short-term experiments:

The PMMA manifold, temperature control layer and perfusion channel were obtained in the appropriate materials using a CO_2 laser cutter (Speedy 100, Trotec). To prevent deterioration when exposed to solvents, the PMMA blocks were cured for 2 h at 90 ˚C. The manifold was then bonded to the temperature control layer (double-sided adhesive) and a glass coverslip containing connecting holes generated using the CO_2 laser-cutting machine. The elastomer perfusion channel was then mounted, sealing the top layers with a microscopy-grade glass coverslip. Rigid Teflon tubing (Cluzeau) was used to connect the chips to the temperature control device as well as to the flow control systems, and sealed using epoxy glue. For the perfusion layer, the inner diameters of these tubings were 0.5 mm (upstream) and 1 mm (downstream), thereby limiting the impact of the chip fluidic resistance on the fluidic network.

Fabrication of chips for long-term experiments:

For long-term experiments, the glass coverslip separating the temperature and perfusion layers was replaced by a plastic coverslip (Electron Microscopy Sciences, Rinzel 72261-60, 280 μm thick), due to the relative weakness of the glass coverslips after laser cutting of the connecting holes. In this case, the temperature control layer was directly engraved within the PMMA manifold using the CO_2 laser machine, and bonding to the plastic coverslip was achieved by stamping of epoxy glue. Connecting holes in the plastic coverslip were made using a drilling machine. The other layers of the chip were identical to those of the devices fabricated for short-term experiments. For simplicity, all the proof-of-concept experiments using mammalian cells were performed using a similar chip structure, in which the temperature control channel was removed (the temperature of the samples was then maintained using high precision hot plates).

Chip preparation and cell loading

All mounted chips were sterilized by treatment with UV for 15 min prior to use. For experiments with non-adherent fission yeast cells, the bottom glass coverslips were coated with lectin (Sigma Aldrich). This was achieved by injecting lectin (0.5 mg/mL) in the chips using manual syringes. After 30 min of incubation, the chips were thoroughly rinsed with deionized water and cells were manually injected in the system. For experiments with adherent mammalian cells, the glass coverslips were similarly coated with fibronectin (0.5 mg/mL) and rinsed with culture medium prior to cell injection. Resuspended cells were then injected and allowed to re-adhere to the glass substrate in a wet chamber placed at 37 °C in a CO_2 incubator. for a minimum of 3 h prior to applying any flow of medium.

Control of the cellular environment in the microfluidic chips

Control of the temperature was calibrated and performed as previously described(Tong Chen et al., 2016). The precise dimensions of the temperature control channel for the calibration were slightly different than for the layer used in the chip (see Supplementary Fig. 2). While the thickness was the same, the length and width was altered

to facilitate the connection of the metal electrodes to the measure instrument. However, the temperature of the sample relies on the thickness of the temperature layer as well as the flow rate in this channel (>5 mL/min, which was validated in all the chips). Thus, the calibrations performed using this channel are valid for the other chips described in this study. Control of the medium flow rates was achieved using flow sensors regulating the operation of pressure controllers (Elvesys). Matrixes of valves allowed rapid media switches (Elvesys). To limit the presence of bubbles within the microfluidic networks, bubble traps (Elvesys) connected to vacuum pumps (KNF) were mounted upstream of the chips. See Fig. 3A for a schematics of the full system.

Cleaning of the chips for reusability

The chips developed in this study can be re-used several times, with the bottom glass coverslip being the only single-use component of the whole system. Prior to re-use, all chips were dismantled and all tubings were thoroughly washed with deionized water, 70% ethanol and dried using pressurized air. The elastomer layer was cleaned in an ultrasound waterbath at room temperature for 15 min, subsequently washed with 70% ethanol and allowed to dry using pressurized air.

RESULTS AND DISCUSSION

A new material for the easy fabrication of complex microfluidic chips

While a host of complex microdevices and microfabrication procedures have emerged for a broad range of applications(Yun Chen, Zhang, & Chen, 2008; Friend & Yeo, 2010; Iliescu, Taylor, Avram, Miao, & Franssila, 2012; Yanyan Xia, Si, & Li, 2016), the integration and popularization of versatile, custom-made microfluidic systems in research laboratories has been hampered by the prevailing microfabrication techniques and materials, requiring high-end equipments, regulated environments and specific expertise. We therefore sought to identify an alternative material that would be readily available to researchers and easily integrated in microfluidic chips dedicated to live-cell imaging. Silicon-based materials are particularly adapted for such approaches, as they are robust and their bonding properties allow the sealing of different layers for the assembly of microscopy-compatible microfluidic chips. Importantly, in order to bypass the requirement for a dedicated clean room as well as advanced fabrication procedures, we focused on materials that are already provided as sheets of precise thicknesses, a critical feature for the production of reproducible microfluidic networks. After a pilot screen to assess the basic properties of a number of existing solutions (*e.g.* bonding characteristics, transparency, short-term biocompatibility; data not shown), the LSR elastomer was selected as the most promising candidate. This materials can be purchased in a range of thicknesses (from 250 µm to 3.2 mm; all the systems described in this study are 250 µm-thick) and it is robust to stretching and deformation (Fig. 1A), making it particularly suitable to routine manipulation. Importantly, we demonstrated that complex microchannel structures can easily be engineered in thin LSR sheets using a CO_2 laser cutting machine (Fig. 1B, C), and found that a 50 µm laser beam, which equips a number of standard laser cutters, allows for the generation of channels as narrow as ~170 µm (Fig. 1D). Therefore, although very small structures are not easily fabricated, this method remains compatible with a broad range of live-cell imaging experiments (as a comparison, a single field of view using high-end large field sCMOS cameras is ~13.3 x 13.3 mm). Undoubtedly, the use of an automated laser cutter provides accuracy and reproducibility at manageable costs. However, such apparatus is not always available in research laboratories, prompting us to assess the fabrication quality of LSR-based microchips using a simple razor blade. Interestingly, we were able to produce simple but perfectly usable channels, whose dimensions were adequate for perhaps the majority of standard live-cell imaging assays (Fig. 1E).

Next, we established the suitability of our strategy with experiments that require the maintenance of a medium flow through the microdevices. To this end, we determined the bonding strength of the elastomer when intercalated between two microscopy-grade glass coverslips, using a method that we previously described(Tong Chen et al., 2016). Briefly, our assay uses a pressure controller connected to the chip to identify the maximum pressure that can be applied within the microsystem without generated fluid leaks. Importantly, we found that the sealing properties of the elastomer in combination with glass at different temperatures (in the range of standard physiological temperatures) are sufficient for robust bonding and the handling of pressures that are compatible with a broad panel of applications (Tables 1 and 2). Moreover, we obtained identical results between new chips and chips that were mounted using an elastomer layer that had been thoroughly washed (see Materials and Methods) and re-used several times. This showed that beyond its ease for manipulation and fabrication, this materials provides re-usability, a clear asset for promoting microfluidic-based approach in the life sciences.

We finally investigated whether the elastomer is compatible with the fabrication and independent use of distinct channels within a single chip. This would allow, for instance, to perform related assays simultaneously

(*e.g.* experiment and controls, different treatments of a single cell line). To test this, we built two distinct channels separated in the center by only 300 µm (Fig. 1F) and intercalated this layer between two glass coverslips. Water was then injected in one of the channels, while the other was perfused with a solution of the fluorescent dye Rhodamine B. Identical and constant flow rates in both channels were maintained for 8 h (20 µL/min; as a reference, the total volume of liquid in each of these channels is ~6 µL), and the fluorescence intensity was measured at different positions (Fig. 1F). Strikingly, we observed no cross-contamination between the channels, even at the narrowest point of the network, demonstrating the compatibility of this material with the design and use of multi-channel microsystems.

Taken together, these results demonstrate that the LSR elastomer is a promising candidate to generate microfluidic devices for live-cell imaging, and is compatible with the fabrication of complex channel networks as well as experimental multiplexing on single chips.

Precise and simultaneous control of the environment in the perfusion channel

We next investigated whether the rapid, precise and simultaneous control of different parameters of the cellular environment during live-cell imaging experiments can be achieved using our microsystem. To this end, we first generated a proof-of-concept microscopy-compatible chip that integrated 1) a perfusion channel built in a 250 µm-thick elastomer sheet and 2) the microfluidic-based temperature control system that we previously used(Tong Chen et al., 2016) (Fig. 2A, B). The latter was fabricated in a medical double-sided adhesive using the CO_2 laser cutter, but similarly to the elastomer perfusion layer, it could easily be fabricated using a simple razor blade (data not shown). Once calibrated to compensate for the heat losses that occur along the microfluidic network (Supplementary Fig. 1), this additional layer allowed not only to maintain a precise and constant sample temperature, but also to induce rapid and reproducible temperature switches both above and below ambient (Fig. 2C). This is a key feature when investigating temperature-sensitive processes or genetic mutants. Importantly, we previously showed that this temperature control system is not significantly influenced by either the flow rate of medium within the cell channel or the type of immersion lens used(Tong Chen et al., 2016). However, these experiments were made with much thinner microfluidic channels and structures than those described in the present study. Nevertheless, we showed that these properties were valid in the elastomer chips as well, for different temperature ranges (Fig. 2D, E). In fact, we observed that higher flow rates could be applied in the elastomer microsystems (60 µL/min affected the temperature in our previous devices(Tong Chen et al., 2016), while the chips presented here could handle the maximum tested flow rate of 80 µL/min). Thus, the elastomer microfluidic chips are compatible with fine and dynamic regulation of sample temperature while monitoring cell behavior by microscopy.

We then assessed the capacity of this perfusion system to perform fast media switches (the channels fabricated for these assays were 5.5 mm wide and 250 µm thick). Using Rhodamine B as a fluorescent marker, we first investigated the dynamics of the media switches as a function of the flow rate. This parameter was set to 5, 10 or 20 µL/min (within the range determined in Tables 1 and 2) using high precision flow sensors that modulate the operation of pressure controllers, and a matrix of valves to induce the changes in perfused fluid (Fig. 3A). After injecting the dye, a rapid switch to water was triggered, and fluorescence intensity in the channel was measured over time. As anticipated, higher flow rates allowed for faster renewal of the medium, with a reduction of 95% of the fluorescence signal after only 4 min when using 20 µL/min (Fig. 3B), while the same was achieved after 9 min and 18 min at flow rates of 10 and 5 µL/min, respectively. However, a lower flow

velocity within the chip can sometimes be preferred when shear stress to the cells is more critical than the timing of the medium switch. Interestingly, when considering, for each condition, the last point at maximum signal intensity and the first point where more than 90% of the fluorescence is lost, we noted timings of 3, 5 and 7 min for flow rates of 20, 10 and 5 µL/min, respectively (Fig. 3B). This suggests that the delays in medium renewal at lower flow rates result for a large part from the time required to displace the volumes of fluid in the connecting tubings rather than within the elastomer perfusion channel. Limiting the length of these tubings is therefore likely to reduce the duration of the media switches when using low flow rates.

In order to assess the homogeneity of the media switches along an axis perpendicular to the flow, as border effects are classical drawbacks of microfluidic devices, we performed the same assay as above at 20 µL/min but determined the fluorescence intensity over time at various distances from the border of the channel (Fig. 3C). This showed that the position within the channel had only limited influence on the dynamics of the changes in medium. The border effect is therefore likely to be negligible for most applications, and only a concern when a very high homogeneity in the channel is essential. Finally, we demonstrated the reproducibility of the media switch dynamics by performing successive renewals within the same microdevice (Experiments 1 and 2 in Fig. 3D) using the same Rhodamine B assay. Importantly, although all the experiments presented above were made with a proof-of-concept design, our conclusions will be applicable to other networks as well, with only minor additional characterizations and optimizations. Furthermore, simple gravity-based flows and manual valves can easily be used to renew and switch the fluids in the chips (data not shown), although they do not provide the degree of precision and reproducibility of more high-end controllers.

While the LSR elastomer cannot be compared to demanding photolithography processes as it does not allow the fabrication of extremely small channels and multilayered structures, our results show that it represents an ideal material for the fabrication of simpler but powerful microsystems. In addition, the possibility to re-use the elastomer layer multiple times is an important advantage, making these microsystems cost-effective, easy to use, and more likely to become widespread in biology laboratories.

Live-cell imaging using the elastomer chips

All the assays described above are proof-of-concept experiments that demonstrate the different features of the microsystems that can be assembled using the elastomer, from their robustness to the possibility of dynamically controlling a range of environmental parameters. However, the goal of this study was to establish a new and easy-to-fabricate system dedicated to live-cell imaging. We therefore set out to validate the optical properties of the elastomer. Indeed, although cells under microscopic observation in the perfusion channel are only separated from the microscope lens by a microscopy-grade glass coverslip, strong autofluorescence of the material could interfere with experiments using fluorescence measurements. We therefore injected medium in a chip, directly exposed the elastomer surrounding the perfusion channel to the most common excitation wavelengths and compared fluorescence intensities to those measured within the channel. Strikingly, we found no differences in signal between compartments, demonstrating that the optical properties of the elastomer are particularly suited for fluorescence microscopy (Table 3).

Next, we assessed the behavior of living cells grown in our microsystems in order to determine the biocompatibility of the elastomer. First, fission yeast cells (*Schizosaccharomyces pombe*) were injected in a chip after coating of the bottom glass coverslip with lectin, thereby promoting their adhesion to the glass substrate. A

constant flow of 20 µL/min of fresh medium was then applied and cells were grown in these conditions at 32 °C for several hours. We previously observed that *S. pombe* cells grown in very confined environments without medium renewal show various phenotypes, including a reduction of their size at division (data not shown). While we surmised that the maintenance of a constant flow of medium may circumvent this issue, the shear stress imposed by such a flow may have other deleterious effects on cell physiology. Using this setup, we therefore determined potential alterations in their division time as well as changes in their size at division and morphology. All these phenotypes are well-described markers that allow the identification of defects in cell cycle progression and cell organization. Comparing cells dividing in both new and re-used microfluidic chips with cells grown in standard batch cultures, we observed no differences in any of these properties after more than 5 hours (Fig. 4A, B). This showed that the elastomer chips are perfectly compatible with the use of fission yeast cells and that the application of a constant flow of fresh medium does not seem to affect cell growth.

Finally, we tested the compatibility of the elastomer chips with adherent mammalian cell lines. To this end, we seeded HeLa cells in either our microsystems or standard cell culture-grade 12-well plates. While the plates were subsequently kept in a controlled CO_2 incubator without medium renewal, a constant flow of fresh medium (5 µL/min) was applied to the chips after the cells were allowed to adhere to the glass coverslip (~ 3 h after inoculating the cells). For ease of manipulation in this assay, the temperature of 37 °C was ensured in the microchannel using a high precision hot plate. Cells were then allowed to grow for 28 h in these conditions. As was the case for fission yeast, we did not observe any detectable difference between the chips and the plates, with similar increases in cell density, no apparent defects in cell morphology and no particular increases in cell death (Fig. 4C). Again not only did this experiment show the compatibility of our devices with the use of mammalian cells, but they also suggest that the shear stress that results from the maintenance of a constant flow of medium in the chips does not seem to strongly affect these cells.

Collectively, these results demonstrate that our microsystems can be used to perform live-cell imaging experiments with different types of cells over long periods of time, without any apparent defect to the cells and without altering their proliferation potential.

Dynamic modulation of the cellular environment and real-time monitoring of cellular responses to perturbations

To fully establish our chips as easy-to-build but powerful systems for live-cell imaging experiments and in particular when dynamic alteration of the medium composition is required, we set out to perform different media switches and monitor the responses of cells to these alterations.

First, we used fission yeast cells operating with an engineered cell cycle control network that is sensitive to inhibition by the ATP analogue 3-MBPP1(Coudreuse & Nurse, 2010). We previously showed that treatment of these cells with high concentrations of 3-MBPP1 results in a G2 arrest and elongation of the cells, and subsequent release into inhibitor-free medium allows for synchronous re-entry into the cell cycle(Tong Chen et al., 2016; Coudreuse & Nurse, 2010). However, like a broad range of small hydrophobic molecules, the 3-MBPP1 inhibitor is absorbed by a number of the most common materials used for microfabrication(Toepke & Beebe, 2006). We therefore started by investigating the absorptive properties of the elastomer within the context of the microfluidic chips. To this end, we took advantage of the effects of the 3-MBPP1 inhibitor on analogue-sensitive fission yeast cells. Indeed, while Rhodamine B absorption is generally used to characterize this aspect

of microfabrication materials(Mukhopadhyay, 2007), our previous studies revealed that, in contrast to our cell-based assay, this method is not sufficiently sensitive to determine the compatibility of a given material with the use of small hydrophobic molecules(Tong Chen et al., 2016). Analogue-sensitive cells were injected in an elastomer chip coated with lectin and subsequently exposed to a constant flow (20 µL/min) of medium containing 0.4 or 1 µM of 3-MBPP1 at 32 °C. These concentrations of inhibitor result in a complete G2 arrest when cells are grown in culture flasks. After 3 h (a bit longer than a cell cycle in these conditions), we monitored the septation index of the cells. Strikingly, we observed significant absorption at the border of the channels, where cells are in close proximity with the elastomer, resulting in high septation indexes (Fig. 5A, B). However, when focusing on cells further away from the material, the impact of this absorption was reduced, and cells at about 1 mm from the borders of the channels were fully arrested, similarly to the control (Fig. 5A, B). These results demonstrate that when using small hydrophobic molecules in the elastomer chips, particular attention must be drawn to discard results obtained from cells that are too close to the material.

Subsequently, we performed an inhibitor block and release assay in the chips. To this end, a similar approach as above was used, but after 2 h 45 min in the presence of 1 µM 3-MBPP1 at 32 °C (duration of a cell cycle in these conditions), we triggered a medium switch in the chip and perfused them with inhibitor-free medium (20 µL/min) for an additional 2 h, assessing the septation index throughout the time course (Fig. 6A). As a control, a similar experiment was performed in batch cultures, inducing the release by filtration. Our results showed a slight delay in the microsystem compared to the control (~ 5 min), likely resulting from differences in the release kinetics. Indeed, while the medium switch is virtually instantaneous when using filtration, the time required to change the medium in the chips at this flow rate, as described in Fig. 3B, is consistent with this 5 min delay. Importantly, we systematically observed a better synchrony when using the chips, with the septation index reaching a higher maximum for both cell cycles after release. We hypothesize that this improved synchrony is the result of a more controlled and stable overall environment in the chips compared to the filtration protocol, which imposes more stress to the cells.

Next, we performed a similar experiment using HeLa cells and the CDK1 inhibitor RO-3306(Vassilev et al., 2006). Cells resuspended after trypsin treatment were injected in the chips or in standard culture dishes and allowed to re-adhere to the substrates for 3 h at 37 °C. 6 µM RO-3306 was then added to the control or perfused to the cells in the microdevices for 20 h. In the latter case, the perfusion was triggered for 10 min every hours at a flow rate of 13 µL/min. This periodic medium renewal was implemented as we observed that a constant flow of medium containing fresh inhibitor over such a long period of time was toxic to the cells (data not shown), an effect that is not observed in the control cultures, in which the inhibitor is not constantly renewed. Cells were then released in inhibitor-free medium for 15 min at 20 µL/min and then at a constant flow rate of 5 µL/min (or through a single medium renewal in the control), and the percentages of both mitotic cells (rounded) and post-mitotic cells (duplets) were determined. We observed similar profiles in both the chips and the control, however with somewhat different fine kinetics. This is likely due to the drastically different conditions between the two approaches, and some toxicity of the RO-3306 may still affect the cells, despite our protocol of periodic rather than constant renewal. Nevertheless, together with our biocompatibility assays in the presence of a constant flow (Fig. 4C), this demonstrates that media switches and the analyses of the responses of cells to such treatments in real-time are also possible for mammalian cells in our microsystems.

CONCLUSIONS

Microfluidic technologies represent a very powerful approach to investigate cell biology, in particular when coupled to high-resolution fluorescence microscopy. However, they are not used to their full potential in research laboratories due to the difficulty of the microdevice fabrication procedures, the requirement for complex and expensive equipments as well as specific expertise that is not common in most research teams in the life sciences. We have developed a system that is not only easy to fabricate, taking advantage of cost-effective solutions in its most basic version, but also to use, while still providing a number of advantages associated with microfluidics. These chips are re-usable, biocompatible, easily coupled with high-end photonic microscopy and allow for a dynamic control of the cellular environment during live-cell imaging assays. Furthermore, in contrast to fully commercially available systems, they remain customizable and permit the implementation of a broad range of fluidic networks. All together, these features make such microdevices very attractive for cell biological studies and their simplicity is likely to promote the expansion of microfluidics in laboratories that do not have expertise in the development of microdevices.

FIGURE LEGENDS

Figure 1. Fabrication of re-usable microfluidic chips using the LSR elastomer.
A. The LSR elastomer is an easy-to-manipulate material that is particularly adapted to the fabrication of microfluidic chips. Left panel: the elastomer is robust to stretching. Right panel: the elastomer is robust to folding. **B.** Versatility of the LSR elastomer for advanced microfluidic chips. Complex patterns can easily be fabricated using a CO_2 laser cutting machine. A schematics of these patterns is presented in Supplementary Fig. 2A. The transparent LSR was painted for ease of visualization. **C.** Microscopy image of a laser-cut piece of elastomer showing the precision of the cutting procedure along the edge of the cut. Bright field image (20X). Scale bar = 100 µm. **D.** The narrowest channel that can be obtained with a 50 µm beam CO_2 laser cutting machine is ~170 µm wide. A piece of elastomer was placed between 2 liners (double-sided adhesive) prior to cutting. Bright field image (10X). Scale bar = 100 µm. **E.** Microchannels can be generated in the elastomer sheet using a simple razor blade. Top panel: comparison of similar channels fabricated using a laser (left) and a razor blade (right). A blue dye is used for ease of visualization. Bottom panel: the use of a razor blade allows for high quality cuts. Brightfield image (20X). Scale bar = 100 µm. **F.** The LSR elastomer is compatible with the fabrication of multichannel microfluidic chips. To demonstrate the absence of cross-contamination between channels, an elastomer chip was fabricated comprising 2 channels (500 µm wide) separated by 300 µm at the middle section (left panel) and intercalated between two glass coverslips. The two channels were injected with either water or Rhodamine B (5 µM) at a constant flow of 20 µl/min, and the fluorescence intensity at different positions of the chip (geometric marks) was measured over time (right panel). T=0 corresponds to 5 min after the start of the perfusion. Data were corrected for the background measured at the entrance of the water channel at T=0. No contamination of the water channel by Rhodamine B could be detected after 8 hours.

Figure 2. Microfluidic-based temperature control of the elastomer microfluidic chip.
A. Schematics of a complete chip fabricated using the LSR elastomer and integrating a microfluidic temperature control system. Assembly of the different layers is easily achieved by hand at room temperature. **B.** Left panel: picture of the different layers used to mount the chip in A. Right panel: image of the assembled chip (top view). An orange dye (temperature control layer) and a blue dye (perfusion layer for medium input) were used for ease of visualization. Connecting tubings were inserted in the manifold and glued using epoxy. The dimensions of the different channels of the chip are described in Supplementary Fig. 2C. **C-E.** All experiments were performed using chips as described in Supplementary Fig. 2B and all temperature measurements within the cell channels were made using metal electrodes deposited on the glass coverslips(Tong Chen et al., 2016). **C.** Fast temperature switches can be achieved using the microfluidic temperature control system. A series of switches were triggered (without medium flow) and the theoretical sample temperature was compared to that measured in the sample channel. The theoretical temperature was calculated for each point based on the calibration equation in Supplementary Fig. 1 and the measured lens and thermalization fluid temperatures. **D.** The temperature of the sample is robust to changes in the flow rate of the culture medium. Sample temperature was set either below (top graph) or above (bottom graph) the ambient temperature, and the flow rate of the culture medium was altered. No changes in sample temperature were measured, even at the highest flow rate tested (80 µL/min). **E.** The temperature of the sample is robust to changes in immersion lens. Sample temperature was set below (top graph), comparable to (middle graph) or above the ambient temperature and the immersion lens was switched (times of the switches are indicated by asterisks) back and forth between a 63X and a 100X objective. To simplify this assay, no medium flow was applied, as it has no impact on the temperature of the sample (see D). Transitory changes in temperature were observed, corresponding to the time windows during which the

microsystem was not in contact with the lenses. However, the channel rapidly returned to the target temperatures after the contact between the lens and the glass coverslip was re-established.

Figure 3. Fast media switches using the elastomer microchips.
A. Schematics of the complete microfluidic setup used to perform fast media switches in the elastomer chips. The flow sensors (FS) downstream of the valves were used to modulate the operation of a pressure controller to maintain an accurate flow rate in the system, independently of the fluidic resistance in the network. In order to limit bubbles in the system, vacuum based bubble traps (BT) were mounted in line with each flow sensor (note that the bubble traps were only added when performing experiments with cells but were not used in B-D). In this schematics, only medium B is perfused (open valve). Switches between medium A and B were simply achieved through operating the valves. **B-D.** All experiments were performed using chips as described in Supplementary Fig. 2C. **B.** Characterization of the dynamics of media switches as a function of the perfusion flow rates. 50 µM Rhodamine B was injected in a microchannel at 20 µL/min for 10 min. At T=0, water was injected at 20 µL/min and the fluorescence intensity in the chip was followed over time. The same chip was then re-used twice using the same protocol but with water perfusion at 10 or 5 µL/min. Data were corrected for the background (measured prior to the initial Rhodamine B injection) and normalized to T=0 (for each flow rate). This assay demonstrates a clear correlation between the flow rate and the timing of medium renewal. **C.** Characterization of the influence of the position within the cell chamber on the dynamics of the media switches. 5 µM Rhodamine B was injected at 20 µL/min for 10 min prior to switching to water at the same flow rate (T=0). Fluorescence intensity was then measured over time at various distances from the border of the channel. Data were corrected for the background (measured prior to the initial Rhodamine B injection) and normalized to T=0 (for each position). Note that the absorption of Rhodamine B by the elastomer influences the measurements close to the border. No dramatic position-specific changes in the dynamics of media switches were observed. **D.** Reproducibility of the media switch dynamics. 50 µM Rhodamine B was injected at 20 µL/min for 10 min in a chip. At T=0 and T=13.5 min (asterisk), the perfusion was switched to water (20 µL/min) and back to Rhodamine B, respectively. Fluorescence intensity was then followed over time (Experiment 1). The same chip was then re-used in an identical experiment (Experiment 2), showing the reproducibility of the media switches. The slopes of the linear regressions for each of the transition phases are indicated. Data were corrected for the background (measured prior to the initial Rhodamine B injection) and normalized to T=0 (for each experiment).

Figure 4. Biocompatibility of the elastomer microfluidic chips.
A, B. Experiments were performed using chips as described in Supplementary Fig. 2C. **A.** Fission yeast cells operating with a modified CDK module that is sensitive to inhibition by the 3-MBPP1 ATP analogue(Coudreuse & Nurse, 2010) were injected in a lectin-coated microchip, and medium was perfused at 20 µL/min, with sample temperature maintained at 32 °C. After 2 h of perfusion, images were acquired over 5 h to calculate single-cell generation times as well as cell sizes at division. Results from a newly cut elastomer chip were compared to those obtained with re-used chips (>10 times) as well as those from control culture flasks. For the generation time in flasks, the standard error of 3 independent experiments is shown. For the size at division in flasks, the average of 3 independent experiments (n>50 for each experiment) is shown with the standard deviation over the entire set of data. For the size at division in chips, the standard deviations are shown for each chip (n>50). **B.** DIC images of cells grown in the chips in A at the indicated times. No morphological defects were observed. Scale bars = 10 µm. **C.** Compatibility of the microchips with the use of mammalian cells. HeLa cells were injected in a chip or in a standard cell culture dish at similar starting densities and grown for 28 h at 37 °C. In contrast to the static conditions in the dish, a constant flow rate of fresh medium (5 µL/min) was applied in the

chip after cells were allowed to adhere to the glass substrate (~3 h after initial injection, T=0). No differences were observed between the conditions. Note that the chip used the perfusion channel as in Supplementary Fig. 2C, but no temperature channel was integrated (direct bonding of a plastic coverslip on the PMMA manifold, see Materials and Methods) as the temperature of the sample was maintained by a high precision hot plate instead of the microfluidic temperature control system in order to facilitate this proof-of-concept assay. For this long-term experiment, the chip and tubings were pre-incubated overnight with 2 mg/mL BSA at 4 °C and washed with medium prior to injecting the cells. Bright field images. Scale bars = 100 µm.

Figure 5. Absorption of small molecules by the elastomer.
All experiments were performed using chips as described in Supplementary Fig. 2C. **A.** The absorption of small molecules by the elastomer restricts the area of the chip that can be monitored when treating cells with such molecules. Fission yeast cells operating with a modified CDK module that is sensitive to inhibition by the 3-MBPP1 ATP analogue(Coudreuse & Nurse, 2010) were injected in a lectin-coated microsystem and exposed to a 20 µL/min flow of medium containing 1 or 0.4 µM 3-MBPP1, with sample temperature maintained at 32 °C. After 3 h, the septation indexes were determined at different distances from the border of the channel. Graphs represent the average of 3 independent experiments (n>50 for each experiment) with standard errors. Note that to facilitate this proof-of-concept assay, the temperature of the samples was maintained using a high precision hot plate. **B.** DIC images of cells in A at the border and at distances of 0.5 and 1 mm from the border of the chip. At 1 mm and more from the border of the chip, both concentrations of inhibitor led to a complete G2 arrest, as seen in the control experiments (cells exposed to 3-MBPP1 in standard batch cultures). The size at division of cells at the border when treated with 1 µM 3-MBPP1 was 23.2 µm (average of 3 independent experiments, standard error: 0.7. n>40 for each experiment), which is significantly larger than in inhibitor-free medium (compare with Figure 4A). This demonstrate that not all inhibitor is absorbed by the elastomer. Scale bars = 10 µm.

Figure 6. Monitoring cellular responses to dynamic changes in their environment.
A. Block and release experiment using fission yeast cells (chip as in Supplementary Fig . 2C). Fission yeast cells operating with a modified CDK module that is sensitive to inhibition by the 3-MBPP1 ATP analogue(Coudreuse & Nurse, 2010) were injected in a chip coated with lectin. Cells were then perfused with 1 µM 3-MBPP1 at 32 °C for 2 h 45 min at 20 µL/min (G2 block) before being released in inhibitor-free medium (T=0) at 20 µL/min. As a control, cells grown in batch cultures at 32 °C were arrested in G2 using 1 µM 3-MBPP1 for 2 h 45 min and released into inhibitor-free medium by three successive washing steps by filtration (T=0). In both assays, the septation index was then monitored over time (n>50 for each time point). The averages of 3 independent experiments are shown with standard errors. The dynamics of release in the chips are similar to those in the batch cultures. Note that the time points in the chips (mounted on a microscope) were acquired every 5 min, a frequency that was difficult to achieve with batch cultures (time points every 10 min). As a result of the higher frequency of acquisition for the experiments performed with the chips, a higher experimental variability in timing can be observed compared to the less resolved batch cultures. **B.** Synchronization of mammalian cell lines using a cell cycle inhibitor (chip as in Fig. 4C). HeLa cells were injected in a microsystem maintained at 37 °C on a high precision hot plate to facilitate this proof-of-concept assay. Cells were then allowed to adhere to the glass substrate for 3 h and subsequently treated with 6 µM of the CDK inhibitor RO-3306(Vassilev et al., 2006) for 10 min (flow rate of 13 µL/min) every hour for 20 h (constant renewal of this inhibitor over 20 h was indeed toxic to the cells - our unpublished data - , in contrast to the situation in control culture dishes where such renewal is not performed). Cells were then released in inhibitor-free medium (T=0; 15 min at 20 µL/min and then 5 µL/min) and followed for 4 h. As a control, cells treated with 6 µM RO-3306 in culture dishes were

washed and incubated in normal medium. The percentages of rounded cells (mitotic) and post-mitotic cell duplets were then quantified. The averages of 3 independent experiments (n>100 for each experiment) are shown with standard errors. The synchronization in the chip showed similar overall dynamics to the situation in control dishes (in particular regarding the timing of mitotic entry). However, differences in the second phase of the process could be observed, likely due to the differences in treatment (frequent renewal of the medium with fresh inhibitor in the chips).

Supplementary Figure 1. Calibration of the temperature control system.
A relationship between the temperatures of the thermalization fluid (T_i, as imposed by Peltier elements), lens (T_{lens}, as measured by a contact sensor) and sample (T_{sample}, as measured by deposited metal electrode on the calibration coverslip) was established (see Materials and Methods, chip as in Supplementary Fig. 2B). Provided the temperature of the lens, this allows for the calculation of the temperature of the thermalization fluid that is necessary to reach the target sample temperature(Tong Chen et al., 2016).

Supplementary Figure 2. Microfluidic designs used in this study.
A. Schematics of the patterns in Fig. 1B. Dimensions are in mm. **B.** Schematics of the temperature and perfusion channels used for the calibration (Supplementary Fig. 1) and for Fig. 2C-E. **B.** Schematics of the temperature and perfusion channels used for Fig. 2B, 3B-D, 4, 5 and 6. Diagrams are not to scale.

ACKNOWLEDGEMENTS

We thank Pei Yun Jenny Wu for critically reading the manuscript and members of the SyntheCell and Genome Duplication and Maintenance teams for useful discussions. JB was funded by a grant to DC from the DGA, France and by Cherry Biotech, France. This work was also supported by a grant from the Région Bretagne, France.

REFERENCES

Bayraktar, T., & Pidugu, S. B. (2006). Characterization of liquid flows in microfluidic systems. *International Journal of Heat and Mass Transfer*, *49*(5-6), 815–824. http://doi.org/10.1016/j.ijheatmasstransfer.2005.11.007

Bhatia, S. N., & Ingber, D. E. (2014). Microfluidic organs-on-chips. *Nature Biotechnology*, *32*(8), 760–772. http://doi.org/10.1038/nbt.2989

Chen, Tong, Gomez-Escoda, B., Munoz-Garcia, J., Babic, J., Griscom, L., Wu, P.-Y. J., & Coudreuse, D. (2016). A drug-compatible and temperature-controlled microfluidic device for live-cell imaging. *Open Biology*, *6*(8), 160156. http://doi.org/10.1098/rsob.160156

Chen, Yuchao, Li, P., Huang, P.-H., Xie, Y., Mai, J. D., Wang, L., et al. (2014). Rare cell isolation and analysis in microfluidics. *Lab on a Chip*, *14*(4), 626–645. http://doi.org/10.1039/c3lc90136j

Chen, Yun, Zhang, L., & Chen, G. (2008). Fabrication, modification, and application of poly(methyl methacrylate) microfluidic chips. *Electrophoresis*, *29*(9), 1801–1814. http://doi.org/10.1002/elps.200700552

Coudreuse, D., & Nurse, P. (2010). Driving the cell cycle with a minimal CDK control network. *Nature*, *468*(7327), 1074–1079. http://doi.org/10.1038/nature09543

Friend, J., & Yeo, L. (2010). Fabrication of microfluidic devices using polydimethylsiloxane. *Biomicrofluidics*, *4*(2), 026502. http://doi.org/10.1063/1.3259624

Haeberle, S., & Zengerle, R. (2007). Microfluidic platforms for lab-on-a-chip applications. *Lab on a Chip*, *7*(9), 1094–1110. http://doi.org/10.1039/b706364b

Hayles, J., & Nurse, P. (1992). Genetics of the fission yeast Schizosaccharomyces pombe. *Annual Review of Genetics*, *26*(1), 373–402. http://doi.org/10.1146/annurev.ge.26.120192.002105

Iliescu, C., Taylor, H., Avram, M., Miao, J., & Franssila, S. (2012). A practical guide for the fabrication of microfluidic devices using glass and silicon. *Biomicrofluidics*, *6*(1), 016505. http://doi.org/10.1063/1.3689939

Lee, C.-Y., Chang, C.-L., Wang, Y.-N., & Fu, L.-M. (2011). Microfluidic mixing: a review. *International Journal of Molecular Sciences*, *12*(5), 3263–3287. http://doi.org/10.3390/ijms12053263

Moreno, S., Klar, A., & Nurse, P. (1991). Molecular genetic analysis of fission yeast Schizosaccharomyces pombe. *Methods in Enzymology*, *194*, 795–823.

Mukhopadhyay, R. (2007). When PDMS isn't the best. *Analytical Chemistry*, *79*(9), 3248–3253. http://doi.org/10.1021/ac071903e

Qin, D., Xia, Y., & Whitesides, G. M. (2010). Soft lithography for micro- and nanoscale patterning. *Nature Protocols*, *5*(3), 491–502. http://doi.org/10.1038/nprot.2009.234

Stroock, A. D., & Whitesides, G. M. (2003). Controlling Flows in Microchannels with Patterned Surface Charge and Topography. *Accounts of Chemical Research*, *36*(8), 597–604. http://doi.org/10.1021/ar0202870

Toepke, M. W., & Beebe, D. J. (2006). PDMS absorption of small molecules and consequences in microfluidic

applications. *Lab on a Chip*, *6*(12), 1484–1486. http://doi.org/10.1039/b612140c

Vassilev, L. T., Tovar, C., Chen, S., Knezevic, D., Zhao, X., Sun, H., et al. (2006). Selective small-molecule inhibitor reveals critical mitotic functions of human CDK1. *Proceedings of the National Academy of Sciences of the United States of America*, *103*(28), 10660–10665. http://doi.org/10.1073/pnas.0600447103

Velve-Casquillas, G., Le Berre, M., Piel, M., & Tran, P. T. (2010). Microfluidic tools for cell biological research. *Nano Today*, *5*(1), 28–47. http://doi.org/10.1016/j.nantod.2009.12.001

Whitesides, G. M. (2006). The origins and the future of microfluidics. *Nature*, *442*(7101), 368–373. http://doi.org/10.1038/nature05058

Whitesides, G. M. (2013). Cool, or simple and cheap? Why not both? *Lab on a Chip*, *13*(1), 11–13. http://doi.org/10.1039/c2lc90109a

Williams, M. S., Longmuir, K. J., & Yager, P. (2008). A practical guide to the staggered herringbone mixer. *Lab on a Chip*, *8*(7), 1121–1129. http://doi.org/10.1039/b802562b

Xia, Yanyan, Si, J., & Li, Z. (2016). Fabrication techniques for microfluidic paper-based analytical devices and their applications for biological testing: A review. *Biosensors & Bioelectronics*, *77*, 774–789. http://doi.org/10.1016/j.bios.2015.10.032

Young, E. W. K., & Beebe, D. J. (2010). Fundamentals of microfluidic cell culture in controlled microenvironments. *Chemical Society Reviews*, *39*(3), 1036–1048. http://doi.org/10.1039/b909900j

FIGURE 1

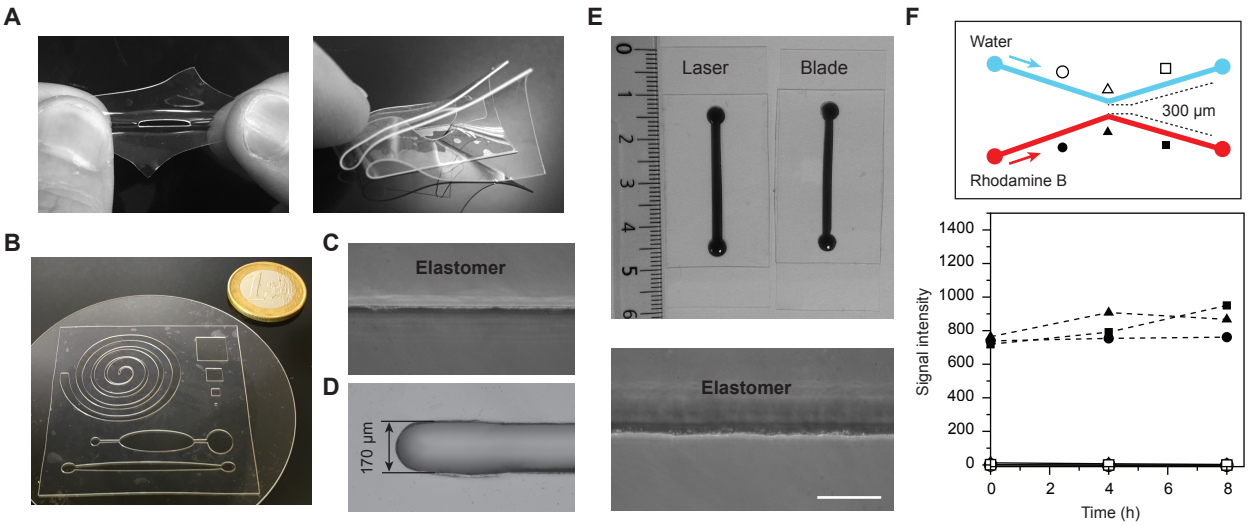
A
B
C
Elastomer
D
170 µm
E
Laser
Blade
Elastomer
F
Water
300 µm
Rhodamine B
Signal intensity
1400
1200
1000
800
600
400
200
0
0
2
4
6
8
Time (h)

FIGURE 2

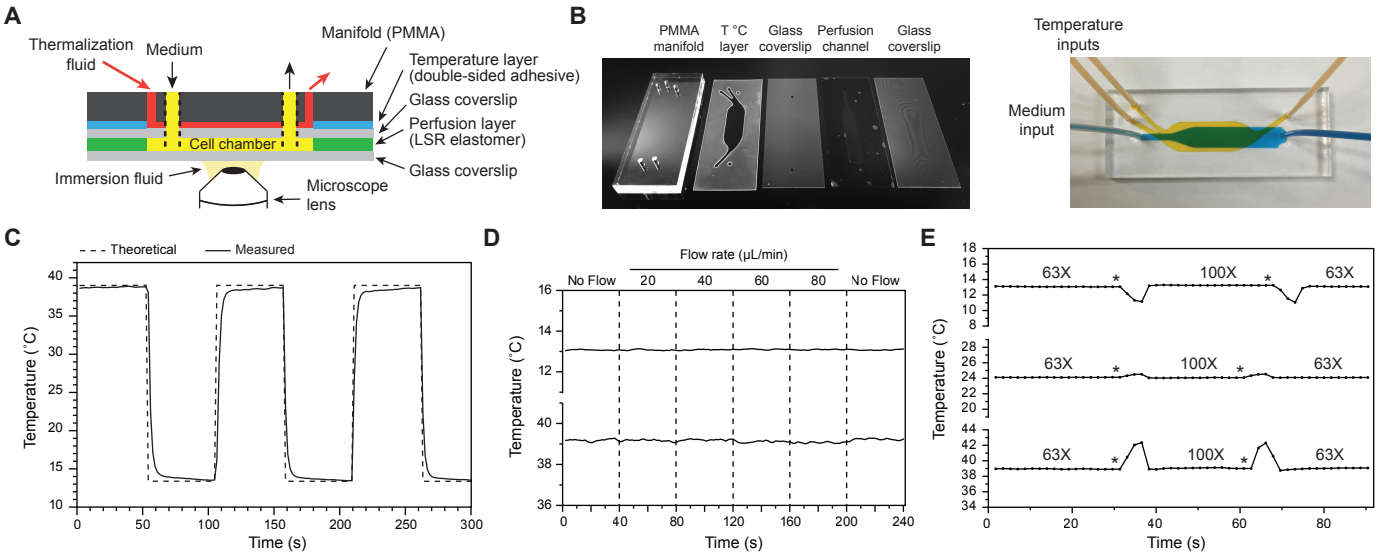
A
Thermalization fluid
Medium
Manifold (PMMA)
Temperature layer (double-sided adhesive)
Glass coverslip
Perfusion layer (LSR elastomer)
Glass coverslip
Cell chamber
Immersion fluid
Microscope lens
B
PMMA manifold
T °C layer
Glass coverslip
Perfusion channel
Glass coverslip
Temperature inputs
Medium input
C
Theoretical
Measured
Temperature (˚C)
Time (s)
D
Flow rate (µL/min)
No Flow
20
40
60
80
No Flow
Temperature (˚C)
Time (s)
E
63X
100X
63X
Temperature (˚C)
Time (s)

FIGURE 3

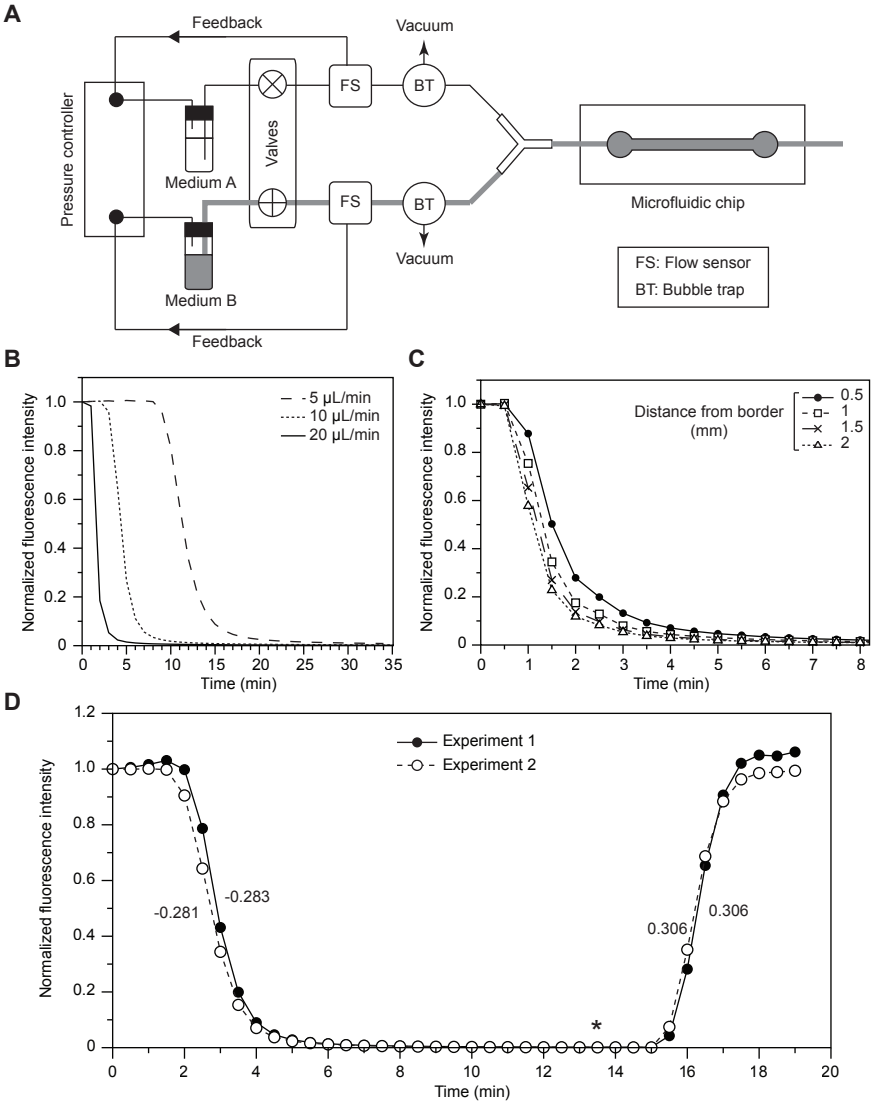
A
Feedback
Vacuum
FS
BT
Pressure controller
Valves
Medium A
Microfluidic chip
FS
BT
Vacuum
FS: Flow sensor
BT: Bubble trap
Medium B
Feedback
B
Normalized fluorescence intensity
5 µL/min
10 µL/min
20 µL/min
Time (min)
C
Normalized fluorescence intensity
Distance from border (mm)
0.5
1
1.5
2
Time (min)
D
Normalized fluorescence intensity
Experiment 1
Experiment 2
-0.281
-0.283
0.306
0.306
*
Time (min)

FIGURE 4

A

	Flask	Chip		
		New	Old_1	Old_2
Generation time (min)	149.5 ± 0.8	145.2	147.5	143.1
Size at division (min)	15.0 ± 0.1	15.2 ± 1.8	14.9 ± 1.0	14.7 ± 1.2

B

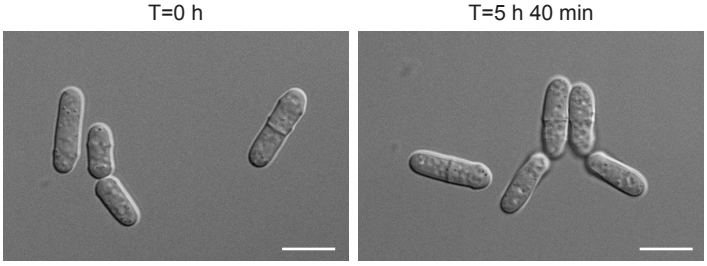

C

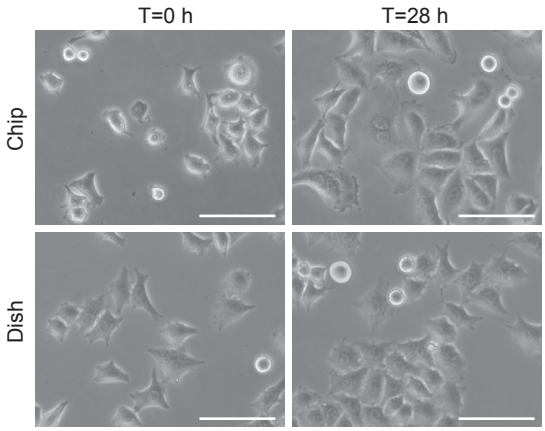

FIGURE 5

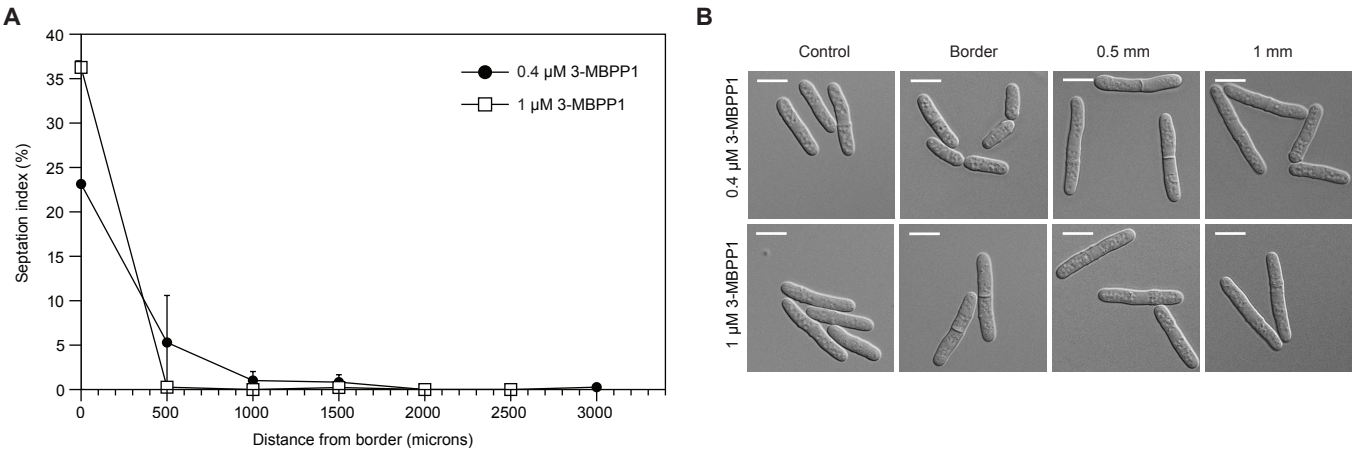
A
B
Septation index (%)
Distance from border (microns)
0.4 µM 3-MBPP1
1 µM 3-MBPP1
Control
Border
0.5 mm
1 mm

FIGURE 6

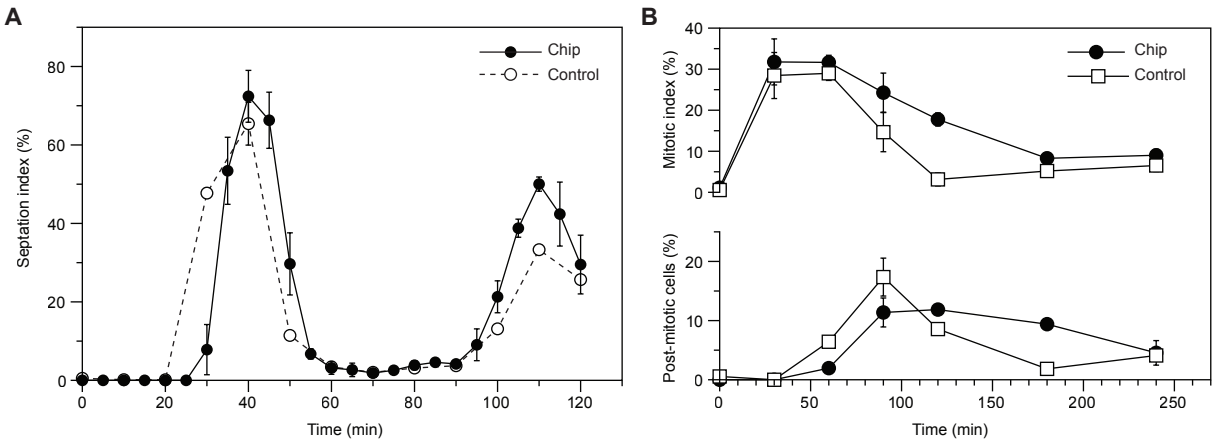
A
Chip
Control
Septation index (%)
Time (min)
B
Chip
Control
Mitotic index (%)
Post-mitotic cells (%)
Time (min)

Supplementary Figure 1

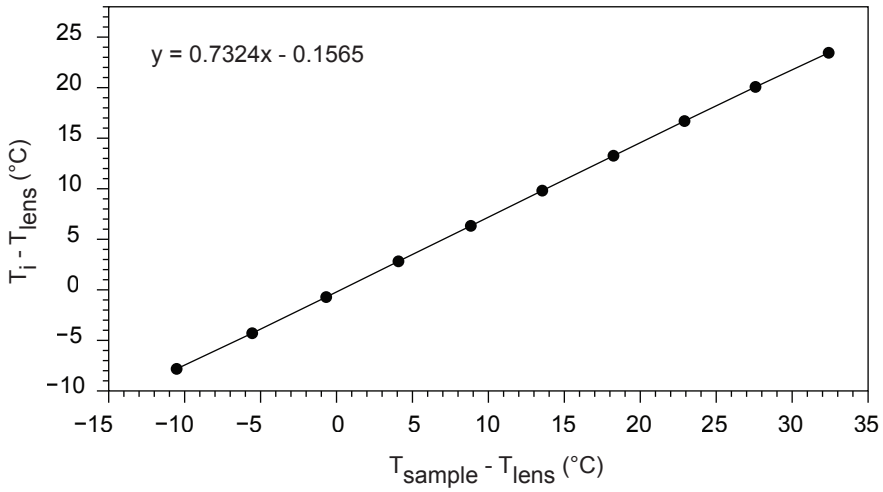

Supplementary Figure 2

A

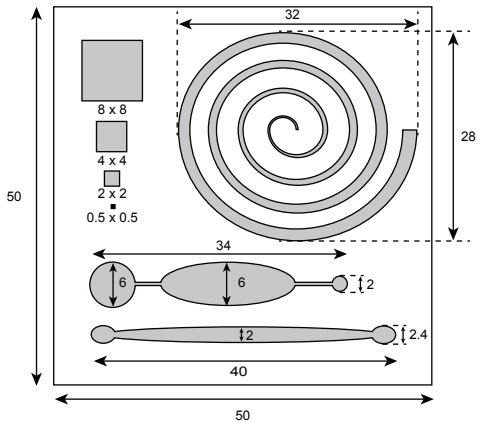

B

Calibration chips

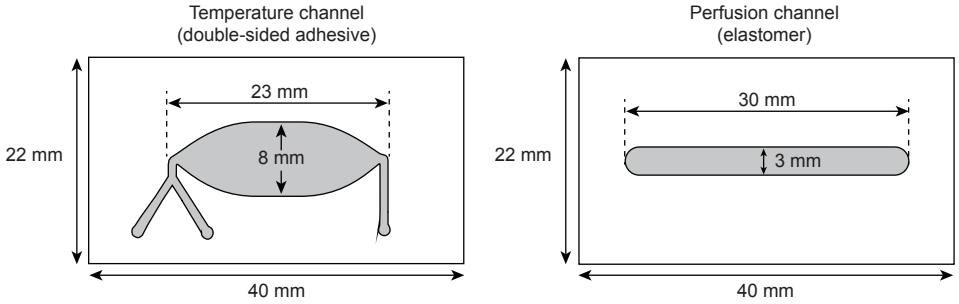

C

Experimental chips

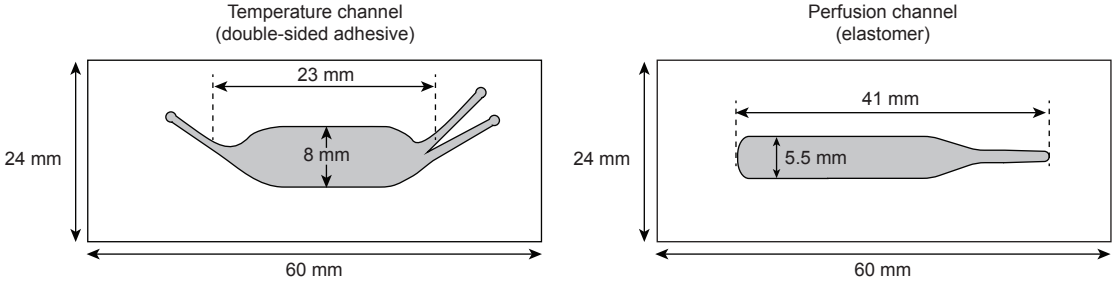

Chapter 3: The membrane chip

The drawbacks of the PDMS (Polydimethylsiloxane) have led researchers to seek for alternative materials for building biocompatible microfluidic chip. However, the use of complex structures and designs, which have been successfully engineered for allowing cell trapping during live-cell imaging, is challenging in such materials. Several fabrication protocols have enhanced the possibility of achieving these complex designs in PDMS, and their replica in plastic materials. However, as previously introduced in chapter 1, the bonding of these materials, especially to microscopy-grade plastic coverslip, has not been successfully integrated in biology laboratories. The other alternative strategy for observing cells at the microscope while perfusing is to use a semi-permeable membrane. However, its integration, especially between hard plastic material, is uneasy and only a few protocols have been established. This chapter presents a novel system, which is membrane-based, which is made of biocompatible materials. It allows constant delivery of fresh medium by diffusion from a feeding channel to a cell channel, and limits the undesired shear stress on cells.

Towards a novel membrane-based microsystem dedicated to live-cell imaging

1. Introduction

Microfluidics have gained considerable attention during the past two decades[1], and opened the door to new investigations in the life sciences. Taking advantage of miniaturization, microfluidic systems circumvent the problems biologists encounter when using conventional methods. They allow the reduction of sample volumes and reagents[2], and provide researchers with a precise and dynamic control of the cell microenvironment in time and space[3], a particularly important feature when performing live-cell imaging. The laminar flow in such devices can be spatially controlled[4] and becomes highly predictable[5]. This allows biologists to mimic as much as possible the ideal physical and biochemical conditions of their biological samples[6]. Being closer to their natural state, the observation of cells under high-resolution microscopy facilitates the understanding of their behaviors and their responses in real-time to perturbations of their microenvironment[7,8]. As of today, the optimal strategy that allows cells to remain in healthy conditions during long-term imaging is microfluidic perfusion[9]. Indeed, microsystems are perfect candidates for achieving constant renewal of fresh medium for ensuring cell proliferation. A myriad of systems and protocols have been developed for realizing such perfusion cultures, but their use in laboratories and their compatibility with various types of cells remains challenging. Even though perfusion systems are compatible with adherent cells, which adhere to their substrate and do not detach in the presence of a constant flow, the possibility of studying non-adherent cells in such systems has been a first challenge. For that, coatings of glass substrates with lectin or poly-L-lysin for insuring their immobilization have been demonstrated to be efficient, but are incompatible with long-term experiments. Moreover, the engineering of complex structures within the perfusion flow allow cells to be trapped and observed during live-cell imaging [10-12]. However, this strategy is not of interest when hydrodynamic shear stress is to be avoided, as it can alter cell behavior[13] and can be deleterious for cell physiology[14]. This non-desired shear stress effect led to the engineering of new designs involving side chambers separated from the perfusion flow, where cells are injected and observed: constant nutritional delivery occurs by diffusion between the cell chamber and the feeding channel[15,16]. The fabrication of such systems requires complex procedures and expensive equipments. Moreover, the injection of cells inside the chambers is not trivial as the use of vacuum through gas permeable materials is often necessary to remove the air trapped[15]. An alternative strategy for avoiding shear stress without involving complex structures is the incorporation of semi-permeable membranes, which separate two channels horizontally and allow exchanges only where the two channels intersect[3]. These membranes act as semi-permeable barriers, allowing nutritional delivery by diffusion and preventing non-desired hydrodynamic shear stress. Importantly, the compatibility with both adherent and non-adherent model organisms and high-quality imaging has been demonstrated[17]. Various membranes have been integrated to separate a cell channel from a perfusion channel, differing by their materials, pore sizes and distributions, thicknesses, and fabrication methods[18]. The dynamics of media switches are membrane-dependent, therefore significant variations in the diffusion timings can be obtained depending on the selection of the membrane, from seconds to hours. For instance, Mirzaei *et al.* demonstrated the possibility of changing medium withing 10 seconds using a 20 µm-thick membrane. Charvin *et al.* used a 30 µm-thick cellulose membrane deposited directly on budding yeast cells, and the switching times were approximately 30 to 40 seconds[19]. However,

these systems had their membrane directly inserted on top of the studied cells, which prevents their movements [17,19], but may lead to physiological and morphological stresses[20].

Significant advances have been made for realizing robust and functional perfusion systems integrating membranes. However, one major challenge has prevented biologists to take full advantage of these membrane-based microsystems. As hard to manipulate, membranes are difficult to integrate in microfluidic chips, and their implementation has been developed mostly between two PDMS layers[21,22]. Although easy to manipulate, the polydimethylsiloxane presents a number of critical drawbacks, making it incompatible with many standard biological assays[14,23]. Its absorption of small biomolecules prevents its usage for a broad range of experiments involving low or precise concentrations of drugs[24], and leads to unreliable chemical characterizations. Moreover, PDMS releases uncross-linked oligomers, and this was shown to have an impact on cell viability[25 26]. Therefore, low-cost plastic microchips have emerged with their fast and complex prototyping[27]. As already described in Chapter 1, fabricating microfluidic chips containing traps or sides chambers in plastic materials is difficult due to their hardness and bonding properties. Integrating a membrane in those systems, which does not interfere with the molecules used in standard cell assays, is also a challenge.

In this study we present our advances on the development of a membrane-based plastic microfluidic chip dedicated to live-cell imaging and compatible with adherent and non-adherent cells. At first, we have used simulations to find the adequate membrane, which would allow the best performances in our system. Other experimental studies were carried out to select the adequate membrane. Finally, we chose to use a 10 µm-thick semi-permeable polycarbonate membrane, which pores of 2 microns diameter allow a constant nutritional delivery by diffusion from the feeding channel to the cell channel. Moreover, this membrane prevents significant hydrodynamic shear stress on cells. This proofs-of-concept of this membrane-based chip have been performed using *S. pombe* yeast cells. We showed that a slight absorption occurred at the border of the channel, even though it is reduced when the width of the channel is increased and cells are observed further from the border. This chip would be of high interest for applications where shear stress is a significant problem.

Materials and methods

1.1. Fission yeast strains and methods

Standard media and methods were used [28,29]. The strain used in this study was DC450[30] (*leu1Δ:Pcdc13::cdc13-L-cdc2as::cdc13-3'UTR::ura4*$^+$ *cdc2Δ::kanMX6 cdc13Δ::natMX6 cig1Δ::hphMX6 cig2Δ::kanMX6 puc1Δ::leu2*$^+$ *ura4-D18 h*$^+$). The Cdc13-L-Cdc2as fusion protein was previously described in [31]. All experiments were carried out in minimal medium plus supplements (EMM6S) at 32˚C. The 3-MBPP1 inhibitor (A603003, Toronto Research Chemical Inc.) was dissolved in DMSO at 10 mM and added to the medium at indicated concentrations.

1.2. Microscopy

All microscopy experiments involving fission yeast were performed on an inverted Zeiss Axio Observer (Carl Zeiss Inc.) equipped with a Lumencor Spectra X illumination system and a Hamamatsu Orca Flash 4.0V2 sCMOS camera. The optical properties of the membranes were analyzed using a spinning disc confocal head and a laser bench (Visitron GmbH). For both systems, images were acquired through VisiView (Visitron GmbH) and analysed using Fiji.

1.3. Microfabrication materials

6 mm-thick extruded PMMA for the chip manifolds was purchased from Weber-Metaux (France). The double-sided adhesive ARcare 90880 (142 µm thick) for the temperature control and perfusion channels, and ARcare 90445 (81 µm thick) for the cell channel were obtained from Adhesive Research Inc. (USA). Polycarbonate membranes were bought from Whatman. SU-8 photoresist was purchased from Gersteltec. PGMEA was obtained from Sigma-Aldrich.

1.4. Fabrication of the first prototype

Fabrication of the SU-8 channels on glass coverslips

Microscopy-grade glass coverslips (~ 170 micron-thick) were coated with SU-8 photoresist. 20-50 microliters of SU-8 were deposited glass coverslips, which were cleaned beforehand with acetone and dried. The resin spread evenly while spinning at 3000 rpm for 30 seconds. The channels were then fabricated using standard photolithography protocols[32]. The final thickness of the SU-8 was approximately 10 microns, according to the parameters we have used for obtaining this thickness on standard wafers.

Bonding polycarbonate membranes to SU-8

Polycarbonate membranes holes were cut using a CO_2 laser cutter (Speedy 100, Trotec). Then the membrane was placed on top the SU-8 channels (on the glass coverslip) and left on a precision heated plate at 145 ˚C for 1 min. This led to efficient bonding of the membrane to the SU-8.

1.5. Fabrication of the final chip

All materials were cut using a CO_2 laser-cutting machine (Speedy 100, Trotec, Austria). A double-sided adhesive containing a cell channel was bonded to a glass coverslip. The polycarbonate membrane, in which holes have made for allowing fluidic circulation, was placed on top of the cell channel. A double-sided adhesive, containing the perfusion channel was then placed above the membrane. Another glass coverslip was then mounted on top of the perfusion channel for complete sealing. This coverslip contained holes, aligned with the inputs and outputs of both cell and perfusion channels, for allowing fluidic connections. A temperature control channel in double-sided adhesive sealed the top coverslip with a 6 mm-thick PMMA manifold. To prevent deterioration when exposed to solvents, the PMMA block was cured for 2 h at 90 ˚C after being cut. Rigid Teflon tubings were inserted in the PMMA holes, allowing for the circulation of media and cells and the thermalization fluid. The use of epoxy around the tubings prevented possible leaks (Figure 1 – a).
In this study, the proof-of-concept experiments involving cells were performed without the temperature control layer, and the perfusion channel was directly sealed to the PMMA manifold.

1.6. Medium control

Control of the medium flow rates was achieved using flow sensors regulating the operation of pressure controllers (Elvesys). To limit the presence of bubbles within the microfluidic networks, bubble traps (Elvesys) connected to vacuum pumps (KNF) were mounted upstream of the chips.

1.7. Chip preparation and cell loading

Glass coverslips were coated with lectin (Sigma-Aldrich) prior to their assembly in the microfluidic chip for immobilizing non-adherent fission yeast cells. All mounted chips were sterilized by treatment with UV for 15 minutes. At the beginning of each experiment, cells were injected manually in the cell channel using syringes. As the membrane is flexible and could eventually break, we stopped the injection before cells penetrated the membrane zone (Figure 1 - b). Most cell volume was then contained in the tubing in which cells were injected. Subsequently, by removing the injecting syringe from the tubing, the medium could spread inside the cell channel by gravity, and no air remained in the channel due to capillary forces. The cell tubings were then closed for avoiding eventual evaporation and the perfusion medium was only injected once cells were inside the cell channel.

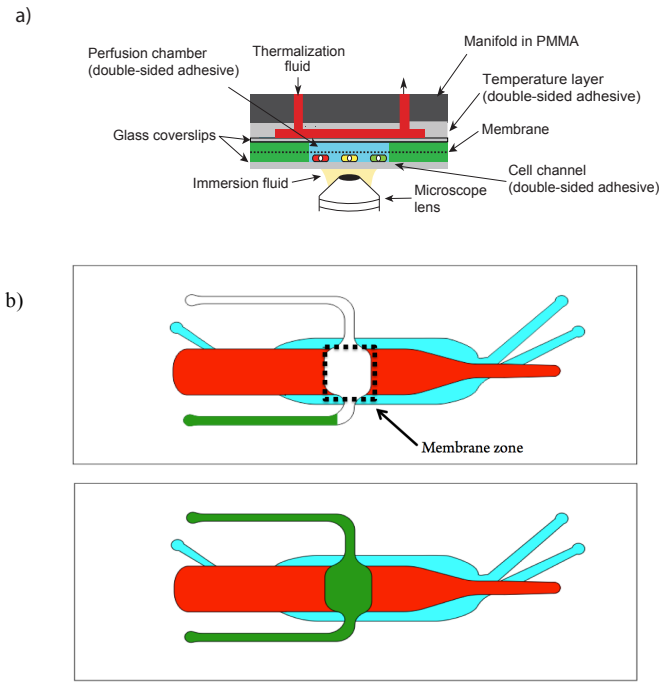

Figure 1: a) Schematic of the membrane chip during live-cell imaging. A membrane separates a channel in which cells are grown from a perfusion channel. Another glass coverslip seals the perfusion channel, and holes allow circulation of media and cells in the perfusion and cell channels, respectively. The top part of the chip is the temperature control channel in double-sided adhesive and the PMMA manifold. b) Schematics of the cell loading procedure. The temperature control channel and perfusion channel are represented in blue and red, respectively. The cell channel is represented in white when filled with air, and in green when cells are present. On the top schematic, cells are injected slowly in the cell channel, using a syringe. The cell channel needs to be partially filled but cells must not be in the area that interconnects the cell channel and the perfusion channel. On the bottom schematic, the needle of the syringe is then removed from the tubing, allowing the cells to fill the channel by gravity and capillarity. The membrane does not let cells or medium pass through during the injection process. Finally, the tubings inserted in the cell channel are closed for preventing medium evaporation.

2. Results and discussion

2.1. Finding the optimal membrane using simulations

Fabricating a microfluidic chip integrating a membrane is not an easy process, and several strategic steps must be followed. Consistent with what Jong *et al.* proposed for implementing a membrane technology on-chip[18], our initial approach was to find the adequate membrane material and type for our targeted applications.

In our study, a particular focus was given on the choice of the membrane, as it constitutes the essential layer of the microchip. Strategic considerations were made regarding our membrane selection: 1) it must allow the fastest diffusion possible while still avoiding convection in the cell chamber, 2) it must be compatible with the flow rates used for rapidly renewing the medium inside the tubings. To help us select the most appropriate membrane, we used a simulation software (using flows and mass transport) for better understanding what are, at the microscaled dimension, the critical parameters allowing the best performances. We first modeled a simple perfusion channel in 2D, and added a cell chamber without any membrane (Figure 2a). This validated that using a laminar flow, even with low velocity in the perfusion chamber, convection in the cell channel still occurs. Integrating a membrane between the two channels is therefore a necessity, and we included a thin membrane in the simulation designs. If we take two points separated by a certain distance, the diffusion dynamics between these two points is directly related to the square of their distance. Thus, chose to implement a thin membrane of 10 micron-thick for obtaining fast diffusion timings. Besides, this thickness is commercially available in several membrane materials. We simulated various pore sizes, with a wide range between 2 µm to 300 µm in diameter. Our results showed that large pore diameters increase convection in the cell chamber, while thin pores reduce switching dynamics, but also decrease the convection inside the cell channel (Figure 2bc). We demonstrated that a microfluidic chip, which cell channel is 90 micron-thick, integrating a 10 µm-thick membrane with pores of 2 µm, separated from each other by 2 µm, enhances diffusion dynamics (more than 95% of the medium is renewed after 30 seconds with a perfusion flow rate of 40 µL/min).

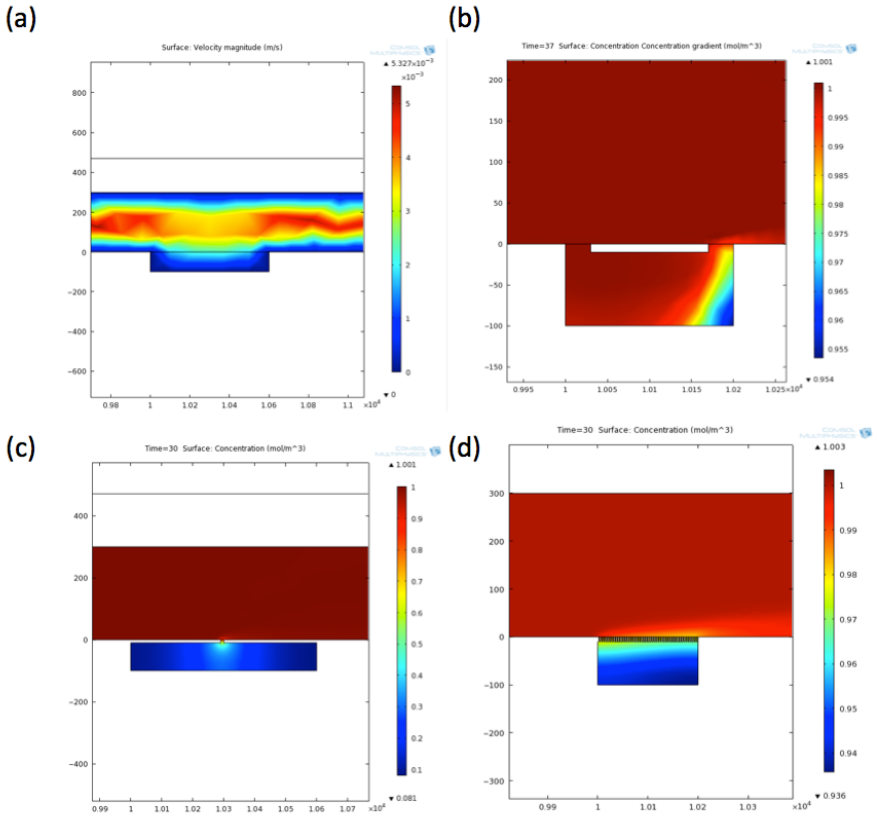

Figure 2: Simulation of a membrane in 2D. In all panels, we designed a perfusion channel and a cell chamber. (a) Simulation of a laminar flow without the integration of a membrane. The simulation includes a 300 µm-thick perfusion channel and a 100 µm-thick cell channel, with a 6 mm length. The colors represent the flux lines, and color gradients show differences in the fluid velocity. Red and blue colors stand for low and high velocity respectively. The blue gradient in the cell channel indicates that convection occurs when no membrane separates both channels. (b) Using the design in a), we modified the channel length to 2 mm and intercalated a simple membrane, consisting of two holes of 300 microns in diameter. We simulated the injection of a drug (Rhodamine B) inside the system (At the entrance of the perfusion channel, concentration C = 1), while having a concentration of C = 0 at the bottom at the cell channel at the beginning. We used the diffusion coefficient D = $5.0x10^{-10}$ $cm^2.s^{-1}$, relatively similar to the Rhodamine B diffusion coefficient. A flow of Rhodamine B (with the diffusion we chose) was simulated at 40 µL/min. We then measured the drug concentration over time. After 37 seconds, the concentration at the cell area is 0.995, meaning that the medium renewal was close to be complete. The concentration gradient observed after 37 seconds in the cell channel proves that the high Rhodamine concentration in the chamber is mainly due to convection and not diffusion. (c) We used the same design as in a) and realized a unique hole of 2 microns, with a membrane of 10 microns thickness. We then measured the concentration with similar parameters as in b). After 30 seconds, the blue color in the cell channel indicates that the concentration is low (< 0.1). Thus, this design shows that only diffusion occurs in the system. (d) Same simulation parameters as in b). We added a membrane with pores of 2 microns. All pores were separated from each other by 2 microns, and the membrane thickness is 10 microns. Results showed that in less than 30 seconds, the concentration at the bottom of the cell channel is nearly equal to 1. The concentration gradient indicates that the drug is brought in the cell chamber mostly by diffusion, although limited convection still occurs. Besides, the flow velocity at the cell area is significantly low (data not shown). The model proves that such a membrane system can be used while having almost no convection in the cell channel.

The simulation we have performed allowed us to validate a 10 µm-thick membrane as the diffusion barrier in our microfluidic system.

2.2. Selection of the membrane material and pore size

To select the final membrane material and pore size, we investigated the diffusion dynamics of several commercial membranes available with a thickness of 10 microns. For these assays, we used simple chips in which membranes were sandwiched between two double-sided adhesives, and a PMMA manifold was used to seal the perfusion channel (See Materials and Methods). Using Rhodamine B as a fluorescent marker, we conducted experiments involving fast media switches on chips fabricated with different membrane materials, such as polycarbonate (PC), polyester (PE), polyethylene terephthalate (PET) and polytetrafluoroethylene (PTFE). Additionally, we tested laboratory-made agarose membranes. However, we decided to exclude the latter, as they were complicated to fabricate reproducibly, and also because they would eventually collapse while having a perfusion flow, preventing their usage during live-cell imaging experiments. Among the commercial membranes tested, the transparency required for obtaining high-quality imaging led to the exclusion of membranes in PET. Moreover, PTFE membranes were only available on culture insert, and cutting the membrane from the insert was not the most adequate option. As a result, we finally compared the PC and PE membranes. The results from Figure 3-a indicate that the switching dynamics when using a polycarbonate membrane with pores of 2 microns in diameter, are less than 5 minutes (4 mins to lose 95% of the rhodamine intensity). However, when using a polyester membrane with pores of 3 microns in diameter, the Rhodamine B intensity was still higher than 20% of its original value after 10 minutes, suggesting slower switching dynamics (Figure 3-b).

The polycarbonate membrane with 2 micron pores showed diffusion timings of about 5 minutes, which could be acceptable for performing fast switches. The pore surface represents 16% of the total membrane surface. Higher pore density was tested using a polycarbonate membrane with pores of one micron (and the same 10 µm thickness). Surprisingly, results indicated slower diffusion timings while using this membrane. This counter intuitive result was obtained for an experiment performed only once, and could be an artifact.

Using the simulation software, we could then establish the theoretical diffusion curve of the experiments we had performed using Rhodamine B with a polycarbonate membrane. Similar parameters were used for the simulations (flow rate, thickness of channel, membrane thickness, pore size and pore distribution). Results in Figure 3a showed similar diffusion timings, even though the slope of the experimental curves is steeper than in the simulations after the injection of water, indicating that slight convection may occur experimentally.

Our experimental results led us select the 10 µm-thick polycarbonate membrane, with pores of 2 microns.

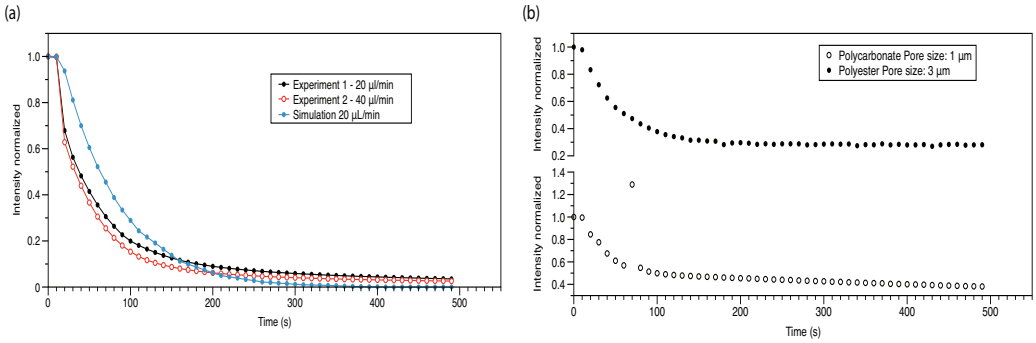

Figure 3: Measurements of the dynamics of media switches using Rhodamine B in membrane-based systems. A) On the left panel, the microfluidic chip used for the experiments is constituted with a 10 µm-thick membrane, with 2 micron pores diameter. The cell channel was perpendicular to the perfusion channel, 81 µm thick and 1 mm wide (See Figure 5b). In both experiments, water was first injected in the perfusion channel. Rhodamine B (50 µM) was then injected in the cell channel. We subsequently started the perfusion of water in the perfusion channel (T = 0), using 20 µL/min (Exp 1) and 40 µL/min (Exp 2). The intensity of the Rhodamine B was measured over time. Values were corrected and normalized by the intensity at T0. Similar values have been used in the simulation (flow rates, membrane pore size and density, thickness and width of the cell channel). For this simulation we measured the concentration at the bottom of the cell channel (C = 1 at T = 0) while injecting medium with a concentration C = 0. Results showed a higher steepness of the experimental curves, indicating that slight convection may occur when the flow of water starts. B) Similar conditions as in a) were used. We compared our results using a polycarbonate membrane with 1) a microfluidic chip containing a 10 µm-thick polyester membrane (with 3 µm pore diameter), and with 2) a microfluidic chip containing a 10 µm-thick polycarbonate membrane with 1 µm pore diameter. The values of the intensity of the Polyester chip were normalized by the value of the intensity at T0. The values of the intensity of the Polycarbonate membrane with one micron pore diameter were corrected then normalized by the value of the intensity at T0. Results showed a slow diffusion for both membranes, compared to the membrane in polycarbonate with pores of 2 microns.

2.3. Fabrication of the chip

Fabrication of a cell channel in SU-8 photoresist

Our choice of using 10 micron-thick polycarbonate membranes with pores of 2 microns allowed acceptable diffusion dynamics. Using a commercial membrane, the fabrication of the system is simpler than having to fabricate a custom-made membrane and then integrate it. We considered different strategies for fabricating the microfluidic system adapted to the polycarbonate membrane. One important criterion for optimal cell observation during live-cell imaging is the use of high-grade glass coverslips. Thus, the cell channel must be built over the glass coverslip and the membrane layer placed on top of the channel. As the diffusion time is directly proportional to the square of the distance, we decided to implement a thin cell channel to allow fast diffusion of nutrients and drugs to cells underneath the membrane. For that, we used photolithography techniques, as they permit the fabrication of thin and precise but customizable channels in various photoresists[33]. In particular, the photoresist SU-8 was well adapted for our project, as this material does not alter cell viability[34]. Moreover, the possibility of realizing microchannels with precise dimensions and thicknesses using soft-lithography processes would be of high interest for studying many cell types[33]. Indeed, the channel thickness can be adapted to the size of the model organism of interest in order to ensure the fastest diffusion possible for all cell types while preventing physical stresses. Standard soft-lithography protocols are using silicon wafers as substrates for depositing thin layers of photosensitive resins. These protocols served as a base for depositing the SU-8 resin onto microscopy-grade glass coverslips. Thus, we adapted the spin coating, curing and UV exposition times for fabricating thin SU-8 channels of 10 µm, 20

μm and 50 μm thicknesses on glass coverslips (See Materials and Methods). Additionally, one advantage of using SU-8 is the possibility of achieving any complex pattern of channels.

Bonding the polycarbonate membrane to the SU-8 layer

The photolithography protocols that we developed (See Materials and Methods) allowed us to generate microchannels in SU-8 photoresist directly on glass coverslips. As the membrane must be placed on top of the cell channels, holes were realized in the membrane using a CO_2 laser-cutting machine (Speedy 100, Trotec) for allowing fluidic circulation inside the cell channel. Bonding the polycarbonate membrane to the SU-8 constituted a great challenge, as both materials are rigid and do not possess adhesive properties. However, we found that reliable bonding could be achieved by using a precision heated plate at 140 ˚C, while keeping the membrane flat for preventing its bending in the cell channels. The second challenge was the bonding of the membrane to a second glass coverslip, for sealing a perfusion channel, which was engraved in a PMMA block. We tried to modify the membrane surface using chemicals, such as APTES[35], GPTMS[36], or silanes[22], as these surface modifications have been reported to improve the bonding properties. We also tested the same thermal bonding that was sufficient to fuse SU-8 with polycarbonate. However, none of these treatments could stick the membrane to the PMMA layer, constituting the perfusion channel. We therefore chose to use a medical-grade double-sided adhesive as a sealing layer, containing a perfusion channel that was cut by laser. Double-sided adhesives are composed of a hard substrate granting rigid properties, sandwiched between two layers of adhesives (generally acrylics or silicone glues). Unfortunately, the glue of the potential adhesives we tested eventually penetrated the cell chamber through the pores of the membrane, preventing any cell injection. The difficulty of intercalating a membrane between SU-8 and PMMA made us opt for a novel fabrication strategy.

Fabricating the final membrane chip using double-sided adhesives

To mount the next generation of chip, we decided to adopt the simple chip configuration that was used for selecting the membrane. As a result, we took advantage of double-sided adhesives for fabricating both cell channel (81 μm-thick) and perfusion channels (142 μm-thick) (Figure 1 - a). Using a thicker cell channel, we surmised the glue of the adhesive on top of the membrane would not block it. Consequently, the protocol for fabricating the cell channel and integrating the membrane was much simpler, as it did not involve time-consuming photolithography processes and complex equipment. However the height of the cell channel in double-sided adhesive resulted in slower diffusion dynamics, which were characterized in Figure 2a, compared to a thinner channel.

On top if the perfusion channel was a second glass coverslip, which separates the perfusion channel from the temperature control channel. The glass coverslip contained holes, which were fabricated to allow the perfusion flow and cells to circulate in their respective channels. Moreover, the temperature control channel was made in a double-sided adhesive (81 μm). Finally, a PMMA manifold sealed the temperature control channel, and contained holes were tubings are inserted, insuring the connections with external flow systems. Using epoxy adhesive around the tubings prevented potential leaks through the PMMA manifold.

2.4. Live-cell imaging using the membrane-based chip

Validation of the optical properties

We have demonstrated that intercalating a membrane in a plastic chip was possible. However, the goal of this study is to establish a membrane-based microfluidic system dedicated to live-cell imaging. We therefore set out to validate the optical properties of this membrane, which is in the field of view. We first investigated whether it could interfere with experiments involving fluorescence measurements with the standard wavelengths used in biology laboratories. For that, we injected cells inside the system to set the focal distance, and measured the auto-fluorescence of the membrane while focusing on cells. Results showed no significant auto-fluorescence intensity at these wavelengths, indicating its compatibility with the use of fluorescent markers (Table 1).

Excitation wavelength	Glass	Polycarbonate membrane
405	100.5 ± 1.8	100.6 ± 1.9
445	102.0 ± 2.2	102.4 ± 2.2
488	104.8 ± 2.8	105.0 ± 2.8
515	100.7 ± 1.8	100.7 ± 1.8
561	101.4 ± 2.0	101.4 ± 2.0

Table 1: Cells grown in culture medium were injected in the cell channel of the chip to determine the appropriate focal distance. Culture medium between two glass coverslips was used as a control (glass). Averages of the fluorescence over more than 2000 pixels along a diagonal line scan with standard deviations are shown for the indicated excitation wavelengths.

We then ensured that the membrane could allow high-quality imaging when using transmission light (DIC). The original chip dimensions (24 x 40 cm) were incompatible with the use of the condenser of the microscope, as the tubings inserted in the PMMA manifold prevented the condenser to be properly positioned while monitoring cells. This resulted in low-quality images, as the pores of the polycarbonate membrane were creating shadows (Figure 4a). We therefore changed the designs of all channels in the system to be compatible with a 24 x 60 cm coverslip, engineering the chip interconnections further away from the condenser area. This allowed the condenser to be used and resulted in better optical properties.

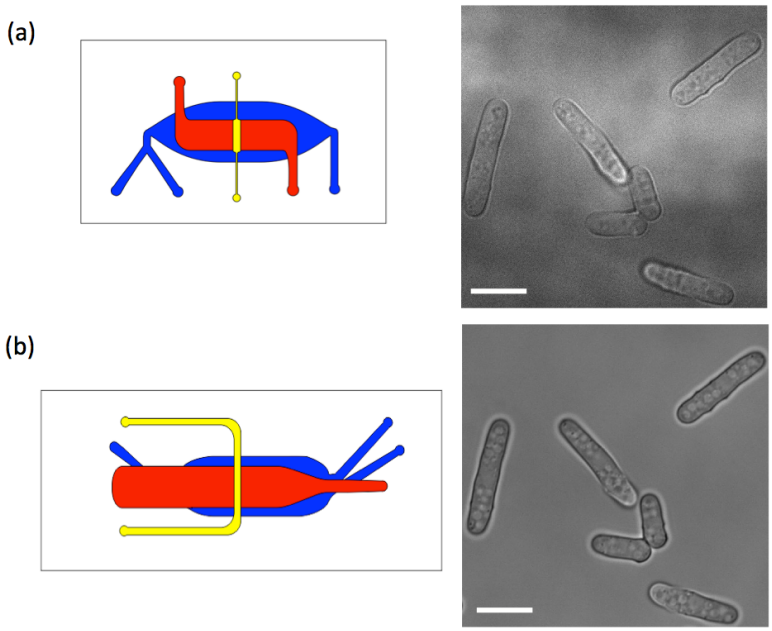

Figure 4: Optimization of chip dimensions. In the schematics, the temperature control channel, perfusion channel and cell channel are represented in blue, red and yellow, respectively. The pictures were acquired in transmission DIC. Cells were grown in the optimized membrane-chip. Scale bar is 10 µm. (a) The schematic represents the original chip dimensions (24 x 40 cm), in which we can observe that the tubings, in which medium flow circulates and which connect the chip to external inputs and outputs, are interfering with the condenser. The picture was taken while the condenser was up. (b) To adapt our microfluidic connections with the use of the condenser, we changed the cell channel dimensions and designs. The schematic represents the chip after optimization of the designs of all channels, allowing space for the condenser during microscopy imaging. The picture were taken while the condenser was down, showing the necessity of having space for the condenser.

Cell observation and tracking in the membrane device

The membrane-based system must be compatible with fast media switches, while preventing hydrodynamic shear stress to the cells. In addition, when non-adherent cells are being monitored at the microscope, even a slight convection may prevent their tracking and monitoring through the entire experiment. Theoretical models using simulation (Figure 2) predicted that convection in the cell chamber was low (although not null) when using a membrane pores of 2 µm and with low flow velocity. However, we assessed it experimentally by injecting fission yeast cells in the bottom channel and perfusing the system with medium at varying flow rates. We tested flow rates of 40 µL/min and 20 µL/min, as both these values are compatible with fast media switches. While focusing on cells under perfusion flow, we could detect movements at both flow rates (Figure 5a). However, coating the glass coverslip with lectin (0.5 mg/mL) prior to the chip mounting would prevent cell movements (See Chapter 2). We therefore tested the effect of lectin during experiments of three hours, perfusing cells for three hours at 20 µL/min. Strikingly, cells in the lectin-free system were still present in the cell channel, but had accumulated in specific areas, likely where the convection is minimal (Figure 5b). On the other hand, the lectin in the other microchip prevented cell movements during the perfusion, as they were homogeneously spread inside their channel (Pictures taken only at T = 0 and T = 180 mins).

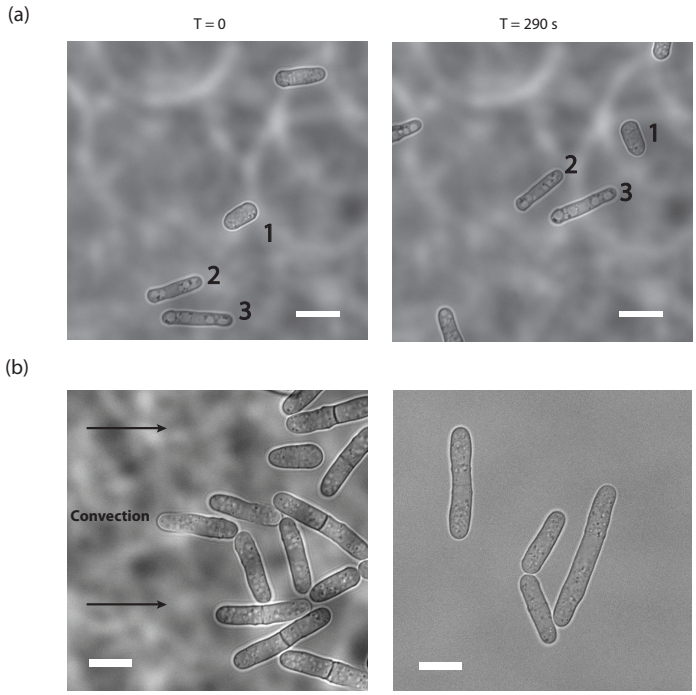

Figure 5: Assessing cell movements inside the membrane-based microsystem. (a) *S. pombe* cells were injected inside the cell channel and a perfusion flow of 20 µL/min was maintained. The pictures acquired at T = 0 (left) and at T = 290 s (right) are proving that the three focused cells have slightly moved during the perfusion after only 5 minutes. Scale bar is 10 µm. (b) Comparison of two systems, one fabricated with a non-coated glass coverslip and one fabricated with a lectin-coated glass coverslip, on the left and right panels, respectively. Cells were injected in both systems, and a perfusion flow of 20 µL/min was maintained for three hours. The pictures were taken after three hours. In the microfluidic chip without coating, we observed areas with high cell density and empty areas. In the system with lectin coating, cells are spread homogeneously in the cell channel, suggesting that the coating prevents their movement. Scale bar is 10 µm.

This first experiment was a proof that the convection in the bottom channel is reduced but still significant, and the usage of lectin is necessary for performing live-cell imaging. Thus, the membrane that we have chosen is not ideal, as it presents slight convection. More research and time of development is needed in order to find the appropriate membrane, which totally prevents convection.

Proof-of-concept experiments with cells

The membrane-based microfluidic system we fabricated allows for constant perfusion of medium. We performed additional validations of the system by assessing the chemical compatibility of the microchip. Thus, we investigated the possibility of using drugs of precise concentrations within the microfluidic device. For that, we injected fission yeast mutants operating with an engineered cell cycle control network that is sensitive to inhibition of CDK by the ATP analogue 3-MBPP1. Treatment of these cells with this inhibitor affects their cell cycle, and arrests them in the G2 phase, resulting in an elongated phenotype. We perfused cells with medium containing the inhibitor for three hours (20 µL/min) at 32 ˚C (Figure 6). As not validated, the microchip had not been calibrated at the microscope, and the temperature of 32 ˚C was achieved using a hot plate. After 3 hours when using 1 µM 3-MBPP1, cells were elongated at the middle of the channel (similarly to cells in the control in flask), but dividing at the borders, showing a slight absorption of the drug by the double-sided adhesive. When using a lower concentration of inhibitor (0.3 µM), cells were dividing in both the middle and the border of the channel, even though they were more elongated in the middle and containing a septum. The control in batch cultures showed a lower percentage of dividing cells (6%) in these

conditions. These results clearly show the existence of absorption gradients from the borders to the middle of the channel. This indicates that the double-sided adhesive absorbs small molecules, but that the constant perfusion flow reduces this effect, as we found in our perfusion chip with the LSR elastomer in Chapter 2. Therefore, having a large chamber (at least 1 mm in width) and focusing on cells at the center of the chamber is likely to be compatible with the use of small hydrophobic molecules.

(a)

Septation index (%)

Concentration: 1 µM		
	Border	Center
Chip 1	17	0
Chip 2	15	0
Control: 0		

Concentration: 0.3 µM		
	Border	Center
Chip	38	8
Control: 6		

(b)

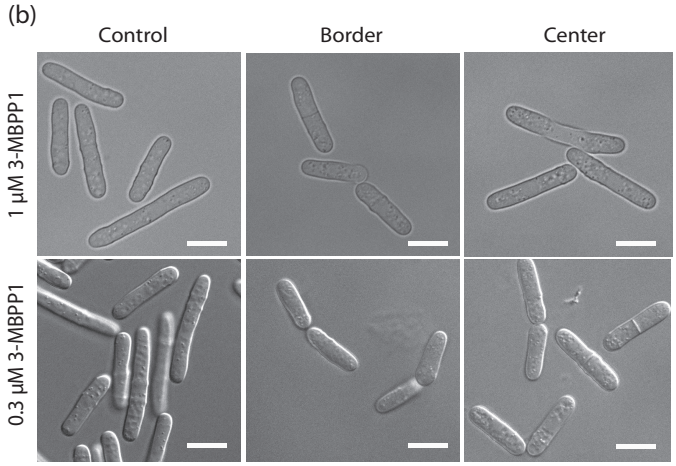

Figure 6: Proof-of-concept of the system using the ATP analogue inhibitor 3-MBPP1. Fission yeast cells operating with a modified CDK module that is sensitive to this inhibitor were injected in a lectin-coated cell channel (1 mm wide), and exposed to a flow of medium containing 1 or 0.3 µM 3-MBPP1 at 32 °C (20 µL/min). After 3 hours, the septation index was measured at the border and in the center of the channel, and in the control batch cultures (*n*>40 for each experiment). As the system was not calibrated for using the temperature-controlled channel, the chips were built without this channel (PMMA – Double-sided adhesive – membrane – double sided adhesive – glass coverslip), and we used a precision heated plate for controlling the temperature of the samples. (a) Septation indexes of three chips. Using 1 µM 3-MBPP1, the two chips present a high septation percentage at the border. Cells at the middle of the channel are similar to those in the control. Using 0.3 µM 3-MBPP1, cells devide at the border of the channel and the septation in the middle is higher than in the control. (b) Images of cells in a) after 3 hours of perfusion at the border and in the middle of the channel. In the control experiments (cells exposed to 3-MBPP1 in standard batch cultures), both concentrations of inhibitor result in a G2 arrest, with a low percentage of cells dividing when using 0.3 µM 3-MBPP1. Scale bar = 10 µm.

This proof-of-concept experiment demonstrates that the double-sided adhesive that we have chosen for integrating the membrane easily is absorbing small molecules. Therefore, it prevents the possibility of performing assays where the concentration of drugs must be precise, even though having a perfusion flow reduces its effect. As previously said, this microfluidic chip is not perfect, and further technological developments were needed, especially on the membrane and its integration, which could have lowered this absorption effect.

3. Conclusion

In this study, we have fabricated a microfluidic chip in plastic materials containing a membrane in polycarbonate. We performed preliminary tests using biological samples and demonstrated its compatibility with non-adherent fission yeast cells. However, additional biological validations needed to be performed for fully characterizing the system. For instance, fast media switches for validating the diffusion dynamics using biological samples could be assessed. Moreover, we have shown that a slight absorption of small molecules occurs in the cell channel, with a reduced effect when cells are at the middle of the channel. The system is

however not adequate for performing experiments involving low or precise concentrations of drugs. For this, the device that we have developed using wax (See Chapter 1) constitutes a better choice. What would be interesting is to increase the cell channel width to validate the concentration gradients steepness using small molecules, as we did for the device with the elastomer LSR. Moreover, as the membrane-chip was not fully validated, we did not calibrate its temperature so that is could be used with a precise temperature at the microscope. Finally, we showed that even with the presence of a membrane in the system, a slight convection occurs, potentially because of the membrane flexibility when perfusion occurs. This proves that the system we have fabricated is not the most robust one, and additional developments were needed for finding a more optimal membrane, which would avoid convection (such as a dense membrane which could be flatter), developing a robust bonding strategy while avoiding the use of absorptive double-sided adhesives, finalizing the characterizations of the system (for instance, finding the maximal pressures inside the system without breaking the membranes) and performing all biological validations using adherent and non-adherent cells.

To conclude, the ideal membrane system for performing live-cell imaging is challenging to fabricate, especially when the materials are biocompatible, and very few systems and protocols exist. Our system is functional, even if not completely validated, and could still be used for experiments requiring low shear stress.

References

1. Whitesides, G. M. The origins and the future of microfluidics. *Nature* **442,** 368–373 (2006).
2. Velve-Casquillas, G., Le Berre, M., Piel, M. & Tran, P. T. Microfluidic tools for cell biological research. *Nano Today* **5,** 28–47 (2010).
3. Young, E. W. K. & Beebe, D. J. Fundamentals of microfluidic cell culture in controlled microenvironments. *Chem Soc Rev* **39,** 1036–1048 (2010).
4. Stroock, A. D. & Whitesides, G. M. Controlling Flows in Microchannels with Patterned Surface Charge and Topography. *Accounts of Chemical Research* **36,** 597–604 (2003).
5. Bayraktar, T. & Pidugu, S. B. Characterization of liquid flows in microfluidic systems. *International Journal of Heat and Mass Transfer* **49,** 815–824 (2006).
6. Duncombe, T. A., Tentori, A. M. & Herr, A. E. Microfluidics: reframing biological enquiry. *Nat. Rev. Mol. Cell Biol.* **16,** 554–567 (2015).
7. San-Miguel, A. & Lu, H. Microfluidics as a tool for C. elegans research. *WormBook* 1–19 (2013). doi:10.1895/wormbook.1.162.1
8. Dahl, J. B., Lin, J.-M. G., Muller, S. J. & Kumar, S. Microfluidic Strategies for Understanding the Mechanics of Cells and Cell-Mimetic Systems. *Annu Rev Chem Biomol Eng* **6,** 293–317 (2015).
9. Kim, L., Toh, Y.-C., Voldman, J. & Yu, H. A practical guide to microfluidic perfusion culture of adherent mammalian cells. *Lab Chip* **7,** 681–694 (2007).
10. Bell, L. *et al.* A microfluidic device for the hydrodynamic immobilisation of living fission yeast cells for super-resolution imaging. *Sensors and Actuators B: Chemical* **192,** 36–41 (2014).
11. Nobs, J.-B. & Maerkl, S. J. Long-term single cell analysis of S. pombe on a microfluidic microchemostat array. *PLoS ONE* **9,** e93466 (2014).
12. Jin, S. H. *et al.* Monitoring of chromosome dynamics of single yeast cells in a microfluidic platform with aperture cell traps. *Lab Chip* **16,** 1358–1365 (2016).
13. Steward, R., Tambe, D., Hardin, C. C., Krishnan, R. & Fredberg, J. J. Fluid shear, intercellular stress, and endothelial cell alignment. *Am. J. Physiol., Cell Physiol.* **308,** C657–64 (2015).
14. Halldorsson, S., Lucumi, E., Gómez-Sjöberg, R. & Fleming, R. M. T. Advantages and challenges of microfluidic cell culture in polydimethylsiloxane devices. *Biosens Bioelectron* **63,** 218–231 (2015).
15. Wang, L. *et al.* Self-loading and cell culture in one layer microfluidic devices. *Biomed Microdevices* **11,** 679–684 (2009).
16. Kolnik, M., Tsimring, L. S. & Hasty, J. Vacuum-assisted cell loading enables shear-free mammalian microfluidic culture. *Lab Chip* **12,** 4732–4737 (2012).
17. Mirzaei, M. *et al.* Microfluidic perfusion system for culturing and imaging yeast cell microarrays and rapidly exchanging media. *Lab Chip* **10,** 2449 (2010).
18. de Jong, J., Lammertink, R. G. H. & Wessling, M. Membranes and microfluidics: a review. *Lab Chip* **6,** 1125–1139 (2006).
19. Charvin, G., Cross, F. R. & Siggia, E. D. A microfluidic device for temporally controlled gene expression and long-term fluorescent imaging in unperturbed dividing yeast cells. *PLoS ONE* **3,** e1468 (2008).
20. Lee, P., Helman, N., Lim, W. & Hung, P. A microfluidic system for dynamic yeast cell imaging. *BioTechniques* **44,** 91–95 (2008).
21. Chueh, B.-H. *et al.* Leakage-free bonding of porous membranes into layered microfluidic array systems. *Anal. Chem.* **79,** 3504–3508 (2007).
22. Sip, C. G. & Folch, A. Stable chemical bonding of porous membranes and poly(dimethylsiloxane) devices for long-term cell culture. *Biomicrofluidics* **8,** 036504 (2014).
23. Futrega, K. *et al.* Polydimethylsiloxane (PDMS) modulates CD38 expression, absorbs retinoic acid

and may perturb retinoid signalling. *Lab Chip* **16,** 1473–1483 (2016).
24. Toepke, M. W. & Beebe, D. J. PDMS absorption of small molecules and consequences in microfluidic applications. *Lab Chip* **6,** 1484–1486 (2006).
25. Gitlin, L., Schulze, P., Ohla, S., Bongard, H.-J. & Belder, D. Surface modification of PDMS microfluidic devices by controlled sulfuric acid treatment and the application in chip electrophoresis. *Electrophoresis* **36,** 449–456 (2015).
26. Regehr, K. J. *et al.* Biological implications of polydimethylsiloxane-based microfluidic cell culture. *Lab Chip* **9,** 2132–2139 (2009).
27. Berthier, E., Young, E. W. K. & Beebe, D. Engineers are from PDMS-land, Biologists are from Polystyrenia. *Lab Chip* **12,** 1224–1237 (2012).
28. Hayles, J. & Nurse, P. Genetics of the fission yeast Schizosaccharomyces pombe. *Annu. Rev. Genet.* **26,** 373–402 (1992).
29. Moreno, S., Klar, A. & Nurse, P. Molecular genetic analysis of fission yeast Schizosaccharomyces pombe. *Meth. Enzymol.* **194,** 795–823 (1991).
30. Chen, T. *et al.* A drug-compatible and temperature-controlled microfluidic device for live-cell imaging. *Open Biol* **6,** 160156 (2016).
31. Coudreuse, D. & Nurse, P. Driving the cell cycle with a minimal CDK control network. *Nature* **468,** 1074–1079 (2010).
32. Friend, J. & Yeo, L. Fabrication of microfluidic devices using polydimethylsiloxane. *Biomicrofluidics* **4,** 026502 (2010).
33. Mata, A., Fleischman, A. J. & Roy, S. Fabrication of multi-layer SU-8 microstructures. *Journal of Micromechanics and Microengineering* **16,** 276–284 (2006).
34. Nemani, K. V., Moodie, K. L., Brennick, J. B., Su, A. & Gimi, B. In vitro and in vivo evaluation of SU-8 biocompatibility. *Mater Sci Eng C Mater Biol Appl* **33,** 4453–4459 (2013).
35. Sunkara, V., Park, D.-K. & Cho, Y.-K. Versatile method for bonding hard and soft materials. *RSC Adv.* **2,** 9066 (2012).
36. Aran, K., Sasso, L. A., Kamdar, N. & Zahn, J. D. Irreversible, direct bonding of nanoporous polymer membranes to PDMS or glass microdevices. *Lab Chip* **10,** 548–552 (2010).

Chapter 4: Avoiding bubbles in microdevices

Bubbles in microfluidic systems are problematic for performing any live-cell assay. They can nucleate spontaneously and accumulate, especially during long-term experiments involving constant perfusion, leading to undesirable cell stresses and affecting viability. Already some solutions have been provided for trapping bubbles, or preventing their accumulation inside a microchip. However, these solutions are mostly compatible with PDMS-based microsystems, and not adequate for plastic microfluidic chip. Moreover, commercial systems compatible with any microfluidic device have been developed and placed upstream the microfluidic chip, however they do not always prevent microbubbles, which may accumulate in the system. In this study, we engineered a novel strategy for removing bubbles that are accumulating at the entrance of a microfluidic channel. This strategy involves the use of vacuum and a side channel, through which bubbles can be removed. This system can be adapted to any material or channel design. It can be automatized and allows performing long-term experiments with live-cells.

The data from this chapter will be part of a Methods in Cell Biology paper, which will be submitted before January 2018.

Preventing the accumulation of bubbles in microfluidic devices

Julien Babic, Laurent Griscom and Damien Coudreuse
SyntheCell team, Institute of Genetics and Development of Rennes, France

Introduction

One common challenge in microfluidic cell culturing devices is the frequent presence of air bubbles(Kim, Toh, Voldman, & Yu, 2007). The formation, accumulation and expansion of these bubbles is not fully understood, although they often arise when residual air is present in the systems as a result of incomplete filling of the channels. However, air bubbles can also spontaneously nucleate in small cavities either along the fluidic control circuit that is connected to the microdevices (*e.g.* fluidic connectors, adaptors, valves) (Kim et al., 2007) or directly within the microfluidic chips(Liu et al., 2007). The potential formation of these bubbles is particularly linked to the geometry of the channel networks(van Steijn, Kleijn, & Kreutzer, 2010) and can be enhanced upon temperature changes(Liu et al., 2007; Wang et al., 2012). Importantly, once bubbles are in the system, it is challenging to remove them and during long-term experiments involving continuous medium flows, they can accumulate, increase in size, and become a real obstacle to the success of an experiment. Indeed, air bubbles in a microchannel in which live-cells are grown can be deleterious for the cells. For instance, their burst can rupture cell membranes(Young & Beebe, 2010), or the samples can dry out, leading to cell death (Wang et al., 2012). In addition, in microenvironments where the flows are highly controlled, bubbles car generate abrupt changes in the flow patterns and properties(VANSTEIJN, KREUTZER, & KLEIJN, 2008), and even block certain channels(Jensen, Goranovi, & Bruus, 2004), thereby disrupting the cell microenvironment and the experimental setup. Finally, they can generate optical perturbations and imaging artifacts as well as alter the capacity of hardware auto-focus systems to maintain a constant focal plan during time-lapse assays.

Bubbles are therefore a well-known challenge for the majority of cell-based assays in microfluidic devices, leading to the development of various protocols that aim at limiting they accumulation and deleterious impact. For instance, pre-treating the tubings and channels with low surface tension fluids (e.g. ethanol) can help preventing air bubbles in the systems (Hansen, Hao, & O'Shea, 2015). Elevating the reservoir of perfusion medium may also reduce the probability of bubble formation in the chip. Strategies to trap the bubbles in the microchips have also been designed to prevent them from disrupting cell cultures. These include diffusion-assisted bubble removal devices, which consist of coupling thin gas permeable membranes fabricated within the channel networks (mostly in PDMS) with vacuum(Johnson, Liddiard, Eddings, & Gale, 2009; Skelley & Voldman, 2008; Sung & Shuler, 2009). However, these approaches involve complex designs and trapping sites that cannot always be easily implemented in the microfluidic networks and that generally require soft-lithography procedures(Frey, Rudolf, Schmidt, & Hierlemann, 2015). Furthermore, the use of vacuum can be difficult if not impossible to apply in devices fabricated using hard materials. As an alternative, plastic membranes have been used inside PDMS-free microfluidic chips. However their integration adds complexity and often requires advanced skills in microfabrication.

Currently, one of the easiest way of limiting the accumulation of air bubbles inside a microfluidic chip is to remove them prior to their entry into the channels(Wang et al., 2012). To this end, various in-line bubble traps have been developed and are commercially available. Similar in principles with some of the bubble trapping systems described above, they rely on the combination of an elastomer membrane, through which micro-bubbles can be separated from the fluids by diffusion under vacuum (Fig. 1) (Skelley & Voldman, 2008). However, these devices are mostly functional when using large volumes(van Lintel, Mernier, & Renaud, 2012) and fail at efficiently preventing micro-bubbles to penetrate inside the

microfluidic channels. Interestingly, we have noticed that even in the presence of upstream bubble traps, the major sources of air bubble formation are the inlets of the microfluidic chips, where the connections are made with the fluidic control circuit. This was particularly striking when using multiple inlets. We therefore developed a simple and powerful protocol that allows the manual or automated removal of such bubbles during long-term live-cell imaging experiments. Our strategy is not specific to any particular microfluidic design and can be adapted to a wide range of materials. Here we describe the principles of the system and the different steps that are necessary to implement it, providing a proof-of-concept assay using a simple microfluidic perfusion system.

Materials and design

Microfluidic chip (PMMA manifold, elastomer perfusion channel and glass coverslip), Teflon and Tygon connecting tubings, low power vacuum pump, high precision hot plate, matrix of valves, pressure controller, and medium reservoirs.

Fabrication of the proof-of-concept microfluidic chip

The perfusion channel was cut in a 250 µm-thick elastomer sheet and subsequently intercalated between a PMMA manifold and a microscopy-grade glass coverslip. We chose this elastomer for its ability to seal PMMA and glass during long-term live-cell imaging experiments, even when using continuous high flow rates of medium in the chip (see Chapter 2). The PMMA and elastomer layers were designed using a computer assisted drawing software and fabricated with a CO_2 laser-cutting machine.

Simple alteration of the microfluidic network for integrating a bubble removal system

The implementation of the bubble removal system that we developed only requires a simple and easy-to-integrate alteration of the design of the microfluidic network in the chip. Specifically, this consists of adding a short side channel at the media inlets. For this proof-of-concept assay, we used a perfusion channel that has only one inlet and one outlet (Fig. 2). This additional connection is directly connected to a low power vacuum pump (when automation is required, a programmable valve is intercalated between the pump and the chip).

Experimental protocol

1. Assemble the microfluidic chip, whose design has been altered to integrate the vacuum channels at the chip inlets (Fig. 3A).

2. Connect the perfusion inlets and outlets of the chip to the medium reservoir and waste container, respectively, using standard tubings. The tubing at the perfusion outlet must be at least 15 cm long to prevent air to come inside the channels upon vacuum (Fig. 3B).

3. Connect the vacuum channel with a high fluidic resistance tubing (Fig. 3C; inner diameter of 100 µm in this example). This prevents that large volumes of medium are vacuumed upon bubble removal.

4. Connect the vacuum channel to a valve (Fig. 3D). While this is not essential for the system, which can be

manually operated, it allows for automatic bubble removal through computer-driven control. In this case, the vacuum can be maintained and open/close valve cycles are generated for bubble removal.

5. Connect the bubble removal line to a waste container to collect the small volumes of medium that may be vacuumed when the valve is open (Fig. 3E).

6. Operate the perfusion system (medium injection for the desired experimental assay).

7. When bubbles form at the inlet of the perfusion channel (Fig. 3F), stop the perfusion (manually or using a valve when making the procedure automatic) and open the vacuum valve for a short period (≤ 2 s). The bubbles are rapidly vacuumed inside the vacuum channel, tubing and reservoir. (Fig. 3G). Re-start the perfusion. Only small volumes of medium in the main channel are displaced. Alternatively, the vacuum valve can be automatically operated at a constant frequency (depending on the type of medium, of the channel design and temperature of the samples) rather than when bubbles are detected.

Conclusion

Bubbles in microfluidic systems are an important obstacle to perform high quality live-cell imaging experiments, and preventing their accumulation in microfluidic chips is a major challenge, often requiring complex trapping systems that cannot easily be implemented. Here we show a simple, versatile and accessible strategy that consists of actively removing bubbles while they form at the inlet of the microsystems. This method is compatible with a wide range of channel designs, materials, chip structures and applications and provides a solution for performing long-term live-cell imaging experiments.

References

Frey, O., Rudolf, F., Schmidt, G. W., & Hierlemann, A. (2015). Versatile, simple-to-use microfluidic cell-culturing chip for long-term, high-resolution, time-lapse imaging. *Analytical Chemistry*, *87*(8), 4144–4151. http://doi.org/10.1021/ac504611t

Hansen, A. S., Hao, N., & O'Shea, E. K. (2015). High-throughput microfluidics to control and measure signaling dynamics in single yeast cells. *Nature Protocols*, *10*(8), 1181–1197. http://doi.org/10.1038/nprot.2015.079

Jensen, M. J., Goranovi, G., & Bruus, H. (2004). The clogging pressure of bubbles in hydrophilic microchannel contractions. *Journal of Micromechanics and Microengineering*, *14*(7), 876–883. http://doi.org/10.1088/0960-1317/14/7/006

Johnson, M., Liddiard, G., Eddings, M., & Gale, B. (2009). Bubble inclusion and removal using PDMS membrane-based gas permeation for applications in pumping, valving and mixing in microfluidic devices. *Journal of Micromechanics and Microengineering*, *19*(9), 095011. http://doi.org/10.1088/0960-1317/19/9/095011

Kim, L., Toh, Y.-C., Voldman, J., & Yu, H. (2007). A practical guide to microfluidic perfusion culture of adherent mammalian cells. *Lab on a Chip*, *7*(6), 681–694. http://doi.org/10.1039/b704602b

Liu, H.-B., Gong, H.-Q., Ramalingam, N., Jiang, Y., Dai, C.-C., & Hui, K. M. (2007). Micro air bubble formation and its control during polymerase chain reaction (PCR) in polydimethylsiloxane (PDMS) microreactors. *Journal of Micromechanics and Microengineering*, *17*(10), 2055–2064. http://doi.org/10.1088/0960-1317/17/10/018

Skelley, A. M., & Voldman, J. (2008). An active bubble trap and debubbler for microfluidic systems. *Lab on a Chip*, *8*(10), 1733. http://doi.org/10.1039/b807037g

Sung, J. H., & Shuler, M. L. (2009). Prevention of air bubble formation in a microfluidic perfusion cell culture system using a microscale bubble trap. *Biomedical Microdevices*, *11*(4), 731–738. http://doi.org/10.1007/s10544-009-9286-8

van Lintel, H., Mernier, G., & Renaud, P. (2012). High-Throughput Micro-Debubblers for Bubble Removal with Sub-Microliter Dead Volume. *Micromachines*, *3*(4), 218–224. http://doi.org/10.3390/mi3020218

van Steijn, V., Kleijn, C. R., & Kreutzer, M. T. (2010). Predictive model for the size of bubbles and droplets created in microfluidic T-junctions. *Lab on a Chip*, *10*(19), 2513. http://doi.org/10.1039/c002625e

VANSTEIJN, V., KREUTZER, M., & KLEIJN, C. (2008). Velocity fluctuations of segmented flow in microchannels. *Chemical Engineering Journal*, *135*, S159–S165. http://doi.org/10.1016/j.cej.2007.07.037

Wang, Y., Lee, D., Zhang, L., Jeon, H., Mendoza-Elias, J. E., Harvat, T. A., et al. (2012). Systematic prevention of bubble formation and accumulation for long-term culture of pancreatic islet cells in microfluidic device. *Biomedical Microdevices*, *14*(2), 419–426. http://doi.org/10.1007/s10544-011-9618-3

Young, E. W. K., & Beebe, D. J. (2010). Fundamentals of microfluidic cell culture in controlled microenvironments. *Chemical Society Reviews*, *39*(3), 1036–1048. http://doi.org/10.1039/b909900j

Figure legends

Figure 1. Standard in-line bubble trap system. Pictures of a commercially available bubble trap device. While participating in limiting the accumulation of air bubbles in the microfluidic chips, such devices are not sufficient to prevent micro-bubbles to enter the fluidic network and alter long-term experiments. **A.** Picture of the device components. **B.** Picture of the assembled device. The tubings on the left allow for medium circulation. The tubing on the right connects the bubble trap to the vacuum pump.

Figure 2. Integration of the bubble removal system in the channel design. A. Schematics of the microfluidic design. A short side vacuum channel is added at the inlet of the perfusion channel. Dimensions are in mm. The holes in the PMMA manifold that allow the circulation of medium are in red. **B.** Picture of the entire setup, including the connection of the system to the vacuum pump. In this example, a valve is used to control both perfusion and vacuum.

Figure 3. Experimental procedure. A. Step 1: microfluidic chip assembled. **B.** Step 2: connection of the chip to the perfusion and the waste reservoir. **C.** Step 3: connection of the vacuum inlet to a high fluidic resistance tubing. **D.** Steps 4 and 5: connection of the vacuum line to a valve matrix and a waste container. **E.** Step 6: Perfusion of water in the channel (T=0). **F.** Step 7: A bubble formed at the entrance of the perfusion channel. **G.** The vacuum valve was opened for 2 s, resulting in removal of the bubble from the perfusion channel (the bubble can still be seen inside the vacuum inlet).

Figure 1. Standard in-line bubble trap system.

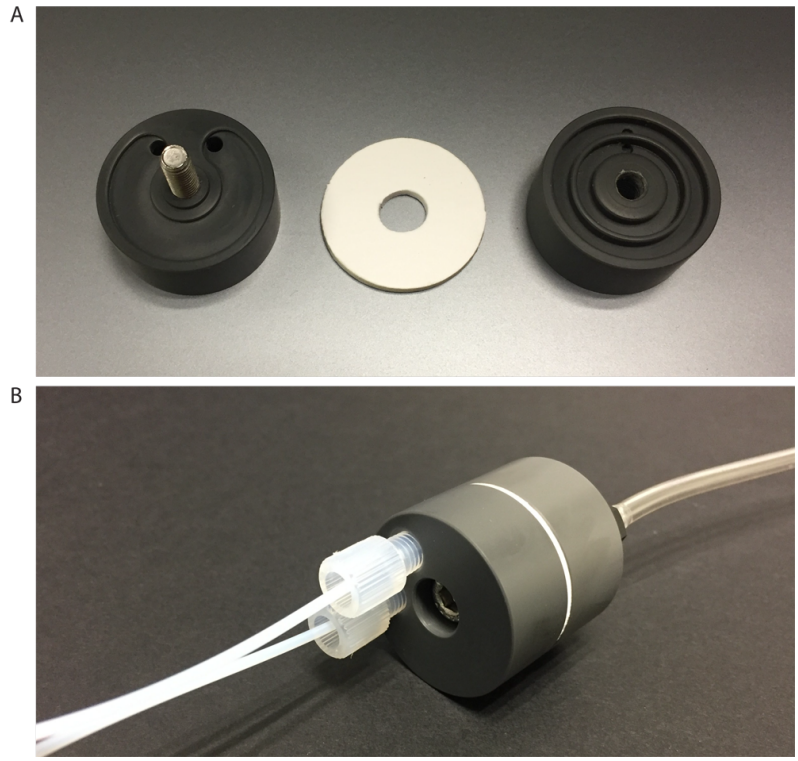

Figure 2. Integration of the bubble removal system in the channel design.

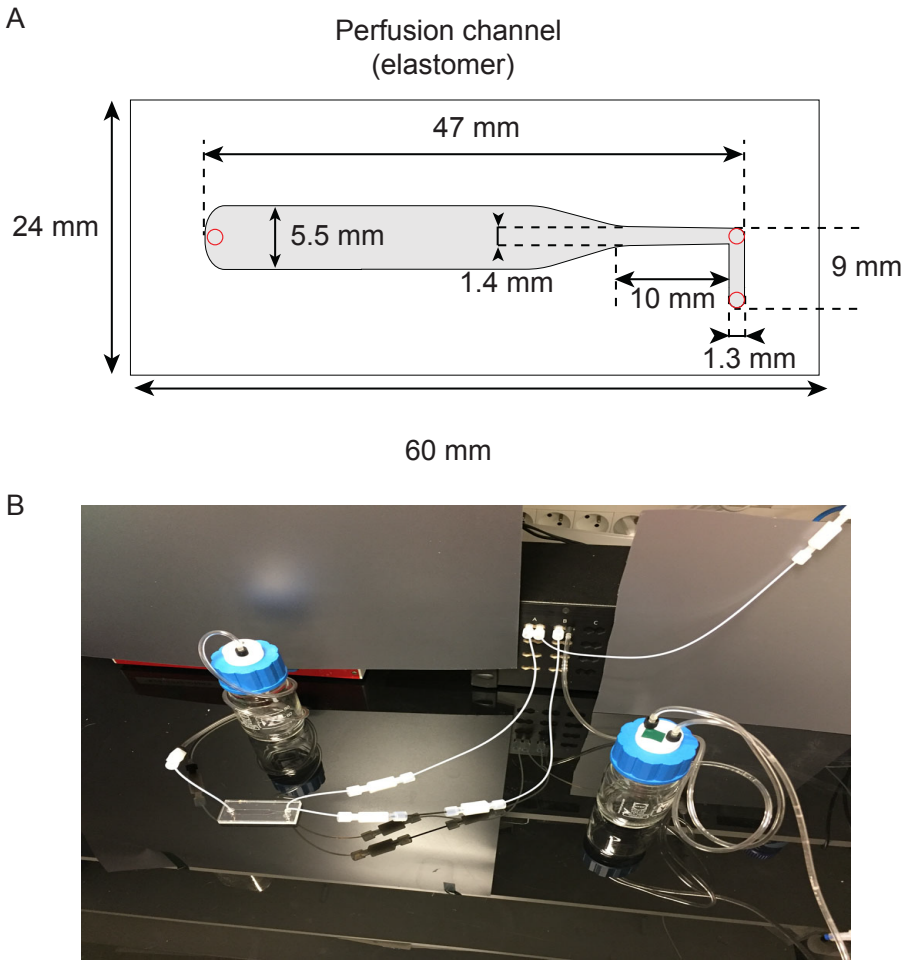

Figure 3. Experimental procedure with pictures.

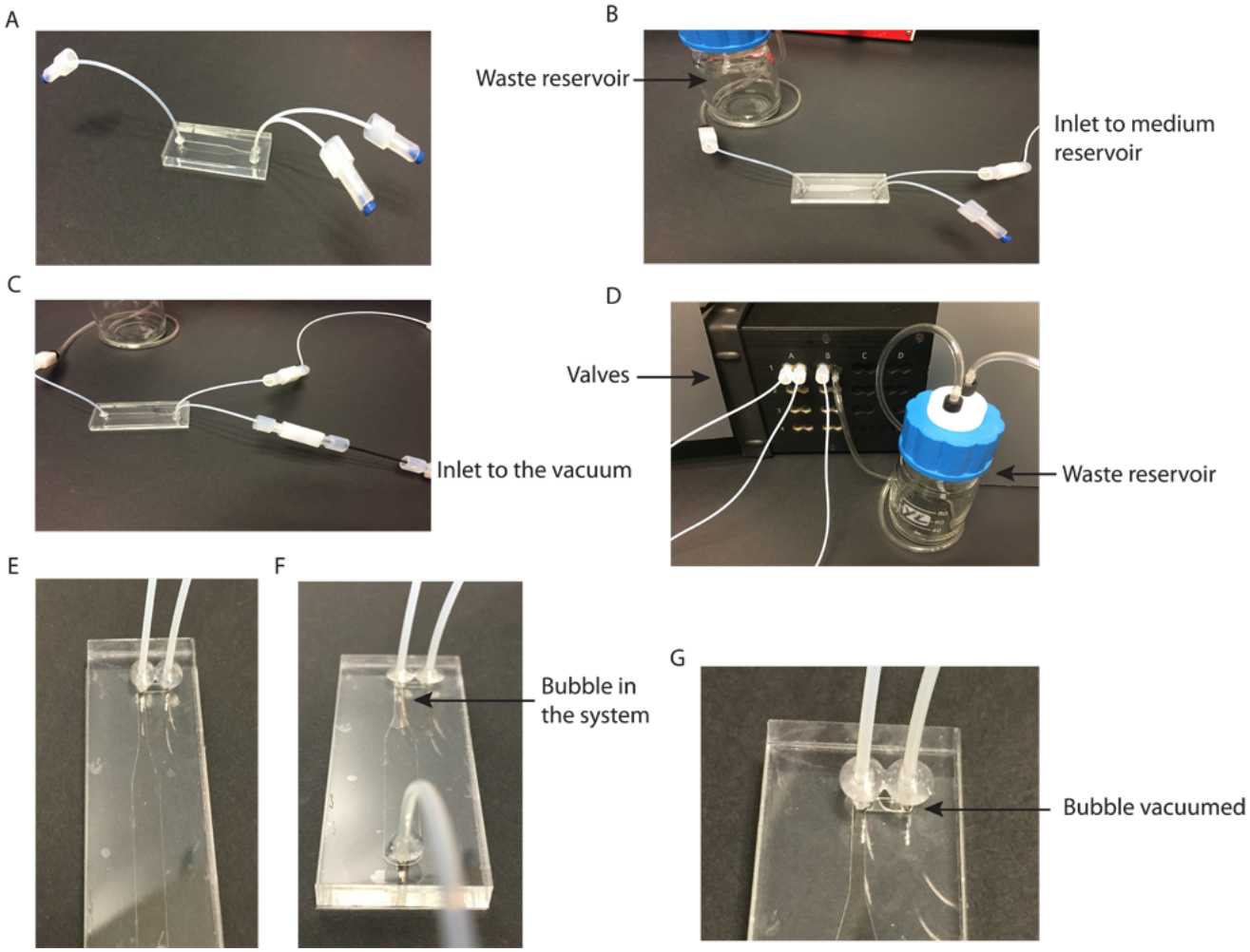

Discussion

Discussion

1 What biological laboratories need: to use simple microfluidic chips

1.1 Microfluidics in biological laboratories: not the expected revolution yet

It has been almost three decades that microfluidics exist, and yet it has not been fully used in biological laboratories. This is reflected by the fact that publications containing the word “microfluidics” are overwhelming in engineering journals, and only a few percentage of them are published in life sciences journals[1]. This discrepancy can be explained: In fact, microfluidics development started while the mechanisms and principles at the micro-scaled dimensions were not fully understood, and scientists needed to build proof-of-concepts of microfluidic potential and applications. Engineering journals have then facilitated the development and growth of microfluidic technologies, and are still major publishers of microfluidic papers. Moreover, the limited amount of microfluidic papers in biology journals may be due to the complexity of microfluidic devices, which retains biologists to use them.

As of today, the physics at the microscaled dimensions are well understood, and the fluidic dynamics in microfluidic systems is highly predictable, due to the laminar flow in such devices. When applied to biology, microfluidics have proven to be adequate, in particular when manipulating cells and their microenvironment is necessary, highlighting such approach as a revolutionary tool for addressing a number of biological questions[2]. In addition, microfluidics allow various advantages such as the reduction of the consumption of reagents and wastes, resulting in a reduction of the global costs of the assay. Furthermore, many protocols have been well established for chip fabrication, connection of the microfluidic chip to external inputs and outputs[3], and cell culturing.

Thus, it is surprising that microfluidics are not as well implemented in research facilities, especially in the fields of chemistry and biology, in which the manipulation of cells and drugs is commonly used. Chemists and biologists are still reticent to microfluidic technologies because of various factors. In fast, standard biological tools and protocols have been established for a wide range of assays and have led to convincing results and discoveries. Conducting assays using microfluidic systems may be reluctant at first sight, as it may require optimizations (of protocols, microchips, control systems, among other things) and increase the time required for discoveries. Moreover, microfluidics is a multidisciplinary field involving specific skills in domains that differ from biology, such as material sciences, fluid mechanics, computer programing, electronics, etc. Hence it is challenging to find researchers possessing this multidisciplinary expertise.

Additionally, microfluidic systems may be avoided because they require expensive equipment and complex systems. One can argue that microfluidics systems are just simple plastic blocs containing channels. In reality, this bloc is just one piece of a bigger picture, as microfluidics globally include all the fabrication equipment for doing soft-lithography, cutting plastics, applying pressures, controlling temperatures, etc., and also relies on several accessories, which represent a certain cost. We could cite tubings, connectors, flow controllers, valves and pumps, actuators, de-bubblers.

To sum up, one of the main obstacle between biology and microfluidic is the complexity of the devices and fabrication methods[4].

1.2 The key: build something simple

For a laboratory with no experience in microfluidics, the first solution that comes to mind is to directly buy microfluidic chips from a supplier. Thus, buying pre-fabricated chips would represent a significant cost, and some of them can be used only once. Furthermore, these chips would require changes in their designs, materials or functions to ensure the compatibility with the biological model of interest, the type of microscope and the targeted applications. Another solution is to use a microfluidic chip that has already been conceived and used by another research group. On the principle, the idea is feasible, but often the fabrication of the chip requires specific equipment and fabrication method, and their use is unique.

In fact, a majority of the microfluidic chips that are published in international scientific journals are qualified as simple, and easy to use, but their fabrication, reproducibility and usage in other laboratories is challenging.

Hence, the development and expansion of microfluidics will only be possible when simplicity will be a major criterion[5].

1.3 An example of simple versus not simple: the temperature control system.

During my three years of thesis, I have been working with the start-up Cherry Biotech, which provides a solution for controlling temperature at the microscope. Cherry Biotech is a young start-up, and even if their temperature control technology is advantageous (for its temperature range, temperature dynamics and its accuracy achieved), the PDMS chips that were provided at early development stages were not robust and user-friendly. In fact, I produced some of these PDMS chips, which was time consuming (2 hours for 4 chips, with 25% wastes). More importantly, the flow rate of thermalized liquid of 5 mL/min that is injected for controlling the temperature prevented long-term usage of the PDMS layer: at this flow rate, leaks through the PDMS holes or through the glass coverslip could not always be prevented.

As part of my training with the laser-cutting machine, I tested the cutting of different materials, as well as the engraving of channels for allowing fluid circulation. I improved the manufacturing process of the PMMA material and conceived robust PMMA chips with channels made in double-sided adhesive. A post-cutting thermal treatment also improved the chemical resistance of PMMA (the thermal treatment re-polymerizes the broken molecular chains), and epoxy glue was applied around rigid tubings inserted in the PMMA holes, which were potential sources of leak. This production resulted in a faster and higher throughput than for PDMS, which fabrication is limited by the size of a wafer (10 chips per hour in a laboratory), and the PMMA chips are reusable several times. Besides, depending on the assay, both PDMS and PMMA chip designs can be modified easily, however the fabrication of these designs require a complete photolithography process for PDMS chip, whereas no additional time is required for PMMA chips, as they are produced using a CO2 laser cutter following drawn patterns. As a result, the robustness, versatility but more importantly simplicity of the chips was significantly improved.

2 Comparison of each chip developed in the laboratory

Our research group has been focusing on building microfluidic chips that are 1) simple to use, 2) easy to fabricate and 3) compatible with biological studies under live-cell imaging with high-resolution microscopy and using the Cherry Biotech temperature controller. In this chapter, I will discuss each microfluidic chip that we have developed in the laboratory. The discussions about the advantages and drawbacks of each, which are not mentioned in the introduction or in the results part, will explain the strategic choices that we have made.

2.1 The wax chip

2.1.1 Introduction and advantages

The wax chip is composed of biocompatible materials that do not absorb small hydrophobic molecules, hence ideal for performing any experiments involving low or precise concentrations of drugs. As of today, there is no other chip available or even described that could perform such multiplexing at the microscope without absorbing hydrophobic molecules.

In addition, this microfluidic chip is realized using photolithography techniques, compatible with a wide range of channel designs, allowing highly precise and reproducible microchannels structures and dimensions. For example, we have produced complex structures consisting of two perfusion channels interconnected by side chambers, where cells are observed. These complex structures allowed us to renew the media while preventing potential shear stress.

This versatility of the chip has proven to be compatible with fast media switches and rapid temperature shifts, thus offering a high level of control of the microenvironment.

2.1.2 Drawbacks

2.1.2.1 State-of-the-art microfluidic chip, but hard to fabricate

This microfluidic chip seems like the perfect chip, preventing any absorption and controlling the temperature and medium flow precisely, dynamically and simultaneously.

On the other hand, fabricating this chip requires specific equipment that not all research laboratories could afford. The fabrication of the chip relies on several steps, starting with a photolithography process to produce a PDMS mold, followed by a thermo-molding process (to replicate channels in COC from the PDMS mold), and a laser-cutting process to cut the PMMA and the double-sided adhesive. The chip fabrication is also limited by the size of the wafer (for the PDMS molds) and the dimensions of the thermo-press (the press used in our laboratory allows to produce one COC layer at a time). Moreover, applying wax on a precision heated plate for bonding COC to glass is not trivial and requires patience and experience. A lack of wax leads to leaks, whereas too much wax clogs the channels.

Moreover, small adjustments of the channel or cell chambers require the whole photolithography process: changing the size of the channels or the cell chambers involves modifications in the initial mask design, and changing the thickness implies other photolithography parameters.

In terms of reusability, it is difficult to wash the cell chamber when the system is closed. The ethanol degrades the wax properties, increasing the probability of leaking during the next experiment. Disassembling the chip remains possible using heat, but completely removing the wax and reassembling the chip is challenging.

2.1.3 Conclusion

This microfluidic chip possesses the great advantage of preventing the absorption, offering the possibility of using fine and precise concentration of drugs during life-cell imaging experiments. Although it is not reusable and requires hand fabrication skills and habits, it allows accurate, precise and dynamic control of the temperature. The perfusion flow is controlled simultaneously, and the medium switch timings, which were shown to be 5-10 minutes longer than in flasks in the setup we have used, are mainly dependent on the length of the tubings after the T-junctions and on the perfusion flow rate.

While challenging to reproduce, especially in other laboratories, this microfluidic chip remains of high interest for any experiments involving low or precise concentrations of drugs.

2.2 The perfusion chip

As biological laboratories are seeking for simple and user-friendly microfluidic chips, we developed the so called “perfusion chip”.

2.2.1 Advantages

2.2.1.1 The simplest fabrication strategy

We built a microchip that would be as simple to produce and to use as possible. For that, we decided to avoid using time-consuming photolithography procedures, which imply specific equipment, but most importantly avoid the possibility of high throughput fabrication (the wafer limits the number of system that can be produced). As a consequence, our strategy was to use only a laser-cutting machine for producing all chip materials. It allows a higher production rate and lowers the costs of material and human timings. Also, the designs can be modified as desired without supplementary timing and cost.

Moreover, we demonstrated that when not using the temperature control channel, all materials could be realized without using the CO_2 laser-cutting machine: the elastomer can be cut with a razor, and holes in the PMMA manifold of the appropriate diameter can be drilled. Also, I gave already-assembled microfluidic chips to beta-testers with no experience in microfluidics, and they could disassemble, clean and re-assemble the chips easily, as well as inject fluids using syringes. This proved that the chip fabrication highly advantageous for users or laboratories that do not possess specific and complex fabrication equipment.

2.2.1.2 Additional development options are possible for making this reusable chip more user-friendly

We engineered a simpler method for using the microfluidic chip by using magnetic field to connect a manifold, containing all tubings that could be reused after each usage, to the rest of the chip (See Figure 1). The microchip that we developed contains magnets, confined inside PMMA blocks using epoxy, and an elastomer, which main function is to seal the chip from any potential leaks. This chip upgrade allows ultra-fast connections between the chip and the microfluidic setup. Furthermore, the development of such system using magnets has been tested on other chips, in which the channels have a higher fluidic resistance, without having leak issues.

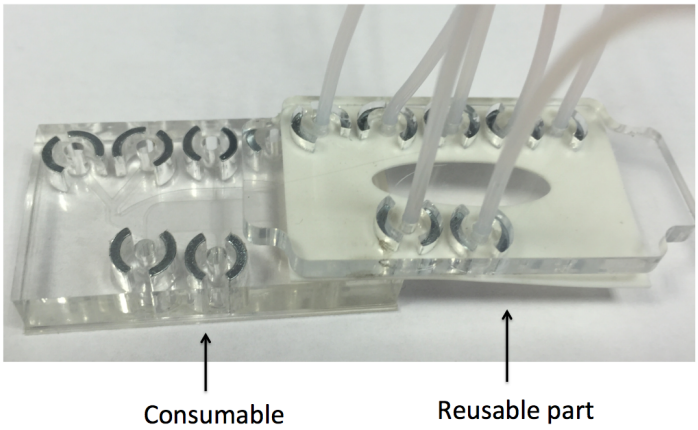

Figure 1: Picture of a membrane-based chip in which magnets have been inserted. An elastomer placed between both attracted magnets allows a robust sealing of the microfluidic chip, even when high pressures of fluids are injected.

A microfluidic chip that provides reusability is a gain of time (production time, or ordering and delivery delays) and costs. While considering the chip materials and fabrication, we had to find the adequate strategy for reusing the chip. Several options were considered.

One possibility of re-using a chip is to use materials that possess the property of bonding other materials and still be detachable: elastomers. In the perfusion chip, one option was to use an elastomer as the temperature control layer, meaning that the top part of the chip would be reusable (including the PMMA manifold and connections) and the bottom part would be used as a consumable (with a perfusion channel made in double-sided adhesive, sandwiched between two glass coverslips). We tested many elastomers but none of them could support the pressure of the thermalized liquid. Our alternative strategy was to use the elastomer for the perfusion channel, whose mechanical properties would be more compatible with the pressure of the perfusion media. The elastomer would bond to glass coverslips, be peeled off after the experiment, cleaned and reused. Finding the appropriate one was not trivial: we tested multiple elastomers, which were not adequate for several reasons: some of them would simply not hold the pressure of the perfusion channel. Others needed the use of a hydraulic press for having the desired thickness, and the process involving hot presses would lead to non-reproducible channel thicknesses. Moreover, all elastomers cannot be cut using a laser, as the borders could deform with heat, preventing a complete flatness of the surface and affecting the bonding. Finally, as sticky materials, they may accumulate dust onto their surface, which can be hard to remove and affect the bonding properties and reuse.

Eventually, we chose the LSR material, which is commercially available with a reproducible thickness, cheap, and presents the adequate bonding properties. Removing the dust from its surface is easy and fast. This option of using the LSR in the system is not unique, but was the simplest solution that we found for allowing the chip to be reusable.

2.2.1.3 Fast media switches

Using this microfluidic chip, cells are directly in the flow. For this reason, media switches in the microfluidic chip are fast, and only depend on the length of the tubings between the microfluidic channel and the T-junction. In the setup we have used, the time for filling the tubing with normal medium induced a 5 minutes delay over the control. Thus, this setup allows for the monitoring of fast cellular responses to perturbations of the microenvironment.

2.2.1.4 The chip can be used by any laboratory

This perfusion system has been developed to be simple so that any research laboratories with little experience in microfluidics could use it. However, we have demonstrated its usage using highly precise, accurate and dynamic control of the perfusion flow and temperature. This high degree of control relies on sophisticated machines, which can be automated, that not all research facilities possess. One must bear in mind that these machines are only providing a high level of control of the flows and temperatures.

In reality, the integration of the temperature control channel allows 1) a precise, accurate and dynamic control of the temperature, with temperature switches in less than 10 seconds, and 2) the possibility of reaching cold temperatures below ambient. While doing simple experiments using one constant temperature above ambient, this temperature control system is not necessary. In the laboratory, we have tested setups using an incubation chamber instead of Peltier elements at the microscope, and performed robust live-cell imaging experiments. Moreover, when following cells over time by microscopy is not of interest, we also demonstrated that we could put the microchips on a precision heated plate.

Similarly, the perfusion control system allows for performing fast media switches and flow control when constancy is necessary. When performing simple perfusion where time and accuracy is less critical, the use of pressurized reservoirs and valves is not essential. For that, simple perfusion systems using gravity can be realized easily and be adapted to the microsystem, and manual valves can be introduced easily. Thus, once the chip is built, controlling the flow and temperature remains accessible for any user even though with less accuracy and robustness.

2.2.2 The drawbacks

2.2.2.1 The temperature control channel makes it challenging to perform long-term experiments

Performing experiments over several days under the microscope using microfluidics can be challenging and many parameters are involved for maintaining cells in a stable microenvironment.

In the second chapter of the Results, the perfusion chip that was used for most experiments has its temperature and perfusion channels separated by a glass coverslip. Indeed, we chose a transparent material so that the light path is not perturbed when doing live-cell imaging. Besides, glass coverslips allow optimal optical properties while using high-resolution microscopy. Moreover, glass possesses a higher thermal conductivity than transparent plastics, thus the temperature gradient from the thermalized channel to the cell focal plan is not significant.

The protocol for the fabrication of holes in glass coverslip using the laser has been optimized for avoiding cracks after cutting, even if the area around the holes became more fragile. However, the thermalization flow pressurizes this glass coverslip, and after several days using the temperature control, the glass could eventually crack and leak. For that reason we had to find an alternative for performing long-term experiments with the temperature control over a couple of days.

Thin plastic sheets are an obvious alternative to glass, as they are transparent. As less heat conductive, the temperature gradient between both channels would be more significant, and using plastic would require increasing the temperature at the Peltier elements to reach the same target temperature in the cell chamber as with glass (if the target temperature is higher than the ambient temperature). When we use these plastics to separate both channels, it created two major inconvenients:

1) The pressure of the thermalized liquid deformed the plastic coverslips. Consequently, the elastomer underneath the plastic is not flat, leaks could happen by capillarity, and cells underneath the plastic could move.
2) The pressure of the thermalization channel eventually detaches the double-sided adhesive, which bonds the PMMA to the plastic layer, again generating leaks.

To circumvent these issues, we tested multiple plastics, seeking for the one presenting the most appropriate mechanical properties (the most rigid one), and also tested various double-sided adhesives, which would be pressure-resistant (heat activated adhesive, acrylics, silicone glues), but the problems remained unsolved.

Finally, we replaced the adhesive between PMMA and plastic coverslips by making highly resistant bonding of the plastic layer directly to PMMA using epoxy. The stamping method using for bonding is not reproducible from chip to chip, thus the thickness of the temperature channel may slightly vary from one chip to the next. Theses variations in thickness do not have a significant impact on the flow rate of the thermalized liquid, neither on the fluidic resistance of the chip. As a consequence it does not affect the temperature inside the system.

Then, we tried to solve the problem of the plastic bending under pressure. At first we used a 500 micron-thick rigid plastic (Rinzel coverslips), which do not deform much with the pressure (due to its thickness). However, the temperature gradient between both temperature and perfusion channels was too important because of the thickness, and the need of elevating the temperature inside the Peltier elements was necessary. This elevation of the temperature (a target temperature of 37 ˚C in the cell chamber with an objective at 25 ˚C comes to injecting 55 ˚C inside the temperature control channel, compared to 42 ˚C using glass) would increase the amount of bubbles inside the channel, which were hard to remove (even with a flow rate of 5 mL/min). When bubbles in this channel were above the observed cells, it induced strong temperature variations (2 to 5 ˚C). We concluded that performing any biological experiment using thick plastics was not possible. Finally, we chose a thinner plastic layer (Rinzel coverslip of 280 microns thick), which still deforms and creates a non-flat surface. However, we changed the designs of the temperature channel so that it is smaller than the cell channel and would not affect the elastomer bonding, even with the slight deformation (Figure 2). This method did not affect the temperature in the cell chambers, as cells are observed in the middle of the perfusion channel, where the absorption is reduced.

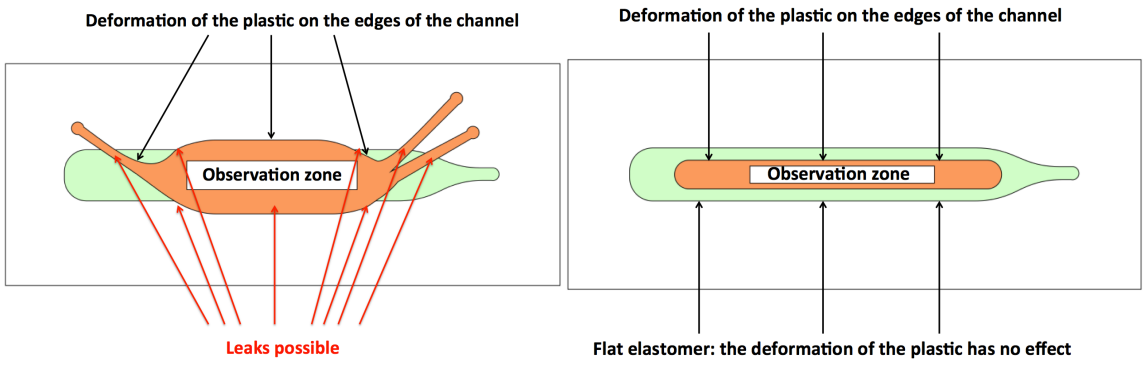

Figure 2: Schematics representing the temperature control and perfusion channels, in orange and green respectively. On the left, the temperature control channel is larger than the perfusion channel. The high flow rate deforms the plastic, which prevents a flat elastomer underneath the plastic layer. On the right, the temperature control channel is narrower than the perfusion channel. The plastic deforms with the pressure, but the plastic bends inside the perfusion channel (this does not have any impact on cell movements) and allows a completely flat elastomer.

All these fabrication issues prove that establishing the structures and protocols to generate simple microfluidic chips can be complicated, especially when it integrates a temperature control channel.

2.2.2.2 The chip cannot be used in static conditions

In order to reuse the microfluidic chip, the strategy chosen was the use of an elastomer for constituting the cell channel. Although we tested various elastomers, all of them showed absorption of small molecules classically used in laboratories. This absorption is linked to:

1) The porosity of the material: a porous material will facilitate the entry of molecules inside its matrix (physical absorption).
2) The type of material: its molecular constitution can have more or less affinity with the drugs in contact of the material (chemical absorption).
3) The surface properties of the material: Depending on the surface hydrophobicity of the material and of the drug of interest, the drug will have more or less interactions with the material.

An elastomer has the ability to deform and is constituted with empty spaces inside its matrix. Consequently, drugs can penetrate easily inside the bulk matrix of the material, and no elastomer that we tested showed significantly reduced absorption.

Despite the absorption, we showed using 1) Rhodamine B and 2) *S. pombe* cells, that having a flow inside the system was circumventing this effect. Indeed, at a given distance from the border (which may need to be determined for each drug), this absorption effect is negligible.

2.2.2.3 Shear stress or continuous flow: a challenge not yet solved.

The systems we used have the drawback of having a flow directly on the perfused cells. Even if media switches are fast, shear stress can still be an issue. In the experiments that we performed for validating the system, we used low flow velocities inside the channel, and showed no major effects on cell physiology.

Indeed, at the slow flow rate of 20 µL/min, *S. pombe* cells had the same generation time and length at division in chips and in liquid culture flasks. Likewise, block and release results were similar to the ones using flasks.

On the other hand, performing experiments with mammalian cells using the system for a longer period of time was challenging. On one hand, we injected a CDK inhibitor RO-3306 to synchronize *HeLa* cells in their cell cycle in the system in static conditions (without renewal of medium and inhibitor). After 20 hours, cells were not blocked due to the absorption effect of the elastomer. On the other hand, when a constant flow with RO-3306 inhibitor was applied for 20 hours, cells would be blocked but would not divide when returning to normal medium. To explain this phenomenon, two hypotheses are possible. The first one is that shear stress is affecting cell proliferation. The second one is that constant renewal of fresh inhibitor alters cell proliferation, which stay blocked even after releasing to normal medium. These two hypotheses were tested while having a sequential renewal of the medium and inhibitor for 20 hours, then a constant flow of medium. Results showed that cells were dividing, and confirmed the second hypothesis.

2.2.3 Conclusion

The system we developed is compatible with live-cell imaging approaches. We have demonstrated its compatibility with adherent and non-adherent organisms. Biological validations revealed issues we did not anticipate or expect. For instance, the perfusion chip was simple to fabricate and to use using yeasts, but adapting it for long-term experiments using mammalian cells was unexpectedly difficult and required some technical engineering and energy.

As cells are directly in the flow, the perfusion dynamics are fast, but may generate shear stress on studied cells. Moreover, we showed that the system was incompatible with low or precise drugs concentrations, even though having a perfusion flow reduces its effect further from the border of the channel. For these applications, we recommend using the wax chip developed previously.

The system that we built could be of great usage for any laboratory without particular experience in microfluidics: the chip fabrication, reuse, flow and temperature control can be realized easily.

2.3 The membrane chip: an ambitious project

2.3.1 Many parameters involved

The membrane chip was the original aim of my thesis. As constituted with several layers, it requires a lot of engineering to be functional and robust. The membrane selection and integration into a microchip is complicated[6]. The selection of the membrane depends on several parameters. Among these, we could cite the thickness, pore size and distribution, optical properties, mechanical properties, absorption properties, bonding methods. We tested several membranes, and fabrication strategies, for obtaining the fastest diffusion timings while preventing hydrodynamic shear stress on cells. The prototype that we developed was not reusable, and the fabrication of one chip was time-consuming. At some point, we decided to prioritize the development of the perfusion chip, which is less complicated and could be use and reused in most biological laboratories.

2.3.2 A first prototype with lots of unknowns

I fabricated a complete membrane-based microfluidic chip (See Results, Chapter 3) by intercalating a polycarbonate membrane between two channels made in double-sided adhesive. I performed some experiments using fission yeast cells with the microsystem developed. Some proofs-of-concept assays were performed: we used *S. pombe* fission yeasts with an engineered cell cycle network, which cell cycle can be synchronized using an ATP analogue inhibitor 3-MBPP1. The injection of this inhibitor in the perfusion channel blocked cells, which were underneath the membrane, in the G2 phase of the cell cycle.

However, we observed that the double-sided adhesive also absorbs small molecules. This absorption comes from the adhesive glue, which surrounds the hard substrate material. Even though we tested various double-sided adhesives for reducing this absorption (temperature-activated adhesives, ultra-thin adhesives of 5 microns thick, etc.), none of these would be appropriate in this system, and we chose to keep this material as the cell channel layer, increasing its width to reduce the absorption effect further from the channel borders. Moreover, we observed a slight convection of fresh medium inside the cell channel increased, which

varies from chip to chip, and the use of lectin prevented cell movements, allowing their observation for long-term experiments at the microscope.

2.3.3 Conclusion

Integrating a membrane in a microfluidic chip is not trivial, as many parameters are interfering in the fabrication process and in the biological validations. The systems that we built during my thesis have shown convincing results of its biocompatibility with non-adherent cells. The membrane we have chosen in polycarbonate allowed a constant delivery of fresh medium to cells underneath, even thou a slight convection inside the cell channel was observed with a perfusion flow of 20 µL/min. What would be interesting is to test slower flow rates, which would not allow convection inside the cell channel, but would be of great interest for performing long-term experiments and for comparing with the results found using the perfusion cells (where cells are directly in the flow).

3 General conclusion

During my thesis, I have participated in the development of the wax microchip and have fabricated both the perfusion and membrane-based systems. These three different chips have their respective advantages and drawbacks. They all allow a precise control of the cell microenvironment while performing live-cell imaging experiments. In fact, the flow in such system can be controlled with accuracy, precision and dynamism. Moreover, these systems allow for a high degree of temperature control at the microscope, as long as cells are observed in the oil area. For instance, using the wax chip, we have reduced the distance between cell chambers so they could all fit in the area.

By being simple and compatible with several model organisms, the usage of the perfusion chip in multiple laboratories could be of great interest, especially since it is cheap, easy to build, and it can be adapted to simple flow and temperature control systems. On the other hand, the wax chip is the most powerful system, as it can be used with precise concentration of drugs. However, this chip is hard to fabricate and cannot be reused, thus is less likely to be a general standard in a broad range of laboratories.

Based on my work, I believe the future of microfluidics relies on the development and use of simple microfluidic chips. For a laboratory that has never done microfluidics, it can take years to develop complex and functional systems. Building complex microfluidic chips is indeed time-consuming, as many parameters are involved, mostly in the fabrication and biological validations steps.

Additionally, one can perform live-cell imaging experiments using a simple system and have undesired microbial contamination. Other experiments may stop because of bubble formation inducing cell drying. In other systems, cells would not proliferate because pH fluctuated, or temperature, or oxygen level. When unexpected conditions happen while utilizing a complex system that takes days to fabricate and operate, we could wonder if the potential results are worth the time consumed. Thus, the expansion of microfluidic laboratories will depend on how simple the microfluidic system is, on the biological questions that is investigated and on the robustness of the results.

Nowadays, research laboratories in microfluidics are mostly focusing on developing state-of-the-art systems, in which complexity is always added. For instance, the development of organs-on-a-chip has been of great interest during the past decade[7], and their aim is to reproduce the complexity of organs. These systems serve as models for tissues or organs to understand the physiological reactions and functions of the human body, as well as to seek for new potential drugs for healthcare[8]. This simulation of tissues or organs is complicated, as a considerable number of parameters are acting in the human body. In these systems, the

first integration and assembly of materials that mimic as much as possible the human tissues, bones, muscles, or other parts of the body, makes the microfluidic chip challenging to fabricate. Furthermore, this complexity is increased when adding flow control, shear stress, complicated structures or designs. Adding cells and validating the system is difficult, because of the numbers of parameters that are involved in the body, and it could take months or years before having valid results. What is surprising is that a large number of organs-on-a-chip systems have been developed, but only a minority of them has reported considerable insights on biological or drug discoveries. This leads to questioning whether the development of such complex systems like organs-on-a-chip, or even more complicated ones as humans-on-a-chip[9], [10], is essential, or whether building these complex but potentially powerful systems is only a trend.

I support the idea that microfluidic is just a tool, whose purpose is to help solving biological problems, and it will become more widespread when the simplicity of microfluidic systems will become a common parameter.

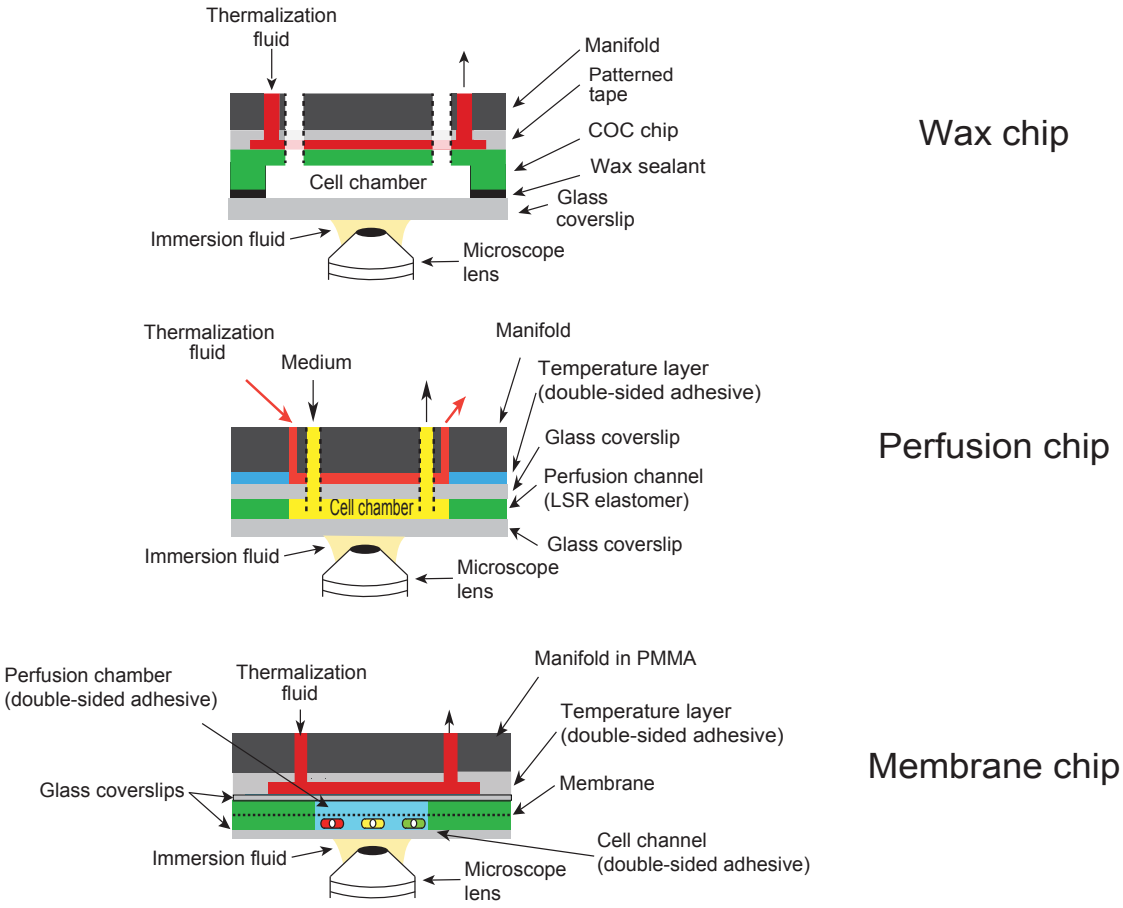

Figure 3: Schematics of the three microfluidic chip developed in the laboratory. On top, the wax chip, containing a channel made of COC. This chip is ideal for performing experiments involving precise concentrations of drugs. In the middle, the perfusion chip. Constituted with an elastomer, this chip is ideal when performing simple experiments. Easy-to-use and re-usable, it could be used as a common tool for any laboratory. At the bottom, the membrane-based chip. Constituted with a membrane, this chip allows for experiments where shear stress is to be avoided.

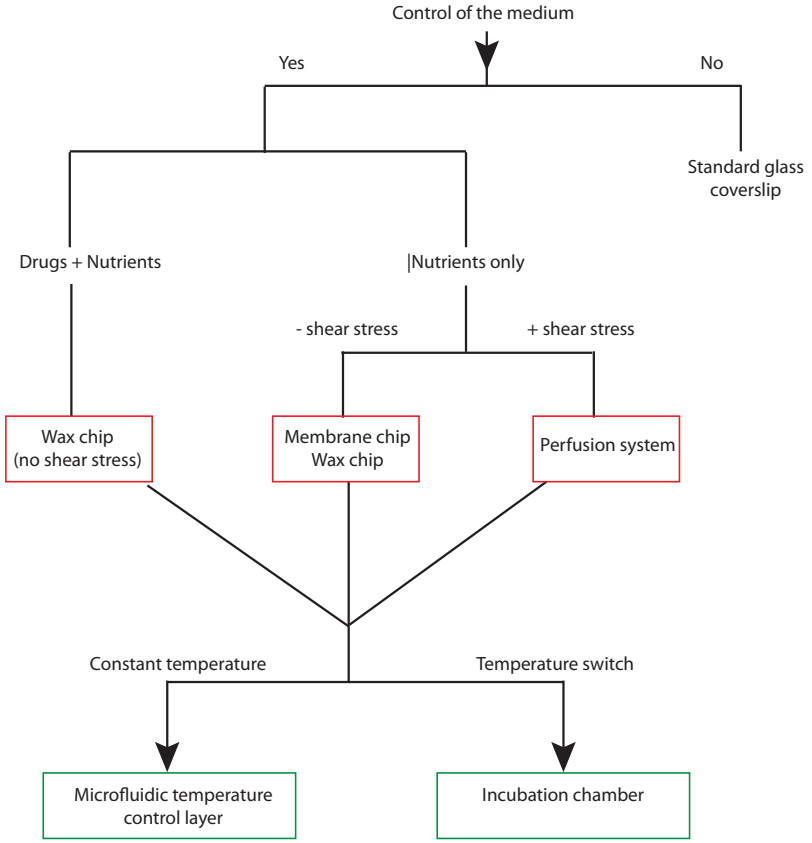

Figure 4: Organigram indicating the appropriate chip to use for the experimental conditions required.

References

[1] E. K. Sackmann, A. L. Fulton, and D. J. Beebe, "The present and future role of microfluidics in biomedical research.," *Nature*, vol. 507, no. 7491, pp. 181–189, Mar. 2014.

[2] "Solving problems," *Lab Chip*, vol. 10, no. 18, pp. 2317–2318, 2010.

[3] Y. Temiz, R. D. Lovchik, G. V. Kaigala, and E. Delamarche, "Lab-on-a-chip devices: How to close and plug the lab?," *Microelectronic Engineering*, vol. 132, pp. 156–175, Jan. 2015.

[4] A. L. Paguirigan and D. J. Beebe, "Microfluidics meet cell biology: bridging the gap by validation and application of microscale techniques for cell biological assays.," *Bioessays*, vol. 30, no. 9, pp. 811–821, Sep. 2008.

[5] G. M. Whitesides, "Cool, or simple and cheap? Why not both?," *Lab Chip*, vol. 13, no. 1, pp. 11–13, Jan. 2013.

[6] J. de Jong, R. G. H. Lammertink, and M. Wessling, "Membranes and microfluidics: a review.," *Lab Chip*, vol. 6, no. 9, pp. 1125–1139, Sep. 2006.

[7] S. N. Bhatia and D. E. Ingber, "Microfluidic organs-on-chips," *Nat. Biotechnol.*, vol. 32, no. 8, pp. 760–772, Aug. 2014.

[8] E. W. Esch, A. Bahinski, and D. Huh, "Organs-on-chips at the frontiers of drug discovery," *Nature Reviews Drug Discovery*, vol. 14, no. 4, pp. 248–260, Mar. 2015.

[9] D. Huh, H. J. Kim, J. P. Fraser, D. E. Shea, M. Khan, A. Bahinski, G. A. Hamilton, and D. E. Ingber, "Microfabrication of human organs-on-chips," *Nat Protoc*, vol. 8, no. 11, pp. 2135–2157, Oct. 2013.

[10] H. E. Abaci and M. L. Shuler, "Human-on-a-chip design strategies and principles for physiologically based pharmacokinetics/pharmacodynamics modeling," *Integr. Biol.*, vol. 7, no. 4, pp. 383–391, 2015.

Résumé :

Connaître en temps réel la réponse et le comportement des cellules et organismes modèles suite à des changements de leur environnement, ou à des modulations de leurs fonctions biologiques est devenu essentiel dans les sciences du vivant. Ces réponses nous permettent ensuite de comprendre les mécanismes qui régissent le fonctionnement des cellules vivantes, avec des implications en recherche fondamentale, appliquée et biomédicale. Un des plus gros défis technologiques reste le contrôle des paramètres environnementaux en microscopie haute résolution. De nos jours, aucun système ne permet de réguler un ensemble complexe de paramètres de manière précise, dynamique et simultanée tout en observant les cellules dans leur environnement.

L'objectif de ma thèse est de mettre au point un tel dispositif permettant a minima une régulation fine de la température, de la composition du milieu, et notamment de la concentration de divers drogues. Ce système doit être compatible avec les applications les plus poussées en microscopie photonique. Mon approche au cours de ma thèse pour élaborer un tel système est l'utilisation de la microfluidique. En effet, c'est la seule technologie qui puisse de réaliser un tel multiplexage. Elle permet de manipuler des petites quantités de fluide à travers un système contenant des canaux de dimensions allant du micromètre au centimètre. Cet ordre de grandeur des canaux constitue un atout majeur (réduction de la consommation des réactifs, réduction des couts, cinétiques des réactions chimiques et biologiques élevées, temps de diffusion court, etc.) et permet d'allier les expériences biologiques à la microscopie. Mon objectif est de concevoir une puce microfluidique qui représentera un pas technologique majeur et ouvrira de nouvelles possibilités de recherche.

Summary:

Monitoring in real-time the response of cells and model organisms to the changes in their environment or to modulations of their biological functions has become essential in life sciences. One of the main technical challenges for biologists is the precise and dynamic control of various environmental parameters while doing high-resolution microscopy.

My thesis consists of building a robust and versatile system, dedicated to live-cell imaging that will be compatible with adherent and non adherent models, that could provide a precise and simultaneous control of 1) the temperature, 2) the media exchanges and 3) the drug concentration while doing photonic microscopy.

My approach is to use microfluidics, which is the best candidate in order to achieve this system and provides all the necessary controls of micro-scaled volumes for culturing, maintaining or analyzing cells. It produces miniaturized systems used as tools for biological experiments, in which channels of a micro-scaled dimension are used for the fluid circulation. The laminar flow in these chips allows fast molecule diffusion as well as fast temperature diffusion. Because of the high surface to volume ratio, the consumption of reagents is reduced, and media switches can be fast. This system will represent a major technical and beneficial step and will open new possibilities of research in biology.

Résumé en français

Introduction

Les enjeux de ma thèse découlent des problématiques majeures liées à l'observation d'échantillons biologiques en microscopie haute résolution. De nos jours, les scientifiques recherchent de plus en plus à contrôler les divers paramètres environnementaux auxquels sont soumis leurs modèles d'étude, soit pour reproduire le plus efficacement possible l'environnement naturel de ceux-ci, soit pour imposer des contraintes liées aux questions biologiques posées. Aujourd'hui, aucun système ne permet de contrôler un ensemble complexe de paramètres de manière précise, dynamique et simultanée tout en observant en temps réel la réponse des échantillons à de telles perturbations.

Ma thèse a pour objectif la mise au point d'un tel dispositif permettant a minima une régulation fine de la température, de la composition du milieu, et de la concentration de divers drogues. Il doit être compatible avec les applications les plus poussées en microscopie photonique. Mon approche pour élaborer un tel système est l'utilisation de la microfluidique, seule technologie qui puisse réaliser un tel multiplexage. Elle permet de manipuler des petites quantités de fluide à travers un microsystème contenant des canaux de dimensions allant du micromètre au centimètre. Cet ordre de grandeur pour les microcanaux constitue un atout majeur et permet d'allier les expériences biologiques à la microscopie. Mon but est de concevoir une puce microfluidique qui représentera un pas technologique majeur et pourrait permettre des avancées importantes en biologie cellulaire et cancérologie, nous permettant de mieux comprendre les mécanismes de prolifération des cellules ou encore leurs réponses aux traitements par des drogues.

Au cours de ces trois années de thèse, j'ai travaillé dans le laboratoire « Synthecell » et avec la start-up Cherry Biotech pour développer ce système et ce rapport est un résumé de mes recherches au cours de ces trois années de thèse.

Objectifs:

L'objectif de ma thèse est de développer un système dédié à l'imagerie de cellules vivantes. Par conséquent, le système idéal doit être compatible avec la microscopie haute résolution. Ce système doit être versatile : il doit être compatible avec des cellules adhérentes et des cellules non adhérentes. Pour permettre aux cellules de proliférer, l'environnement cellulaire donc la température et le milieu cellulaire doivent être contrôlés de façon précise et dynamique. De plus, le matériau PDMS (polydimethylsiloxane), principal matériau utilisé en microfluidique, doit être évité, en raison de ses propriétés d'absorption non désirées.

La fabrication d'un tel système est contraignante : le rendre simple à fabriquer et facile d'utilisation, ainsi que réutilisable est d'autant plus difficile. En considérant toutes les contraintes, nous avons conclu qu'un système unique et idéal est impossible à réaliser. Par conséquent, nous avons opté pour une stratégie différente : construire trois systèmes

différents, ayant leurs avantages et inconvénients respectifs, couvrant ta totalité des besoins et des applications en biologie cellulaire. Dans ces trois systèmes, les matériaux doivent être compatible avec la microscopie, la température et la perfusion de milieux doivent être contrôlés précisément, dynamiquement et simultanément.

Resultats :

1) La première puce microfluidique

Au cours de ma thèse, j'ai développé une première puce microfluidique dédiée à l'observation de cellules sous microscope en temps réel. Les systèmes similaires existant sont fabriqués en PDMS. Le système dont j'ai participé au développement possède l'avantage de ne pas contenir ce matériau, qui est préjudiciable pour la prolifération cellulaire. En revanche, les matériaux thermoplastiques ont émergé en replacement du PDMS dans le domaine de la microfluidique pour les expériences avec des cellules vivantes. Cependant, la fabrication de ces dispositifs en plastique, et surtout leur collage avec une lamelle de verre, essentielle pour la microscopie de haute résolution, reste un défi pour les chercheurs. Nous avons testé la compatibilité de ces matériaux avec les drogues classiquement utilisées en laboratoire, et avons choisi le COC (cyclic olefin copolymer), duquel l'absorption est négligeable, permettant la possibilité d'injecter des milieux avec les drogues de concentration précise. Dans le système conçu, nous avons établi des microcanaux dans le COC dans lesquels les cellules sont injectées et observées, et dont les designs et structures peuvent être complexes et avantageuses. Nous avons obtenu un haut degré de contrôle du micro-environnement. En utilisant la levure de fission *S.pombe*, nous avons démontré la possibilité de réaliser des changements rapides de milieux. De plus, nous avons implémenté un canal de contrôle de température qui permet de contrôler la température de façon précise et dynamique tout en observant les cellules sous microscope.

2) La deuxième puce microfluidique

Même si la microfluidique s'est répandue dans de nombreux laboratoires de recherche, la complexité des systèmes jusqu'alors développés, ainsi que les équipements de fabrication onéreux peuvent être un frein à leur intégration dans certains laboratoires de recherche. Nous nous sommes donc intéressés au développement d'une puce microfluidique qui soit simple à utiliser et à fabriquer, et qui pourrait s'intégrer facilement dans des laboratoires de biologie. Pour se faire, nous nous sommes intéressés au développement d'un système dont la simplicité est le paramètre le plus important à considérer, tout en possédant les avantages inhérents à la microfluidique. La puce que nous avons développée est composée d'un matériau élastomère composant le canal principal de perfusion. L'élastomère permet d'assurer l'étanchéité du canal mais aussi la réutilisabilité de la puce microfluidique. Ce canal permet un renouvellement de milieu en continu tout en observant les cellules sous microscope. En conséquence, les cellules sont directement dans le flux de milieu et sont soumises à des contraintes pariétales. Des tests ont été établis et ont prouvé que ce stress n'altère pas la

physiologie des cellules non adhérentes *S.pombe* (collées à la lamelle de verre par l'utilisation de lectine) et les cellules adhérentes *HeLa*. Cependant, l'absorption non négligeable de l'élastomère empêche toute expérience utilisant des quantités de drogues faibles ou précises, même si le flux de milieu rend cette absorption négligeable sur les cellules au milieu du canal, loin des bords de l'élastomère. J'ai réalisé les mêmes systèmes de contrôle que pour la puce précédente par des expériences avec changement de milieux ou de température de façon dynamique, prouvant la robustesse du système. De plus, tous les matériaux constituant cette puce sont coupés facilement par une machine laser à CO_2. Nous avons montré qu'il est aussi possible de les couper sans machine laser, prouvant l'accessibilité à tout utilisateur. De plus, le contrôle des températures et flux de milieux peuvent être réalisés sans contrôleur, qui peut être onéreux, si la précision et la justesse ne sont pas des paramètres importants.

3) La troisième puce microfluidique

Les désavantages du PDMS ont poussé les chercheurs à trouver des alternatives afin de fabriquer des systèmes biocompatibles. Cependant, ces matériaux ne permettent pas forcément des designs et structures complexes, qui ont été auparavant ingénieusement conçus avec le PDMS, en formant par exemple des pièges pour les cellules non adhérente et ainsi permettre leur observation au cours d'une perfusion sans utiliser de drogue pour qu'elles adhèrent (lectine). Il s'agit de méthodes de fabrication permettant de réaliser un moule en PDMS et leur réplica en plastique pour obtenir des structures complexes et ainsi piéger les cellules afin de les visualiser sans qu'elles soient mobiles avec le flux de milieu. Comme évoqué précédemment, le collage de ces plastiques à une lamelle de verre, essentielle à la visualisation sous haute microscopie, reste un challenge.

Toutefois, une autre approche pour visualiser les cellules non adhérentes sous microscope est l'utilisation d'une membrane perméable. Les pores de cette membrane sont une surface d'échange de milieux de façon diffusive et non convective, par conséquent les cellules ne sont pas soumises aux contraintes pariétales (pas de convection). En revanche, peu de protocoles ont été développés pour intégrer des membranes dans des systèmes ne comportant pas de PDMS. J'ai dû développer un protocole afin d'intégrer une membrane semi-perméable en polycarbonate entre des matériaux plastiques biocompatibles.

En conclusion, la puce microfluidique développée présente trois canaux distincts :

- Un canal de cellules, ou celles-ci sont injectées et visualisées.
- Un canal de perfusion, séparé du canal de cellules par la membrane perméable qui apporte en continu le nouveau milieu, ou les diverses drogues.
- Un canal de température, ou est injecté un liquide caloporteur qui contrôle la température à l'intérieur du système.

Des tests préliminaires ont été effectués et montrent que le système est fonctionnel avec les cellules non adhérentes *S.pombe*. De plus, la fonction de la membrane est validée : le stress subit par les cellules est négligeable (convection limitée dans le canal des cellules).

4) Les bulles dans les systèmes microfluidiques

Les bulles dans les systèmes microfluidiques sont problématiques dans les expériences sur cellules vivantes. En effet, elles peuvent nucléer spontanément et s'accumuler, surtout lors d'expériences à long terme incluant une perfusion, résultant en stress indésirable sur les cellules et affectant leur comportement et viabilité. Quelques solutions ont déjà été établies et sont disponibles dans le commerce, mais restent compatibles seulement avec les systèmes en PDMS (pas adéquat pour les systèmes en plastiques). Des systèmes commerciaux standards ont aussi fait leur apparition pour limiter l'accumulation des bulles, cependant lors d'expériences à long terme ces systèmes ne sont pas efficaces. Au cours de ma thèse j'ai donc développé une nouvelle stratégie pour enlever les bulles déjà accumulées dans les systèmes microfluidiques. Cette stratégie inclut l'utilisation d'une pompe à vide et un canal isolé, dans lequel les bulles peuvent être aspirées. Ce système est adapté à tout type de matériau et de design de canaux. Il peut être automatisé et permet des expériences à long terme sur des cellules vivantes.

Conclusion

Au cours de ma thèse, j'ai participé au développement de trois puces microfluidiques distinctes, et ai élaboré un protocole afin de réaliser des expériences de longue durée sous microscope en temps réel avec des cellules vivantes. Celles-ci ont leurs avantages et inconvénients respectifs, et permettent à plus grande échelle de couvrir la totalité des applications en biologie.